NOTE TO USERS

Page(s) not included in the original manuscript and are unavailable from the author or university. The manuscript was scanned as received.

112

This reproduction is the best copy available.

UMI®

FACTORS GOVERNING THE DESIGN, SELECTION AND CLEAVAGE OF SUGAR-MODIFIED DUPLEXES BY RIBONUCLEASE H

Maria M. Mangos

Department of Chemistry
McGill University
Montreal, Canada

January 2005

A Thesis submitted to McGill University
in partial fulfillment of the requirements for the degree of
Doctor of Philosophy

Your file Votre référence
ISBN: 0-494-12899-2
Our file Notre référence
ISBN: 0-494-12899-2

This thesis is dedicated to my loving parents, Helen & Mike, whose suffering during its writing has been long, but not silent.

ABSTRACT

The antisense principle bases its premise in the exquisite complementarity of a synthetic, chemically-modified oligonucleotide to tightly bind with a unique target RNA sequence. Rapid and selective genetic discrimination, as driven by the formation of multiple points of target contact, constitutes a central goal of oligonucleotide therapies. Most synthetic designs have, however, provided little structural insight on the role of the antisense oligonucleotide (AON) in triggering RNA cleavage of preformed hybrids, as catalyzed by a ubiquitous, intracellular enzyme known as ribonuclease H. The use of RNase H to assist AON inhibition of gene expression is crucial to mainstream antisense technologies, yet the precise mode by which this enzyme acts on AON/RNA duplexes remains unclear.

To address the role of substrate structure on enzyme activation, a dominant theme of this thesis highlights the design, synthesis and structural studies of novel AONs comprised of rigid 2'-deoxy-2'-fluoroarabino (2'F-ANA) or native (DNA) nucleotides, containing interspersed flexible (*e.g.* "2',3'-seconucleotides") or anucleosidic (*e.g.* butyl) residues. This unique AON class combines both pre-organization & flexibility within the hosting heteroduplex, which on their own usually prove detrimental towards enzyme trigger. Their combination, however, synergistically activates both *E. coli* and human RNases H, leading to potent destruction of duplexed RNA. These compounds thus represent the first examples of modified AONs lacking deoxyribose sugars that elicit RNase H activity comparably to the native (DNA) systems. DNA-derived AONs with acyclic residues also amplify enzyme-catalyzed target degradation, suggesting the added flexibility imparted to the substrate structure to be vital for ameliorating the protein/nucleic acid interaction. Melting and circular dichroic experiments have revealed that the enhanced dynamics associated with a particular acyclic modification remain globally undetectable, indicating the acyclic residues induce only local structural deformations to the helix architecture.

Intricate comparisons of the structural and biological properties of various acyclic residues (*e.g.* butyl, propyl and ethyl interresidue spacers) designed to locally compress or expand the AON helix backbone at a defined axial site has enabled a deeper understanding of the conformational factors that underlie the observed enhancements.

Stemming from this work is the discovery that these subtle changes in local flexibility have relatively minor impacts on enzyme tolerance, whereas strong RNase H induction profoundly relies upon both the inter- and intrastrand placement of the flexible unit.

The exceptional processivity imparted toward canonical A-like heteroduplexes upon modification with an acyclic residue is extended to characteristically poor substrates (*e.g.* dA_{18}/rU_{18}), which normally fail to achieve adequate enzyme activation by virtue of suboptimal helix geometries. Surprisingly, these hybrids can likewise be engineered to invoke relative rates of RNase H-mediated cleavage that far surpass those attainable with their unmodified cognates. These studies collectively unveil a strong dependence on the helical disposition of the hybrid housing the modification, with A-like duplexes preferentially activating the enzyme upon antisense derivatization whereas those with compressed minor grooves elicit high activity only upon sense-strand modification.

We last present compelling evidence for an elegant substrate orienting mechanism involving amino acid intercalation that serves to rationalize some of these key observations. These are elucidated via competition experiments involving linker-containing AON/RNA hybrids in the presence of human RNase H1 using as 'inhibitor' an aromatic tripeptide to mimic core protein binding interactions that presumably occur during formation of the enzyme-substrate complex.

RÉSUMÉ

La théorie antisens s'appuie sur la remarquable complémentarité entre un oligonucléotide chimiquement synthétisé et modifié et une séquence particulière d'un brin d'ARN visé. La sélection rapide et spécifique d'un gène (grâce à une reconnaissance en multiples points) est la caractéristique principale des traitements à base d'oligonucléotides. Toutefois, la plupart des molécules synthétisées ne permettent pas de bien comprendre le rôle, au niveau structurel, de l'oligonucléotide antisens (ONA) dans la dégradation d'hybrides préformés par une enzyme ubiquitaire et intracellulaire : la ribonucléase H. L'emploi de la ribonucléase H dans l'inhibition de l'expression génétique par l'ONA est essentiel aux technologies antisens, même si son mécanisme précis d'action sur les duplex ONA/ARN n'est toujours pas clair.

Afin de mieux comprendre le rôle joué par la structure du substrat dans l'activation de l'enzyme, nous avons modélisé, synthétisé et fait l'étude structurelle de nouveaux ONA comprenant des nucléotides rigides, tels que les 2'-désoxy-fluoroarabinoses (2'F-ANA), ou natif tel que l'ADN; et comprenant des unités flexibles (2', 3'-seconucléotides) ou non nucléosidique (butyle). Cette classe unique d'ONA combine flexibilité et pré-organisation au sein des hétéroduplexes hôte, qui séparément s'avèrent généralement avoir un effet négatif sur l'activation enzymatique. Toutefois, leur combinaison permet l'activation synergétique aussi bien de l'*E. coli* que de la ribonucléase H humaine, ce qui entraîne la dégradation du duplex d'ARN. Ces composés sont donc le premier exemple d'ONA modifiés ne contenant pas de désoxyriboses, capables d'activer la ribonucléase H aussi bien que l'ADN natif.

Les ONA dérivés de l'ADN ayant une unité acyclique, amplifient aussi la dégradation par catalyse enzymatique du brin visé, semblant ainsi démontrer que le surcroît de flexibilité est important pour améliorer les interactions protéines/acides nucléiques. Les expériences de température de fusion et de dichroïsme circulaire démontrent que l'amélioration dynamique observée par l'insertion d'un bras acyclique est globalement indétectable, ce qui indique que les parties acycliques ne provoquent qu'une déformation structurelle localisée de l'architecture en hélice.

Une comparaison détaillée des propriétés structurales et biologiques de nombreux bras acycliques (bras écarteurs : butyle, propyle et ethyle), modélisés pour compresser ou espacer le squelette de l'hélice ONA à un site axial précis, a permis de mieux comprendre les facteurs conformationnels sous-jacents à l'amélioration observée. Grâce à ces travaux, nous avons découverts que ces changements subtils dans la flexibilité locale ont très peu d'impact sur la tolérance de l'enzyme, tandis qu'une forte induction de la ARNase H repose de manière importante sur le placement inter et intra de l'unité flexible dans les brins oligonucléotides.

L'exceptionnelle réactivité observée chez les hétéroduplexes natifs de conformation A lors de la modification par une unité acyclique s'étend jusqu'aux substrats généralement peu réactifs (dA_{18}/rU_{18}) qui, à cause de la géométrie de leur hélice, ne peuvent suffisamment activer l'enzyme. Etonnamment, ces hybrides peuvent être modifiés afin d'obtenir un taux relatif de dégradation médiée par la RNase H largement supérieur a celui de leur pairs non modifiés. Toutes ces études mettent en évidence une forte dépendance vis à vis de la structure hélicoïdale de l'hybride modifié : les duplexes de conformation A activent l'enzyme si le brin antisens contient la modification, tandis que ceux qui ont un petit sillon compressé ont une plus grande réactivité lorsque la modification se trouve dans le brin sens.

En dernière partie nous présentons des données éloquentes sur un mécanisme d'orientation du substrat qui agit par intercalation des acides aminés. Il nous permet de rationaliser quelques observations clés. Celles-ci sont élucidées par le biais d'expériences de compétition entre des hybrides ONA/ARN contenant un bras écarteur, en présence de l'enzyme humaine ARNase H1 et avec pour inhibiteur un tripeptide aromatique mimant les interactions de liaison protéinique fondamentales qui interviennent vraisemblablement lors de la formation du complexe enzyme-substrat.

ACKNOWLEDGEMENTS

This thesis was shaped with some unexpected turns over the years. Its direction, as with my own, was guided with great wisdom, solid ideas, and sharp insight generously shared by my supervisor, Dr. Masad J. Damha. Along with his constant wealth of enthusiasm, inspiration, strong encouragement and optimism, he taught me to embrace the unpredictable nature of research with passionate beliefs yet critical judgement. Much more than just an outstanding scientist, his benevolence, patience, cheerful humor and good company are few of the things I shall treasure most from my experience at McGill. Thank you.

My warmest thanks to Dr. Karine Auclair for granting me unrestricted access to her facilities and use of the CD instrument at a moment's notice. I appreciate your trust and gracious hospitality. Drs. David Harpp and George Just, for their often colourful tidbits of advice both professionally and ethically, also made my stay at the university all the more pleasant.

I am deeply indebted to the many scientists who worked with me behind the scenes but nevertheless enriched the quality and depth of my understanding and studies tremendously: Mr. Nadim Saade and Dr. Antisar Hlil are thanked for their technical proficiency and speed in providing FAB and MALDI mass spectral acquisitions; Drs. Paul Xia and Fred Morin, for dutifully convincing me that NMR can be a friendly, if not useful, tool when treated with a little affection; and Dr. Kyung-Lyum Min, a talented collaborator and friend, whose assistance with and practical expertise in the world of RNase H immeasurably strengthened my own skills and knowledge in this area. A special thanks is owed to Dr. Ekaterina Viazovkina who always made the time to lend a helping hand when needed. She and Dr. Mohamed Elzhageid are sincerely thanked for their great assistance with both solution and solid-phase syntheses of 2'F-ANA.

I am so honoured to have worked with a creative, ambitious, amazing group of people throughout my Ph.D. studies. For ensuring a stimulating and fun environment in which to learn and grow, I owe a very special thanks to my good friends at McGill, in particular, Anna Tedeschi, Debbie Mitra, and Bénédicte Pâtureau, all of whom lightened the mood

and enlivened the atmosphere. Bénédicte – un deuxième grand merci for translating the abstract, you are impressive.

My most heartfelt appreciation is extended to a very dear friend and past colleague of mine, Dr. Sandra Carriero, who became a truly exceptional part of my surrogate family during the many years spent here, and for her continued involvement and moral support thereafter. I will fondly remember our late work sessions together in the lab, sharing laughs, frustrations and triumphs, often times in a single night.

To my parents, Helen and Mike Mangos, you have never asked anything from me other than my happiness, yet have dedicated your lives with steadfast courage and grace for the dreams and futures of your children. It is a small fraction of your hard work that rests upon these pages now. I hope in some way I have given you one shining moment of pride, much as that you have always given me. You are my greatest sources of love, strength and inspiration, and two of the finest people I have ever known.

Huge thanks to my brother John, who will always be my best friend and most thoughtful listener, even if I don't see him as much as I used to. You are my greatest role model.

Thanks to the rest of my family and friends in Toronto, for reminding me that life and busy schedules should always be second to a hot cup of coffee with a good ear beside you. Thanks for always being there.

An extra special thanks to my best friend Karen, for her unique ability to share with me the humour in every situation, and for still being the first person I call whenever back in my hometown.

My two little companions, B & C, whose endless plots to destroy these pages I can only hope were done out of love – thanks for keeping an eye on me.

To all of you in the department who never forgot the importance of a smile or friendly gesture, and for those whom I've unintentionally left unmentioned, thank you.

TABLE OF CONTENTS

ABBREVIATIONS & SYMBOLS

A	adenosine
Å	angstrom
A. fulgidus	*Archaeoglobus fulgidus*
A_{260}	UV absorbance measured at 260 nm
ABu	2'-O-aminobutyl
Ade	adenine
AE	2'-O-aminoethyl
amp^r	ampicillin resistance gene
ANA	arabinonucleic acid
AOE	2'-O-aminooxyethyl
AON	antisense oligonucleotide
AP	2'-O-aminopropyl
APS	ammonium persulfate
ara	arabino
Arg	arginine
ATT	6-aza-2-thiothymine
B	base
BIS	*N,N'*-methylene-bisacrylamide
BLAST	basic local alignment search tool
bp	base pair
BPB	bromophenol blue
Bz	benzoyl
C	cytidine
ca.	*circa* (approximately)
calc.	calculated
CD	circular dichroism
cDNA	complementary DNA (*i.e.* reverse transcribed)
CE	β-cyanoethyl
CMV	cytomegalovirus

COSY	Homonuclear Correlation Spectroscopy
CPG	controlled pore glass
Cyt	cytosine
d	days
DCC	1,3-dicyclohexylcarbodiimide
DCE	1,2-dichloroethane
DCI	4,5-dicyanoimidazole
DCM	dichloromethane
ddH_2O	double distilled and deionized water
DEAOE	2'-O-(N,N-diethylaminooxyethyl)
DEC	1-(3-dimethylaminopropyl)-3-ethylcarbodiimide hydrochloride
DEPC	diethyl pyrocarbonate
DIPEA	diisopropylethylamine
DMAOE	2'-O-(*N,N*-dimethylaminooxyethyl)
DMAP	2'-O-(*N,N*-dimethylaminopropyl), *i.e.* sugar modification
DMAP	*N,N*-dimethyl-4-aminopyridine
DMF	*N,N*-dimethylformamide
DMSO	dimethyl sulfoxide
DMT	dimethoxytrityl
DNA	2′-deoxyribonucleic acid
ds	double stranded
dsRBD	double stranded RNA binding domain
dT	thymidine
DTT	dithiothreitol
E. coli	*Escherichia coli*
e.g.	for example
EDTA	disodium ethylenediamine tetraacetate dihydrate
EG	ethylene glycol
EOM	2'-O-ethoxymethylene
eq	equivalent(s)

Et	ethyl
EtOAc	ethyl acetate
2'F-ANA	2'-fluoro-2'-deoxyarabinonucleic acid
F	phenylalanine
FAB-MS	Fast Atom Bombardment Mass Spectrometry
G	glycine
g	gram(s)
G	guanosine
gCOSY	gradient COSY
Gua	guanine
h	hour(s)
H	hyperchromicity
HATU	O-(7-azabenzotriazol-1-yl)-1,1,3,3,-tetramethyl-uronium hexafluorophosphate
*Hin*dIII	*Haemophilus influenzae* restriction enzyme
HIV-1	human immunodeficiency virus type 1
HPLC	High Pressure Liquid Chromatography
Hz	Hertz
i-	iso
i.d.	internal diameter
i.e.	that is
ICAM	intercellular adhesion molecule
i-Pr	isopropyl
IPTG	isopropyl-β-thiogalactopyranoside
K	lysine
LB	Luria-Bertani medium
λ	wavelength
LCAA-CPG	long chain alkylamine controlled pore glass
Lys	lysine
M	molar
M. jannaschii	*Methanococcus jannaschii*

m/z	mass to charge ratio
MALDI TOF	Matrix Assisted Laser Desorption/Ionization Time of Flight
max	maximum
MD	molecular dynamics
Me	methyl
MeO	methoxy
mg	milligram
min	minute(s)
MIOE	methyleneiminooxy
µL	microliter(s)
mL	milliliter(s)
µM	micromolar
mM	millimolar
MMT	monomethoxytrityl
mod.	modification
MOE	2'-O-methoxyethyl
mol	mole
mRNA	messenger RNA
MS	mass spectrometry
MW	molecular weight
n-	normal
N	north (C3'-*endo*)
NBA	nitrobenzyl alcohol
nm	nanometer
nM	nanomolar
NMR	nuclear magnetic resonance
Non	nonyl
nt	nucleotide
ODN	oligodeoxynucleotide
ODU	optical density units
PAGE	polyacrylamide gel electrophoresis

PCR	polymerase chain reaction
PEG	polyethylene glycol
Pen	pentyl
Phe	phenylalanine
PNK	polynucleotide kinase
PO	phosphodiester
ppm	parts per million
Pr	propyl
pre-mRNA	precursor mRNA
PS	phosphorothioate
Pu	purine
Py	pyrimidine
®	registered trademark
r.t.	room temperature
R_f	retention factor (*i.e.* TLC analysis)
RISC	RNAi induced silencing complex
RNA	ribonucleic acid
RNAi	RNA interference
RNase	ribonuclease
rRNA	ribosomal RNA
RT	reverse transcriptase
S	south (C2'-*endo*)
S. cerevisiae	*Saccharomyces cerevisiae*
sec	second(s)
SEC	size exclusion chromatography
ss	single stranded
SVPDE	snake venom phosphodiesterase
t-	tertiary
Taq	*Thermus aquaticus*
TBAF	tetra-*n*-butylammonium fluoride
TBDMS	*tert*-butyldimethylsilyl

TCA	trichloroacetic acid
TEA	triethylamine
TEMED	*N,N,N',N'*-tetramethylethylenediamine
TeOE	2'-O-methyl[tetra(oxyethyl)]
THF	tetrahydrofuran
Thy	thymine
TLC	thin layer chromatography
T_M	melting temperature
TMS-Cl	trimethylchlorosilane
TOE	2'-O-methyl[tri(oxyethyl)]
TREAT-HF	triethylamine trihydrofluoride
Tris	2-amino-2-(hydroxymethyl)-1,3-propanediol
tRNA	transfer RNA
Trp	tryptophan
Tyr	tyrosine
™	trademark
U	units (of enzyme)
U	uridine
Ura	uracil
UV	ultraviolet
UV-vis	ultraviolet-visible
v/v	volume per volume
W	tryptophan
w/v	weight per volume
XC	xylene cyanol
*Xho*I	*Xanthomonas holcicola* restriction enzyme
Y	tyrosine

LIST OF FIGURES

CHAPTER 1.

CHAPTER 2.

CHAPTER 3.

CHAPTER 4.

LIST OF TABLES

CHAPTER 1.

CHAPTER 2.

CHAPTER 3.

CHAPTER 4.

CHAPTER 6.

CHAPTER 1 – IMPORTANCE OF SUGAR-MODIFIED NUCLEIC ACIDS: SHAPING BIOLOGY BY STRUCTURE

1.1. HISTORICAL AND TECHNICAL CONTRIBUTIONS TO ANTISENSE TECHNOLOGY

The discovery of the double helix structure of deoxyribonucleic acid (DNA) in 1953 forever changed the face of modern biological science. Its famous description by James Watson and Francis Crick, an interwoven, two-stranded helical molecule held together by hydrogen bonding between the nitrogenous bases, with the two strands running in opposite (antiparallel) orientations, has since become the most celebrated finding of our time.[1,2] The base pairing mystery had partly been solved by the biochemist Erwin Chargaff some years earlier, who recognized that equal proportions of complementary bases (adenine:thymine and cytosine:guanine) are present in all DNA molecules regardless of biological origin.[3] Crystallographic evidence of the helical structure, independently captured by chemist Rosalind Franklin, provided the last crucial missing link, prompting revisions of earlier models proposed by Watson, Crick and Linus Pauling – including one with bases at the outside – to that which is widely known today (**Figure 1.1**).[4-6] Thus was born the concept of a molecule capable of its own self-replication and propagation from a simple four-base alphabet, through the unzipping of the duplex and replacement of missing bases along the unwound strands in an elegant, predictable fashion.

The next half-century would soon confirm these monumental revelations and add a few of its own.[7,8] Pioneering theories, including that of genetic inheritance set forth by Gregor Mendel in the 19th century, and of evolution by Charles Darwin, were strongly revived with the discovery of cellular processes capable of transmitting the genetic message carried within DNA to a more practical, usable form. The coding instructions, relayed through an intermediary ribonucleic acid 'messenger' (mRNA) via a process of *transcription*, established the next vital link between 'latent' DNA sequence information and active cellular synthesis of functional proteins (see **Figure 1.2** panel **A**). Decoding, or *translation,* of the message would ultimately require the help of other nucleic acid participants assimilated within a multi-protein complex termed the ribosome. Included among these are the ribosomal (rRNA) and transfer RNAs (tRNA), the latter so named

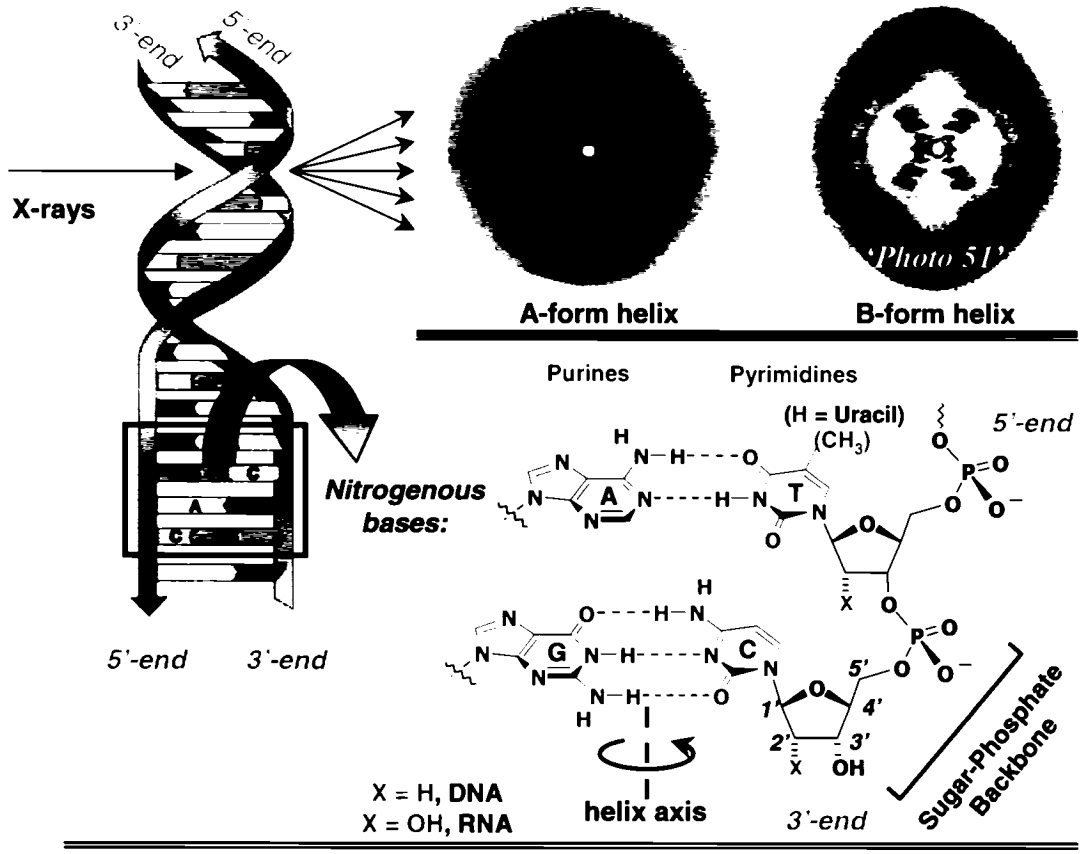

	A-form (RNA:RNA)	B-form (DNA:DNA)
Helical Sense	Right	Right
Residues per helical turn	11	10.4
Rise per base pair (bp)	2.56 Å	3.3 - 3.4 Å
Helix Diameter	25.5 Å	23.7 Å
Major Groove Dimensions	Narrow & deep	Wide & deep
Minor Groove Dimensions	Broad & shallow	Narrow & deep
Sugar Conformation	C3'-*endo* ('North')	C2'-*endo* ('South')
Base Tilt	20°	-6°

Figure 1.1: Watson and Crick's description of DNA as an antiparallel double helix, inspired by X-ray crystallographic evidence for the A- and B-forms of suspended DNA fibers. First photographed by Franklin, the hydrated ("B") form of DNA is that found within a living cell, while RNA duplexes characteristically adopt the A-form. Hydrogen bonding between bases via Watson-Crick complementarity (A:T and G:C) and average parameters of the A- and B-form helical conformations are also given below. Photographs courtesy of the Cold Spring Harbor Archives. Nucleic acid structural parameters adapted from Blackburn, G.M. and Gait, M.J. In *Nucleic Acids in Chemistry and Biology*; Blackburn, G.M. and Gait, M.J., Eds; Oxford University Press: New York.

for their ability to decipher the mRNA sequence and supply the necessary amino acids to elongate the growing polypeptide chain.

Yet despite such drastically different functional roles, both DNA and RNA are exquisitely similar in chemical composition and primary structure. Each is composed of a linear polymeric array of D-2-deoxyribose or D-ribose sugars respectively, strung together by interconnecting phosphodiester linkages (**Figure 1.1**). Upon carbon 1' of the sugar moieties sits any one of four nitrogenous bases, or heterocycles, with uracil (U) replacing thymine (T) in RNA. Further dissecting the polymeric composition of each biomolecule reveals a repeating combination of furanose (sugar), base and phosphate that collectively define the monomeric 'nucleotide' subunits. While the heterocycles engage in reciprocal base interactions, the scaffolding sugar-phosphate backbone primarily fulfills a structural role. Accordingly, both deoxy- and ribonucleic acids follow identical base pairing guidelines upon recognition of complementary polynucleotide strands, yet intrinsic chemical differences at the sugar 2'-position of each polymer profoundly influence their respective associations. Whereas DNA:DNA duplexes typically adopt a 'B-form' helicity, as identified by an elongated intertwined structure having a smaller diameter and fewer base pairs within each helical turn, RNA:RNA duplexes assume the 'A-form', characterized by a tightly wound right-handed helix with an expanded diameter and greater tilting of base pairs lining the internal hydrophobic cavity (see description in **Figure 1.1**). As will be revealed in later sections, the chemical nature underlying these vast structural differences owes to the presence and conformational influence of the hydroxyl group at the 2'-carbon sugar in RNA, which accounts for many of its global variations from those of the native B-form DNA duplexes.[9,10]

1.1.1. The Molecular Biology Revolution & Birth of 'Genetic Medicines'

Spurred forward by these groundbreaking insights, the last half of the 20th century has seen an emphatic shift of the scientific community into a world of genetics, giving us the fully sequenced human genome, stem-cell research, and endless promises of rationally designed gene therapy. By coupling chemical and molecular biology techniques, newer perspectives in molecular medicine have also generated elegant tools that have revolutionized the way in which gene-based intervention is achieved. One important

approach involves the antisense strategy, which fundamentally seeks to selectively inhibit protein biosynthesis altogether by tying up the genetic message on the corresponding 'sense' RNA messenger template using a synthetic 'anti'-sense oligonucleotide and established Watson-Crick base pairing rules (**Figure 1.2**).[11-13]

As such, the antisense era has been marked by exciting improvements spanning over 3 decades of active research. Its inception dates back to the early 1960's when Nirenberg *et al.* first observed that not only could nucleic acid secondary structure influence the efficiency with which an mRNA template is read and translated, but whose landmark

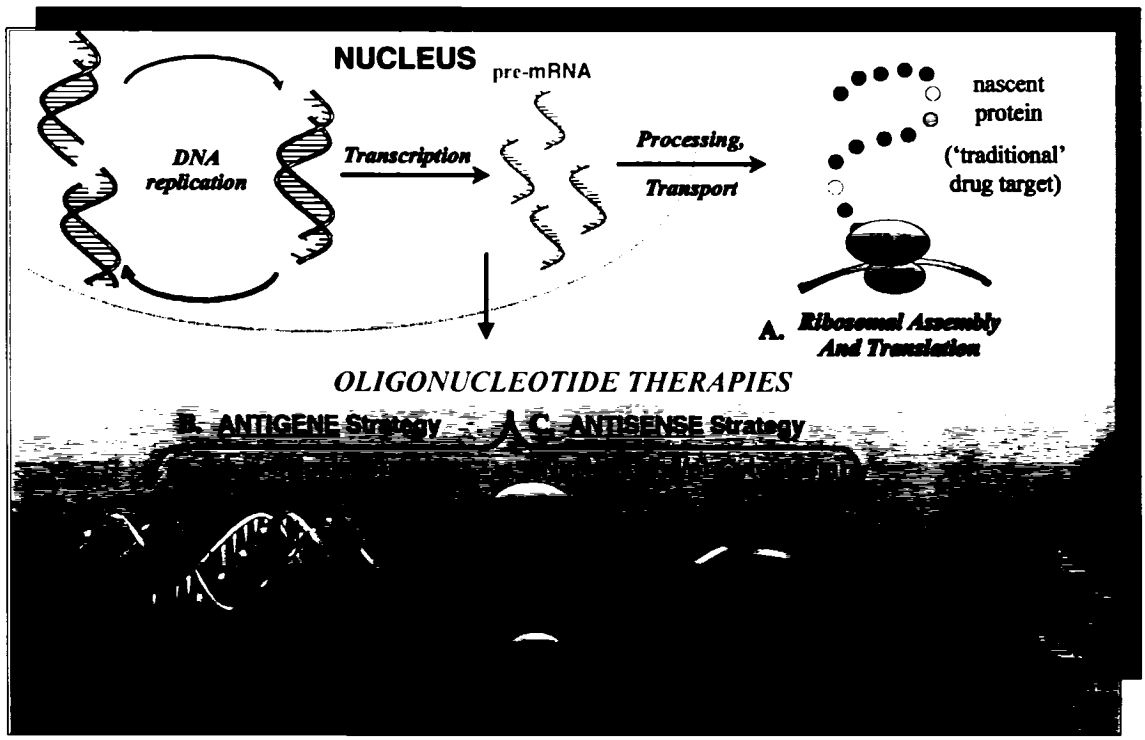

Figure 1.2: **A.** Intracellular fate of an mRNA transcript (red) under normal cellular conditions. While traditional 'small molecule' approaches attempt to sequester an aberrant protein to control a particular disease state, oligonucleotide strategies seek to suppress its biosynthesis altogether. **B.** In the antigene strategy, a synthetic oligonucleotide recognizes a specific genomic region in the DNA duplex and hybridizes at that site to form a triple helix, thereby blocking further activity by preventing transcription. **C.** The antisense approach aims to target the nascently transcribed messenger instead, which is relatively more abundant and accessible within the cell. In the above example, mRNA inactivation occurs by steric block of the message via duplex formation, but other inhibitory mechanisms may further be invoked. These and associated biological consequences of the antisense pathway are discussed in the text.

studies first captured the essence of selective gene silencing by demonstrating that hybridization of polyribouridylic acid with an oligoadenylate complement could specifically prevent the translation of polyphenylalanine from the ribouridylic acid template.[14] This was also the first demonstration of oligonucleotide single-strandedness as a necessary requisite for protein biosynthesis.

Shortly thereafter came the first suggestion of nucleic acid therapy as a potential combatant against naturally occurring genetic anomalies,[15] followed by the first successful demonstration of antisense-induced suppression of viral activity in cell culture.[16]

Certainly, many plausible gene-based applications of a therapeutic focus may now be envisioned which can *suppress* aberrant genetic activity (**Figure 1.2**), or *restore* proper splice site selection in otherwise erroneously spliced nuclear precursor mRNA (pre-mRNA). Indeed, as of 1999, a total of 11 antisense oligonucleotides (AONs) successfully entered clinical trials for the prospective treatment of a variety of hereditary and viral diseases. Since that time, a large number of promising antisense biotherapeutics have entered the clinical stage, only to encounter unexpected physiological complications later on.[17] Hence, the need for optimizing the technology to improve the pharmacological properties of potential candidates while minimizing their toxicity is still met with an explosive level of activity in the field. Although a number of antisense compounds are currently in late stage clinical trials, the only one to be approved thus far, Vitravene,™ belongs to the phosphorothioate class of compounds wherein the internucleotide phosphodiester bond is replaced by an enzymatically more stable phosphorothioate (PS) linkage[18] (**Figure 1.3**). Unfortunately, first generation AONs that contain this structural motif are characterized by relatively poor binding affinities toward complementary RNA targets as compared to unmodified DNA, which is thought to arise from the diastereomeric nature of the PS bridges.[19] This is potentially problematic as the activity of one or more distomers (*i.e.* a biologically active stereoisomer that may induce unintended effects) may account for the rather high toxicity profiles of PS-AONs.[20] The phosphorothioates also participate in sequence-specific and non-sequence specific interactions owing to a strong propensity for the sulfur-containing linkage to engage in

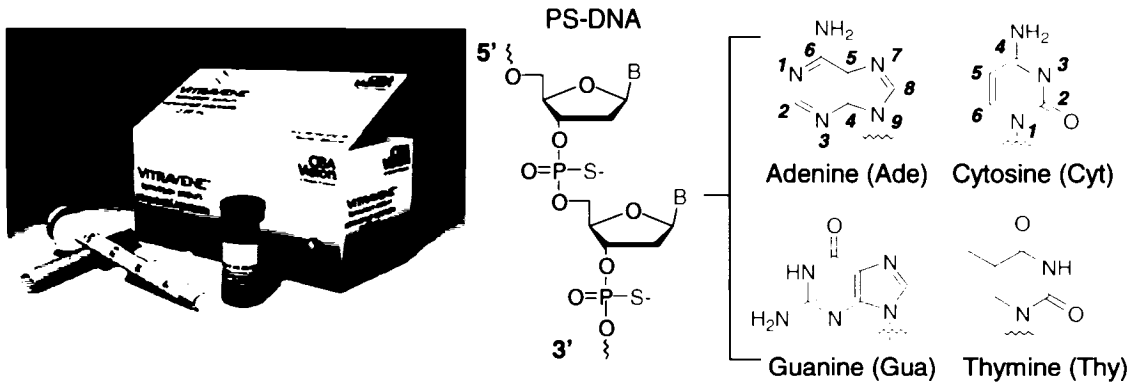

Figure 1.3: Vitravene™, a formulation comprising a phosphorothioate DNA analogue as the active medicinal ingredient, was first approved for clinical use in 1998 by the Food & Drug Administration. Administered by intravitreal injection in the treatment of CMV-induced retinitis, the chemical structure of PS-DNA differs only by sulfur substitution for one of the nonbridging phosphate oxygens; constituent nucleobases and numbering are identical to those of the native oligodeoxyribonucleotides.

binding towards serum and cellular proteins.[21,22] Certainly, this has spawned the development of newer AON chemistries with potentially greater levels of therapeutic safety.[23] Nevertheless, because the development of antisense is hypothetically much quicker than that of the more conventional small molecule drugs, a strong potential exists for creating a broad-reaching therapeutic of very specific action. This translates to a mode of pharmaceutical intervention that is both highly general yet specific at the same time, in that a given antisense design can be used to target many disease genes by simply altering the base sequence of the AON candidate.[13]

Dissecting the various molecular features that enable strong molecular recognition upon introduction of new modifications in a synthetic antisense has been a long standing goal. Pivotal to the imminent success of the technology has been the enormous impact and progress that modified oligonucleotides have had from a practical perspective. The current variety of analogues is overwhelming, with many precedents describing modifications of the carbohydrate, backbone linkage and nucleobase moieties. We have primarily focused on modification of the furanose portion of these molecules, because these seem to govern many nucleic acid recognition events with proteins usually without severely compromising the hybridization attributes of the nucleic acid. For this reason and for the sake of simplicity, we have chosen to gear this discussion upon some of the

more salient features of carbohydrate modified AONs and their use in an antisense strategy of gene interference. Alternatively, the implementation of other types of modifications, specifically those relating to nucleobase and phosphate surrogates have been the focus of several excellent reviews and are not discussed further here but should be consulted by the reader if desired.[24-28]

1.2. Minimum Requirements of Modified Oligonucleotides

Suitability toward *in vivo* applications[18,23] is usually gaged by the ability of an AON candidate to possess a multi-fold mechanism of action that involves: (i) sufficient metabolic stability under physiological conditions; (ii) cell penetration and liberation of the encapsulated AON from endocytic vesicles into the cytoplasmic space;[29] (iii) strong and selective discriminatory behaviour for full complements in the presence of different sequences of partial complementarity; (iv) prevention of ribosomal-assisted translation of an RNA transcript by precluding the association of RNA processing enzymes involved with protein synthesis; and (v) activating ribonuclease H (RNase H) to degrade the RNA transcript of the resultant hybrid (*vide infra*).[30]

As a general rule, the length of the construct is usually designed to range from 15 to 25 nucleotide units in order to ensure that optimal identification and binding takes place with a unique sequence[12,31] in the mammalian genome and not with similar genetically redundant elements. Statistical analyses specify a 12 base sequence in *E. coli* or 11-15 base paired human sequence as the theoretical lower limits for sufficient recognition of a single genomic region. In practice, however, a slightly longer AON is commonly used to compensate for low melting transitions that may become manifest at physiological temperature. Furthermore, excessively long AON sequences are not always advantageous either, as irrelevant and partial hybridization to non-targeted sequences may occur and subsequently disrupt some other vital cellular function.[32]

1.3. Amplifying AON Therapeutic Potency: The Catalysis Criterion

An attractive biochemical pathway that could aid in effective suppression of gene activity appears to considerably depend on both the endo- and 3'→5' exonuclease activities of

RNase H, a constitutive and ubiquitous enzyme that is present in most viral, bacterial and eukaryotic organisms.[33] Its widespread existence implies an important role in many biological processes, including DNA replication (to remove RNA primers generated during lagging strand synthesis),[34] transcription and viral reverse transcription events.[35,36] More specifically, the RNase H family comprises a class of enzymes that have the unifying property of recognizing and cleaving the RNA constituent of various RNA:DNA heteroduplexes having non-canonical topologies[37,38] that are intermediate between the pure A- or B-form helicities adopted by dsRNA and dsDNA, respectively. This activity cleaves the RNA strand to liberate 5'-phosphate and 3'-OH nucleotide fragments,[39] and essentially inactivates the mRNA toward further cellular anabolic processes. Ideally then, if an AON:RNA hybrid duplex possesses the correct conformational features for RNase H recognition, the potential exists for creating a therapeutic with sufficient potency at sub-stoichiometric concentrations relative to the cellular RNA targets, as enzyme-activating AONs become endowed with the ability to inhibit multiple copies of the target RNA (**Figure 1.4**).

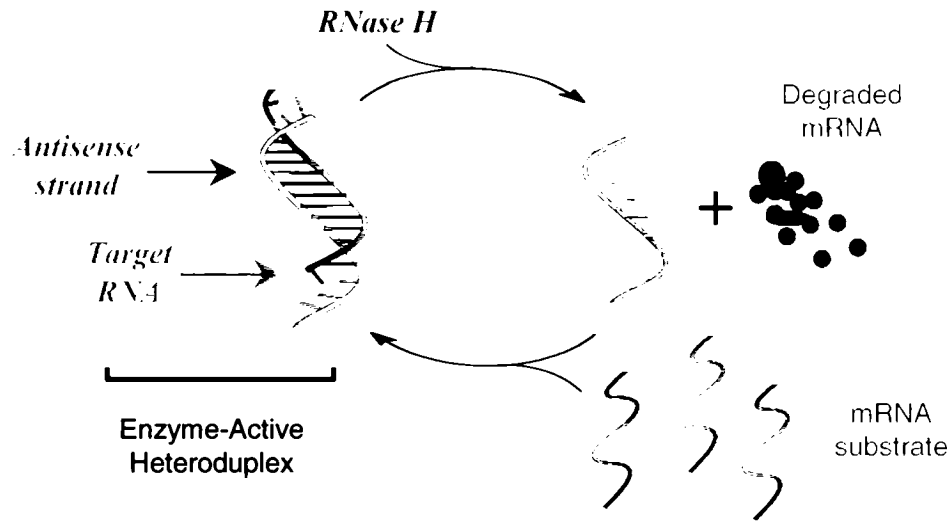

Figure 1.4: Ribonuclease H-mediated RNA destruction. Most AONs work by inhibiting assembly of the ribosome along the mRNA, yet this requires high doses for optimal gene suppression. Others however, initiate rapid and permanent destruction of the antisense-bound RNA through the help of a cellular enzyme, ribonuclease H, which selectively degrades the RNA strand of suitable substrates. This event frees the intact 'enzyme-active' antisense for multiple rounds of inhibition.

It is noteworthy, however, that the stringency with which RNase H activity is recruited to a native target is rather low, and as little as a 4 to 5-base complementary region of enzyme-activating deoxynucleotide stretches bound to the target, regardless of nucleotide sequence[37,40] may be sufficient to induce degradation of the RNA. On the other hand, chemical changes of the sugar constituents, or alterations in the orientation of the sugar to the base all can dramatically diminish RNase H activation.[41]

1.4. Prospects of RNase H Therapy

Unfortunately, most backbone and sugar modifications do not support RNase H activity yet confer many pharmacological advantages to oligonucleotides (*e.g.* drug stability). Thus, an important consideration regarding RNase H recognition involves a survey of the steric composition and spatial dimensions of the minor groove, which is known to be the primary locus of action of the enzyme.[42] Duplex RNA has a minor groove width of 10 – 11 Å and is not degraded at all.[9,43-45] Moreover, the canonical A-form adopted by pure RNA duplexes and similar AON progeny is believed to interact with and inhibit the enzyme.[46] Alternatively, the native DNA:RNA substrate shows a slight contraction of the minor groove (*ca.* 9 Å), the dimensions of which lie intermediate between canonical A- and B-form duplexes (**Figure 1.5**).[47,48]

DNA:RNA hybrids are also the only architectural variants of the three classes which are processed by the enzyme, thereby setting a standard by which subsequent AON-derived hybrids with RNA are evaluated. The associated stimulatory properties have, however, proven difficult to reproduce upon chemical modification of the native DNA strand. Among the currently expanding list of modified AONs that retain RNase H-mediated cleavage of the mRNA message are the phosphorothioates, phosphorodithioates,[49,50] boranophosphates,[51,52] arabino- (ANA) and 2'-deoxy-2'-fluoro-β-D-arabinonucleic acids (2'F-ANA),[53,54] cyclohexene nucleic acids (CeNA)[55] and more recently, α-L-*ribo*-configured locked nucleic acids (α-L-LNA).[56] Interestingly, the extent of cleavage by each of these classes varies significantly but all appear to share the same minor groove width dimensions, which are believed to be key to maintaining RNase H activity.

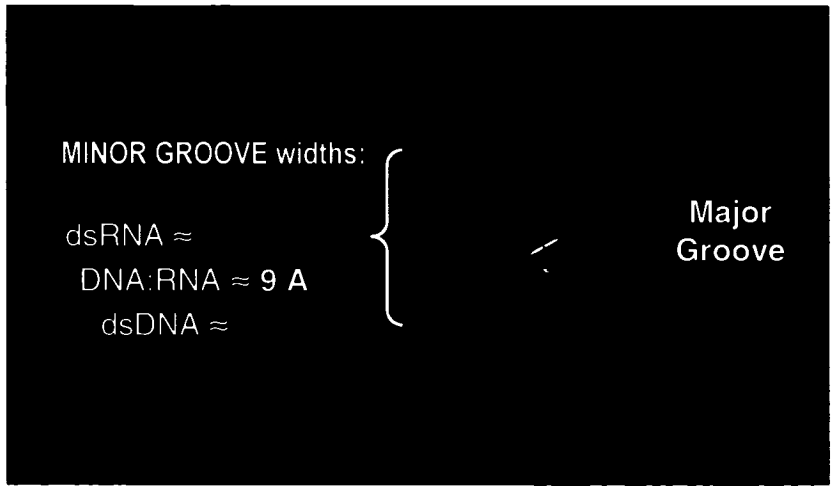

Figure 1.5: Superimposition of the two canonical duplex morphologies adopted by dsRNA and DNA helices, showing expansion and compression of the minor groove widths, respectively. DNA:RNA heteroduplexes adopt an intermediate architecture, the minor groove dimensions of which serve as key recognition elements for RNase H.

1.5. RNase H-Independent Mechanisms Illustrate the Importance of a Catalytic Mode of Gene Suppression

There are, however, other mechanisms by which the antisense approach can be employed to modulate gene expression without relying on RNase H activity but which may also culminate in the cleavage and degradation of a target RNA by antisense. Many endogenous enzymes such as RNase III,[57-60] RNase P,[61,62] and RNase L[63,64] may be utilized towards this feat. Although mammalian RNase L typically targets dsRNA indiscriminately in response to viral induced 2',5'-oligoadenylate synthesis, its activity may be directed to specific targets if the oligoadenylate portion is tethered to an antisense strand.[65]

Alternatively, the antisense construct can be engineered to contain inherent cleaving activity (*e.g.* ribozymes, DNAzymes), which effectively relinquishes any dependence on enzymatic assistance.[66] Scission of the RNA can also be accomplished by an oligonucleotide-linked cleaving agent which selectively accesses and severs the target strand upon hybridization. Yet conjugation of the AON to an alkylating or photoactivating species is sometimes associated with potentially hazardous biological effects, as random alkylation *in vivo* has often been noted.[12,41]

Interestingly, each approach stresses the importance of designing a catalytic AON species in an attempt to provide an optimal inhibitory effect on protein biosynthesis. Additionally, since the newer oligonucleotide chemistries presently being developed mostly do not rely on RNase H-dependent cleaving mechanisms, the above examples suggest a place for the future application of non-RNase H active AONs that may therefore exhibit greater inhibitory potency by a different biochemical pathway of target RNA destruction.

1.5.1. Sterically Acting AONs Target Translation or Direct Spliceosomal Rerouting in pre-mRNA

Alternatively, antisense oligonucleotides that do not direct sense strand hydrolysis, yet exhibit high binding avidities toward complementary RNA may also sufficiently downregulate the expression of a targeted transcript directly. For example, an AON that selectively interferes with the formation of the translation initiation complex on the transcript may ultimately interfere with other metabolic processes by exerting its effects through steric block of ribosomal assembly factors rather than RNase H-promoted cleavage of the mRNA (**Figure 1.2**, panel **C**). However, the mode of action of an enzyme-inactive AON largely depends upon its mRNA binding site location and as such, is generally limited to genomic regions outside of the coding region of the transcript.[11,41] Importantly, it has been noted that steric block of ribosomal assembly may only contribute minimally to a potent antisense effect.[67,68]

In contrast, a prime application of modified oligomers that do not activate RNase H lies in their ability to mask the selection of aberrant splice sites in incorrectly spliced mRNA, thereby redirecting the splicing machinery to the correct splice site and restoring proper gene function (**Figure 1.6**). Here, it is crucial that RNase H not be activated so that the target pre-mRNA is preserved yet the message that it carries can now selectively be altered.[69]

Another interesting application relates to the use of a fully modified 2'-O-methoxyethyl (MOE) oligonucleotide capable of prolonging the expression of E-selectin, a transiently produced cellular adhesion molecule, by interfering with and redirecting the

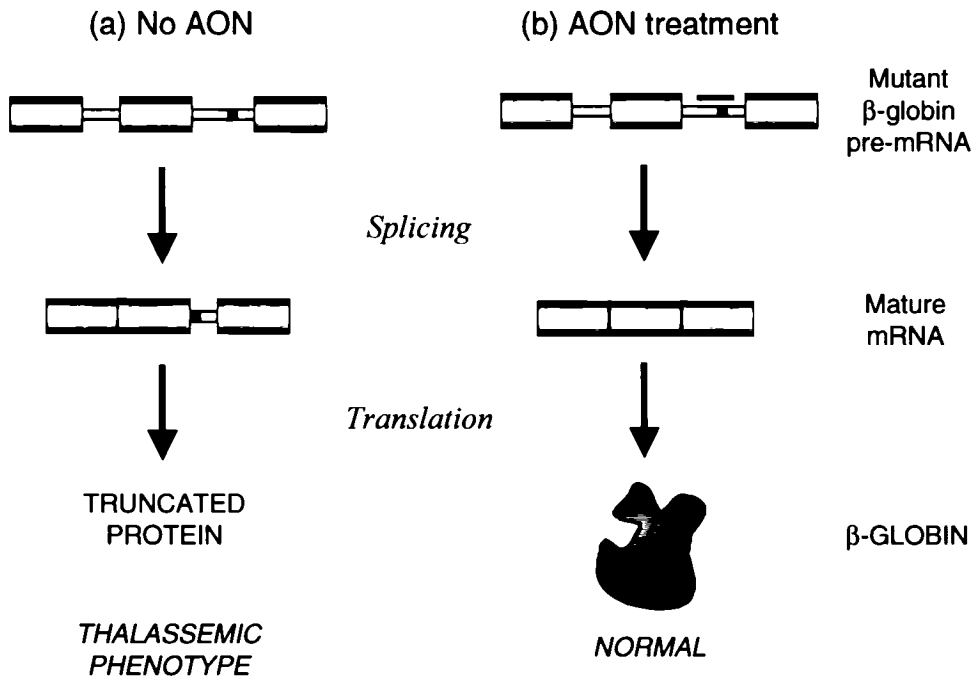

Figure 1.6: **A.** Point mutations in an intronic segment of β-globin pre-mRNA activate a cryptic 3'-splice site (▪) upstream of the normal 3'-intron-exon junction. Although translation still occurs in this example, the spliced transcript now encodes a premature UGA stop codon in the intron remnant, and ultimately produces a defective protein. **B.** Hybridization of an AON complementary to the intron region spanning the damaged site masks its recognition by the splicing machinery and restores proper splice site selection.[69]

polyadenylation event to an alternate cryptic polyA site on the pre-mRNA transcript, resulting in prolonged stability for the transcript and a subsequent increase in the abundance of the message.[70] Such a unique mode of genetic intervention may find significant therapeutic utility toward diseases in which a particular protein is underexpressed due to the inactivation of one allele, and is likely to be pursued in the future.

In summary, a mode of action that effects degradation of the target transcript may simply be more potent than one which merely interferes with other metabolic processes; however, the complementary nature of these mechanisms from a medicinal viewpoint suggests many diverse roles for enzyme-active and inactive AONs as effective mediators of gene expression.

1.6. DUPLEX STABILITY IS DICTATED BY THE NUCLEOTIDE SUGAR

Clearly, the most important determinants of antisense activity - high affinity AON:target binding and possible enzyme recruitment – depend on AON single strand dynamics and consequent hybrid helical architecture.[37,38,71] Duplex stability owes much to sugar conformation in this respect as many of the global structural morphologies that are seen in the generic A and B helical families arise from the individual twists – or puckering profiles – of the sugar residues within each participating strand of the hybrid.[9]

This occurs because the furanose ring is not planar and – depending on how the atoms in the ring are displaced from the plane[72] – the residues can act cooperatively to influence the macromolecular architecture of both the single stranded and hybrid states.

The sugar pseudorotamers adopt one of 3 predominating forms in solution that act interdependently to sculpt the overall helical curvature. Thus, the B family is characterized by C2'-*endo* (or Southern) conformations whereas A-form duplexes contain C3'-*endo* disposed sugars. However, the sugars can be quite heteromorphic in solution and dynamically interconvert through the O4'-*endo* antipode which itself gives rise to a helicity that is intermediate between the two classic forms (**Figure 1.7**, panel **A**).[9]

As such, duplex helicity is tuned by the geometry and dynamic transitions of the furanoses, which together specify a pseudoaxial (A-form; Northern) or equatorial (B-form; Southern) inclination of the adjoining heterocycles and therefore the corresponding intrahelical stacking efficiency. This is crudely evident in the observation that A-form duplexes usually constitute greater thermally stable structures than B-form helices because the bases are placed closer together and exhibit more proficient stacking. In this way, changes in the chemical nature of the sugar ring impact dramatically on the thermodynamic stability of the duplex.[73,74]

In turn, the ring geometry is stereochemically controlled to preferentially assume a C2'-*endo* or C3'-*endo* pucker as harmonized by the competing forces of the anomeric and the O4'-C1'-C2'-O2' (endocycle) and O2'-C2'-C1'-N (base) *gauche* effects. Consequently, the adoption of a pseudoaxial nucleobase disposition in RNA strands maximally invokes anomeric stabilization as well as O2'-C2'-C1'-O4' *gauche* effects while disfavouring the weaker O2'-C2'-C1'-N interaction with the heterocycle.[73-76]

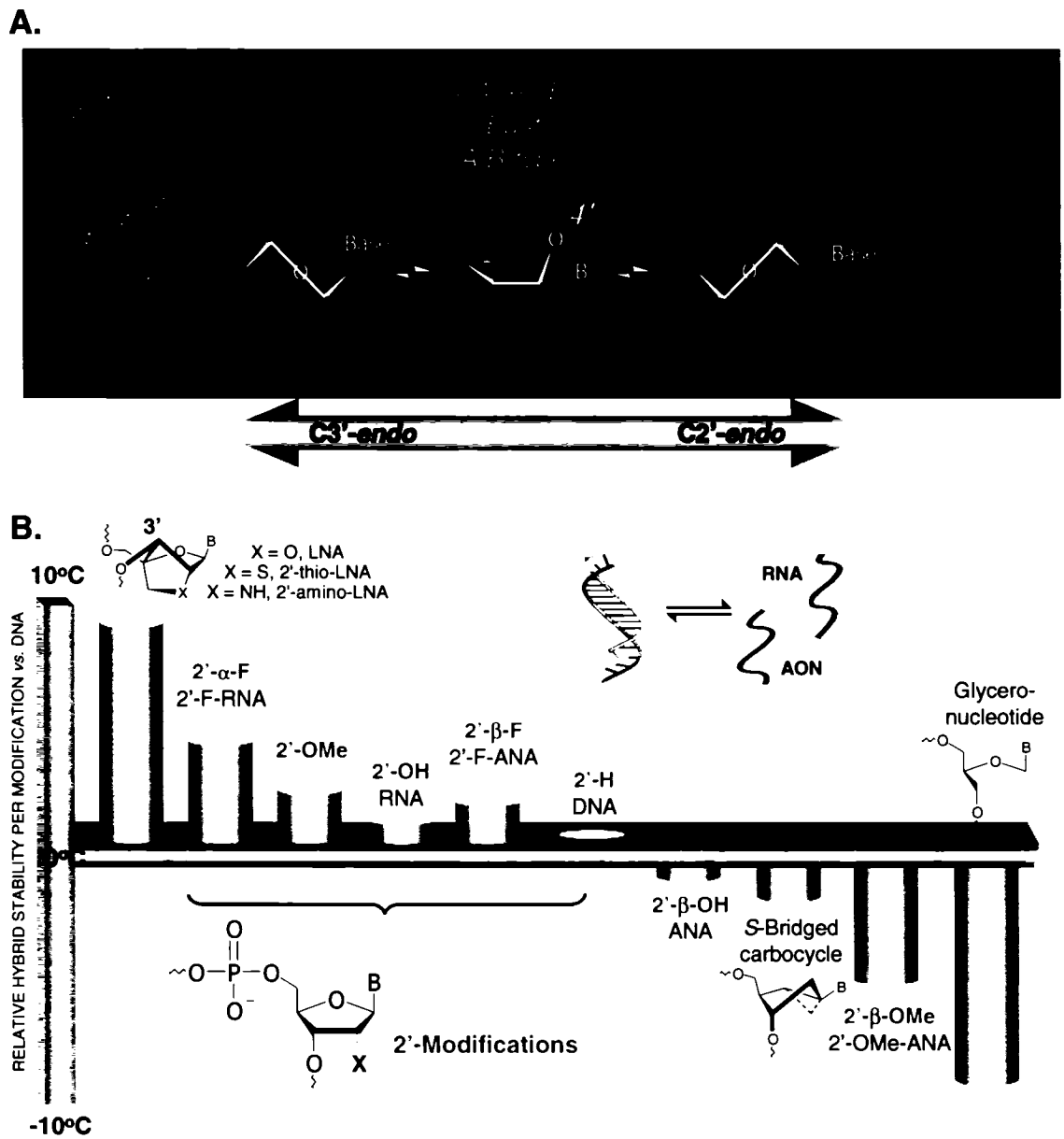

Figure 1.7: A. Interconversion pathway of the furanose through the 3 lowest energy conformations. **B.** Representative examples of each type of sugar-modified substituent as well as general sugar puckering preference and associated thermal reductions per modification relative to native DNA:RNA heteroduplexes are indicated; note, however, that the preferred disposition of the residue may be quite variable as, for *e.g.*, deoxynucleotides can assume all 3 forms. The thermal penalty inherent upon glyceronucleotide incorporation within the parent AON is also shown to illustrate the importance of sugar unit preorganization on duplex stability. See text for further details.

In principle, any position that is chemically altered within the sugar ring would be expected to redefine energetic contributions of a stereoelectronic nature and hence the expected conformations of the furanose ring. Therefore, most sugar modifications primarily exploit the *gauche* effect to influence pseudosugar ring equilibria and global strand dynamics.

1.7. Modulation of Biopolymer Properties by the Sugar 2'-Substituents

Accordingly, the orientation and identity of the C2'-substituent has a profound influence on the macromolecular conformation and resultant hybrid stability (**Figure 1.7**, panel **B**), with the degree of A-form character in the AON strand approximating the B-form with diminishing electronegative character of the 2'-position. Thus, a strongly electronegative 2'-substituent can lock the sugar conformation into a single predominant form and confer added binding capacity to the polymer while enhancing nucleolytic stability.

Additionally, the 2'-position of a nucleoside appears to be one of the easiest locations to introduce various substituents as this site has been demonstrated to be more tolerant towards significant deviations in size and structure of a particular modification.[26,77] This is because the 2'-position is located close to the exterior of the helix, and as such, the probability with which a duly appended substituent will interfere with subsequent intermolecular interactions with other nucleic acids is rather small. This location also suggests that there should be little change in hydration pattern around the 2'-group in going from a single stranded to a double stranded form and therefore little loss in entropy upon duplexation that sometimes occurs as when the modified substituent is placed elsewhere on the residue.[78] Thus, only minor changes in sugar solvation accessibility accompany duplexation from the single-stranded state and are therefore insignificant destabilizing factors.

However, because the 2'-appendages point toward the face of the helix minor groove, they invariably disrupt RNase H recognition of potential substrates. Nevertheless, placement of an electronegative substituent at this position typically confers an RNA-like sugar puckering of the antisense oligonucleotide (*i.e.* C3'-*endo*). This results in a preorganized structure that favours an RNA-like conformation and should greatly improve the binding affinity to the target RNA.

1.7.1. RNase H-Inactive 2'O-Modifications that Elevate Duplex Stability

Hence, the simplest strategies thus far adopted have centered on the design of 2'O-, 2'C- and heteroatom substituents of the more conventional ribosyl-based analogues. Without exception, uniformly 2'-alkoxy modified AONs exert their antisense effects via RNase H-independent mechanisms. Increasing the length of the alkoxy chain (**Table 1.1**, entries **1-3**) correlates negatively with heteroduplex formation as the larger alkyl chains are highly prone to unfavourable contacts with other parts of the duplex or may disrupt the water structure in the minor groove.[26]

Alternatively, a major consequence of the presence of an alkyl group at this position is that the resulting polymer becomes more resistant to cleavage by alkali and by a wide range of natural RNA and DNA specific nucleases. This is mainly due to the effect that the alkyl group has on reducing the nucleophilic character of the 2'-oxygen and on imposing a physical barrier to hydrolysis by 2'-O participation. Indeed, the larger moieties of the alkyl series serve to enhance nuclease resilience in the analogue by creating a sterically compromised environment around the phosphate group that thereby prohibits its accessibility to external hydrolytic factors.[79] For instance, Monia and coworkers found significant *in vitro* exonucleolytic resistance of a 2'-O-pentoxy PO/PS chimera that dropped in the series from pentoxy > propoxy > methoxy > fluoro ≈ deoxy (**Table 1.1**).[79]

The 2'-OMe analogues owe their thermal stabilities to a shift in the S ⇌ N equilibrium but also to a purported 'hydrophobic effect' in which the methyl groups are suggested to force the nucleobase in a pseudoaxial position in order to avoid steric clashing with the vicinal phosphate and as a consequence reflect increased base stacking.[80] Furthermore, the 2'-OMe groups adopt exclusive *gauche* orientations that maximize the interatomic distances with adjacent 3'-phosphates, thereby resulting in the disposition of the Me groups in the minor groove,[37] which in turn probably adversely affects optimal recognition of the duplex by RNase H.

Although unable to induce enzymatic cleavage, fully modified 2'OMe-RNA:RNA heteroduplexes can competitively interact with the natural substrate for the enzyme's active site and slow the rate of hydrolytic cleavage. In this respect, the rate of hydrolytic

Table 1.1: Some representative biological properties of 2'-modified oligonucleotides.

Entry	AON Designation[a]	2'-X unit	ΔT_M / mod. (°C)[b]	Rel. Nuclease Resistance[c]	Reference
1	OMe	—O-Me	0.8 – 1.4	7	81,82
2	OPr	—O⁄⁄	0.7	10	26,82
3	OPen	—O⁄⁄⁄⁄	-0.1	>10	26,82
4	MOE	—O⁄⁄O-Me	0.9 – 1.6	24	81,83
5	TOE	—[O⁄⁄]$_3$O-Me	0.8 – 2.1	>48	81
6	TeOE	—[O⁄⁄]$_4$O-Me	0.4	n.d.[d]	26
7	Fluoroethoxy	—O⁄⁄F	1.3	n.d.[d]	26
8	EOM	—O⁄O⁄⁄	-1.2	16	26,81
9	AE	—O⁄⁄$\overset{+}{N}H_3$	1.0	n.d.[d]	84
10	AP	—O⁄⁄⁄$\overset{+}{N}H_3$	-1.8 – 0.3	360	85
11	DMAP	—O⁄⁄⁄$\overset{+}{N}HMe_2$	-0.2 – 1.2	>360	86
12	AOE	—O⁄⁄O⁄NH_2	1.2	*ca.* 24[e]	87,88
13	DMAOE	—O⁄⁄O⁄NMe_2	1.1 – 1.4	>24[e]	88
14	DEAOE	—O⁄⁄O⁄NEt_2	1.0 – 1.5	>>24[e]	88
15	MIOE	—O⁄⁄O⁄$N{=}CH_2$	1.2	*ca.* 24[e]	87

[a]See list of abbreviations for an explanation of terms. [b]The reported change in thermal stability (*i.e.* ΔT_M) corresponds to that per modified unit relative to its deoxynucleotide counterpart when bound to an RNA complement. [c]Oligonucleotide half-lives are relative to those obtained for the unmodified deoxynucleotides using snake venom phosphodiesterase (SVPDE), a 3'-exonuclease. [d]Not determined. [e]Values for AOE and corresponding derivatives have been estimated from comparison to the MOE compounds.[83,86,88,89]

cleavage in thioate-DNA:RNA complexes drops 3-fold upon chimeric derivatization of the thioate strand with 2'-OMe termini.[46] The authors suggest that this rate reduction is actually the result of a decreased size of the deoxynucleotide gap, which results in a smaller proportion of binding events at the correct position for enzymatic hydrolysis. Indeed, others have observed similar hydrolytic rates with respect to the efficiency of the bacterial enzyme towards the chimeric substrate.[37] It is, however, noteworthy that a secondary – though minimal – contribution to the reduced efficiency may be imagined to originate from a short-lived occupancy of the 2'-OMe portion of the hybrid with the enzyme active center, which may momentarily obstruct the hydrolysis.

1.7.2. 2'-Modifications that Reduce Duplex Stability and do not Activate RNase H

In contrast to the increase in duplex stability observed with electronegative substituents at the 2'-position, 2'-sulfur or 2'-carbon linked modifications tend to be very destabilizing. Destabilization due to 2'-α-alkyl substitution has been explained by the propensity of these substituents to shift the conformational equilibrium of the sugar toward the C2' *endo* pucker and away from the C3' *endo* pucker found in pure RNA duplexes. On the other hand, 2'-β-methyl substituted residues can drive the sugar equilibrium toward the North antipode, yet poorly associate with RNA complements (ΔT_M = -3.1°C/mod.),[26] this time owing to severe steric repulsion of the bulky methyl substituent with the adjacent *cis*-oriented heterocycle that thereby destabilizes the A-form duplex.

By analogy to the above, *ribo*-configured 2'-sulfur linked substituents lead to a decrease of the 3'-*endo* conformer compared with the 2'-hydroxyl substituent, again owing to the poorly electron withdrawing capacity of sulfur.[90] In fact, it has been well documented that the ratio of the 3'-*endo* conformer population increases linearly with the electronegativity of the 2'-pendant groups such that a relation for preferential C3'-*endo* puckering, duplex stability and A-like character has been shown to conform to the following trend: 2'-OMe-RNA:RNA (A-form) > DNA:RNA > 2'-SMe-RNA:RNA (B-form).[91] Accordingly, the 2'-thiomethylated nucleosides exhibit a substantially greater S-population relative to the deoxynucleosides with purine analogues showing an average of > 90% S pucker, followed by their pyrimidyl analogues which exhibit > 75% S-

population[92] predominantly due to an absence of O4'-C1'-C2'-S2' and N-C1'-C2'-S2' endocyclic *gauche* effects. Interestingly, the thiomethyl modification also confers greater structural rigidity to its anchoring furanose relative to the deoxynucleoside counterparts, although the methylated site itself appears to have unhindered rotation about the C-S bond. The puckering in the hybrid duplex shows an average orientation towards the C1'-*exo*/C2'-*endo* domains which parallels the individual nucleosides, with the methylated substituents now directed toward the cleft of the major groove where intraresidual steric contacts are minimized and where they would not be expected to obstruct minor groove recognition and binding by RNase H. Furthermore, based on an examination of minor groove widths, the authors have postulated that the 2'-SMe substitution may trigger RNase H activity, since the dimensions of the minor groove fall within those seen for unmodified hybrids. Unfortunately, no experimental RNase H evidence is yet available to authenticate these results, however, the fact that this modification results in a drop in duplex stability in the area of 1.5°C / SMe residue to as much as –4.5°C / residue in the higher S-hexyl homologues,[90] highlights an important limitation of these molecules as antisense candidates.

1.8. Stabilization Associated with the Ethylene Glycol Motif

A striking correlation between molecular architecture and stability immediately becomes apparent on examination of some of the modifications discussed above. The driving force for macromolecular conformation is as mentioned before the interplay of different *gauche* and anomeric effects within the furanose. However, these may be dramatically affected by introducing subtle changes to the sugars in the AON. Indeed, nucleosides preferentially adopt conformations that maximize the number of *gauche* interactions between adjacent lone pairs and/or polar bonds.[73,75,93] In these molecules, the *gauche* effect is a manifestation of the stability conferred via a $\sigma \rightarrow \sigma^*$ donation of electron density from the bonding orbital of the polarized C-H bond to the nonbonding orbital of the C-O bond.[94] This interaction is an important structural determinant of conformational architecture.

Many bulky 2'-modifications are aptly suited for enhanced RNA binding when composed of repeating ethylene glycol (EG) units, which possess an associated *gauche* orientation

of the side chain (**Table 1.1**, entries **4-6**). Most modifications of this type have demonstrated enhanced binding affinities relative to an unmodified deoxy control.[81] For instance, 2'-substituents with as many as four conjoined EG units still retain strong heteroduplexation; even a nonyl group has been well tolerated at the end of an EG chain.[26] However, changing the ethylene spacer to methylene or higher alkyl homologues has a deleterious effect on binding efficacy (**Table 1.1**, entry **8**), indicating that the second oxygen of the 2'-ethylene glycol pendants results in a conformation of the side chain consistent with duplex formation.

Furthermore, appending an EG unit within an AON is a straightforward mode of adjusting polymer lipophilicity and the ensuing cellular permeability. For instance, high molecular mass PEG moieties have been introduced as tethers on AON conjugates in order to impart more favourable pharmacological properties to the oligonucleotide.[95] Moreover, the conjugated polymers do not compromise the thermal stability or structure of the duplex nor do they impede RNase H assisted antisense effects but merely serve as a means of effective protection of the molecule from biodegradation.

1.8.1. 2'-O-MOE RNA: Retention of the Exocyclic Gauche Effect

These stabilizing origins are deeply rooted in 2'-O-MOE containing oligonucleotides and have been scrutinized from high-resolution crystal structures of an RNA decamer duplex containing a completely 2'-O-MOE modified RNA strand.[91] Of particular relevance, the furanose ring is further rigidified by the EG-type tether, which sterically promotes the A-form helicity and specifies the hydration pattern along the spine of the minor groove by establishing 3-point contacts that coordinate water molecules in the vicinity of the MOE ether oxygens and the adjacent bridging oxygen of the phosphate. The highly intricate attunement of 2'-O-MOE RNA conformational properties has been invoked to explain the greater relative affinity of these derivatives for RNA than DNA, with *ca.* 1.0 – 1.5°C increase in binding affinity to RNA over the unmodified deoxy residues.

Likewise, molecular dynamics studies have shown the MOE functionality of the fully modified mixed sequences to possess a relatively stable geometry throughout the simulation with little movement observed for the appended MOE atoms.[96] Indeed, the *gauche* orientation around the central linkage of the -O-C-C-O- side chain, along with the

added steric space occupied at the helical perimeter, forces the interdependent and synchronous rotation of each neighbouring functionality within the polymer to avoid unfavourable contacts with each other. Interestingly, added motility is observed for the free MOE nucleosides, although the characteristic *gauche* state of the central C-C bond in the side chain is retained.

1.8.2. Protonated Amino Side Chains

Conversely, analogues with cationic tethers or 'zwitterionic oligonucleotides' introduced into the minor groove such as the 2'-O-AP[97] and 2'-O-DMAP[86] oligonucleotides (**Table 1.1**, entries **9-11**) display predominantly enthalpy-driven affinities towards RNA complements as conferred by the aminated species rather than the preferential 3'-*endo* twist of the furanosides.

Although the available evidence is somewhat conflicting,[84,85,98] the behaviour of these analogues generally depend on: (i) the relative proximities of the internal positively charged amino groups of the residues – *i.e.*, contiguous stretches of 2 or more of the modified residues markedly destabilize the duplex, likely as a result of intrastrand charge repulsion that presumably counteracts any entropic assistance towards hybrid formation; (ii) an inherent charge attraction of the side chain with the phosphate backbone of the opposing strand which aids in faster nucleation or 'strand-zipping' by neutralizing the negative charges upon intermolecular mingling of the two single strands; and (iii) lack of a *gauche* effect in the aminoalkyl side chain (*vide supra*) which compromises the binding affinity of these residues toward their targets. The lack of the *gauche* effect in the alkylamino chains minimizes any entropic advantage imparted to this modification upon binding to RNA and acts to reduce the T_M in some instances by an amount comparable to a hydrocarbon chain of the same length.[99]

Nevertheless, modifications such as these involving charged side chains show the highest exonucleolytic resistance to date. The explanation lies in the fact that the amino groups in 2'-O-AP derivatives are protonated at physiological pH (pK_a–NH_3^+ = 9.4) and so can displace a metal ion cofactor present in the nuclease's active site, thereby rendering its phosphodiesterase function inactive. Other cationic groups would be expected to display similar properties.

Despite these potential advantages, there is undisputed likelihood for the charged analogues to engage in nonspecific binding with cellular proteins and thereby lead to general cytotoxicity. In addition, the positively charged modification is not well tolerated in the active site of *E. coli* RNase H presumably due to putative electrostatic repulsions with the surface of the active site cleft or with interference of bound Mg^{2+} and/or Mn^{2+} cofactors.[100-102] Even single substitutions flanking a deoxynucleotide gap have shown substantially reduced rates of cleavage of the chimera over the wild type substrate by the enzyme, suggesting that multiple insertions in an enzyme active AON background may actually abolish activity or engage in non-specific binding toward other oppositely charged cellular constituents.

Furthermore, oligonucleotide analogues such as this which have been constructed to carry one or more positive charges and which exhibit higher binding affinities usually do so at the expense of unchanged specificities. Although facile target binding is optimized via opposite and attractive charge interactions with the phosphate backbone of the complement strand (especially at low ionic strengths where the charges are more unshielded/exposed), the positive charge is likely to raise the affinity for binding all nucleic acids, since all carry more or less the same regularly spaced negative charges.[103]

1.8.3. Uncharged Amino Side Chains

Kawasaki *et al.* demonstrated that many of the important structural features of the MOE and aminoalkoxy groups (*vide supra*) could be retained and improved upon by the construction of pseudoisosteric analogues possessing a neutral hydroxylamino function (**Table 1.1**, entries **12-15**).[83] The 2'-O-aminooxyethyl derivatives were expected to retain the important stereoelectronic properties of their prototypical MOE relatives while offering entropically favourable preorganizational attributes to the oligomers via the added restricted motion around the N-O bond. This is due in part to the unusual properties of the N-O bond, which is unprotonated at physiological pH and exists as the most stable conformer with bonds and lone pairs fully eclipsed and has high barriers to nitrogen inversion or rotation.[104]

In fact, the 2'-O-AOE and MIOE modifications exhibit similar binding affinities and nuclease resistance as the MOE group (**Table 1.1**, entries **4**, **12**, and **15**).[83] This factor, combined with the undesirably high reactivity of the hydroxylamino group, which precludes facile oligonucleotide assembly, has led to the derivatization of this analogue to the more stable DMAOE and DEAOE derivatives.[88,89] The N-dimethyl and ethyl analogues (2'-O-DMAOE, 2'-O-DEAOE) exhibit higher binding affinity and higher nuclease resistance with the improved steric effect from alkyl chains contributing to the enhanced nuclease resistance (Table **1.1**, entries **13** and **14**). Nevertheless, while each of the analogues within this series display subtle differences in nucleolytic character, all maintain the requisite *gauche* orientation with respect to the furanosyl and 2' oxygen atoms and display higher specificity to RNA over DNA though the origin for this selectivity has not yet been described.

1.8.4. Fluorination of the 2'-Position

Fluorine as heteroatom substantially raises the duplex melting temperature such that hybrids of 2'F-RNA and RNA produce A-form segments that are stabilized *ca.* +2.5°C / fluorinated residue relative to that with DNA as antisense.[99] Like its fluorinated 2'F-ANA epimers (*vide infra*), the fluorine electronegativity influences the ring conformational equilibrium, this time leading to C3'-*endo* biased analogues which predominate over the S-conformation by over 90% in solution and entropically predestine the single stranded oligomers to engage in remarkably tight target binding.[105] However, the ribosyl-based congeners are unable to activate RNase H since they are preorganized to form pure A-type duplexes rather than the requisite non-canonical A-like forms. They also show far greater susceptibility to nucleolytic hydrolysis,[46] although much improvement is obtained upon replacement of the phosphodiester scaffold with a thioate backbone.[87]

The fluorine atom has also found some use in the design of 2'-O-trifluoromethylated analogues.[106] The fraction of N conformer is estimated at 31%, which is surprisingly lower than that found for the ribo- or 2'-OMe-ribosyl counterparts (*i.e.* 36% N and 42% N respectively, by NMR),[107] but reflects the relatively diminished group

electronegativity of the OCF_3 moiety.[108] Yet relative to 2'F-RNA, the decreased N character is not entirely unexpected since the F atoms are now further removed from the other endocyclic heteroatoms and so exert less control over the antipodal pseudosugar equilibrium. Hence, it is not surprising that these derivatives behave much like their methoxy analogues, and show RNA selective properties with an overall B-like conformation when bound with DNA but are only slightly more resilient to 3'-exonucleases, and are comparable to the methylated analogues in this respect as well.[106]

1.9. 2'-MODIFIED AONS THAT ACTIVATE RNASE H: ANA AND 2'F-ANA

Clearly, for most ribose-based antisense nucleotides, enzyme activity is invariably precluded by projection of the C2'-substituents into the docking site of the substrate where they likely interfere with one or more processive functions of the enzyme. Newer perspectives in analogue design have capitalized on this intrinsic biological 'handicap' by introducing atoms on the furanose ring with alternate stereochemistries. For example, a switch in chirality of the C2'-OH group in ribose residues to the β-configuration (**Figure 1.8**) was explored as one of the first structural manipulations to conceivably retain

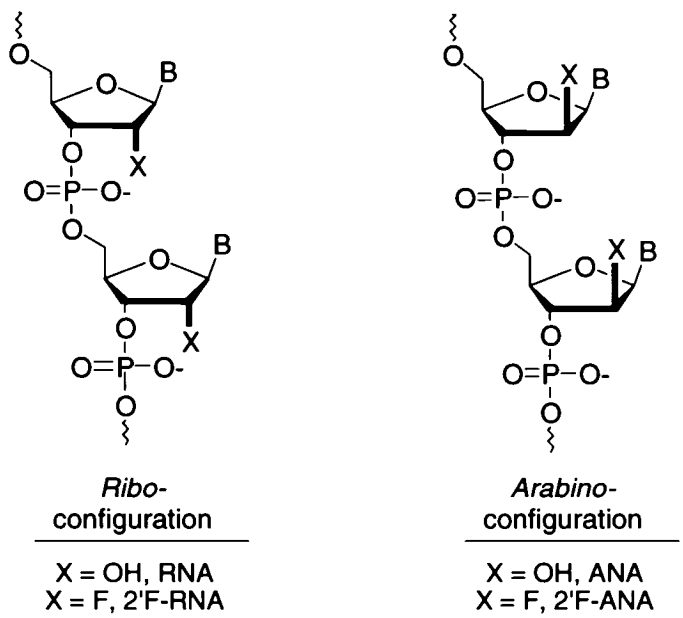

Figure 1.8: Inversion of configuration at the 2'-position of RNA and 2'F-RNA gives the corresponding epimeric arabinonucleic acids (ANA and 2'F-ANA).

enzyme activation. Interestingly, the chirality switch also enforces a shift in the conformational equilibrium away from the Northern hemisphere (*i.e.* C3'-*endo*), almost opposite to the trends described above which have thus far precluded enzyme activity.

Accordingly, Giannaris and Damha first investigated the functional consequences of inverting the stereochemistry at the 2'-position in their work with oligoarabinonucleotides (ANA).[109] Preliminary investigations showed that arabinoadenylate heteroduplexes displayed generally beneficial characteristics, although thioation of the arabinoadenylate backbone significantly destabilized the heteroduplex with RNA and to a lesser extent, DNA. Although these first examples demonstrated sufficient promise with both nucleic acid complements, the initial pairing trends were found to be the exception rather than the rule, as mixed-base PO sequences were later shown to exhibit selective pairing with ssRNA in contrast to the poor pairing behaviour with ssDNA.[53]

Furthermore, oligoarabinonucleotides (*i.e.* ANA:RNA hybrids) of mixed-base composition[53,110] have since been shown to generally display weaker binding affinities (ΔT_M= 0.5 – 2.1°C/mod.) relative to native heteroduplexes with RNA, perhaps due to inherently impaired heterocycle associations within the duplex as imposed by the sterically demanding β-C2'-OH group which is now oriented into the major groove of the helix where efficient base stacking is likely to be disrupted.[111] Some evidence for this has been provided by molecular dynamics (MD) simulations of ANA:RNA duplexes[112] which have indicated prevalent C2'-*endo* geometries in the ANA strand resulting from a combination of stereoelectronic effects and probable intrasugar hydrogen bonding between the 2'-α-substituent and the C5'-oxygen. This 'locked' conformation may alter the torsional preference of the glycoside and therefore the heterocycle orientation, which could hypothetically contribute to the observed thermal destabilization.

Interestingly, a comparison of the CD spectral signatures of DNA:RNA and ANA:RNA complexes reveals similar global geometries between the two classes of compounds. Even more remarkable is the fact that the latter retains the ability to direct RNase H-mediated phosphodiester hydrolysis of the target, thereby proving to be the first sugar-modified AON capable of supporting RNase H-mediated degradation of the sense RNA. The fact that target hydrolysis occurs with poorer efficiency than with the native

substrates has been rationalized in conjunction with the lower affinity of ANA for RNA targets, which may act to present a lesser amount of AON substrate duplex to the enzyme, thereby diminishing the overall catalytic effect.[53] In contrast, alternate explanations derived from MD simulations have suggested that subtle structural deviations of the arabinose residues are responsible for the less than optimal binding of RNase H toward preformed ANA:RNA hybrids.

Yet this latter interpretation seems unlikely given the recent and unequivocal NMR determination[113] of the ANA sugar conformational properties. Not only have these refuted earlier MD analyses, they have also clearly outlined a structural similarity of ANA with DNA at the nucleotide level (**Figure 1.9**). As such, the arabinose sugars clearly appear to occupy an Eastern pseudorotational disposition (*i.e.* O4'-*endo* geometries) and lack intraresidue C2'-OH/5'O interactions.[111] Thus, in spite of the reduced activity, the requisite O4'-*endo* conformation which is widely hypothesized as an underlying asset for enzyme activation is retained in ANA. Accordingly, Noronha *et al.* have shown that the extent of target cleavage increases dramatically when the substrate and enzyme are incubated at ambient rather than physiological temperatures.[53,114] This

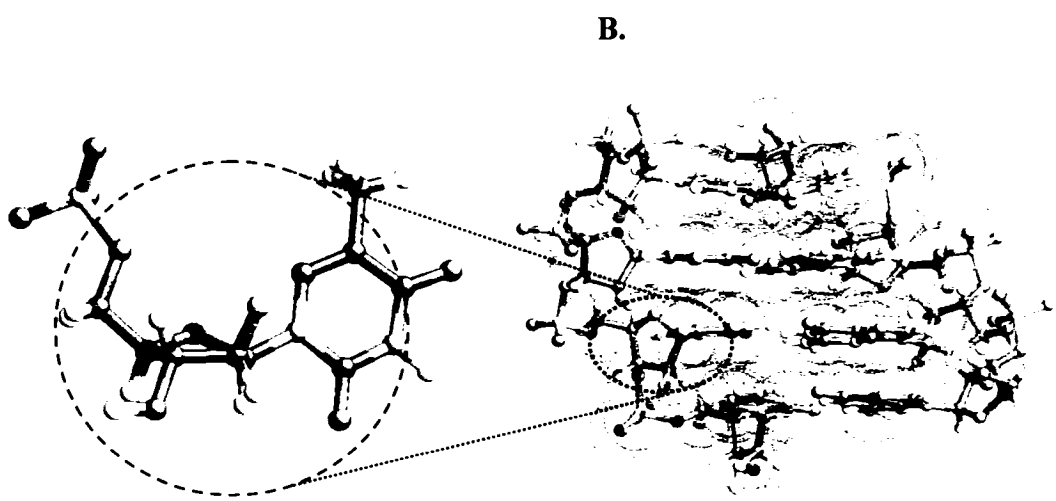

Figure 1.9: Illustration of (**A**) the O4'-*endo* structure of the arabinose sugar of 2'F-ANA upon (**B**) hybridization to complementary RNA as elucidated by NMR.[111,113,115] Adapted from Damha *et al.*[111]

provocatively suggests that poor enzyme recruitment is solely a consequence of suboptimal hybrid formation.

Remarkably, the above trends are readily extended to and improved upon in the fluorinated ANA homologues (**Figure 1.8**, 2'F-ANA), which display enhanced enzyme activation relative to their arabinose-derived counterparts. Replacing the ara-2'-OH group with a smaller 2'-F atom to give 2'F-ANA results in compounds with elevated duplex stabilities towards a multitude of targets.[53,110,116] Quite conceivably, simple substitution with a more electronegative atom on the β-face of the sugar drives the N ⇌ S equilibrium toward the S hemisphere, as endocyclic *gauche* effects now become more pronounced and easily predominate over any counteracting anomeric forces.[105,117] However, as with ANA, subtle differences are seen in the conformation of the fluorine containing isomers when duplexed with RNA. The pseudosugars adopt an O4'-*endo* (or Eastern) conformation[115] which lies halfway between the C2'- and C3'-*endo* puckers and places the sterically innocuous fluorine atom within the major groove (**Figure 1.9**). Once again this preference over a C2'-*endo* spatial arrangement presumably occurs to relieve steric interactions between the proximal heterocycle and the F atom (specifically C6-H6 in pyrimidines; C8-H8 in purines), which is now accommodated surprisingly well at this position by adopting a more eastern geometry.[105] Yet unlike ANA sugars, NMR and modeling analyses show a through space interaction between the 2'-F atom and H6/H8 which has been suggested to stabilize the strand topology[118] and which is absent in ribofluoronucleosides as well as arabinofluoronucleosides with an α-oriented heterocycle.

A comparison of ANA and 2'F-ANA further reveals that the increased T_M for the latter may reflect the reduced steric interactions of the F atoms (*vs.* OH groups), while greater thermal stability over DNA hybrids presumably results from a higher preorganizational state as orchestrated by the β-fluorine atom relative to the single-stranded DNA counterparts. The fluorinated derivatives are also more robust towards intra- and extracellular nucleases than are the native DNA strands and markedly resist depurination by virtue of the electron withdrawing character of the vicinal fluorine atom. From the perspective of RNase H-mediated antisense effects (*vide supra*), the most intelligible

approach for designing an antisense agent that retains RNase H activity seems to necessitate physical clearance of the minor groove cavity of the substrate to enable optimal enzyme binding. This principle is most easily adhered to with the arabinose-derived AON:RNA hybrids which project the 2'-substituent of the AON into the major groove at a site where steric contacts with the binding cleft of the enzyme are likely not possible.

This observation, along with a molecular dynamics evaluation of 2'-OMe-ANA conformational properties have extended the opinion that ANA progeny may in principle be adept at retaining enzyme activity with a variety of modifications in the 'up' position, although with some steric consequences imposed on the flanking heterocycles.[91] However, while 2'F-ANA retains and improves upon many essential features for enzyme activity that are crudely evident in ANA, other carbohydrate modified AONs that have focused on the inclusion of more rigid ANA-derived chemical moieties in the antisense are unable to invoke the same activation characteristics with respect to RNase H.[119]

1.9.1. Bicyclo-ANA and LNA: the Case for Structural Preorganization and High Binding via Monomer Rigidity

Facile hybridization by monomeric rigidity is a recurrent theme in mainstream antisense methodologies and is one of several key features invoked in the fluoroarabino compounds as well. Strand preorganization is of great utility in this sense because it can raise both the avidity and fidelity with which an AON anneals to a complementary sequence. In this respect, a ligand can be designed to resemble the bound conformation even before the requisite association occurs, such that the consequential rearrangement of the binding ligand is no longer required to establish optimal base pairing contacts to its target. This reduces the associated pairing entropy but also thwarts undesired binding to fallacious targets (*e.g.* mismatched sequences).[103]

Accordingly, many 'locked' nucleic acids have a definite entropic advantage thereby enabling tight and efficient hybridization with a target strand. Strategic placement of a bridging network of atoms freezes the resulting polycyclic sugars to favour a conformation that predisposes the AON to engage in strong and rapid RNA selective hybridization over the natural ODNs (**Figure 1.10**).

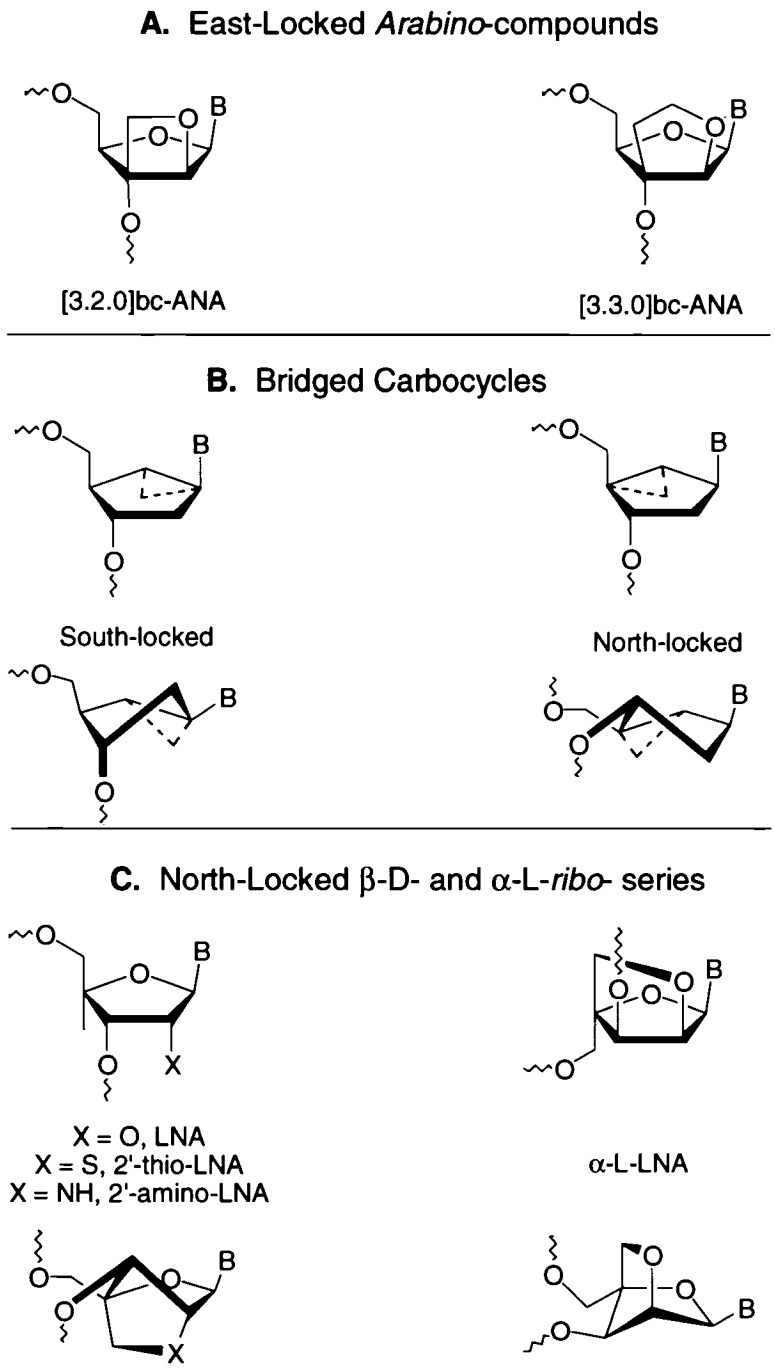

Figure 1.10: Structural anatomies of some conformationally frozen bicyclic nucleic acid sugars. The indicated conformations are also the only ones adopted by each type of derivative.

This is exemplified in work by Christensen *et al.* in which a systematic evaluation of the binding properties of 2 different 2'-O, 3'-C-linked bicycloarabinonucleoside analogues was undertaken (**Figure 1.10**, panel **A**).[120] While the [3.3.0] congeners exhibit strong and selective recognition for RNA over DNA complements, positive effects on duplex thermal stabilities towards either target have only been obtained with the fully modified oligonucleotides, which raise the duplex melting temperature *ca.* 1°C per modification. The 2'-*arabino*-configured bicyclonucleotides (*i.e.* bc-ANA) obviously have an entropic advantage during duplex formation, which is further accompanied by favourable enthalpic effects that are likely manifest via increased base stacking. Quite unexpectedly then, alternating sequences of [3.3.0]bc-ANA with unmodified deoxynucleotide residues largely reduce hybrid thermal stability (*ca.* -3°C per insert) with complementary RNA (rA_{14}).[121] This suggests that conformational preorganization can be a beneficial design strategy but may sometimes severely distort the preferred structural disposition of the accommodating AON. For instance, in cases such as this where an oligomer is constructed from two different nucleoside analogues, it may be difficult to obtain a stereoregular structure that is conformationally identical within every nucleotide unit. Therefore, it could be that fusion of the rigid *arabino*-configured bicyclic ring to the furanose kinks the parent AON at each deoxy / bc-ANA junction into a structure that poorly recognizes its RNA complement. Other reasons have also been presented that suggest the hydration pattern along the spine of the AON to be periodically disrupted upon introduction of the modified nucleosides within an otherwise uniform deoxy chain.[122]

Conversely, [3.2.0]bc-ANA with a smaller bicyclic ring binds well to both RNA and DNA complements and exhibits better stability than its [3.3.0] homologue[120] (**Figure 1.10**, panel **A**). The smaller bridge – and consequently more compact sugar environment – promotes duplexation with RNA even when alternated with deoxynucleotides in the antisense strand.

Both [3.3.0] and [3.2.0] derivatives exist exclusively in Eastern conformations (O4'-*endo*/C1'-*exo*).[119,120,123] Quite significantly, only sugar geometries that fall within the O4'-*endo* range within the AON have been postulated to actively induce RNase H-assisted sense strand cleavage, a principle which surprisingly has not been adhered to

with the [3.3.0] fused systems.[123] The CD signatures of the [3.3.0]bc-ANA fully modified complexes with rA_{14} show that the hybrid shape of each complex is similar to that of the unmodified DNA:RNA duplexes, in spite of the lack of enzyme induction in these examples. This may indirectly suggest impeded catalysis by the constrained molecules rather than poor enzyme binding. More specifically, the bicyclic sugars likely induce an uncharacteristically high energy barrier to catalysis by preventing conformational manipulation of the substrate by the enzyme, which disables further processing in the bc-modified duplexes as opposed to an inherently flexible alternative (*vide infra*). Alternately, the bulkiness of the bridging atoms in the [3.3.0]bc-ANA analogues may physically hinder the binding event and preclude hydrolysis in this manner.

A more defined picture of the structural origins that are responsible for the abolished activity should be attainable by comparison to other ANA-derived AONs, such as the [3.2.0]-bicyclic surrogate, which itself is also unable to activate RNase H.[123] Indeed, the sugars of this derivative are likewise held in an O4'-*endo* geometry by the more rigid – yet relatively compact – 4-membered bicycle, which rigidifies the residues to a greater extent than the fused five-membered ring analogues, but occupies less steric space above the furanose ring. In light of this evidence, and the notion that the fused rings sit at the brim of the duplex major groove away from the primary locus of enzyme binding, it is improbable that this event is impeded by any physical obstruction presented by either bicyclic AON surrogate. Rather more likely is the concept that an active duplex conformation for hydrolysis cannot be achieved by the enzyme once bound, owing to the impliable nature of the core bicyclic sugar residues.

Certainly, an extension of these observations to other Eastern fixed tri- and polycyclic systems with an arabinose framework[124] will also be necessary to determine if this conformation generally gives favourable binding and potential enzyme activation as empirically demonstrated by the deoxy- and fluoroarabinonucleotides.

It is noteworthy that these and similar pseudosugar designs primarily attempt to preorganize the AON strand into a structure compatible with A-type duplex formation. This effectively eliminates a large entropy cost since the fused analogues already possess the predefining structural elements required for tight duplexation. Further examples

relate to the N- and S-configured methanocarbanucleotides, which display opposite pairing tendencies. In this respect, the 1',6'-methylene bridged nucleosides are customized to favour a Southern conformation (B-form), which decreases duplex stability with RNA;[125] yet moving the bridge to the neighbouring furanosyl ring carbons, as in 4',6'-methanocarba-nucleic acid (**Figure 1.10 B**), elevates the T_M with RNA, and shifts the sugar to the C3'-*endo* domain (A-form).[126,127] Thus, heteroduplex stabilization clearly correlates with the tendency of methanocarba-oligonucleotides to adopt a northern conformation.

Likewise, the locked nucleic acids (LNA) and related chemical variants,[128-131] which possess a [2.2.1]bicyclic ribosyl-configured frame (**Figure 1.10**, panel **C**), have taken advantage of conformational restriction to induce unparalleled increases in the thermal stability of duplexes toward complementary DNA and RNA (ΔT_M/monomer = 3 – 11°C *vs.* a DNA reference).[132,133] The *ribo*-configured methylene bridging bicycle that connects the 2'-oxygen with the 4'-carbon atom freezes the sugar in the C3'-*endo* conformation so that the LNA residues essentially mimic their RNA prototypes. These features are evident in the CD spectra of LNA:RNA duplexes, as well as X-ray and NMR analyses,[134,135] which show the oxymethylene bridge to be situated along the face of the minor groove of the duplex.[128,136,137]

Interestingly, LNA 'mixmers' with interspersed ribo- or deoxynucleotides reveal that the LNA constituents act in concert to elevate the T_M to a greater degree than otherwise expected from the individual contributions of the monomers in the analogous fully modified LNA AONs. This profoundly contrasts what is seen for bc-ANA monomers and may be related to the placement of the bicycle on the α-face of the furanose along the minor groove cleft (**Figure 1.11**) rather than on the β-face as with the bc-ANA compounds. Moreover, the α-oriented bridge fusion within LNA residues appears to be influential in dictating the conformation of neighbouring deoxy- or ribonucleotides to adopt a preference for the N-conformation[138] or by aligning the heterocycles to favour increased intrastrand base stacking, an observation that has independently been noted by other investigators for these bicyclic systems.[139,140]

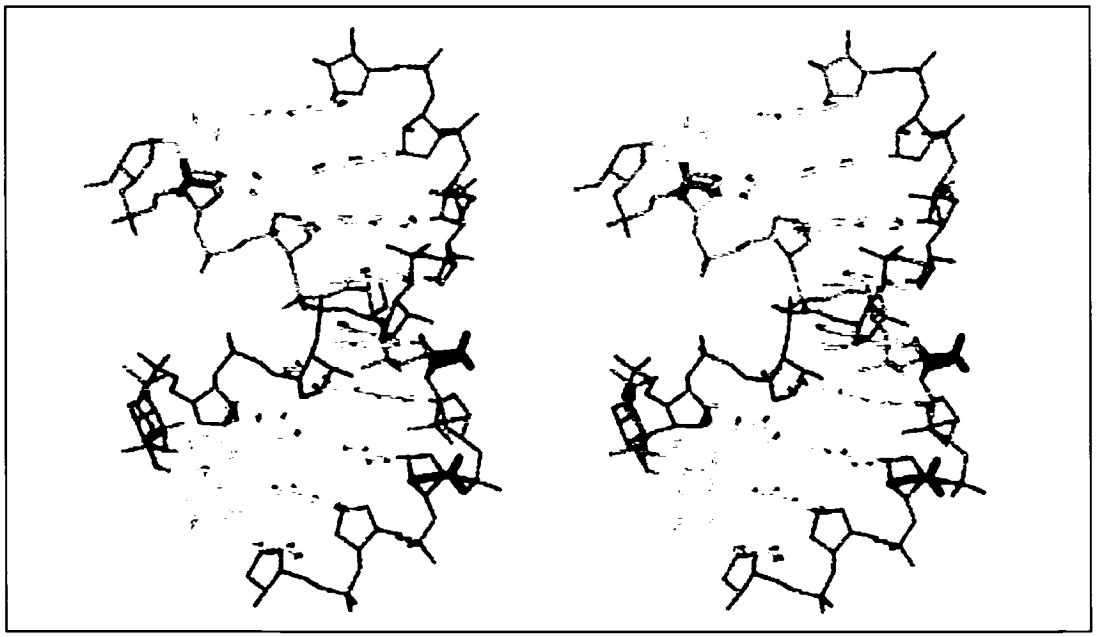

Figure 1.11: Stereoview of an LNA-DNA mixmer hybridized to an RNA complement, showing projection of the LNA oxymethylene bicycle bridges (blue) into the minor groove face of the duplex, where they are likely to interfere with RNase H action. Also evident is the A-form mimicry of the double stranded structure despite a predominant deoxynucleotide content in the AON strand, as induced by preferential adoption of the N-conformation in flanking deoxynucleotides by the imposing LNA inserts. (*e.g.* compare with **Figure 1.7 A**). Adapted from Petersen *et al.*, 2002.[141]

It has since been shown that an alternating LNA-DNA copolymer assembly consisting of 6 isolated deoxynucleotides and 9 interspersed LNA residues can support slow but detectable *in vitro* cleavage by *E. coli* RNase H.[142] Although the activity was quite minimal in comparison to an LNA-DNA-LNA gapmer with six adjacent deoxy residues, it represents an interesting example of retention of enzyme activity in the AON strand in the absence of an uninterrupted stretch of the naturally recognized deoxynucleotides. Unfortunately, subsequent reports that further probed this characteristic with gapmer or fully modified LNA sequences have refuted the activity in other sequence contexts, suggesting that the specificity may be sequence dependent and/or influenced by nearby unmodified residues.[56,143] Naturally, fully modified oligonucleotides of this composition would not be expected to retain enzyme activation simply on account of the minor groove occupancy of the fused ring structure, which would expectedly disrupt the formation of productive contacts in the resultant enzyme-substrate complex.

Yet unlike LNA which mimics the RNA conformational properties and likely displays characteristics that make it unsuitable as an enzyme-activating AON, α-L-LNA is a preferential DNA mimic (2'-*exo*),[129,130] with the 2'-C,4'-C-oxymethylene linker now conveniently directed within the major groove duplex cavity[144] (**Figure 1.10**, panel **C**). Moreover, modified α-L-LNA:RNA duplexes have overall helical topologies that closely resemble the native duplexes, with the AON strand fully capable of maintaining antiparallel Watson-Crick association with the target.

Additionally, the monomers have surprisingly little influence on the conformations of adjoining deoxy residues which exist in S-puckers in the mixmer α-L-LNA, and are able to effect adequate yet retarded *in vitro* activity with *E. coli* RNase H toward the ribonucleotide targets, although only after prolonged incubation times using high concentrations of enzyme.[56] Unfortunately, further data on this peculiar property has yet to be reported in sequences comprising a fully modified α-L-LNA phosphodiester duplexed with a homogenous RNA target. Rather, a DNA / α-L-LNA / DNA gapmer was initially shown to induce enzyme-mediated hydrolysis within a chimeric ribonucleotide composed of a central ribouridylate tract inclosed by 2'-OMe-RNA wings.

Recent studies have, in fact, outlined greater promise for numerous chimeric variants of a general α-L-LNA / DNA phosphorothioate design to induce an RNase H pathway of target RNA destruction. Importantly however, uniformly thioated chimeric derivatives with high α-L-LNA content (*ca.* 90% in the hexadecamer, with 2 isolated deoxynucleotides) were unable to efficiently downregulate luciferase mRNA expression, as ultimately ascribed to an inability of these molecules to activate RNase H cleavage.[145] Hence, the ability of α-L-LNA nucleotides to only partially support RNase H activity may well depend on the structural plasticity of the heteroduplexed form in addition to shared structural similarities with the natural (*i.e.* DNA:RNA) substrates. Accordingly, if enzyme catalysis requires the bound duplex to be steered into a more reactive conformation,[42,146] it follows that these substrates would necessarily experience a greater amount of strain energy when distorting the backbone at the vicinity of the reacting phosphate linkage into a more desirable orientation for hydrolysis relative to an all-DNA antisense strand. Hence, the reduced degradative capacity of the target strands

is likely influenced by the rigid nature of the locked residues in the α-L-LNA AON complement.

It is clear, however, that preorganization of the modified backbone can be beneficial in retaining some of these requisites and therefore deserves careful consideration in future designs of antisense agents. Indeed, while strand complementarity via preorganization presents itself as a useful solution to optimizing target avidity, an unfortunate yet recurrent consequence is the substantial loss of enzymatic activity, which inevitably accompanies these approaches. Consequently, substrate flexibility appears to be emerging as a critical mediator of protein-nucleic acid recognition, however the significance of the flexibility of the sugar component towards *both* nucleic acid recognition and enzymatic compatibility has only recently been addressed.[147,148]

1.9.2. Acyclonucleotides: Biological Effects of Monomer Conformational Mobility

Indeed, several research groups have actively investigated 'flexible' nucleic acids where the deoxy- or ribose component of respective DNA or RNA residues is replaced by an acyclic sugar component that is free of associated ring strain.[149-151]

These analogues are attractive for a variety of synthetic and biological reasons.[152-154] For instance, the acyclo or '*seco*'-nucleotides are much simpler to synthesize and easily cease the progression of 3'-exonucleolytic digestion to exhibit excellent *in vitro* stabilities, with minimal degradation reported after 19 h in cell culture (*i.e.* 98% intact oligomer remaining).[154] Secondly, the lipophilic character of the residues can easily be adjusted to promote unimpeded entry of the oligonucleotide into the cellular space. The documented efficacy of many of the monomeric nucleosides as effective antivirals[155] and consequently as good probes of enzyme function may also earn this class a special place in future AON designs that attempt to invoke sense strand cleavage by enzyme participation.

In principle, many different bond scissions of the furanosyl endocyclic frame can be chemoselectively accomplished to produce a variety of acyclic derivatives. **Figure 1.12** (panel **A**) highlights the various '*seco*' skeletons that are obtained from different cleavage modes of the parent congener. Furthermore, removal of the O4'-C1' linkage or complete

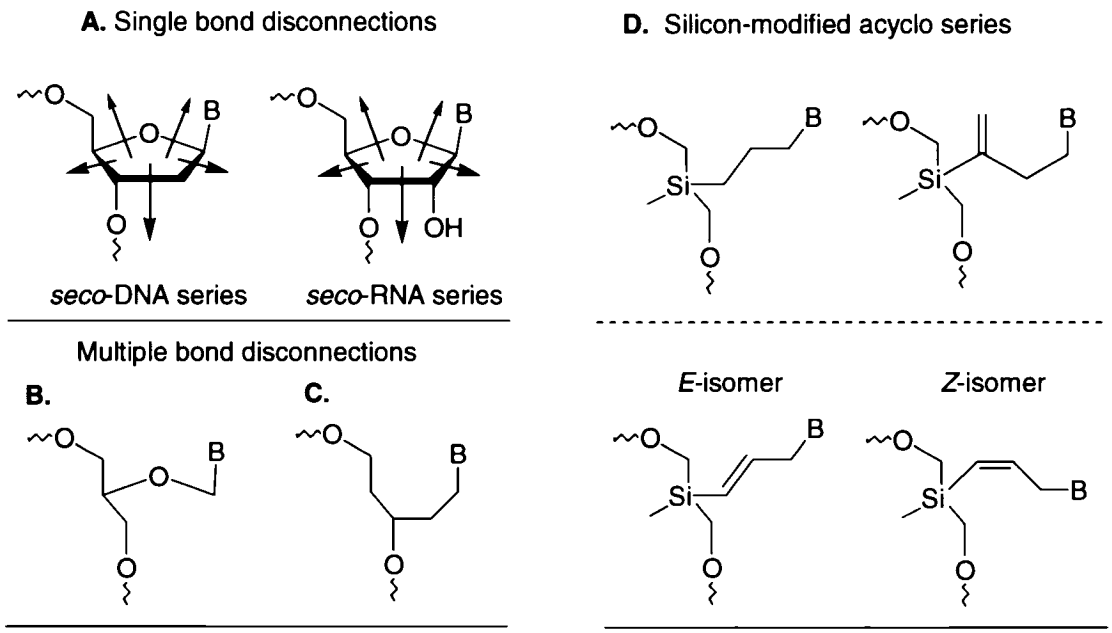

Figure 1.12: **A.** Acyclic nucleotides of the '*seco*' class of compounds may be obtained by almost any bond disconnection of the natural deoxy- or ribofuranose parent. **B.** Removal of the C2' fragment generates the glyceronucleotide class. **C.** Seconucleotides in which the O4' atom is removed exhibit enhanced glycosyl stability. **D.** *Sila*-acyclonucleotides improve lipophilicity via silicon incorporation within the residue.

deletion of the O4' atom from the furanose altogether can give building blocks that resemble the natural nucleosides but lack the chemical instability associated with the natural glycosidic linkage and therefore strongly resist depurination (**Figure 1.12 C**). Unfortunately, completely modified oligomers constructed of this type form poor associations with complementary DNA targets and discriminate less among the four natural nucleotides when in a double helix. [154]

Acyclic functionalization of the natural oligonucleotides has originally been stimulated by the glyceronucleoside family, whose members lack the characteristic C2' fragment of the natural deoxynucleosides (**Figure 1.12 B**).[156-160] Unfortunately, hybridization of DNA with glyceryl-substituted oligonucleotides lowers the duplex melting temperature significantly, comparable to the amount of a G-T mismatch (*ca.* 12 – 15°C), and uniformly functionalized thymine-containing homopolymers are unable to bind with a DNA complement at all.[156]

The *sila*-acyclic analogues (**Figure 1.12 D**) represent an interesting diversion from the *seco* class in that a silicon surrogate is employed for the normal 4'-carbon of the deoxyribose, while carbon-2' and the carbohydrate oxygen are removed entirely, to enhance hydrophobicity.[161] A propyl – rather than ethyl – spacer separates the nucleobase from the silicon atom in order to avoid facile β-elimination of the base in mildly alkaline conditions. However, the accompanying entropic cost associated with insertion of the *sila* acyclonucleosides within oligodeoxyribonucleotides induces a similar decline in base pairing that equates to a 7.5 – 12°C drop in thermal stability per modified residue. The unsaturated thymine congeners have since been prepared,[162] however their hybridization potential has yet to be reported, although an improvement in the integrity of duplex formation is anticipated based on the relative rigidity of these compounds with respect to their previously synthesized *sila*-acyclic nucleotides.

In summary, replacement of the carbohydrate with almost any acyclic chain has conferred strong endo- and exonuclease resistance to all seconucleotides examined thus far, despite a significantly decreased integrity of the duplex formed with natural DNA. While this has mostly halted further research on acyclonucleotides as antisense agents, much of the literature in this area has not examined their behaviour towards RNA complements. Although this may be a minor oversight, it is well known that binding affinities with DNA are not necessarily predictive of relative RNA affinities (*i.e.* the intracellular target). Hence, compounds such as 2',3'-seconucleotides could in theory present a unique mode of intra- or interstrand hydrogen bonding of the free hydroxymethyl arm with available hydroxyls on the ribose residues of the opposing RNA strands; any added intermolecular contacts could thus strengthen the association with RNA.

1.10. Revisiting the Preorganizational Approach from the RNase H Perspective: The Neighbouring Nucleotide Flexibility Hypothesis

The reduced thermal stabilities observed with acyclonucleotides presumably owe to their high multiconformational characters, which inevitably lead to huge entropic disadvantages for hybrid formation. However, the more successful AON technologies have usually neglected to include flexible chemical moieties in an otherwise rigid AON as a possible means of maintaining a high degree of enzyme activity. Hence, combining

both properties (*i.e.* preorganization and flexibility) while preserving favourable target recognition by the construct is a difficult undertaking but one that may open new opportunities for a detailed examination of RNase H tolerance toward target hybrids. We speculated that any entropic disadvantages generally inherent in the acyclic residues could likely be overcome by their interdispersion within a rigid backbone scaffold, in order to maintain high association affinities while potentially endowing the chimeric polymers to retain elevated and efficient RNase H cleavage of complementary RNA sequences. In fact, such a seemingly incompatible union of these properties has presented a unique opportunity to examine and dissect the various molecular features that enable facile scission of target sequences by RNase H.

A less obvious yet pertinent extension of this concept clearly highlights the importance of intrahelical conformational mobility on enzyme hydrolytic efficiency. Specifically, pronounced enhancements in enzyme activity are evident in chimeric AONs comprised of 2'F-ANA with varying deoxynucleotide content. In fact, introduction of even a single deoxynucleotide within an otherwise all-2'F-ANA thioated AON derivative markedly elevates the susceptibility of the target strand towards enzyme scission.[163]

Moreover, multiple deoxy insertions in 2'F-ANA phosphodiesters significantly increase the level of target degradation, so that 2'F-ANA sequences with 50% deoxy content display activity that is equal to or significantly better than the uniformly modified 2'F-ANA AON strands or even all-DNA (**Figure 1.13**).[164] Thus, whereas most enzyme eliciting AONs such as 2'F-ANA are typically less potent enzyme activators than DNA, the introduction of small segments of the relatively conformationally labile deoxynucleotides ($\leq$ 3 neighbours in an 18mer) in the former enable it to supersede the degradative potential of the natural DNA antisense. Specifically, alternating trinucleotide repeats of DNA with 2'F-ANA (*i.e.* 'altimers') possess superior antisense properties to all-DNA and suggest that strand flexibility may be accountable.[164,165] Indeed this class of AON has only recently surfaced as one of the first examples of artificial constructs that elevate the RNase H – directed vulnerability of their targeted RNA complements over that of the wild type substrates.

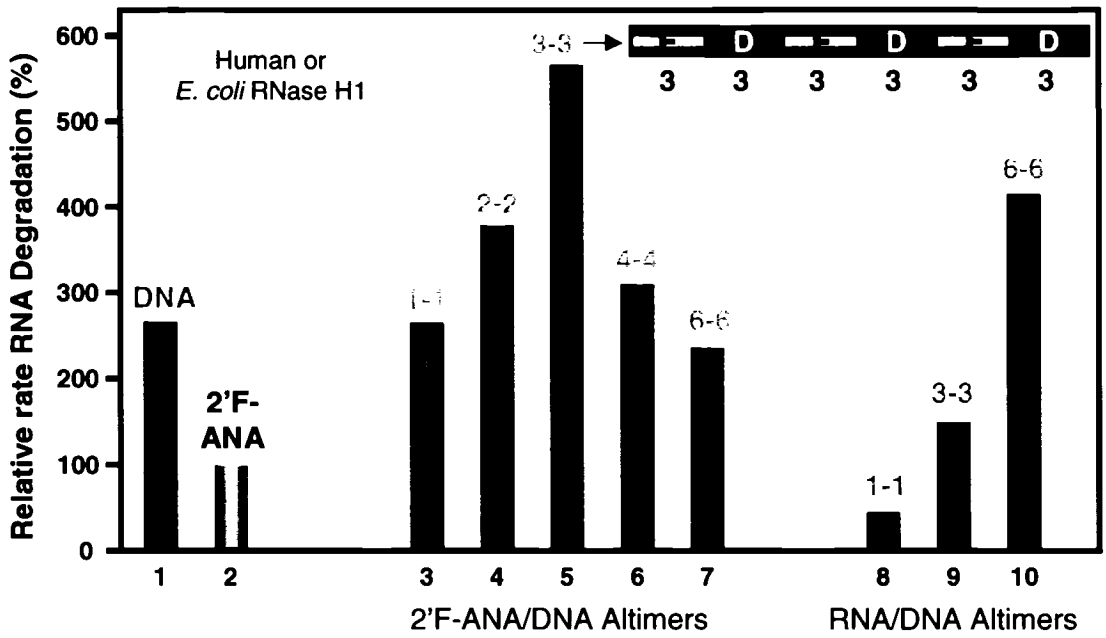

Figure 1.13: Alternating segments of flexible (DNA) and rigid (2'F-ANA) nucleotide repeats in an 18mer AON markedly elevate the efficiency with which human RNase H1 cleaves the duplexed RNA component and far surpass their native surrogates in this regard. F = 2'F-ANA; D = DNA. 2'OMe-RNA-DNA altimers with similar alternating compositions (AONs 8 – 10) do not induce RNase H-mediated RNA degradation as efficiently, with the exception of "gapmer" constructs which comprise a central uninterrupted stretch of 6 deoxynucleotides flanked by enzyme-inactive 2'-methoxyribose sugar termini. Analogous trends are observed when target degradation is induced by the bacterial counterpart (*E. coli* RNase H1). Adapted from Min *et al.*, 2002.[164]

1.11. CeNA: A Monomer of Flexible Capacity

The cyclohexene nucleic acids (CeNA) constitute another unique paradigm in antisense design that capitalizes on the flexible virtues of the intrastrand AON residues.[166,167] Cyclohexene in place of the carbohydrate as the nucleotide anchor is accommodated fairly well in the DNA or RNA component of the heteroduplex as these residues are suggested to adapt reasonably well to either environment.[55] Moreover, the $^{3}H_{2}$ conformation (analogous to C3'-*endo* in furanose residues) is slightly favoured over the $^{2}H_{3}$ antipode (2'-*endo* like) although the energy differences of these conformers are quite small (*ca.* 0.4 kcal/mol for interconversion; **Figure 1.14**). It is noteworthy that the energy gap for N $\rightleftharpoons$ S interchange in the natural furanose nucleosides is correspondingly higher, and ranges from 3 – 6 kcal/mol.[9] Accordingly, greater thermal stability is imparted to hybrids of CeNA and RNA (ΔT_M = +1.2°C / mod.)[168] rather than with DNA as sense

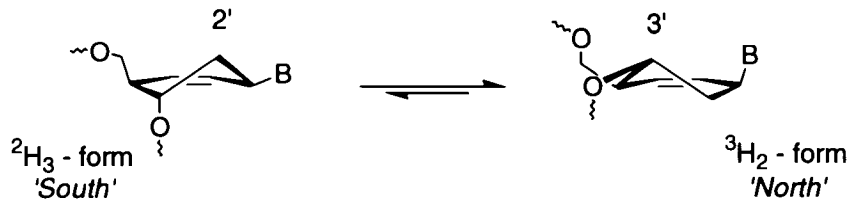

Figure 1.14: Conformational interchange of cyclohexenyl (CeNA) sugar residues. The preference for the 3'-*endo* antipode is estimated to be smaller than that of the natural residues.

strand (ΔT_M = 0.0°C), which together reflect a modest degree of monomer preorganization in the cyclohexene residues that is surprisingly well tolerated with the latter targets.

Evaluation of target RNA lability towards *E. coli* RNase H-assisted degradation in the presence of cyclohexenyl-containing antisense segments with flanking deoxynucleotide tracts shows that sufficient hydrolysis is supported by the constructs, although the extent to which cleavage occurs is comparably lower than that observed for the wild type hybrids.[55,167,169] Notably, the oligonucleotides were designed such that enzyme activity was kept confined within the CeNA/RNA duplex region of the hybrids by similarly inclosing the ribose tract of the sense strand within 2'-OMe flanking segments (*i.e.* double chimeric design comprising DNA–CeNA–DNA as antisense, bound to a 2'-OMe-RNA–RNA–2'OMe-RNA target). Importantly however, the influence of the flanking deoxy/2'-OMe hybrid regions needs to be defined more carefully, especially since the observed effects may not be reproducible in an all-RNA target. Nevertheless, it is remarkable that both these derivatives and α-L-LNA are able to effect cleavage within the RNA component at all, in light of their relative structural diversities.

1.12. Challenges and Opportunities of Future Research

The opportunity to predictably improve AON binding properties has been spurred by an expanding awareness of the precise molecular properties that promote and stabilize nucleic acid double helices. For instance, it is now fairly clear that an increase in affinity for complementary mRNA can more or less be routinely obtained by the use of either conformationally biased (*e.g.*, 2'F-RNA) or conformationally frozen (*e.g.*, bicyclo- and

LNA) AONs, all of which favour the C3'-*endo* conformation. Unfortunately, steric inhibition of mRNA processing is likely to contribute only minimally to a potent cellular antisense effect given that preorganization of these AONs into a pure north conformation produces an AON/RNA duplex not generally recognized by RNase H.

As RNase H is strongly implicated as a critical step in the mechanism of action of antisense drugs, predictive improvements in its activation are only poorly pending. The failure to activate RNase H can usually be traced back to the conformational properties of the AON. Among the properties that appear promising for RNase H recruitment include A-like character in the hybrid and eastern (O4'-*endo*) geometry in the AON sugars. While the latter element has certainly been a notable exception in other enzyme-activating AONs, namely CeNA and α-L-LNA, there is little evidence that disputes the importance of this conformation in other sequence and/or structural contexts. Indeed, as both CeNA and α-L-LNA modified AONs are unlikely to acquire an O4'-*endo* disposition which is believed to be a key factor in retaining activity, it is important to point out that the influence of flexible deoxynucleotide neighbours in the mixmer and gapmer constructs associated with these AON designs is not yet known. This is an especially critical consideration, given that neither of these AON classes has yet been shown to induce RNase H activity in the absence of one or more deoxynucleotide segments in the hosting AON.[55,56,145,167]

Conversely, while modifications that impart substantial rigidity to a particular nucleotide have often been poor activators of enzyme function, less work has highlighted the importance of sugar conformer flexibility along the AON strand, which may act in concert with the global helical architecture of the duplex to govern interactions between RNase H and the substrate. Nevertheless, a unifying theme set forth by each enzyme activating AON class thus far centers on the inclusion of more flexible neighbouring nucleotide moieties within the AON.

Yet even with the 'optimal' enzyme inducing AON at hand, there are disadvantages to an RNase H pathway of RNA destruction, primarily that the enzyme may recognize unstable and partial duplexation arising from the transient binding of the AON to mismatched, non-target mRNA.[32] In fact, non-specific RNA cleavage arising from PS-DNA induced

RNase H activity is considered to be an important contributor to the toxicities associated with this AON class.

Another potential problem that has recently surfaced is the formation of N-truncated proteins arising from the 3'-cleavage product of the transcript. It may therefore be dangerous to over-generalize the *in vitro* effects of all AONs, since gene down-regulation in few instances provides an opportunity for creating stable protein remnants from the 3'-fragment of the partially degraded mRNA transcript, which is still polyadenylated and therefore stable to 3'-exonucleolytic hydrolysis.[170,171] This might be especially problematic in human systems, which are characterized by relatively low levels of 5'-exonuclease activity and therefore are poorly proficient at degrading the poly-A fragment in a 5' → 3' manner. However, mammalian cells have a dedicated decay pathway where poly(A) removal occurs prior to 3' → 5' degradation of the body of the mRNA, as catalyzed by a complex of exonucleases.[172-176] Nevertheless, the poly-A tail of truncated mRNA species is known to support cap-independent translation initiation and as such, has been observed to direct the synthesis of N-terminally truncated versions of the full protein.[170] The biological consequences and deleterious effects – if any – of these remnants are not yet known but imply that adequate analyses of resulting cellular activity is crucial to fully understanding and controlling the antisense assisted target degradation of mRNA by an RNase H pathway of inhibition.

1.12.1. Gene Suppression by RNA Interference

Alternate modes of biochemically induced target destruction may provide a way to side step this potential problem. Indeed, RNA interference (RNAi) by short dsRNA segments (*ca.* 21-23 nt) has fruitfully been explored as a viable method of selectively blocking protein synthesis in an antisense-'like' manner.[58-60] The underlying steps in this mechanism involve RNase III-assisted fragmentation of an exogenously added double stranded RNA (usually > 150 bp) into segments of 'short interfering' RNA duplexes (siRNA) of 21-23 bp which subsequently trigger the degradation of the endogenous mRNA cognates (**Figure 1.15**). Recognition of the cognate strand occurs after incorporation of the siRNA 'guide' sequence into a multicomponent aggregate of nucleases known as the RNA-induced silencing complex (RISC), whereupon the 'guide'

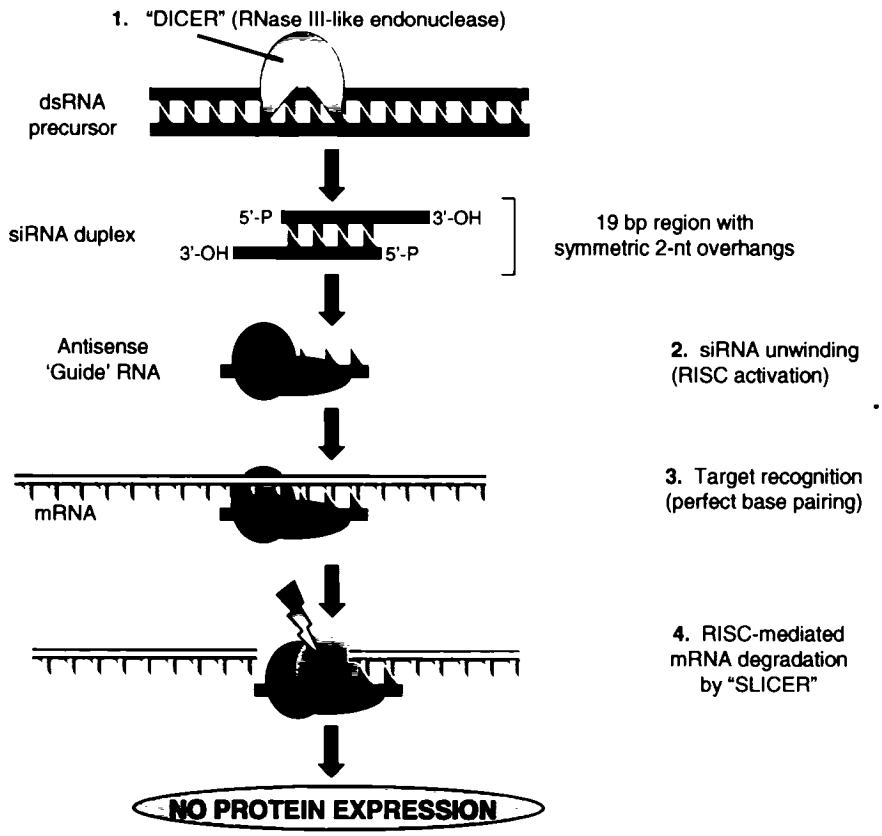

Figure 1.15: Steps in the RISC-mediated gene silencing of cellular mRNA. Exogenous dsRNA in the cytoplasm enters the RNAi pathway, where it is recognized by an RNase III-like endonuclease (Dicer) and cleaved to produce a set of short RNA duplexes. These are then incorporated into the RISC complex and unwound by an ATP-dependent helicase activity to generate the single-stranded antisense 'guide' RNA. The guide strand ultimately serves to hybridize with and direct the destruction of homologous mRNA sequences by the action of an intimate component of the protein complex, termed Slicer. As with RNase H-dependent gene therapies, silencing of the target gene occurs sequence specifically in a catalytic manner. Note however that siRNAs with partial sequence matches may induce translational repression and still down-regulate protein expression (see text for details).

seeks and hybridizes with its complementary target messenger. One of the RISC components, termed "slicer" then catalyzes cleavage of the target mRNA at the center of the base paired region.

Accordingly, two features of siRNA differ from antisense approaches: (i) duplex RNA (not DNA/RNA hybrids) is recognized and (ii) gene inhibition involves RISC – rather than RNase H – to promote recognition and cleavage of the mRNA target. In addition, direct application of siRNAs in gene manipulation via RNAi follows a different set of

molecular guidelines.[177] These include: (a) 5'-phosphorylation at the ends of the siRNA duplex, (b) the presence of a 5'-A/U-rich region, (c) a 2-nt 3'-end overhang, and (d) the ability to form a pure A-form helical structure once bound to the target mRNA. As such, gene interference by RNAi presents a new and important application for many C3'-*endo* biased AONs that are currently inactive by an RNase H assisted pathway of gene suppression.

Also unlike antisense, RNAi occurs posttranscriptionally, and thereby necessitates that exogenous dsRNA be complementary to exon sequences of the target gene in order to elicit inhibition.[178] No suppression occurs when the target sequence involves an intronic segment,[178,179] necessarily limiting the number of genomic regions and/or cellular intermediates within the RNA metabolic pathway that may be accessed. In addition, because the length of the exogenous strands is rather large, these present foreseeable problems toward cell delivery and oligonucleotide uptake. There has also been some evidence pointing to a potential role for this biochemical pathway toward global suppression of cellular protein biosynthesis in mammalian systems, leading to cell apoptosis which may be associated with using RNAi at later stages of cellular differentiation in the organism.[180,181] Thus, while suitable for use in mammalian embryos, the use of dsRNA (100 – 1000 bp) is not universally applicable to all cell lines. This is because as little as one molecule of dsRNA longer than 30 nt can induce the antiviral/interferon response pathway in differentiated somatic cell types. These non-specific effects in many mammalian cells have paved the way for the use of synthetic siRNAs instead (*ca.* 19 – 29 bp in length), themselves long enough to serve as substrates for Dicer yet small enough to evade the interferon response.[58,182] However, recent reports have shown that some siRNAs may still induce the interferon pathway, indicating that improved designs and delivery systems may still be required to overcome this effect.[177]

Mismatches in siRNA can also be tolerated, leading in some cases to an observed phenotype caused by the suppressed expression of off-target cellular proteins.[183] This occurs through a second RNAi pathway involving translational repression of targets with partial complementarity to the siRNA guide.[184] In certain instances, these short RNAs

can affect expression of cellular genes with as many as 3-4 mismatches and additional G-U wobble pairs, the latter of which are recognized as authentic base matches by the RNAi machinery.[185] This documented tendency for non-specific silencing of unintended transcripts will only be controlled once the pathway is better understood.

Nevertheless, while many features of siRNA differ from that of antisense approaches, these two seemingly complementary modes of gene inhibition may share more in common than previously believed. Recent studies have elucidated the crystal structure of a key signature component of the RISC complex, an Argonaute protein better known as Slicer, which participates in the terminal step of the pathway to cleave the duplexed mRNA target.[186] This protein possesses many of the architectural and mechanistic hallmarks of the RNase H family, indicating strong functional similarity despite structurally different nucleic acid substrate requirements. Evidently, much may further be learned by comparisons made between these two classes, pointing to a vital applicability of the knowledge garnered through antisense studies to the RNAi mechanism.

1.13. Thesis Objectives

Antisense oligonucleotides clearly have enormous potential and scope for use in biotechnology and therapeutics. The ability to target and inhibit the expression of individual genes with a high degree of specificity distinguishes oligonucleotide therapy from other treatments in development. However, current AON technology is far from ideal and will likely see much improvement in the coming years. Certainly, innovative designs of newer AON classes with higher safety profiles, coupled with a precise elucidation of the mechanistic features that characterize RNase H – dependent therapies, will likely represent only few of the significant advancements made in the criteria needed for antisense utility.

Our laboratory has had a long standing and intense interest in designing[53,187,188] and defining[54,110,111,113,115,164] the structural properties of synthetic nucleic acids capable of unleashing and exploiting the power of cellular enzymes such as RNase H for effective and selective gene regulation geared toward eventual therapeutic benefits.[163,189] At the same time, we have actively engaged upon expanding the

available knowledge on the substrate specificities of ribonuclease H enzymes in an effort to evolve newer, more potent generations of antisense oligonucleotides.

With this in mind, the chapters of this thesis are structured to build upon and delineate some of the underlying molecular features governing the structural stringency by which RNase H specifically targets RNA destruction of heteroduplexed nucleic acids. Chapter 2 provides the first insights that strategically placed flexible (*i.e.* acyclic) residues within the antisense (DNA or 2'F-ANA) component of enzyme-active double helical substrates may favourably adjust enzymatic recognition and accelerate RNA sense strand hydrolysis within the resultant heteroduplexes. The synthesis, characterization and influence of acyclonucleotides derived from 2',3'-ribose bond disconnections on AON duplexation strength with RNA complements is also explored and contrasted with similar flexibly-designed duplexes hosting a butanediol interresidue connection (*i.e.* anucleosidic unit) at the analogous duplex position. Attempts to rationalize the enzyme acceleratory properties to the added intrinsic backbone plasticity imparted by the acyclic modification of respective AON:RNA hybrids are extensively described, along with their evaluation against a biologically relevant RNA species containing regions of significant secondary structure.

The precise anatomical requirements of localized DNA:RNA flexible anucleosidic regions giving rise to superior RNase H activation and their dynamic effects on hybrid duplex morphology are expanded upon in Chapter 3. Here, we conduct a systematic investigation of the thermal and enzymological properties of AONs containing centrally placed single anucleosidic insertions of various intraresidue lengths, designed to compress or extend the helix backbone at the insertion junction upon duplexation with complementary RNA. Along with related duplex derivatives hosting single modifications in the RNA component of the pair, enzyme susceptibility is assessed in an effort to deduce both the strand-specific influence of the flexible linker and its structure-specific role in driving RNase H-mediated RNA hydrolysis. Associated consequences on both the binding and catalytic activities of the enzyme toward these substrates is revealed, which collectively support a proposed model detailing the likely origins for the observed enhancements.

In Chapter 4, key conformational criteria of established RNase H-competent hybrid substrates are challenged in an effort to extend the utility of the anucleosidic structural effect to poorly-cleaved or enzyme-inactive nucleic acid duplex classes. Accordingly, the inclusion of local flexible elements within duplexes possessing suboptimal macromolecular architectures that span a broader range of the B $\rightarrow$ A conformational spectrum is investigated with respect to the role the anucleosidic site may play in orienting these substrates along the enzyme surface for ultimate target strand scission. We further evaluate the mechanistic basis governing the enzyme-substrate interaction through a series of competitive inhibition experiments aimed at identifying the participation of local amino acids implicated in nucleic acid hybrid processing by RNase H.

CHAPTER 2: SYNTHESIS AND SELECTION OF ENZYME-ACTIVE FLEXIBLE DUPLEXES

2.1. INTRODUCTION – THE NEED FOR AN RNASE H PATHWAY OF GENE INHIBITION

Antisense oligonucleotides (AONs) certainly represent an attractive and promising class of clinically useful compounds that are rationally designed to alter gene expression patterns.[13,190] As more sophisticated methods evolve for their construction, their widespread use in functional genomics, drug target validation, and as human therapeutics may soon be realized.[23,32,191] Prospects for quick and facile customization of a particular AON candidate to suit a diverse range of cellular targets further add to the excitement of this approach. Accordingly, the design of antisense-based therapeutics should be quite feasible without prior knowledge of the protein structure, and immediately accessible with the complete sequence of the human genome now at hand.[192] Yet adequate optimization of the biological properties of chemically-modified AONs is paramount to the success of this and related technologies. Good exo- and endonucleolytic robustness, efficient cell entry, and tight and specific binding with their intended genetic targets in the presence of cellular proteins with minimal residual expression of the target gene,[32] are few of the criteria important for establishing the chemotherapeutic potential of AONs.

Additionally, a desirable mechanism which could provide a catalytic mode of supressing gene activity in eukaryotic cells, relies upon the activity of ribonuclease H (RNase H), a ubiquitous enzyme of many vital intracellular functions.[30,33,193] As previously described, these activities ultimately culminate in the destruction of the RNA component when duplexed with DNA or a suitable AON variant of the latter.[38,42,101] Thus, a single enzyme-active AON can ideally induce the specific destruction of multiple copies of an RNA transcript (*i.e.* AON recycling), and exhibit greater biological activity than those that do not activate RNase H.[13,194,195] Importantly, these events hinge upon presentation of the correct hybrid shape by the substrate duplex to the enzyme for subsequent hydrolysis of the targeted species.[101] To date, however, most AONs lack the appropriate structural attributes for enzyme trigger, and consequently display less than optimal cellular potencies. Indeed, oligonucleotide "gapmer" modifications that combine

intervening enzyme-active AON segments (*e.g.* DNA) with conformationally restricted residues (*e.g.* 2'-O-alkyl RNA) at the periphery may still effect cleavage of their intended targets.[26,37,196] However, these usually focus on preorganizing the antisense strand to adopt a more compatible structure that affords tighter target binding, while compromising high RNase H induction.[71,120,138]

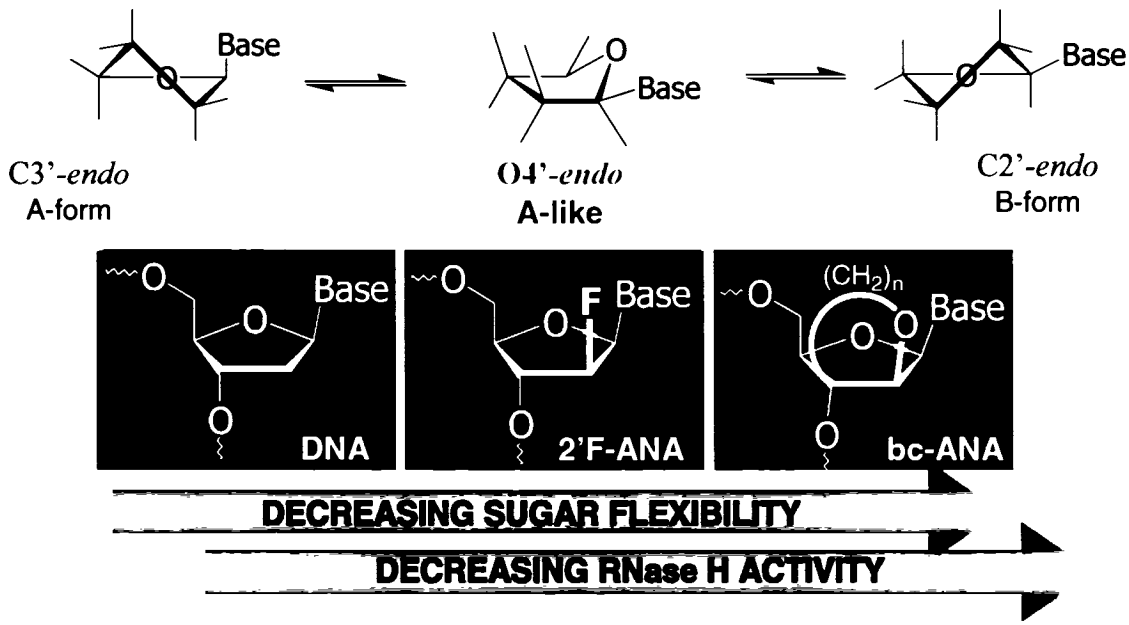

Figure 2.1: RNase H recognition of AON:RNA heteroduplexes depends on antisense sugar pucker, yet with large variabilities within this class. Native deoxynucleotides elicit superior enzyme activity presumably by virtue of the flexible deoxyribofuranose ring, which exists as a diffusely populated mixture of all 3 conformations (*ca.* 40 % O4'-*endo* population).[48] ANA and 2'F-ANA derivatives are more closely clustered toward the O4'-*endo* conformation[113,115] whereas this is the only one available to the locked pseudosugar frame of the bicyclic ANA analogues;[120] n = 1, [3.2.0]bc-ANA; n = 2, [3.3.0]bc-ANA. See chapter **1** for details.

Our previous discovery[53,54,110,111,163] that arabinose-derived AONs (*e.g.* ANA & 2'F-ANA) can induce RNase H degradation of the target RNA species has established that an O4'-*endo* conformation[105,112,117] in the antisense sugar residues is of prime importance for recognition;[113,115,117] yet, other carbohydrate-modified AONs with this same antipodal bias have been unable to sustain any level of enzymatic activity (*e.g.* [3.3.0]bc-ANA; **Figure 2.1**).[119,120,123] As a consequence, pre-organization of the antisense strand, while crucial for maintaining high binding affinity towards

complementary RNA, appears to be detrimental for RNase H activity, even if the antisense strand adopts a "DNA-like" (O4'-*endo*) conformation. A general survey of the trends and conformational properties in various ANA analogues clearly provides evidence for this, and suggests that the inherent flexibility of these sugars profoundly impacts on the ability of the enzyme[113,163] to bind to and recognize hybrids of ANA-derived AONs and RNA (**Figure 2.1**).

2.2. PROJECT OBJECTIVE

As an outcome of the preceding observations, we wished to explore the significance of imparting conformational variability in both the native DNA antisense (**I**) and 2'F-ANA (2'-deoxy-2'-fluoro-β-D-arabinonucleic acid, **II**) to determine whether the insertion of a flexible acyclic residue in a known RNase H-active AON could accelerate the enzymatic degradation. This was accomplished by the systematic introduction of acyclic nucleotides consisting of a 2',3'-secouridine synthon **III** (constructed from a 1-[1,5-dihydroxy-4(*S*)-hydroxymethyl-3-oxapent-2(*R*)-yl]-uracil unit) or a butanediol linker **IV** into either one of the two enzyme-active AON backbone types (**Figure 2.2**). We surmised that this

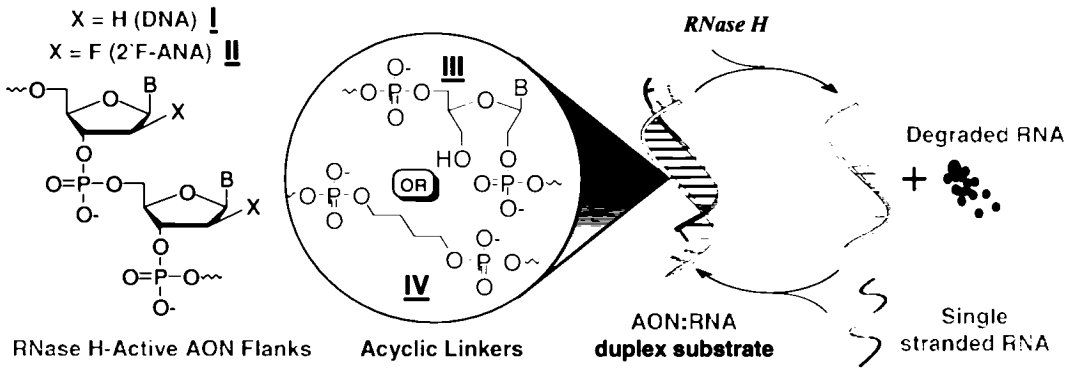

Figure 2.2: Substrate design and RNase H activation of heteroduplexed AON constructs containing acyclic internucleotide units. Central inclusion of a seco-uridine (**III**) or aliphatic butanediol linker (**IV**) within an enzyme-active tract of deoxy- (**I**) or 2'-fluoroarabinonucleotides (**II**) provides localized flexible sites within the helical structure that may render the target more amenable to ultimate hydrolysis.

relatively unconstrained molecular architecture would improve RNase H induction properties as well as afford some insight towards elucidating the structural factors that may provide the 'optimal' AON/RNA substrate. Moreover, such a strategy should enable

us to directly investigate and compare the potential synergistic attributes of intermingling sites of flexibility within the native DNA polymers *vs.* their synthetic 2'F-ANA surrogates, the latter being notably less efficient at activating the enzyme than their unmodified counterparts.

2.3. Chemical Synthesis of Secouridine 2'-Phosphoramidites For Oligonucleotide Assembly

Acyclic nucleosides consisting of a suitably protected 1-[1,5-dihydroxy-4(*S*)-hydroxymethyl-3-oxapent-2(*R*)-yl]-uracil unit (2',3'-seco-nucleosides) for solid phase oligonucleotide assembly were prepared by variations of published protocols. Indeed, the preparation and characterization of these compounds was first described by Khym & Cohn[197] and others,[198,199] who attempted to distinguish between deoxy- and ribonucleosides by final structural confirmation of the latter following a simple oxidation-reduction of the 2',3'-*cis* diol function. Although now known for over 3 decades, most of the available literature has described applications of this initial scheme to functionalizing the ribose sugar precursor as a means of generating the unprotected trihydroxy compounds,[200] which themselves have mostly been limited to study as potential antivirals and as inhibitors of nucleic acid metabolism.[201,202]

Of critical importance to successful oligonucleotide chain incorporation, however, is the selective protection of the 5'-hydroxyl group on the ribose sugar precursor prior to subsequent reactions in order to ensure preservation of chirality at the C4' center on the furanose framework (**Figure 2.3**).[203] Regioselective masking of the primary alcohol function on the uridine precursor (**2.1**) was thus effected by selective monoprotection of the free primary functionality as its monomethoxytritylated (MMT) derivative (**2.2**). As this group is entirely amenable to the conditions of solid phase synthesis (*vide infra*), and compatible with subsequent solution reaction conditions, its early incorporation in the overall reaction scheme should ultimately prevent loss of stereogenicity at C4' during subsequent manipulations of the sugar core. Conversion of the sugar moiety to its C2'-C3' disconnected acyclic derivative then proceeded upon treatment with an aqueous solution of sodium periodate at room temperature to generate an intermediate, unstable dialdehyde. As such, no attempts were made to isolate this compound, which was

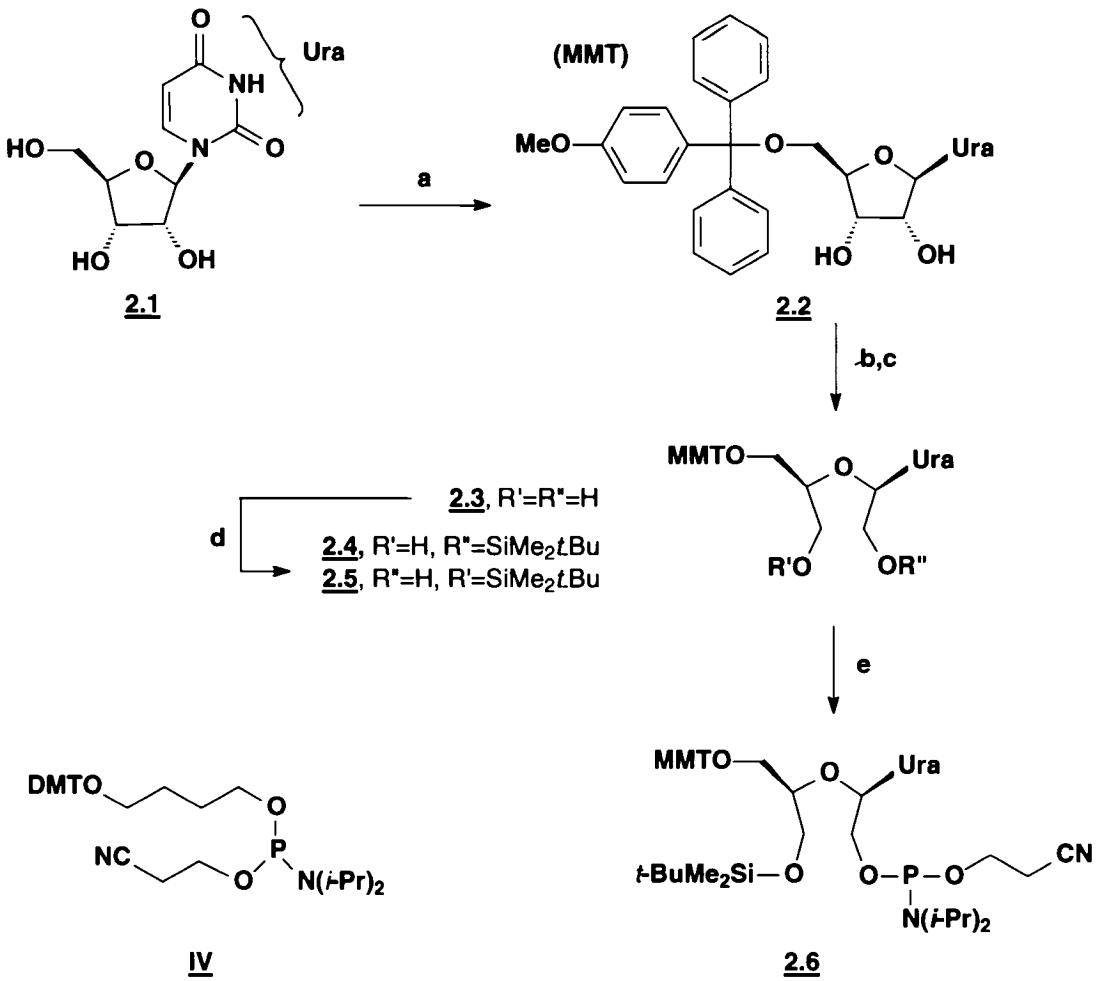

Figure 2.3: Synthetic steps in the chemical conversion of uridine to its 2',3'-disconnected acyclic pseudosugar phosphoramidite derivative, shown alongside the dimethoxytrityl (DMT)-protected 1,4-butanediol phosphoramidite synthon (**IV**; ChemGenes Corp., Ashland, MA). Reactants: (a) MMT-Cl, pyridine (80 %); (b) $NaIO_4$, dioxane, H_2O, 2 h (quantitative); (c) $NaBH_4$, dioxane, H_2O, 15 min (quantitative); (d) *t*-BDMS-Cl, $AgNO_3$, THF, 24 h (**2.4**, 22 %; **2.5**, 14 %); (e) Cl-P(OCE)N(*i*-Pr)$_2$, DMAP, EtN(*i*-Pr)$_2$, THF, 2.5 h (99 %).

immediately reduced *in situ* following the addition of sodium borohydride to the reaction medium, ultimately generating two primary hydroxyl functions on the acyclosugar (**2.3**) under alkaline conditions (pH 10 – 11). As these reactions generally proceed with extremely high efficiency, complete conversion of the starting material to the acyclic pseudosugar can be realized, which thereby circumvents the need for tedious chromatographic purifications following the reaction work-up. Accordingly, direct monoprotection of either of the free hydroxyl functions of **2.3** was subsequently achieved

nonselectively in a solution of *t*-butyldimethylsilyl chloride, added dropwise at an equimolar ratio to a cooled (0°C), dilute solution of nucleoside, primarily in an attempt to maximize the product distribution in favour of the monosilyl regioisomers (**2.4** & **2.5**). Despite these precautions however, this step proved to be particularly problematic as much of the starting compound was converted to its disilylated derivative while a significant portion of diol (**2.3**) remained unreacted. Of note, the reaction system employed in this work (*i.e.* *t*-BDMS-Cl in THF/$AgNO_3$/pyridine), when used upon the natural 5'-protected ribonucleosides, yields good selectivity for the 2'- over the 3'-hydroxyl function and typical combined yields of *ca.* 80% of the monosilylated product can be attained.[204-206] However, monoderivatization of primary diols is known to be significantly challenging, owing in part to the difficulty in differentiating between the two chemically equivalent and relatively unhindered primary hydroxyl groups.[207]

We have likewise found this to be the case with the corresponding acyclic (2',3'-seco) adenine and cytosine-containing dihydroxy analogues, for which similar studies as with **2.3** have yielded essentially the same outcome despite the use of a variety of reaction conditions and solvents designed to optimize the monoprotection reaction[207-209] (data not shown). Although a DMSO/imidazole system ultimately proved quite successful for the adenine analogue, yielding 27% and 36% isolated yields for the 2'- and 3'-silylated isomers respectively (63% combined *vs.* unoptimized yields of less than 20%) with negligible amounts of disilyl product formed, these conditions proved unsuccessful when implemented to the uridine series. Further complicating this step was the consequent difficulties encountered upon separating the two regioisomers using typical flash column elution conditions applicable to the standard monosilylated ribonucleosides.

Fortunately however, the secouridine regioisomers (**2.4** & **2.5**) could rapidly be resolved and both starting material and side product cleanly recovered following flash column purification using a 25% gradient of acetone in dichloromethane, with the latter recycled back to the dihydroxy compound upon short treatment with tetra-*n*-butylammonium fluoride (TBAF).[204,210] This scheme essentially provided the most efficient method of regenerating the more useful starting diol from the unwanted disilyl product, which could then be used to ultimately reproduce the desired monoprotected products.

A final step involving phosphitylation of the remaining hydroxyl moiety on **2.5** and

complete conversion to its respective phosphoramidite (**2.6; Figure 2.3**) thus provided a straightforward synthetic route to the corresponding antisense molecule, which was subsequently obtained by conventional solid phase protocols (see **section 2.3.2.**).

2.3.1. Structural Characterization of Secouridine Nucleosides

To prove the structure of the 2',3'-secouridine nucleoside **2.3**, the newly synthesized compound was subjected to 2D-NMR and Fast-Atom Bombardment mass spectrometry (FAB-MS) analyses, both of which demonstrated distinct spectral differences from those of the parent ribonucleosides (**2.2**). The structural characterization of **2.3**, as verified by establishing ^{1}H-^{1}H homonuclear correlations within the acyclosugar framework, is illustrated in the corresponding COSY spectrum shown in **Figure 2.5**, which also served as a sufficient means of assessing the purity of the compound. Immediately identifiable from this data is the presence of a nonexchangeable triplet centered at 5.8 ppm, corresponding to H1' on the acyclosugar, itself split by the appended H2' and H2" protons at the adjacent 2'-carbon. By contrast, H1' in the ribonucleoside precursor (**2.2**) appears as a doublet (**Figure 2.4**), owing to the presence of only a single appended proton at the analogous adjacent position, thus providing the first evidence of a precise disconnection between the 2',3'-bond in the pseudosugar moiety of **2.3**.

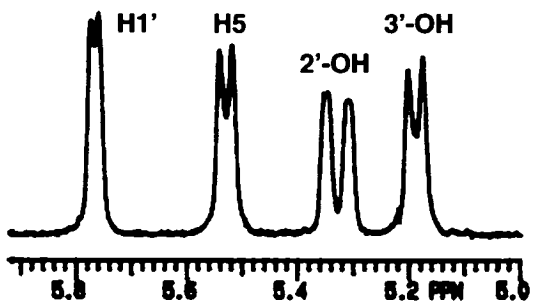

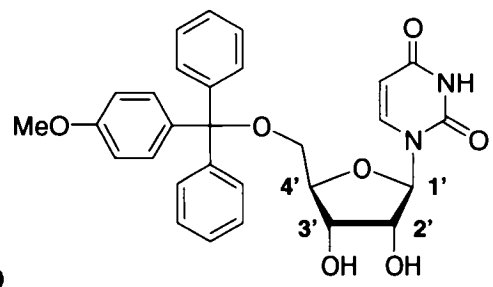

2.2

Figure 2.4: Expansion of the anomeric region in the ^{1}H-NMR spectrum of **2.2**, taken at 200 MHz using DMSO-d_6 as solvent.

Further tracing through the spectrum of **2.3** reveals an isolated network of correlations among H1', H2' & H2" and the 2'-hydroxyl protons, as well as a second network of proton couplings running along the C3' to C5' portion of the molecule (**Figure 2.5**).

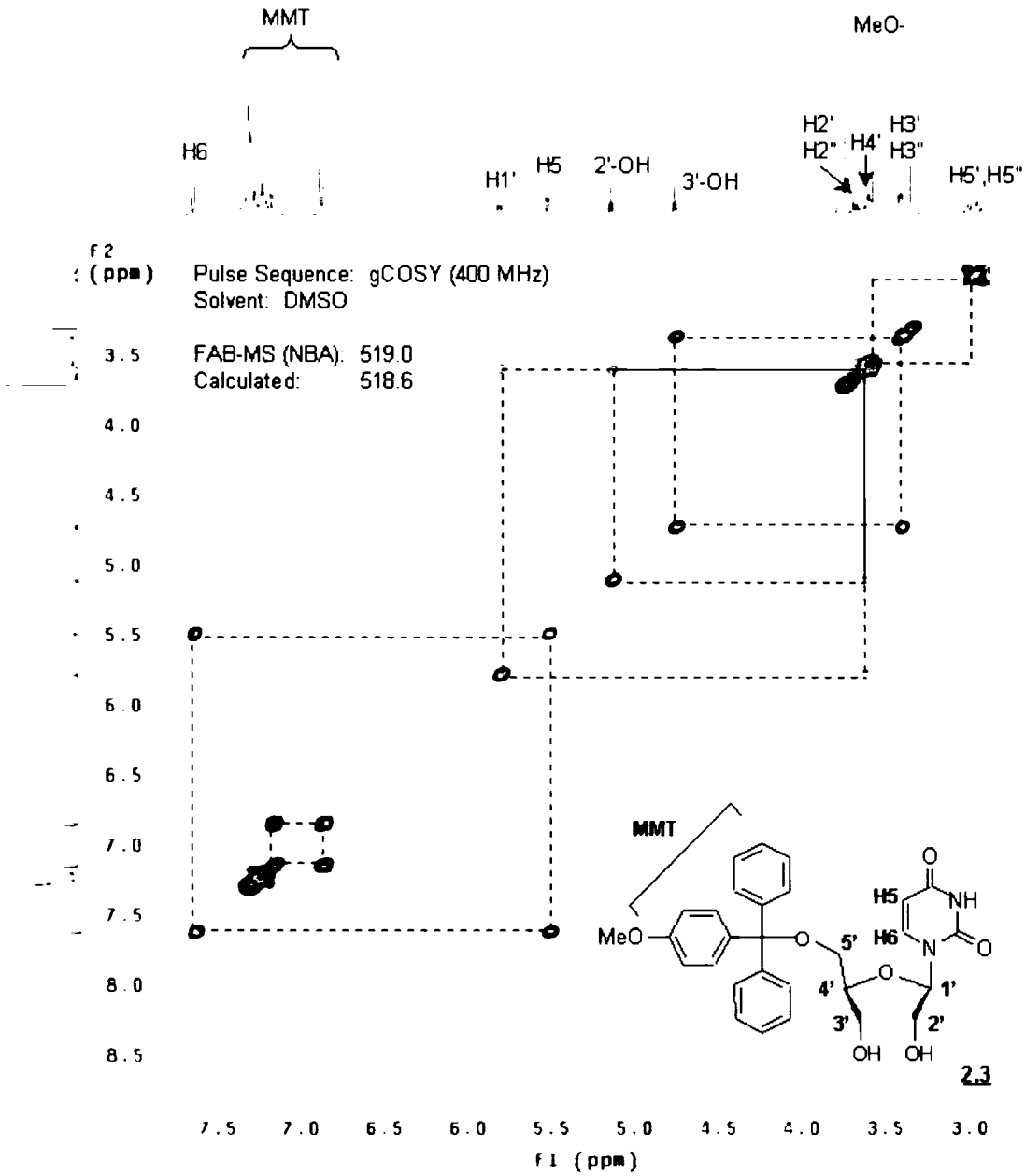

Figure 2.5: Structural characterization of the 2',3'-disconnected uridyl sugar derivative (**2.3**). The 1D proton spectrum (400 MHz, DMSO-d_6) is plotted along each axis, with peak assignments given at top corresponding to the identification of peaks off the diagonal in the grid below. For simplicity, the traditional numbering system of the natural nucleosides is preserved in the acyclic analogue in order to underline their similarities.

Along with the appearance of 2 distinct exchangeable triplets at 5.1 and 4.75 ppm arising from 2'- and 3'-hydroxyl protons respectively, both of which undergo moderate exchange in acetone-d_6 with concomitant peak broadening arising from the coalesced signals, these data collectively substantiate the structure and assignment of **2.3** as that of the 2',3'-secouridine dihydroxy derivative. Molecular weight determination by FAB-MS also gave values in strong agreement with those calculated, further confirming the existence and isolation of this molecule.

In a similar fashion, the 2'- and 3'-silylated regioisomers of **2.3** were distinguished on the basis of ^{1}H-^{1}H COSY cross-peak correlations, again used to demonstrate the connectivity of the protons in the acyclosugar. In both spectra, the H1' protons are split by the nonequivalent H2' and H2" protons into a doublet of doublets which suggests a certain degree of structural rigidity around the C1'-C2' bond, likely imparted by the presence of the bulky *tert*-butyldimethylsilyl group. More significantly, a single well-resolved hydroxyl peak is observed for both **2.4** and **2.5** in DMSO-d_6, which negates rapid chemical exchange of these moieties. As a result, the effect of the protons at C2' of **2.5** is transmitted to the 2'-hydroxyl proton which in turn appears as an overlapping doublet of doublets. In **2.4**, splitting of the hydroxyl peak is also observed, however it shows correlations with H3' and H3" and therefore rules out the presence of a silyl group at the 3'-position. Taken together, these data along with mass spectral characterizations confirmed the assignment of **2.4** and **2.5** as the 2'- and 3'-monosilylated isomers, respectively (see **section 6.7.1.**).

2.3.2. Solid-Phase Synthesis of DNA and 2'F-ANA Oligonucleotides with Acyclic Inserts

Oligodeoxy-, ribo- and 2'-fluoroarabinonucleotides were synthesized by standard phosphoramidite methodology[206,211,212] on an automated DNA synthesizer using the appropriate monomers for each step of the cycle (*e.g.* DNA, or 2'F-ANA phosphoramidite synthons with **2.6** or commercially available **IV**). The 2'-fluoroarabinonucleoside phosphoramidites required for this task were synthesized and graciously provided by Dr. Katya Viazovkina of the Damha laboratory. Indeed, not only these, but virtually all types of nucleic acid chemistries and modifications may suitably be

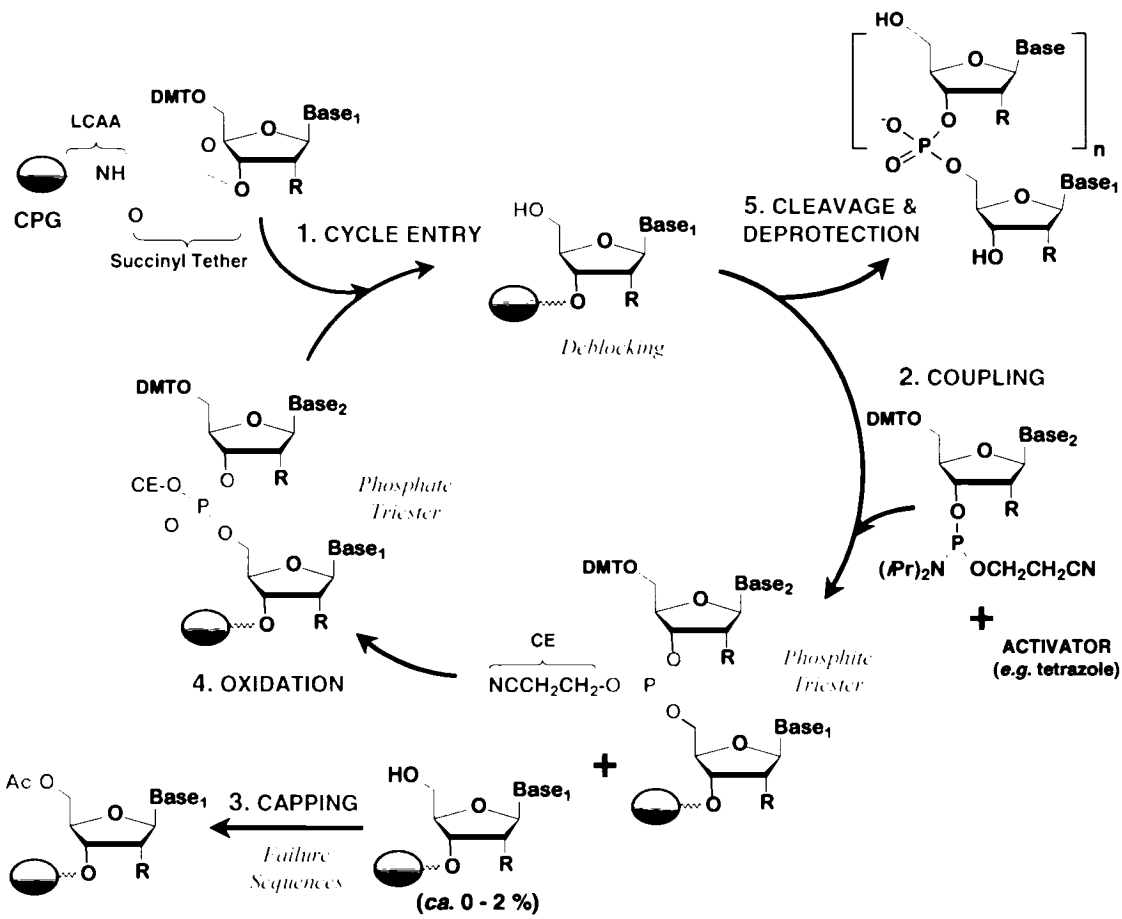

Figure 2.6: Automated solid phase oligonucleotide synthesis cycle via phosphite triester chemistry, showing the key steps necessary for successful chain extension. Cycle entry is initially preceded by manual attachment of an appropriately protected nucleoside to a solid support, followed by capping to ensure masking of free hydroxyl sites on the CPG surface. Synthesis then proceeds by sequential detritylation of 5'-MMT or DMT protecting groups (step 1); phosphoramidite-mediated extension of the oligonucleotide (step 2); capping of unreacted failure sequences (step 3); and oxidation of the trivalent internucleotide phosphite linkage (step 4). Final cleavage from the support and deprotection of the assembled oligomers after n repetitions of the cycle completes the synthesis (step 5). CPG, controlled pore glass; LCAA, long-chain alkylamine; R = H, DNA; R = OH, RNA; R = F (β-orientation), 2'F-ANA.

implemented as synthons in the construction of oligonucleotides by the phosphoramidite approach. The general scheme allowing automated coupling, chain extension and deprotection of the desired nucleic acid is shown in **Figure 2.6**, whereby chain assembly is carried out by the stepwise addition of an excess of phosphoramidite building block to nucleoside or nucleotide hydroxyl termini pre-immobilized on a solid support until the

relevant sequence is obtained.

Briefly, each cycle is initiated upon acid-catalyzed detritylation and unmasking of the 5'-hydroxyl moiety of a CPG-tethered terminal residue in a solution of 3 % trichloroacetic acid in dichloroethane, followed by its quick and almost quantitative coupling with an incoming, activated nucleoside phosphoramidite (step 2). The efficiency of this and successive couplings is conveniently monitored by spectroscopic quantification of liberated trityl cations, and typical coupling yields of 98 – 99 % per cycle can generally be realized. For the small fraction of incomplete sequences still present however, a subsequent acetylation, or 'capping' step ensues, specifically to block any remaining unreacted support-bound hydroxyl termini from participating in future couplings. This precautionary step ultimately serves to minimize the growth of shorter oligomers that may otherwise contaminate and complicate isolation of the final pure product.[213] Oxidation of the newly formed internucleotide phosphite triester linkage[214,215] is next accomplished by exposure of the reaction column contents to an aqueous solution of iodine and pyridine in THF to afford the more stable pentavalent phosphate triester (step 4). Accordingly, numerous repetitions of this scheme are conducted until the desired length of oligonucleotide is obtained, with full-chain synthesis of species as long as 20 nts generally deemed complete in a mere matter of hours.

For our purposes, the assembly of 2'F-ANA sequences was conducted under virtually identical conditions as for DNA sequences, but longer coupling times for the former (*ca.* 10 fold) were required to ensure comparable stepwise efficiencies. The coupling efficiencies of each of the acyclic phosphoramidites typically exceeded 99%, as monitored by the release of the mono- or dimethoxytrityl cations (λ_{max} = 478 nm for MMT^+; 504 nm for DMT^+) after each monomer addition with no need to optimize the standard coupling times to accommodate the differential reactivities of these specialized synthons. Newly synthesized oligonucleotides were cleaved from the solid support, with phosphate and exocyclic amino protecting groups on the nucleobases concomitantly removed under basic conditions (*i.e.* aqueous ammonia solution; see **section 6.3.2.**). For oligoribonucleotides or secouridine-containing AONs, additional deprotection of the *tert*-butylsilyl ethers was effected by treatment with triethylamine-trihydrogen fluoride (TREAT-HF)[216] to release the masked hydroxyl groups. This step is necessarily

performed last to ensure complete compatibility with the relatively labile internucleotide phosphodiester linkages which are otherwise susceptible to strand breaks via neighbouring group 2'-hydroxyl participation when in a basic environment.[217]

A final purification of the naked oligomers was undertaken using polyacrylamide gel electrophoresis (16 – 20 % PAGE with 7 M urea added as denaturant) and/or anion exchange HPLC, followed by desalting of the oligonucleotides after gel or chromatographic isolation to complete the procedure. Analytical amounts of the purified material were separately analyzed by either of these techniques to confirm sample purity, and oligonucleotide compositions subsequently verified by Time-of-Flight Matrix Assisted Laser Desorption mass spectrometry (TOF MALDI-MS), which demonstrated only negligible deviations between the calculated masses and those measured for each oligomer (**section 6.7.1.**).

2.4. Preparation and Analysis of DNA & 2'F-ANA AON Heteroduplexes with RNA: Thermal and Enzymatic Properties of "Flexible" Hybrids

To accumulate a comparative picture on the biophysical properties of the newly synthesized strands, the UV thermal denaturation profiles for each of the preformed AON:RNA duplexes was first evaluated, using conditions mimicking the physiological environment. Prior to their assessment, AON and complementary target RNA oligonucleotides were mixed in equimolar ratios in 140 mM KCl, 1 mM $MgCl_2$, and 5 mM Na_2HPO_4 buffer (pH 7.2), to provide a total duplex concentration of *ca.* 2.5 μM. All samples were heated to 90°C for 15 min to ensure full dissociation of any partially bound species in solution, then cooled slowly to room temperature, and stored at 4°C overnight before taking measurements in order to promote maximal annealing of complementary strands. The homogeneous AON/RNA duplex solution was then exposed to increasing temperature at 1 minute intervals (0.5°C/measurement), and the UV absorbance at 260 nm was determined after temperature equilibration at each increment. From the resulting temperature *vs.* absorption profiles, hybrid thermal melting (T_M) values corresponding to the absolute temperature at which approximately half of the duplex population has dissociated to the single-stranded state, could then be extracted. These data are reported

Table 2.1: Sequence Anatomies, Melting Temperatures (T_M) and Relative RNase H-Mediated Hydrolysis Profiles for the AON/RNA Heteroduplexes[a]

Entry	Sequence type[b, c] (5'±3')	T_M (°C)	ΔT_M	Rates (k_{rel}) of enzyme cleavage[d]
	(i) DNA			
2.1	ttt ttt ttt ttt ttt ttt	39	---	1
2.2	ttt ttt ttt Btt ttt ttt	33	-6	2.7
2.3	tta tat ttt ttc ttt ccc	53	---	1
2.4	tta tat ttt Btc ttt ccc	48	-5	3.4
2.5	tta tat ttt ctc ttt ccc	40	-13	0.7
2.6	tta tat ttt B ttc ttt ccc	48	-5	2.5
	(ii) 2'F-ANA			
2.7	TTT TTT TTT TTT TTT TTT	53	---	1
2.8	TTT TBT TTT TTT TTT TTT	49	-4	0.6
2.9	TTT TTT TTT BTT TTT TTT	47	-6	7.9
2.10	TTT TTT TTT TTT BTT TTT	49	-4	5.1
2.11	TTT TTT TTT STT TTT TTT	47	-6	1.6
2.12	TTT TTT TTS STT TTT TTT	42	-11	2.8
2.13	TTA TAT TTT TTC TTT CCC	64	---	1
2.14	TTA TAT TTT BTC TTT CCC	55	-9	3.5
2.15	TTA TAT TTT CTC TTT CCC	55.5	-8.5	0.9
2.16	TTA TAT TTT tTC TTT CCC	63	-1	1.6
2.17	TTA TAT TTT B TTC TTT CCC	57	-7	2.3

[a]Aqueous solutions of 2.38 x 10^{-6} M of each oligonucleotide, 140 mM KCl, 1 mM $MgCl_2$, 5 mM Na_2HPO_4 buffer (pH 7.2); all measurements were obtained in triplicate with an uncertainty in T_M of ±0.5°C. [b]Upper case letters, 2'F-ANA nucleotides; lower case letters, deoxynucleotides; C, arabinofluorocytidine or c, deoxycytidine mismatch residue; B, butanediol linker; S, 2'-secouridine insert. [c]Target RNA sequences correspond to rA_{18} (sequence code # **2.23**), or 5'-r(GGGAAAGAAAAAAUAUAA)-3' (sequence code # **2.24**). [d]Human enzyme; relative rates shown are those obtained at 22°C and have been normalized according to the parent strand of each series.

in **Table 2.1**, as calculated using the first derivative method with an associated uncertainty of ± 0.5°C following three independently executed measurements.

2.4.1. Purification of RNase H Isotypes and Induction Assays

Along with the hybridization behaviour of AON:RNA heteroduplexes, these studies assessed the effect of one or more acyclic linker inserts on enzyme activity. Both bacterial (*E. coli*) and human sources of RNases H were cloned, purified and kindly provided by Dr. Kyung-Lyum Min from the Damha laboratory while under the supervision of Dr. Michael Parniak at the Lady Davis Institute (Montreal, QC; see **section 6.5.2**), with subsequent results described in this chapter also obtained with his assistance. RNase H induction assays were carried out at 14-15°C and/or room temperature (*ca.* 22°C), with the exception of *HRAS*-derived sequences (**section 2.6.**) in which assays were conducted at 37°C. Nucleic acid duplex substrates were prepared by mixing the AONs (3 pmol) with 5'-^{32}P-labeled complementary target RNA (1 pmol) in 10 µL of 60 mM Tris-HCl (pH 7.8) containing 60 mM KCl and 2.5 mM $MgCl_2$, followed by heating at 90°C for 2 minutes and slow cooling to room temperature. Duplex substrate solutions were allowed to stand at room temperature for at least 1 h prior to use. Reactions were then initiated by the addition of human RNase H1 or *E. coli* RNase H1, and aliquots were removed at various times and quenched by the addition of an equal volume of 98% deionized formamide containing 10 mM EDTA, 1mg/mL bromophenol blue and 1 mg/mL xylene cyanol. After heating at 100°C for 5 min, reaction products were resolved by electrophoresis on 16% polyacrylamide sequencing gels containing 7 M urea, visualized by autoradiography, and product formation was quantified by densitometry. **Table 2.1** summarizes the relative propensities (k_{rel}) by which each of the AONs affects the rate of target strand RNA hydrolysis by human RNase H, as extracted upon analysis of each of the respective degradation reactions. The initial cleavage rates reported are those obtained from the slope of the best fit line for the linear portion of the plot representing the amount of cleaved RNA over time, which comprised in general, data from at least four time points (see **section 6.6.3.**).

2.5. Results and Discussion

(A) Duplexation Studies. In assessing the thermal behaviour of the AONs, it has been noted without exception that a drop in hybrid stability is characteristic of all strands with single acyclic inserts (**Table 2.1**). While this was expected for butyl-containing AONs (*e.g.* entries **2.7** *vs.* **2.9**), we were nonetheless surprised to find that the 2',3'-secouridine containing 2'F-ANA surrogates (sequence **2.11**, constructed using acyclic synthon **2.6**; **Figure 2.3**) offered no improvement in binding affinity towards the complementary RNA target relative to the former. The effect was approximately additive upon incorporating a second secouridine residue (**2.12**), suggesting minimal base pairing and/or interresidue base stacking with the opposing helical ribonucleotide at this location. The extent to which the linkers were destabilizing was also contingent upon base sequence, *i.e.*, mixed 2'-fluoroarabino sequences with the butyl linker (**IV**; **Figure 2.3**) were *ca.* 3°C more destabilizing than their homopolymeric counterparts upon duplexation (entries **2.9** & **2.14**; **Table 2.1**). Single substitutions were also less tolerated at the center (**2.9**; ΔT_M = -6°C) as opposed to the ends of these heteroduplexes (**2.8** & **2.10**; ΔT_M = -4°C), which is an expected and recurrent phenomenon[150,154] that is likely manifest from end-fraying of the duplex, the effects of which partially suppress the magnitude of the destabilization. Interestingly, placement of a C-A mismatched base pair in either of the mixed sequence AON backbones significantly destabilizes their hybrids with RNA, with the deoxy sequence (**2.5**) proving less competent toward retaining adequate target avidity as compared to the 2'F-ANA complements (**2.15**). Furthermore, only modest destabilization occurs upon insertion of one deoxynucleotide in the all-2'F-ANA mixed sequences (entry **2.16**), which is consistent with the notion that the 2'-fluoroarabino residues enhance thermal stability via relatively greater rigidity at the nucleotide level leading to consequent strand preorganization over the native deoxynucleotide residues, yet do not perturb the stereoregular structure of the AON to any appreciable degree.

(B) RNase H Assays. Fortunately, the destabilization introduced into the AON by the acyclic linkers is largely outweighed by the high stabilization afforded by the rigid 2'F-ANA backbone. Indeed, when linked to a proven RNase H-competent analogue, *e.g.*, 2'F-ANA, an acyclic insert in the middle of an 18-nt oligomer enhances RNase H-

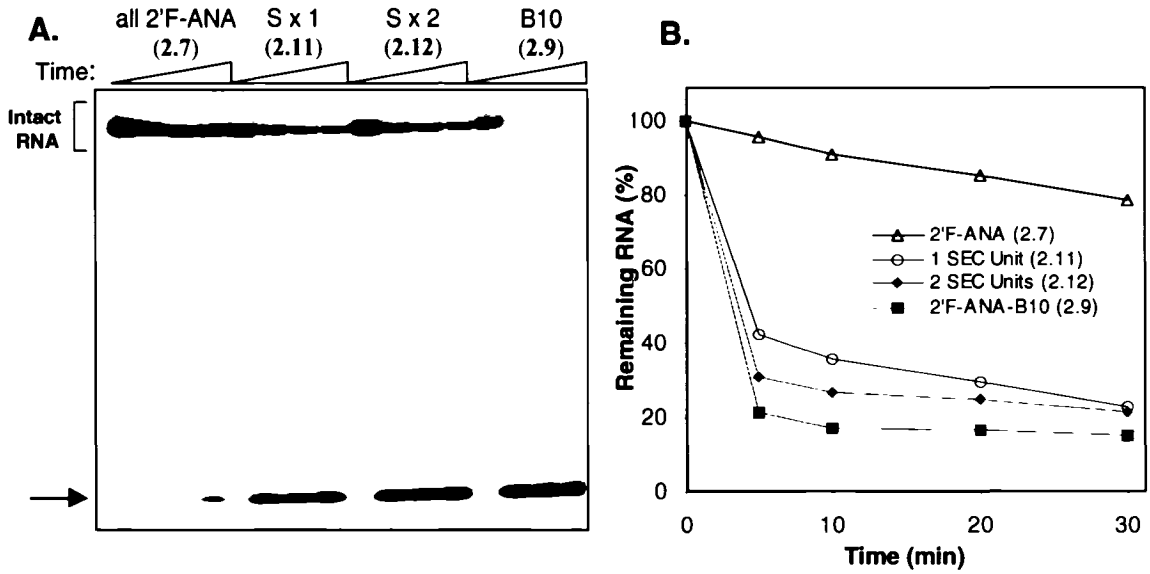

Figure 2.7: Flexible inserts in 2'F-ANA enhance RNase H-mediated degradation of the duplexed RNA component. **A.** PAGE results showing enzyme cleavage of 5'-^{32}P-end labeled RNA. Assays comprised 1 pmol of target 5'-[^{32}P]-rA_{18} and 3 pmol of test AON in buffer (10 μL) consisting of 60 mM Tris-HCl (pH 7.8), 2 mM dithiothreitol, 60 mM KCl, and 2.5 mM $MgCl_2$. Reactions were started by the addition of human RNase H1 (22°C; lanes represent 0, 5, 10, 20, and 30 min time points); the arrow indicates coalesced 5'-scission products obtained from multiple cleavages within the same duplexed target strand. **B.** Quantification of the remaining full-length [^{32}P]-RNA signal, obtained by UN-Scan-It digitizing software (Silk Scientific Inc.; Orem, UT).

assisted sense strand hydrolysis (**Figure 2.7**). Moreover, a second contiguous insert amplifies the effect, whereas the incorporation of a single butanediol insert in the middle of the same sequence potentiates the targeted destruction of the AON-chimera:substrate duplex even further, as much as *ca.* 8-fold relative to the uniformly modified control AON (**Table 2.1**, *e.g.* **2.7** and **2.9**). This methodology is entirely applicable in DNA backbones as well, in which the relative rate enhancements easily approach a 3-fold improvement in target degradation over the native strands (*e.g.* **2.1** *vs.* **2.2**; **2.3** *vs.* **2.4**). The enhancement in rate, coupled with a distinct cleavage pattern upstream of the site of the inserts in the AON, is also apparent in mixed sequence 2'F-ANA analogues (*vide infra*), suggesting the generality of the structural effects on the conformational discretion of the human enzyme.

A possible, yet partial, explanation for the elevated RNA degradation may owe to an increased turnover efficiency of the enzyme for the linker-modified duplexes, which may arise from an enhanced rate of dissociation for these hybrids over their thermostable

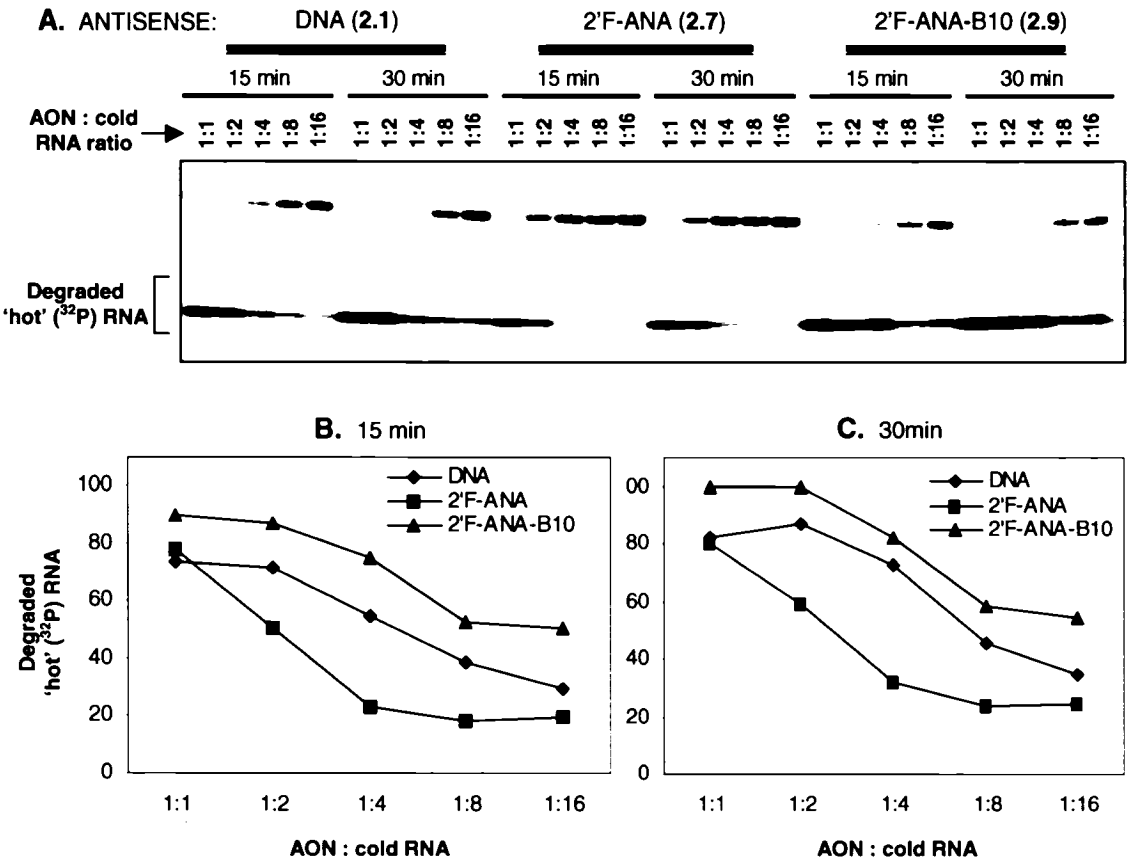

Figure 2.8: RNase H degradation of AON:RNA heteroduplexes in the presence of increasing amounts of nonlabeled ('cold') RNA in the reaction mixture. Turnover experiments were performed by varying the concentration of 'cold' rA_{18} (1 – 16 pmol) in the presence of 0.05 pmol of 5'-^{32}P labeled ('hot') rA_{18}, and 1 pmol of dT_{18}, 2'F-ANA or 2'F-ANA-B10 oligothymidylates as antisense oligonucleotide, respectively. After the addition of human RNase H1, samples were incubated for 15 or 30 min at room temperature and then quenched with an equal volume of gel loading dye. RNase H-generated degradation products were electrophoretically resolved (14% acrylamide sequencing gels containing 7 M urea), visualized by autoradiography (Kodak XOMAT film), and quantified by densitometry. Panels **B** and **C** indicate the amount of cleaved RNA product obtained with the different AONs at 15 and 30 minute time points.

counterparts (*e.g.* ΔT_M = -9°C for **2.14** versus **2.13**). For instance, 2'F-ANA, which forms stronger duplexes, exhibits reduced turnover relative to DNA and 2'F-ANA-B10 hybrids and therefore might partially seem to accommodate such a trend (**Figure 2.8**). This is evidenced by a relatively greater attenuation in the amount of cleaved 'hot' ^{32}P-RNA upon increasing the amount of unlabeled target species in the reaction mixture, specifically with the contiguous 2'F-ANA homopolymeric sequences (panels **B** and **C**;

1:1 → 1:2 ratios of AON:cold RNA). On the other hand, the activity is diminished in mismatched DNA and 2'F-ANA AON mixed sequences, where a respective deoxy- or arabinofluorocytidine mismatch replaces the butyl linker (**Table 2.1**, entries **2.5** and **2.15**). Because the mismatch also induces an equivalent (2'F-ANA) or larger (DNA) drop in duplex thermal stability relative to the butyl insertion, it appears that increased turnover is simply not the sole basis for preferential enzyme discrimination towards the flexible AONs in these examples. Quite possibly, residual activity may be retained in mismatched sequences by virtue of this characteristic alone (*i.e.* increased turnover arising from faster duplex dissociation events), which could conceivably become operative in segments of partial complementarity.

2.5.1. Linker Position in 2'F-ANA:RNA Hybrids

In order to examine the relevance of enzyme turnover efficiency and of the actual cleavage event in other contexts, AONs with butyl linker **IV** at various positions along the double helix were next prepared to determine whether optimal activity might depend upon the exact site of the acyclic insertion unit (**Table 2.1**; 2'F-ANA sequences **2.7** – **2.10**). Moreover, this strategy should lend further credibility to the precise pattern and rate of cleavage that accompanies the movement of the linker along the 2'F-ANA backbone (*vide infra*). Close inspection of the autoradiogram in **Figure 2.7** reveals that the exact location of RNase H – executed primary cuts on the RNA strand is difficult to measure under ambient temperature for the homopolymers, which were now known to be good substrates for the enzyme. As we were more interested to see where the first cuts were occurring, this information was instead extracted from assays conducted at a lower temperature (**Figure 2.9**), under which enzyme activity was retarded just enough to enable a qualitative comparison on the preferred cleavage modes toward each substrate. At higher temperatures, the pattern becomes less interpretable as it results from the superimposition of multiple cleavages on a single target by the enzyme (see **Figures 2.7 & 2.8**). As such, when the assay temperature is dropped from ambient to 14 – 15°C, a distinct pattern of cleavages emerge for each set of modified 2'F-ANA substrates that seems to corroborate intrinsic differences in the initial mode of the enzyme-substrate interaction (**Figure 2.9**) as experienced by these hybrids when incubated with RNase H.

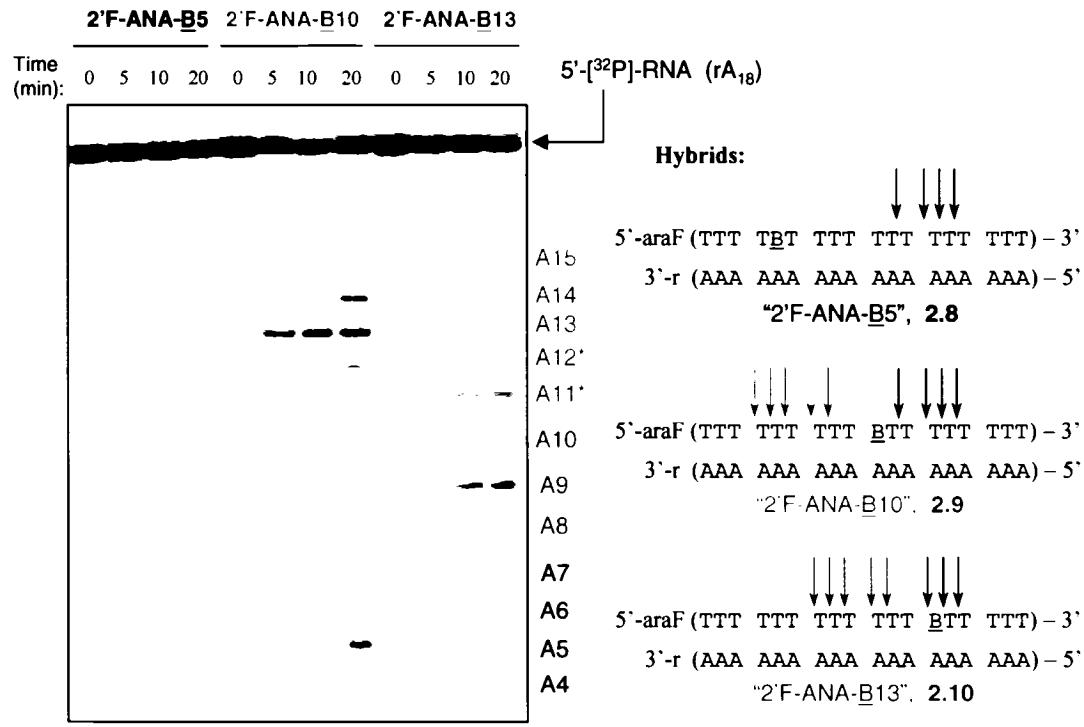

Figure 2.9: Gel (PAGE) showing linker-dependent human RNase H1 mediated hydrolysis patterns of duplexes. Assays (10 μL final volume) comprised 1 pmol of 5'-[^{32}P]-target RNA and 3 pmol of test oligonucleotide in 60 mM Tris-HCl (pH 7.8, containing 2 mM dithiothreitol, 60 mM KCl, and 10 mM $MgCl_2$. Reactions were initiated by the addition of RNase H and carried out at 14-15°C for 20 minutes. Lengths of the RNA fragments generated via enzyme scission and corresponding position along the AON are indicated. The asterisk along rA_{12} and rA_{13} RNA fragments denotes common cleavage sites for both B10 and B13 heteroduplex substrates.

We observe an overall enhancement in target degradation in the order of 2'F-ANA-B10 (**2.9**) > 2'F-ANA-B13 (**2.10**) > 2'F-ANA (**2.7**) > 2'F-ANA-B5 (**2.8**). Furthermore, all of the butyl-containing AONs induce additional primary cuts at the 3'-end of the RNA except for 2'F-ANA-B5, which coincidentally, is the only AON superseded in rate by all-2'F-ANA. As such, the B5 and B13 homopolymeric substrates show large differences in activation potencies, in spite of the fact that their sequences are virtually identical and equally thermostable, yet with opposite directionalities with respect to the butyl site in the AON (see **Table 2.1**). Indeed, the different activities of these two compositions contrast their thermal and structural similarities, and suggest a minor – if not absent – role for the turnover effect. The diminished rate enhancement in the AON with butyl at position 5

might alternatively reflect the remote positioning of RNase H along the substrate, which is known to bind near the 3'-end of the AON in the hybrid duplex[218] and so may be unaffected by the butyl insertion. This does not explain, however, why there is a reduction in the relative degradation rate of this duplexed AON:RNA species as compared to all-2'F-ANA counterparts, although an adverse effect on the catalytic activity of the enzyme – which initiates cleavage at downstream RNA segments with respect to binding along the hybrid – may be accountable.

2.5.2. 2'F-ANA *vs.* DNA in Human and *E. coli* Enzyme Homologues

The above findings thus far prompted us to explore the activating potential of the purely artificial 2'F-ANA constructs directly to those of systems mainly incorporating the native deoxyribose residues in the antisense strand. While a mismatching residue in either DNA or 2'F-ANA mixed base sequences imposes a negligible effect on the overall enzyme hydrolytic efficiency as compared to the parent AONs, (*e.g.* **2.5** *vs.* **2.3** & **2.15** *vs.* **2.13**; **Table 2.2**) a substantial acceleration in degradation rate is readily achieved by sequences incorporating a modest degree of flexibility in the antisense strand. For example, substitution of a central arabinofluoro residue in 2'F-ANA **2.13** with a more flexible

Table 2.2: Relative Rates of RNA Target[a] Degradation Among Mixed Sequence DNA and 2'F-ANA AON Constructs

Entry	Sequence Type[b]	k_{rel} (human)[c]	k_{rel} (*E. coli*)[c]
2.3	DNA	4.6	8.8
2.5	DNA-c10	3.3	7.1
2.13	2'F-ANA	1.0	1.0
2.14	2'F-ANA-B10	3.5	1.4
2.15	2'F-ANA-C10	0.9	1.3
2.16	2'F-ANA-t10	1.6	2.6

[a]Target RNA: 5'-r(GGG AAA GAA AAA AUA UAA)-3'. [b]AON sequences are abbreviated as follows: c10, C10, B10 and t10 denote deoxycytidine, arabinofluorocytidine, butyl or deoxythymidine residue in place of the 10th nucleotide in the mixed sequence AON, respectively; complete descriptions are given in **Table 2.1**. [c]RNase H assays were conducted at 22°C; rates are normalized according to the all-2'F-ANA AON (entry **2.13**).

deoxy sugar (**2.16**) elevates the activity of both RNase H isotypes. In the human system, an immediate and pronounced increase in target degradation is likewise apparent upon interchange of a thymidine (dT) in the rigid 2'F-ANA antisense for a butyl linker (AON **2.14**), which closes the efficiency gap between 2'F-ANA (k_{rel} 3.5) and DNA-derived (k_{rel} 4.6) AONs considerably.

Even more intriguing is the finding that the preference for a more flexible duplex substrate is a property displayed by the bacterial (*E. coli*) enzyme as well, such that target strand hydrolysis is accelerated in the presence of a single deoxy or butyl insert within the parent AON (**Table 2.2**). It is noteworthy, however, that the discriminatory properties of the two isotypes display some subtle variations. Specifically, the bacterial homologue shows greater tolerance for dT containing constructs over the butyl containing 2'F-ANA strands, in contrast to that observed with its human counterpart. The reasons for this disparity are presently unclear, but could be related to variations in the placement of catalytically active residues between the two isotypes.

2.5.3. Effect of 'Looping' Butyl Linker

As enzyme efficiency may be related to the energetic cost of distorting the duplex into a more catalytically reactive conformation, placing the linker outside of the helix should enable closer scrutiny into the dynamic nature of the RNase H–AON complex interaction. As such, when the non-nucleotidic linker is shifted *outside* of the helix by inserting a nucleotide complementary to the RNA single gap region (*e.g.* **2.6** and **2.17**, **Table 2.1**), this gives an oligonucleotide of 19 units in length with 2 nonameric nucleotide segments that are capable of forming perfect complexes with the RNA.

In this regard, the 2'F-ANA-B-Lp sequence (**2.17**, **Table 2.1**) contains unifying elements of both the 2'F-ANA (**2.13**) and 2'F-ANA-B10 (**2.14**) mixed sequence oligonucleotides. These consist of a localized flexible site in the center of the sequence (similar to 2'F-ANA-B10 **2.14**) as well as the ability of this oligonucleotide to fully hybridize with the target RNA (similar to 2'F-ANA **2.13**). For this sequence, AON binding to the RNA is likely accompanied by a local compression of the AON backbone at the extrahelical site to project or 'loop' the linker away from the duplex core. Such a compensatory distortion of the helix may further be reconciled through kinking in the overall conformation of the

hybrid which probably also occurs to maximize the number of residues that form base pairs between this oligonucleotide and the RNA. This is reflected in a modest gain in the thermal stability of this sequence relative to 2'F-ANA-B10 (ΔT_M = 2°C), which although not as high as all-2'F-ANA, indicates that some linker-induced motility of the strands surrounding the junction may be necessary to relieve local intrastrand steric effects.

In contrast, DNA with a looping butyl linker (DNA-B-Lp, **2.6**) is incapable of promoting stable base pairing between butyl-anchoring residues and the opposing RNA strand, as this sequence exhibits the same thermal stability as when the linker resides completely parallel with the helix axis (*e.g.* AON **2.4**). This is not entirely unexpected however, as the deoxynucleotides themselves are considerably more flexible than 2'F-ANA residues and so would be more likely to experience greater intrahelical disorder around the backbone region flanking the linker insertion.

In either case, we speculated that forcing the linker out of the helix in this manner could potentially disrupt some of the interactions between RNase H and the two strands by reducing the number of stable contacts between the enzyme and the duplex minor groove. Remarkably, enzyme assays with both 2'F-ANA-B-Lp (**Figure 2.10**) and the analogous

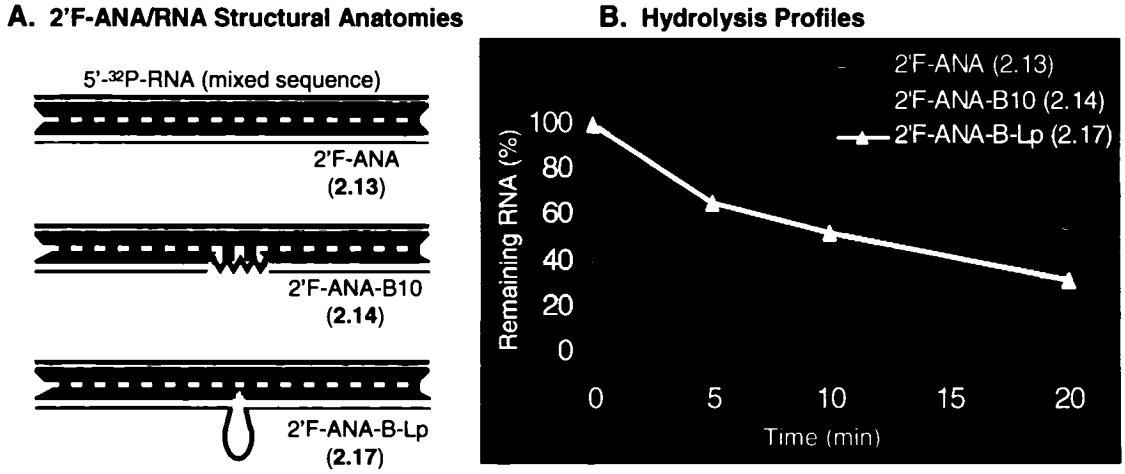

Figure 2.10: A. Schematic depiction of 'stretched' and 'looped' butyl-containing mixed sequence 2'F-ANA constructs with RNA. In either case, insertion of a butyl linker in these derivatives (**B**) or in DNA-based AONs (**Table 2.1**) accelerates the RNA hydrolysis reaction with RNase H. Hydrolysis data from the human enzyme (22°C) is shown above.

DNA-derived oligonucleotides suggest that such a protrusion is only associated with a minor energy penalty for enzyme docking and subsequent processive activities. In fact, both the DNA and 2'F-ANA sequences still considerably enhance RNA degradation (compare k_{rel} values of oligomers **2.13** *vs.* **2.17** & **2.3** *vs.* **2.6, Table 2.1**), which suggests that flexibility in the antisense strand is important for effective RNase H induction, *irrespective of whether the flexible linker resides directly within or extends away from the helix axis.*

The converse is true when a mismatching residue occupies a central position within the antisense strand. For instance, the mismatched nucleotide in DNA-c10 (**2.5**) and 2'F-ANA-C10 (**2.15**) oligonucleotides should likewise occupy an external position along the hybrid duplex (similar to 'B-Lp' AONs **2.6** and **2.17**), as steric prohibition with the opposing RNA nucleotide likely occurs to 'bulge' the mismatch away from the helix. However, if proper enzyme interaction with these substrates necessitates subtle repositioning of the strands within the AON:RNA complex, a high energy penalty associated with this event could reduce the enzyme's overall capacity to bind to and cleave the mismatched substrates. This presumably disables extensive processing in these duplexes as opposed to an inherently flexible alternative. In the butyl-modified duplexes where the linker loops out of the helix, enzyme activation is conceivably retained as steric interactions are relieved via an induced spatial rearrangement of the linker by the enzyme upon substrate docking. It is especially noteworthy that a possible transient delay in catalysis due to such repositioning of the looping linker during the enzyme interaction may be responsible for the reduced rates relative to DNA- (**2.4**) and 2'F-ANA-B10 (**2.14**) substrates in which the linker resides parallel with the helix and likely requires minimal distortion.

2.6. Targeting Structured RNA

Folded RNA usually precludes antisense effects *in vivo* by rendering most of the molecule inaccessible to intermolecular base pairing with complementary nucleic acids. As the extent and rate of RNA cleavage should therefore also depend on the structure, length and base composition of the target polyribonucleotide, we next evaluated whether the flexible AONs could accelerate cleavage in a highly structured, physiologically

relevant RNA species. These efforts particularly examined the specific reduction of target RNA levels using an *in vitro HRAS* model system, especially since hyperactivated forms of both point mutant and nonmutated mammalian *HRAS* protooncogenes are frequently implicated in various human cancers,[219-222] thus making this a desirable therapeutic target. As such, the linker-modified antisense oligonucleotides were directed to hybridize with an internal 18 nucleotide region in the *RAS* mRNA encompassing the translation initiation site of the gene and corresponding to residues –19 to +21 of the full length transcript. For comparison, a similar set of targets was designed to comprise longer (*i.e.* –24 to +26; 50 nts) or shorter segments of the *RAS* transcript, each encompassing the common AON binding region. Probable secondary structures of these targets were extracted using the MFOLD program,[223,224] which estimates ΔG°_{37} values for self-complementary duplex formation (**Figure 2.11**). The program incorporates many

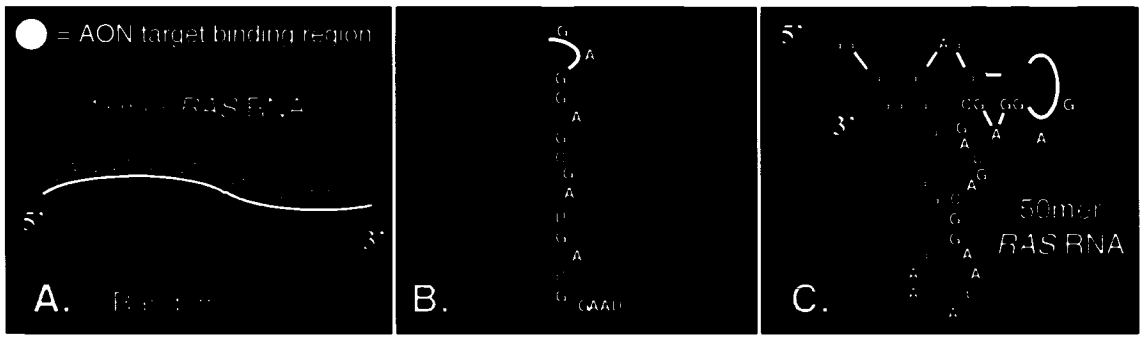

Figure 2.11: Probable secondary structures adopted by 18, 40, and 50mer *HRAS* RNA targets, as generated using the Turner-Zuker algorithm.[223,224] Residues denoting the common AON binding region are shown in white. Sequence designations are as follows: 18 nt *RAS* target, **2.25**; 40mer, **2.26**; 50mer, **2.27**.

adjustable parameters to improve the predictions and as such, each sequence was set to fold at a simulated temperature of 37°C, with sodium and magnesium counterion concentrations set to 145 mM and 1 mM, respectively, to mimic the experimental solution ionic conditions (see **section 6.7.**).

While the shorter 18 nt target species fails to exhibit any intramolecular association properties under these conditions, the calculations argue for the existence of a single predominant species for the longer *RAS* target (40 nts; **2.26**) in which most of the target site (*ca.* 75%) is sequestered in a stable 25 base hairpin structure (**Figure 2.11,** panel **B**).

This prediction is supported by analysis of the UV thermal profiles of the 18 and 40mer species, which indicates biphasic melting behaviour only for the latter, likely due to structural changes induced by the unfolding of the RNA and/or denaturation of self-associated (*i.e.* intermolecular) RNA complexes (data not shown). That all of these characteristics are closely reproduced in a longer *RAS*-derived target spanning residues –24 to +26 of the full length transcript (panel **C**), further corroborates these observations. Despite apparent differences in secondary structures among the various RNA species, none of these intricate morphological features markedly affect the abilities of the AONs to invade and hybridize with the complementary binding site in the RNA sequences

Table 2.3: Melting temperatures (T_M) of DNA, & 2'F-ANA constructs upon hybridization with an 18, 40 or 50 nt *HRAS* RNA species.[a]

Entry	Legend	5'-AON-3' 18mers	RNA Target Length: T_M (°C)		
			18 nts		50 nts
2.18	*r*-2'F-ANA	ATT CCG TCA TCG CTC CTC	>80	82	82.5
2.19	*r*-2'F-ANA-B10	ATT CCG TCA BCG CTC CTC	72.1	71.7	71
2.20	*r*-DNA	att ccg tca tcg ctc ctc	72	69.9	69.8
2.21	*r*-DNA-B10	att ccg tca Bcg ctc ctc	62.6	58.2	59
2.22	*r*-DNA-dC10	att ccg tca ccg ctc ctc	64	63.1	63.6

[a]Aqueous solutions of 2.38 x 10^{-6} M of each oligonucleotide, 140 mM KCl, 1 mM $MgCl_2$, 5 mM Na_2HPO_4 buffer (pH 7.2); All measurements were obtained in triplicate with an uncertainty in T_M of ±0.5°C. [c]Upper case letters, 2'F-ANA nucleotides; lower case letters, deoxynucleotides; c, deoxycytidine mismatch residue; B, butyl linker. Predicted structures and sequences of RNA targets **2.25** – **2.27** are presented in **Figure 2.11**.

(**Table 2.3**). In fact, AON binding to both 40 and 50 nt *RAS* targets (**2.26** & **2.27**) occurs just as strongly as when the target exists in a random coil conformation (*i.e.* 18 nt *RAS* complements) thereby demonstrating that the presence of folded regions within a more organized, less accessible molecular framework does not impede the consequent association of these nucleic acids with a given antisense composition as examined herein.

2.6.1. RNase H Acceleration of Cleavage within Folded *HRAS* RNA Complements

Having examined both the structural and thermal hybridization properties of each *RAS* RNA target system, we next evaluated the ability of linker-containing AONs to induce RNase H-assisted cleavage in the folded segment using the 40mer target oligoribonucleotide (**2.26**; **Figure 2.11**) as model system for subsequent enzyme analyses. The results for both DNA- and 2'F-ANA AONs as well as their butyl-modified derivatives are shown in **Figure 2.12**. Somewhat surprisingly, for DNA-based AONs within this series (**2.20** – **2.22**), an increase in human RNase H1-mediated target degradation is not apparent upon interchanging a deoxynucleotide residue in the parent strand for a butanediol linker (*i.e.* **2.21** & **2.22**; **Figure 2.12**) and appears to be consistent with prior work by other groups.[225-227]

Alternatively, the lack of an acceleratory effect may be explained in part by a decreased propensity for this AON to associate with the RNA, resulting in a non-homogeneous AON:RNA population and consequently a lesser amount of substrate duplex presented to the enzyme for cleavage. Duplex heterogeneity seems even more likely given that hybrid formation with *r*-DNA-B10 (**2.21**) produces the least intrinsically stable duplex within the series (**Table 2.3**). Consequently, greater competition for intramolecular folding of the *RAS* target as opposed to its intermolecular duplexation with a DNA-derived AON counterpart could conceivably mask any observable differences in cleavage rates.

However, this is not the case for the 2'F-ANA linker-modified constructs. Indeed, substitution of the arabinofluoronucleoside residue in *r*-2'F-ANA **2.18** with a more flexible butanediol linker elevates the activity of human RNase H1 against the respective duplexed substrates rather dramatically, with a *ca.* 23-fold enhancement observed over the parent compounds. As such, the rate attained by this 2'F-ANA construct closely approaches the level of enzyme-induced degradation attainable with the native oligodeoxynucleotides (*e.g.* compare **2.19** *vs.* **2.20**; **Figure 2.12**, panel **B**). Once again, these properties are consistently reproduced when the 2'F-ANA-based constructs are directed against a slightly longer *RAS* 50mer RNA (data not shown), indicating that a significant enhancement in target hydrolysis may readily be achieved by the butyl-modified AON, even when targeting a highly structured RNA species.

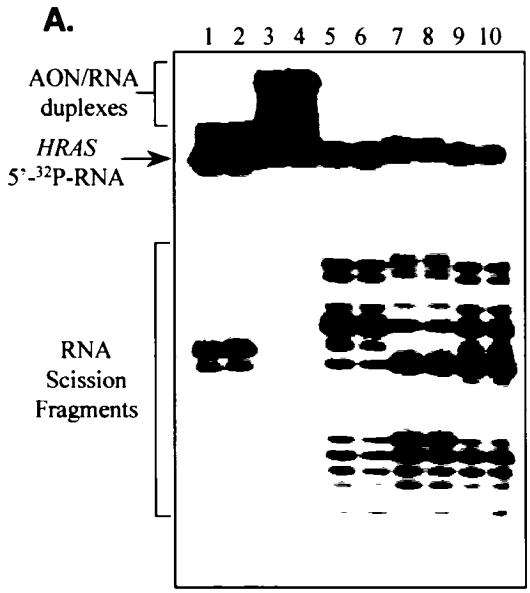

B.

Entry	Legend	Relative rates (k_{rel}) of enzyme cleavage
2.18	*r*-2'F-ANA	1
2.19	*r*-2'F-ANA-B10	23.3
2.20	*r*-DNA	33.8
2.21	*r*-DNA-B10	31.6
2.22	*r*-DNA-dC10	31.9

Relative rates of cleavage:

DNA ≈ DNA-B10 > 2'F-ANA-B10 >> 2'F-ANA

C. AON:RNA Scissile sites

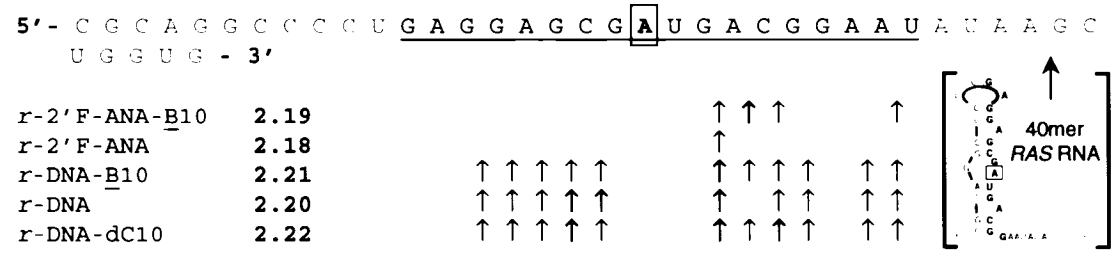

Figure 2.12: **A.** Denaturing PAGE illustrating human RNase H1 mediated cleavage of 5'-^{32}P-labeled *HRAS* 40 nt RNA (**2.26**; 1 pmol) duplexed with mixed base AON sequences (5 pmol) at 37°C. Lanes 1 and 2: *r*-2'F-ANA-B10 (**2.19**), 10 and 20 mins; lanes 3 and 4: *r*-2'F-ANA (**2.18**), 10 and 20 mins; lanes 5 and 6: *r*-DNA-B10 (**2.21**), 10 and 20 mins; lanes 7 and 8: *r*-DNA (**2.20**), 10 and 20 mins; lanes 9 and 10: *r*-DNA-c10 (**2.22**), 10 and 20 mins. The slowly migrating band in lanes 3 and 4 is that of the 2'F-ANA:RNA duplex (sequence **2.18** bound to **2.26**; T_M > 80°C), which withstands the denaturing conditions of the electrophoresis and the heating of the sample prior to being loaded onto the gel. **C.** Lengths of the RNA fragments generated via enzyme scission and corresponding position along the AON are indicated. Bold arrows represent the major cleavage sites; the boxed A residue in the RNA sequence denotes the residue opposite the insertion position of the linker in the AON; underlined residues correspond to the AON binding tract, with kinetic data (k_{rel}) of RNA cleavage provided in panel **B**. See **Figure 2.11** & **Table 2.3** for complete list of sequences.

2.7. CONCLUSIONS

This chapter has directly demonstrated for the first time the importance of achieving an optimal balance between flexibility and rigidity in the AON as one step towards improving its biological properties and ultimate therapeutic potency. The stimulation of RNase H activity appears to require a flexible component in the duplexed substrate, which itself appears essential for enhancing targeted destruction of the hybrid duplex by the enzyme, provided that other geometrical elements around the actual cleavage site still retain the necessary requirements that have thus far been demonstrated – *i.e.* Eastern sugar conformation and B-like character[111-113,115] in the AON strand. Remarkably, 2'F-ANA constructs derived by insertion of a flexible acyclic residue within the AON sequence (*e.g.*, **2.14**) represent the first examples of modified antisense compounds devoid of deoxyribose sugars that elicit RNase H activity with comparable efficiency to the native (DNA) systems, yet even the deoxy strands themselves may be fashioned to accelerate enzyme cleavage upon linker modification.

Indeed, the incorporation of acyclic linkers with high degrees of flexibility in the AON strand – either a 2',5'-linked secouridine residue **2.6** or a butanediol linker **IV** – appear to better accommodate the stringent conformational requirements of the enzyme without disrupting other fundamental recognition elements within the inclosing AON segments. Sizeable increases in enzyme-mediated scission of target RNA occur upon substituting an acyclic linker in the middle of a known RNase H-competent analogue (*i.e.* DNA or 2'F-ANA). The susceptibility of these hybrids to RNA hydrolysis remains fully operative in various sequence contexts as well, with up to 8-fold enhancements observed over strands lacking the acyclic insertion. Furthermore, in sequences where the acyclic inserts are moved along the 2'F-ANA scaffold, a significant change in activity is observed that depends specifically on the helical insertion site. The greatest activity occurs in constructs with a centrally placed acyclic linker, although differences between 5'- *vs.* 3'-end insertion are also observed, with a greater amount of enzyme processing occurring when the linker is placed near the 3'-end of the AON.

A more practical model exploiting the *in vivo* difficulties that are sometimes encountered with antisense oligonucleotides was also investigated to scrutinize the ability of each AON composition to achieve efficient hydrolysis in a folded RNA target. The target

species for these studies was shown to be more representative of the biological complexity typically assumed by various mRNA species in the physiological environment, where the adoption of numerous folded segments in the molecule usually preclude its consequent association with an invading AON. In fact, this is where the relatively greater preorganizational ability of the rigid 2'F-ANA scaffold provides the most obvious benefits toward strand scission, such that considerable activating potency is restored to the respective linker-modified constructs which approach *ca.* 23-fold improvements in enzyme recruitment over the parent strands (*e.g.* **2.19**). By contrast, DNA-based AONs show little discernible variation in enzyme rate among contiguous or linker-modified sequences within this structural context. More importantly however, 2'F-ANA hybrids, although typically much less adept at inducing RNase H activity as compared to the native deoxynucleotide AONs, become strongly proficient at directing enzyme destruction of the duplexed RNA component in a manner that closely approaches that attainable with the latter systems, while still retaining relatively greater duplexation strength. These experiments thus clearly outline an impending need to further explore the structural attributes that define high enzyme recruitment, especially within other rigid AON contenders in an effort to ameliorate their subsequent use in biological and/or therapeutic applications.

In conclusion, we have demonstrated that RNase H induction can remarkably be improved by introducing subtle changes in local 2'F-ANA or DNA strand dynamics that might enable better adherence and processing of the hybrid substrate by the enzyme. The malleability of the duplex backbone region surrounding the acyclic modifications likely better accommodates the enzyme into the minor groove[42,101,228] and may aid in more efficient hydrolysis during the catalytic event, thereby giving rise to the observed rate enhancements. These and future studies with DNA, 2'F-ANA and similar constructs should afford valuable insight into the substrate requirements of the enzyme, and further provide a versatile method in generating a new repertoire of more potent antisense compounds. A clearer understanding of the molecular nature underlying the RNase H binding and cleavage events in other similarly deformable hybrid substrates, as explored in the chapters that follow, will undoubtedly offer much foresight to these endeavours.

CHAPTER 3. THERMAL, STRUCTURAL AND MOLECULAR EFFECTS OF LINKER ANATOMY AND LOCATION IN RNASE H-COMPETENT HETERODUPLEXES

3.1. INTRODUCTION – MOLECULAR DIVERSITY AND BIOLOGICAL ROLES OF RNASES H

Ribonuclease H enzymes are critical participants of various biological processes in both eukaryotic and prokaryotic organisms, and constitute one of the best studied examples in the life cycles of certain retroviruses.[30] As all enzymes within this family ensure the accurate replication or transcription of DNA, their ubiquitous presence and importance for cellular viability is undisputed. During pro- and eukaryotic replication, RNases H actively remove RNA primers generated during synthesis of the lagging DNA strand.[229] They also participate in DNA repair events,[230,231] in some cases excising single misincorporated ribonucleotides from within a replicating DNA template,[34] and retroviral reverse transcription[232] as well, in which the enzyme selectively degrades the viral RNA from heteroduplexed intermediates, allowing for subsequent integration of the nascently transcribed cDNA genome into the host gene pool.

Mammalian RNase H (for Hybrid) was the first of the family to be discovered[233] and was termed a class I enzyme to designate it as the first to display this unique RNA cleaving property. A second human enzyme later emerged on the basis of different physical, biochemical and serological characteristics and was subsequently named RNase HII to distinguish it from the former.[102,234] Later, the amino acid sequence for human RNase HI was determined and shown to display significant homology to the class II RNase H of *Escherichia coli*, which itself corresponds to the least active of the two isoforms present in the bacterial kingdom.[235] In fact, all known mammalian RNases HI and HII are now presumed to be sequence homologues of bacterial RNases HII and HI, respectively.[236,237]

These and other discrepancies in the general nomenclature of the mammalian and prokaryotic enzymes, coupled with recent discoveries of new RNase H genes, has prompted the creation of at least 2 major categories of RNases H based either on the enzymes' biochemical properties or sequence homologies. Currently, prokaryotic and eukaryotic RNases H are widely designated by class (roman numerals – I or II) to

characterize members with comparable serological, physical and biochemical characteristics including similarities in peptide molecular weights, isoelectric points, sensitivity to sulfur blocking reagents and ability to use Mn^{2+} as a cofactor. *E. coli* RNase HI is the best characterized of this group, and is also closely related in sequence to the RNase H domain of HIV-1 reverse transcriptase.[238]

Alternatively, a newer system of classification specifies the enzymes by type (arabic numerals – 1 or 2), which corresponds to those members that display close sequence homologies rather than similar biochemical attributes (**Figure 3.1**). A need for revising

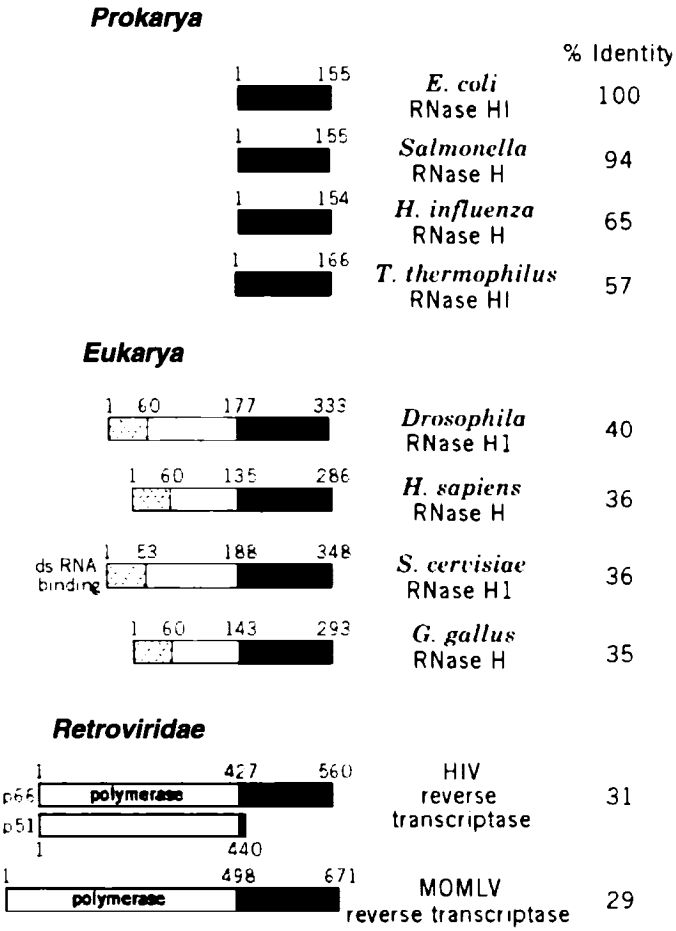

Figure 3.1: Primary structures of type 1 RNases H isolated from representative species, showing residue numbering and positioning of the RNase H domain (black shading). Additional domains in the human isotype comprise a mitochondrial localization signal (residues 1-27), a dsRBD-like motif (28-73) and variable spacer region (74-135) at the N-terminus of the polypeptide.[239-242] The percent identity of each RNase H domain to that of the *E. coli* enzyme is indicated. Adapted from Ohtani *et al.*, 1999.[243]

the current nomenclature has arisen however, mainly because of various intricate discrepancies between the two classification modes and the ensuing confusion when drawing comparisons across different organisms. For instance, these inconsistencies are evident in the classification of human RNase HI – a class I, type 2 enzyme – when contrasted with *E. coli* RNase HI – a member of the type 1 category. Further compounding this problem is the possible existence of more than two isoforms in a given organism. *Saccharomyces cerevisiae*, for example, encodes three active RNases H,[237] for which some investigators have thereby preferred to designate the enzymes simply by molecular weight, as in *S. cerevisiae* RNase H(35). Here, the number in brackets refers to the molecular weight of the protein in kilodaltons; in this example, the 35 kDa yeast enzyme is also widely termed as a class I, type 2 enzyme.[244] By this account, the type and class designations poorly correlate with one another at best, and a more accurate way of placing the enzymes may need to draw upon several additional criteria.

Regardless of origin, all RNases H share a strongly conserved catalytic triad of amino acid residues and common core folding motif, consisting of a five-stranded β sheet sandwiched by two α helices, all of which superimpose well in the ternary protein structure (**Figure 3.2**). A common catalytic mechanism is likely shared as well, considering that all members of this family function primarily as endonucleases, acting exclusively upon the RNA moiety of RNA/DNA hybrids to yield products with 5'-phosphate and 3'-hydroxyl termini. The degradation reaction first begins with an endolytic cleavage at a ribonucleotide involved in the duplex and then processes exolytically in a 3' to 5' direction,[245,246] with respect to the DNA component of the paired strands, in a process requiring divalent metal cations (Mg^{2+} or Mn^{2+}), and a free 2'-hydroxyl group in the sense (RNA) strand. For *E. coli* RNase H1, the mechanism by which internucleotide phosphodiester hydrolysis occurs has recently been shown to proceed via in-line attack of a water molecule opposite the side of the leaving 3'-hydroxyl group with configurational inversion at phosphorus.[247] The entire interaction takes place at the face of the duplex minor groove, away from any steric influence of the nucleic acid heterocycles which themselves project into the major groove cavity.

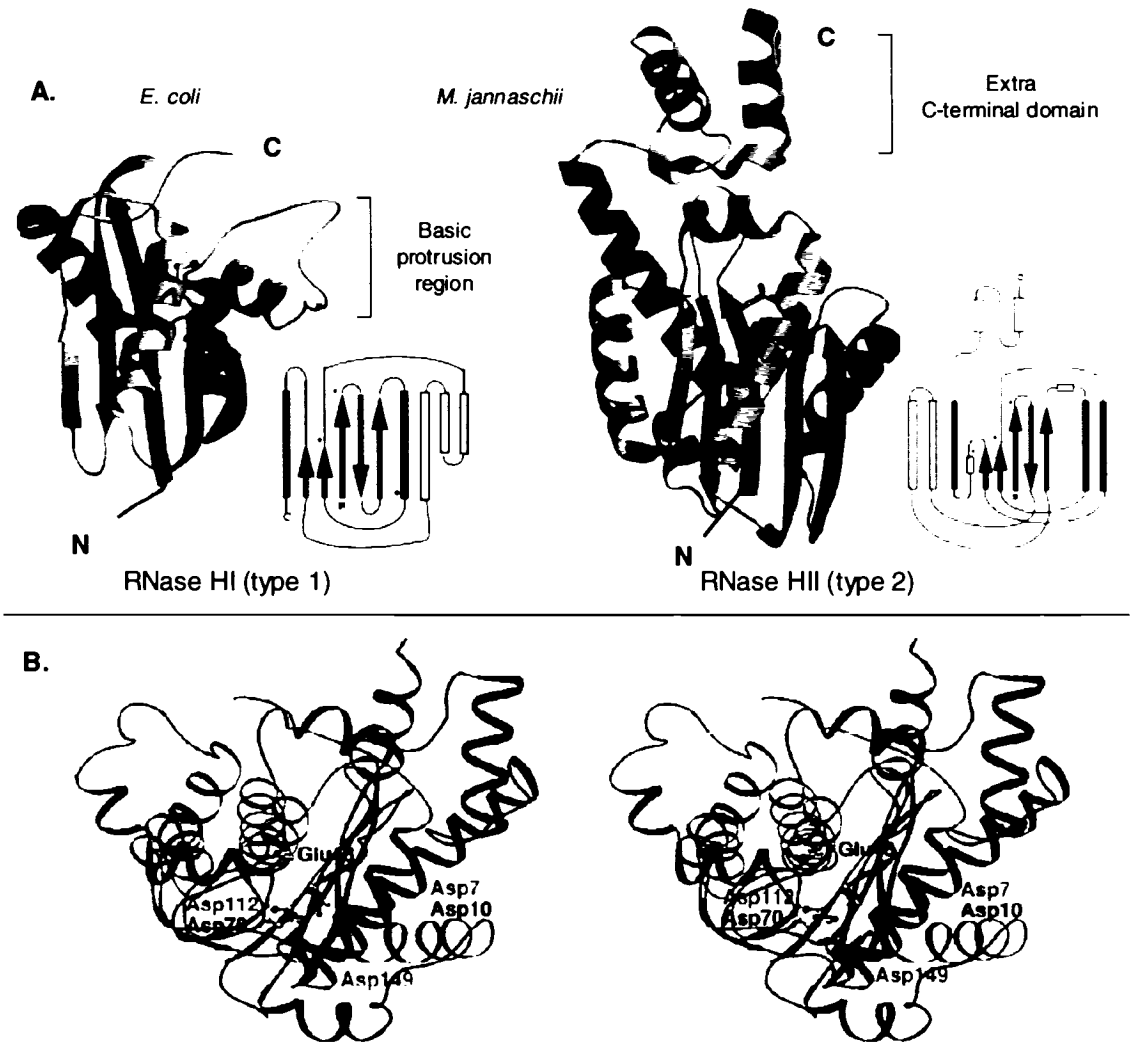

Figure 3.2: **A.** Structural topology of a bacterial RNase HI and archaeal RNase HII, showing structural conservation of the canonical RNase H fold, as depicted in the schematic on the right, despite poor sequence similarities. Secondary structural elements of the RNase H fold are colored (red, orange, yellow, green, blue, purple, pink) as ordered in the protein sequence; the arrows represent β-strands and cylinders represent α-helices **B.** Stereoview of the superimposed enzymes shown in **A**, highlighting functional conservation of catalytic residues, *M. jannaschii* = blue, *E. coli* = green. Adapted from Lai *et al.*, 2000[248] and Song *et al.*, 2004.[186]

As such, RNase-H mediated cleavage usually proceeds with minimal sequence specificity, implying that almost any DNA/RNA hybrid can serve as a suitable substrate for these enzymes. Accordingly, the use of antisense oligonucleotides (AONs) as selective inhibitors of gene expression offers a rational approach for the prevention and treatment of many genetic disorders. The RNase H-mediated degradation of a target mRNA is considered to be the most effective mode of action of AONs,[12,194] for it is

simply more potent than ones that are limited to interfering with the splicing or translational machinery. This is because the antisense-bound RNA is rapidly and permanently disabled by RNase H, thereby freeing the intact antisense for successive rounds of inhibition. This also offers a powerful approach for selectively inhibiting the production of an encoded disease-causing protein, to enable reversal of the disease phenotype and ultimately restore normal cellular function.

3.2. Conformational Flexibility of AONs in the Activation of RNase H

As noted previously, of the hundreds of modified AONs tested, only a handful are currently capable of supporting RNase H-induced RNA cleavage. Among these 'active' variants, none sufficiently attain enzyme activity in a manner comparable to that of the native DNA surrogates. 'Locked' α-L-LNA heteroduplexes with RNA, in particular – while mimicking the global features of natural substrates – only poorly activate the enzyme,[56,145] likely because the sugar-phosphate backbone is too stiff to optimally establish multiple contacts in the nucleoprotein complex (**Figure 3.3**). Clearly, as with our previous findings, the plasticity of the phosphodiester backbone dictates the feasibility with which this event can occur.[147,249] Along these lines, NMR[250] and CD

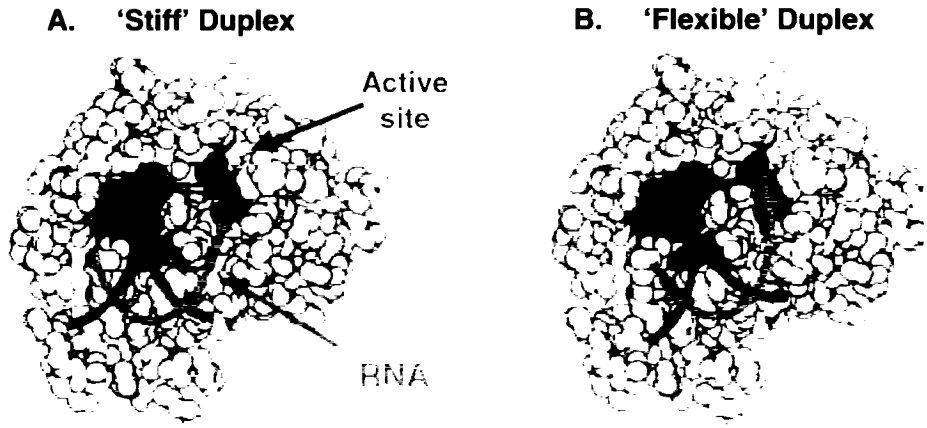

Figure 3.3: Molecular model of the interaction of core protein residues in HIV-1 RT RNase H with its substrate, showing proximity of the catalytic (red) and binding domains (blue). A-like duplexes of the correct minor groove width can interact with both sites, but rigid substrates (**A**) resist enzyme-induced conformational restructuring of the helical trajectory, thereby undergoing comparatively suboptimal catalysis as opposed to that of a more flexible alternative (**B**). Modified from Nielsen *et al.*, 2000.[250]

studies[42] of bound substrates have further delineated an active role for the substrate and enzyme, characterized by induced bending or 'kinking' of the helix axis just prior to target strand hydrolysis.[251]

3.3. Project Overview and Design

The molecular basis by which flexibly-designed DNA or 2'F-ANA heteroduplexes with RNA render the target more amenable to enzyme hydrolysis by RNase H[147,249] is currently unclear. However, as this and similar designs might prove directly vital to improving ultimate AON therapeutic utility, we have sought to expand upon this class of compounds through the introduction of anatomically and flexibly variable regions in one or both components of the heteroduplex. We expected these modifications to highlight the functional role and possible differences for each single-stranded component of the heteroduplex toward enzyme discrimination. In doing so, we further hoped that varying the linker composition itself and relative deformability might further fine-tune and drive the susceptibility of the duplex toward hydrolysis more favourably.

Several other key structural aspects of the natural interaction of RNase H and its substrate that were probed in this study, included: (1) *importance of chain length in the sugar-phosphate backbone*. Native 3',5'-linked oligonucleotides have a backbone composition consisting of 3 carbon atoms that form a portion of the sugar core, and are linked by adjoining phosphodiester groups. This uniform repetition of equal numbers of atoms along the periphery of the native 3',5'-linked helix gives rise to a defined geometry in which minimal distortion or bending of the macromolecule is expected to occur; (2) *influence of local sites of conformational mobility*. Removal of the sugar and heterocyclic component of an intrahelical nucleotide would conceivably disorder the resulting hybrid helix with RNA at this specific junction, by removing the strain imposed by the natural furanose ring, as well as eliminating the possibility of interstrand base pairing with the opposing ribonucleotide partner of the pair; and (3) *variations in helical curvature of linker-modified hybrids*. One likely consequence of forced mispairing in hybrid helices is the potential formation of bulges or loops within defined helical regions,[252-255] especially when the mispaired site consists of an 'extended' or 'shortened' spacer arm. It is currently unknown whether these structural anomalies can influence the formation of

curved tracts within the duplex that may ultimately contribute to differential enzymatic discrimination upon presentation to the enzyme for hydrolysis.

Each of these characteristics were scrutinized in modified heteroduplexes, themselves specifically used as probes toward the type 1, class II human RNase H enzyme (*i.e.* RNase H1), as this isozyme is presumed to be the major player in intracellular antisense effects.[256] Notably, the type 2 human enzyme has yet to be cloned in an active form.

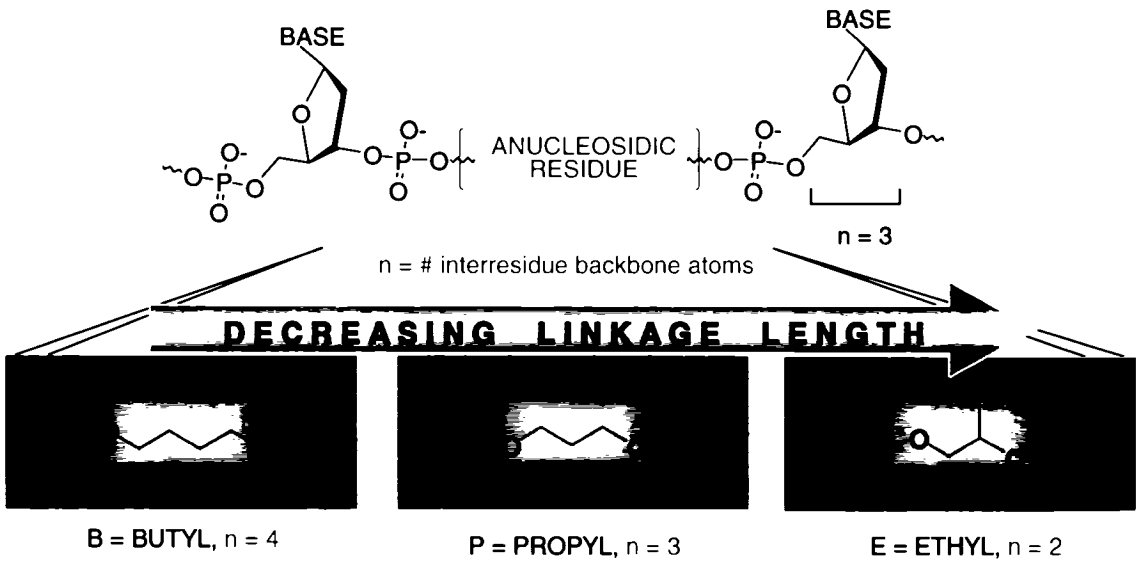

Figure 3.4: Incorporation of different acyclic linkers of varying length and flexibility in a 'rigid' enzyme-active antisense may provide insight on the structural factors that give rise to the 'optimal' AON/RNA substrate for RNase H.

3.3.1. Chemical Synthesis of Propyl and Ethyl-linked Oligonucleotides

In order to further optimize the potential ability of oligonucleotides to enhance target RNA degradation, a series of linker constructs was chosen to probe the requirements for enzymatic binding and cleavage (**Figure 3.4**). We examined sequences corresponding to the most potent members previously identified, with the chosen site of the linker insertion analogous to that previously tested (**Table 3.1**). For these studies, mixed sequences were used in order to prevent base pairing misalignment upon complexation and the possible formation of heterogeneous duplex populations that might otherwise preclude the precise identification of enzyme-induced cuts within the strands.

Table 3.1: Sequence Composition and Yields of Antisense and RNA Targets

Entry	AON Designation	Sequence (5'-3')[a]	ε x 10^4 ($L mol^{-1} cm^{-1}$)[b]	Crude Yield[c] (ODU)	Isolated Yield[d] (ODU)
		(a) Antisense Sequences			
2.3	DNA	TTA TAT TTT TTC TTT CCC	15.5	72.7	13.0
2.4	DNA-B10	TTA TAT TTT BTC TTT CCC	14.7	67.3	15.3
2.6	DNA-B-L	TTA TAT TTT B TTC TTT CCC	15.6	76.0	9.8
3.1	DNA-P10	TTA TAT TTT PTC TTT CCC	14.7	53.5	11.2
3.2	DNA-P-L	TTA TAT TTT P TTC TTT CCC	15.6	65.1	14.3
3.3	DNA-E10	TTA TAT TTT ETC TTT CCC	14.7	50.4	8.0
3.4	DNA-E-L	TTA TAT TTT E TTC TTT CCC	15.6	51.9	6.1
2.5	DNA-dC10	TTA TAT TTT CTC TTT CCC	15.4	72.0	17.1
		(b) RNA Targets			
2.24	all-RNA	GGG AAA GAA AAA AUA UAA	21.1	48.0	13.6
3.5	RNA-B9	GGG AAA GAB AAA AUA UAA	20.3	35.9	9.0

[a]All syntheses were performed using a 1 μmol synthesis scale. B = butyl linker, P = propyl linker, E = ethyl linker, C = deoxycytidine mismatching nucleotide. [b]Molar extinction coefficients (ε) were calculated using the nearest neighbour approximation of Puglisi *et al.*[257] [c]Crude yields are those obtained following solid-phase synthesis and deprotection. [d]Isolated yields represent the fraction of pure, desalted oligonucleotide recovered following purification of one-half of the starting crude material.

The oligodeoxynucleotides and RNA complements were synthesized on an ABI 381A DNA synthesizer using standard phosphoramidite chemistry and reagents (**Table 3.1**). Linker phosphoramidites (ChemGenes Corp., Ashland MA) were attached to the additional port of the machine, and like the standard deoxynucleoside phosphoramidites, were efficiently coupled to the free 5'-hydroxyl termini of support bound oligonucleotides, as indicated by trityl analysis of released DMT cations with only modest coupling times necessary (120 sec). This step in particular is key to the success of the synthesis, and as such, chain assembly was conducted using 4,5-dicyanoimidazole

(DCI) as phosphoramidite activator during the coupling step, rather than the more conventional choice of 1*H*-tetrazole[211,258,259] (**Figure 3.5**). This is because DCI, being more nucleophilic than tetrazole, increases the rate and efficiency of the nucleoside phosphoramidite coupling reaction *ca.* 2 fold.[260,261] It is also more soluble in acetonitrile, allowing for the use of a greater effective concentration of activated phosphoramidite-azolide intermediate in solid-phase syntheses.

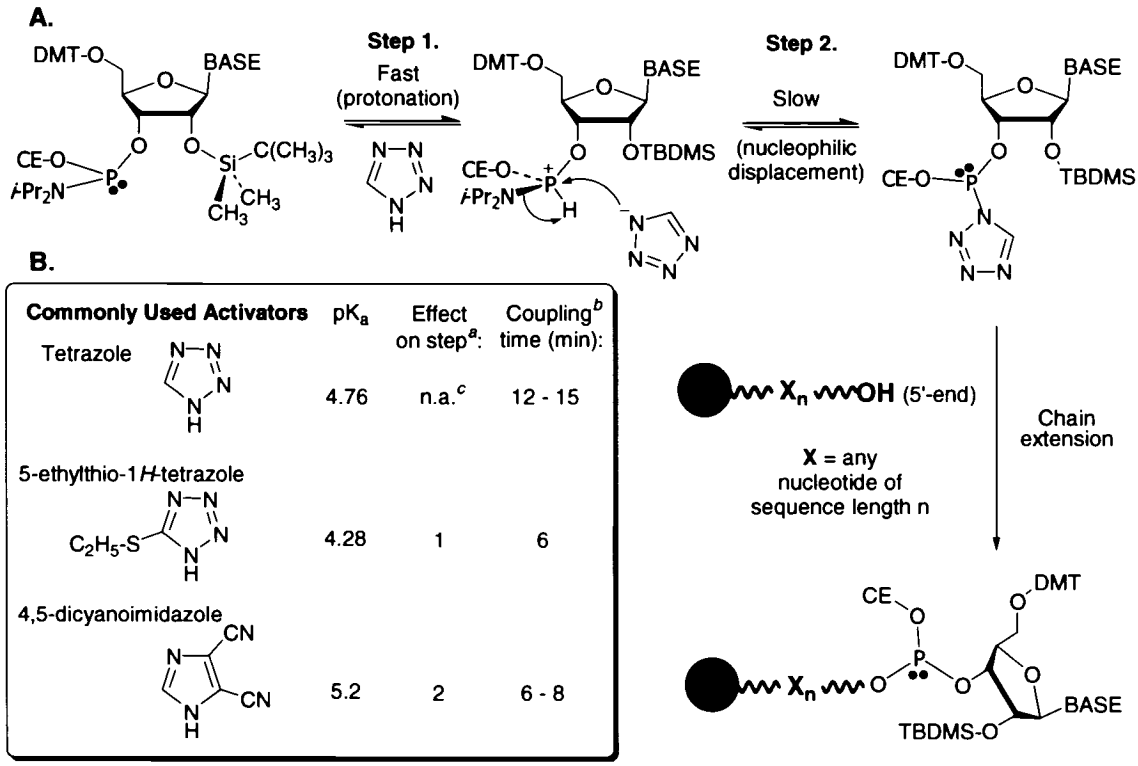

Figure 3.5: **A.** Mechanism of phosphoramidite activation and coupling, the most crucial step in the success of solid-phase synthesis. Most tetrazole derivatives[262] speed up activation by faster protonation of trivalent phosphorus[258,263] (step 1), but the increased acidity of the solution inevitably produces concomitant detritylation of a small fraction of support bound species. **B.** Increasing the nucleophilicity of the activator enhances the second step. [a]indicates an acceleration in the respective step relative to tetrazole; [b]coupling times are those commonly used for 2'-O-substituted ribonucleoside phosphoramidites; [c]n.a. – not applicable.

Furthermore, DCI is less acidic (pK_a 5.2) and thereby minimizes any occurrence of premature detritylation that sometimes becomes evident when using more acidic alternatives (*e.g.* tetrazole). In the latter case, partial detritylation corrupts the integrity of

the final product by allowing multiple couplings to occur within a single cycle, thereby leading to a small amount of n + 1 insertion mutations ('longmers') in the crude product. The extent of longmer formation in oligodeoxynucleotides has also been shown to proceed in a nucleobase-dependent manner, with an increase in n + 1 content paralleling the preferred order of detritylation as follows: dG > dA > dC > T.[264]

These considerations have even greater relevance in the synthesis of oligoribonucleotides, the monomeric precursors of which are relatively sluggish to react by virtue of the added steric bulk conferred by silyl protection at the adjacent 2'-position. As the coupling times in this case are generally 5-fold longer for effective chain extension relative to oligodeoxynucleotide synthesis, these species remain in contact with the activator solution for extended periods. Consequently, the additional time required to complete this step of the cycle ultimately increases the potential for acid-catalyzed deblocking of the 5'-hydroxyl, thereby leading to undesired side-reactions. In contrast, formation of longmer (n + 1) insertion products are typically absent when phosphoramidite coupling is catalyzed by DCI (**Figure 3.6**).

Regardless of the apparent success of the crude reactions, all oligodeoxy- and ribonucleotides were purified and rigorously analyzed by gel electrophoresis and anion

Figure 3.6: 20% preparative denaturing PAGE purification of 35 OD units of crude RNA **3.5**, demonstrating the relative abundance in yield of full length oligoribonucleotide over shorter failure sequences and an absence of longer (n + 1) species, attainable when using DCI as activator. Unlike the preparative gel shown above, the failure products are barely detectable in analytical separations. XC, xylene cyanol FF; BPB, bromophenol blue.

exchange HPLC prior to pursuing subsequent biophysical and biochemical characterizations. Accordingly, the immobilized oligomers were detached from the solid support, with concomitant deprotection of exocyclic base- and phosphate protecting groups by treatment with an aqueous ammonia/ethanol mixture (see chapter **6**).

Oligodeoxynucleotides **3.3** and **3.4**, constructed using an orthogonally protected glycerol unit, were deprotected in a similar fashion. In this instance, orthogonal masking of the dual primary hydroxyl functionalities in the respective 1-dimethoxytrityl-3-levulinyl glycerol-2-phosphoramidites (**Figure 3.7**) was essential in ensuring the monodirectional elongation of the corresponding oligonucleotide strands during these syntheses. This is possible because the levulinyl protection is compatible with the acidic conditions used during solid-phase synthesis.[265-267] As such, it is normally suited for applications that necessitate its selective removal during chain assembly, which is effected at near-neutral conditions using a hydrazine monohydrate/pyridine/acetic acid mixture,[268] as for example, in the construction of triple-helical forming "branched" ODN molecules of mixed sequence and length at each of the branches.[269,270] Treatment with hydrazine was not necessary for our purposes, however, as the levulinyl ester could quantitatively be cleaved using standard ammonolysis conditions (*vide supra*).

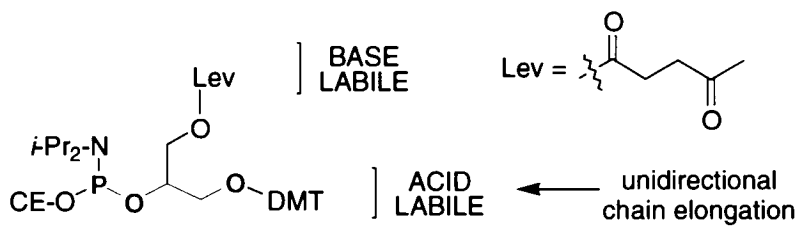

Figure 3.7: Structure of the asymmetric glycerol phosphoramidite. The ethyl fragment of the molecule ultimately connecting adjacent nucleotides in the oligonucleotide backbone is indicated in blue.

After deprotection, purification and successive desalting, the chemical composition of all modified DNA and RNA strands was verified by MALDI-TOF mass spectrometry measurements (see **section 6.8.**), which gave masses in accordance with the expected structures.

3.4. Duplex Destabilization Varies With the Identity of the Anucleosidic Linker

Thermodynamic and structural studies of nucleic acid duplexes containing abasic lesions, mismatches, or other anomalies in stereoregular duplex formation indicate that such structural defects, while often imparting profound energetic penalties, only induce localized structural perturbations in overall duplex helicity and architecture.[253,271-273] As we were interested in ultimately determining whether the presence of similar localized imperfections could also influence the relative susceptibilities of flexibly-modified linker-containing duplexes to RNase H discrimination and processing, we constructed a series of anucleosidic duplexes consisting of either central 'holes' or 'bulges' in *one* or *both* of the associating strands, that upon duplexation produced hybrids comprising either (a) a linker-modified antisense strand bound to a full RNA target (**2.24**); (b) unmodified antisense strand bound to a butyl-modified RNA target (**3.5**); or (c) doubly-modified or 'bistranded'-anucleosidic duplexes in which both the antisense and RNA targets were engineered to contain a single linker insert, structurally/geometrically aligned opposite one another in the hybridized duplex as dictated by the complementarity of flanking nucleobases (**Figure 3.8**). This convenient 'mix-and-match' strategy of combining the various DNA and RNA complements (**Table 3.1**) would thereby enable rapid screening and analysis of key structural contributors to both antisense- (AON) and sense- (RNA) induced effects on helical morphology, flexibility and ensuing protein recognition.

3.4.1. Thermal Properties of 'Asymmetric' Linker-Modified Duplexes: Butyl (C4), Propyl (C3), and Ethyl Spacers (C2) in the AON Strand

We first probed the effect of centrally-placed single anucleosidic insertions of various intraresidue lengths (*i.e.* butyl *vs.* propyl *vs.* ethyl), that could assume either a stretched (DNA-X10) or 'looped/bulged' orientation (DNA-X-L) along the DNA antisense backbone once bound to its target (**Figure 3.8**, panel **C**); each of these AON designs would thereby produce either an 'orphaned' or partially paired ribonucleotide in the RNA component, respectively. Accordingly, it came as no surprise that intra- or extrahelically inserted linkers ('stretched' or 'looped/bulged' designs) exhibited pronounced reductions

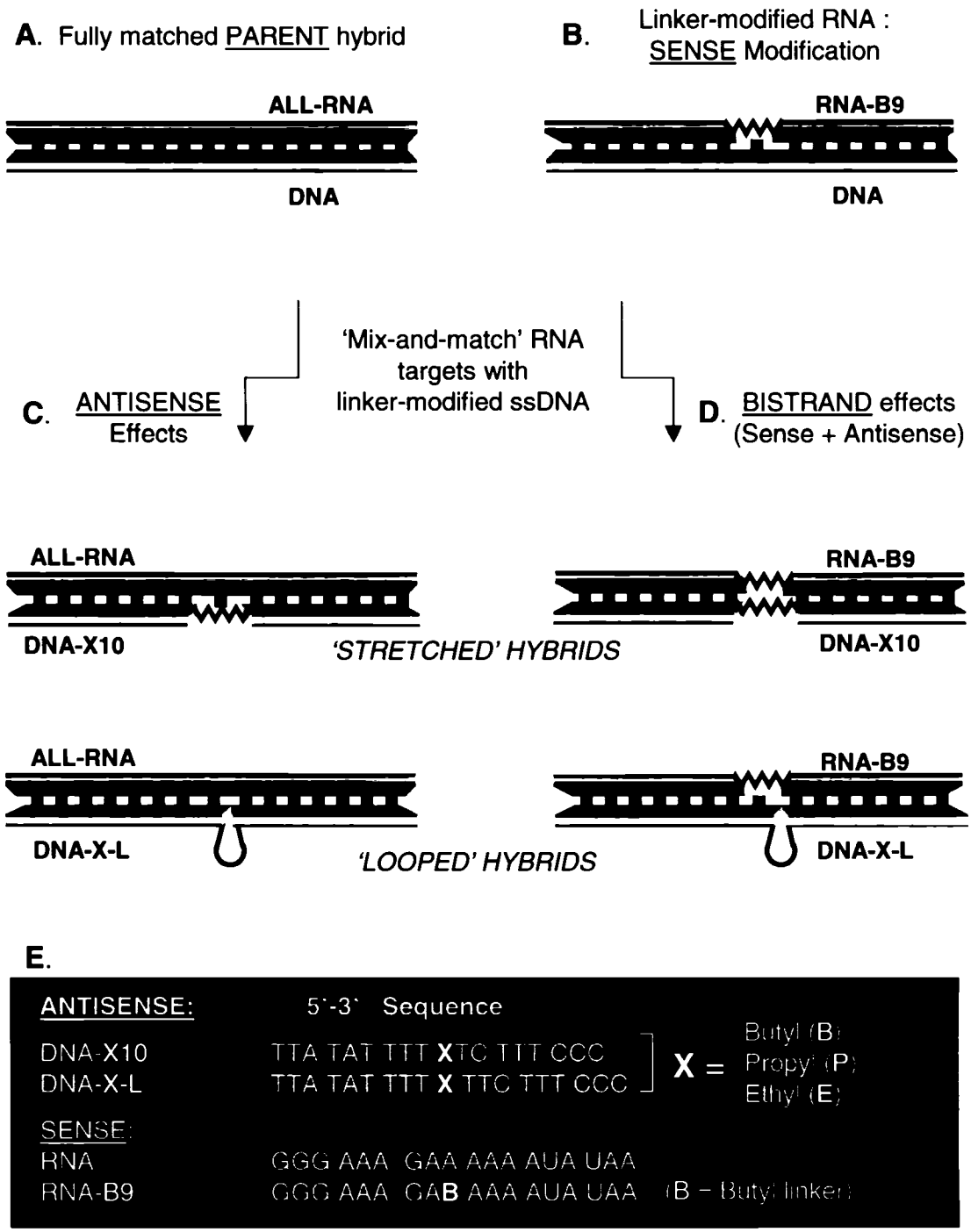

Figure 3.8: Representative structural anatomies of (**A**) fully-matched DNA:RNA hybrids and anucleosidic constructs (**B** – **D**), generated by mixing and matching unmodified or linker-containing single stranded DNA with either of the two RNA complements shown in (**E**). 'Bistrand'-modified hybrids (**D**) were designed to contain paired linkers in opposing strands upon hybridization. Sequence designations in (**E**) correspond to those shown in **Table 3.1**. The sequence numbering used is from the 5'-end of the oligonucleotides.

in thermal stability *vs.* the unmodified parent hybrids, regardless of the type of linker-derived localized structural 'defect' investigated (*e.g.* B *vs.* P *vs.* E).

(A) Stretched Helical Linkers. Within the DNA-X10 series in particular, (**Table 3.2**; AON sequences bound to all-RNA **2.24**), the magnitude of linker-induced thermal reductions to consequent hybrid formation was surprisingly rather variable, with stretched propyl backbones constituting the least stably tolerated modification (entry **3.1**; ΔT_M = -15°C), while butyl constructs were comparatively well accommodated (**2.4**; ΔT_M = -5°C) and the ethyl spacer assumed an intermediate value (**3.3**; ΔT_M = -12°C). In fact, this thermal trend was rather unexpected given the congeneric natures of the propyl surrogate and native 2-deoxyribofuranose backbones (4 interphosphate/intraresidue bonds each). Even more remarkable was the conservation of this trend within a homopolymeric sequence context, in which propyl insertion at the center of a polydeoxythymidine AON strand was found to be more destabilizing than B or E-derived constructs when hybridized to an rA_{18} target (ΔT_M = -3°C for P *vs.* E or B; data not shown). Yet on the basis of purely anatomical considerations alone, one would have expected P-containing duplexes to bear the greatest structural resemblance to the unmodified duplexes (*i.e.* **Table 3.2**, sequences **2.3:2.24**) and consequently to exhibit the least dramatic thermal perturbations to hybrid structure.

However, the observed thermal variabilities associated with each of these flexible 'defects' cannot be explained by rationalizing the intrinsic structural distortions associated with intraresidue bond length alone (*i.e.* C2, C3, C4 hydrocarbon spacers), nor are they solely the result of an absent base-pairing partner at this location of the duplex. In the latter case, removal of an intrahelical deoxynucleotide and its replacement with an aliphatic, anucleosidic linker completely obliterates any canonical Watson-Crick base-pairing and associated stacking interactions at this junction, regardless of the length or composition of the incorporated linker. Thus, all modifications would be expected to destabilize the hybrid to the same extent solely on this account. In contrast, the existence and energetic consequences of structural deformations or irregularities arising from linker-induced extensions (*e.g.* butyl; C4) or compressions (*e.g.* ethyl; C2) at this region

Table 3.2: Melting Temperatures (T_M) and Percent Hyperchromicity Values of Mono- or Bistranded Anucleosidic Duplexes[a] with all-RNA or RNA-B9

		All-RNA Target **2.24**			RNA-B9 Target **3.5**		
Entry	AON Designation	T_M	ΔT_M[a]	% H	T_M	ΔT_M[b]	% H
2.3	DNA	52.1	---	20.5	40.1	---	14.0
2.4	DNA-B10	47.1	-5	16.9	34.1	-6	15.4
2.6	DNA-B-L	48.0	-4	18.7	35.2	-5	15.6
3.1	DNA-P10	37.1	-15	15.6	31.4	-9	14.9
3.2	DNA-P-L	44.0	-8	15.9	32.4	-8	15.2
3.3	DNA-E10	40.2	-12	16.2	36.0	-4	14.2
3.4	DNA-E-L	47.0	-5	17.7	36.0	-4	15.1
2.5	DNA-dC10	39.9	-12	n.d.	n.d.	n.d.	n.d.

[a]Aqueous solutions of 2.38 x 10^{-6} M of each oligonucleotide. Results were derived from three independent measurements; uncertainty in T_M is ± 0.5°C. Scans were recorded at 260 nm and measured from 5°C – 85°C in buffer consisting of 140 mM KCl, 5 mM Na_2HPO_4, 1 mM $MgCl_2$ (pH 7.2). The reported differences in T_M are those relative to [a]fully matched (**2.24**) or [b]butyl-modified (**3.5**) RNA targets; n.d., not determined.

of the helix, indicate the underlying presence of more subtle effects not discernible from the melting data alone. Likely, they reflect a complicated interplay between enthalpic destabilization, associated with variable degrees of stacking propensity in adjacently paired nucleobase flanks, and balancing entropic countereffects, associated with the inherent flexibility of the linker under examination.

One can also envision a further compensatory effect on hybrid formation in ethyl-modified AON, arising from favourable water contacts between the anchored hydroxymethyl side chain on this linker (**Figure 3.7**), which could conceivably be solvent exposed and accessible. The tether may thus act to 'bridge' the gap with the orphaned base in the RNA strand through water-mediated hydrogen-bond formation, thus stabilizing the duplex cavity and organizing the helix via solvation.[274,275] Accordingly, the exact structure and composition of the anucleosidic lesion exerts seemingly unpredictable impacts on the magnitude of destabilization imparted to the helix. Among

these, changes in duplex solvation, propagation of stability through the phosphate backbone itself and local helical organization by the penetrating ability of water into the anucleosidic site as dictated by the size of the cavity, are few of the factors that may collectively contribute to the observed differences.

(B) Looped Linker Series. In comparison to the above, some thermal stability among each of the sequences could be recovered by forcing each of the respective linkers to 'loop' away from the helical axis of the hybrid with concomitant restoration of partial base pairing (DNA-X-L series bound to all-RNA **2.24**). Once again, similar trends to the X10 series were evident, indicating that P-L sequences were largely destabilizing in a looping context as well. However, a larger degree of thermal compensation occurs with this modification as with the ethyl surrogate, in comparison to the butyl looped linker (*e.g.* $\Delta\Delta T_M$ = +7°C for **3.1** and **3.2** *vs.* $\Delta\Delta T_M$ = +3°C for **2.4** and **2.6**; **Table 3.2**), thus suggesting these shorter hydrocarbon linkers to experience fewer energetic consequences than butyl when forced to loop out of the helix. In addition to other factors (*vide supra*), such thermal reductions may further be rationalized by the propensity with which the former two modifications influence the localized melting or 'breathing' of the helix in the vicinity of the anucleosidic site.

3.4.2. Thermal Properties of 'Symmetric' or Bistrand Linker-Modified Duplexes

We were also interested in determining the thermal behaviour of duplexes containing linkers within 2 opposing sites in the helix (*i.e.* bistranded defects; linker-modified DNA sequences bound to RNA-B9 **3.5**), accompanied by the removal of all interresidue hydrogen bonding associations between the dT-rA pairing partners comprising the central 2 nucleotide units in the native fully matched octadecameric duplexes. This was generated by single- (DNA-X-L:RNA-B9) or double-deletion (DNA-X10:RNA-B9) of these two residues, and their replacement with one of the 3 hydrocarbon spacers in the two pairing strands (**Figure 3.8**).

Inspection of the melting data (**Table 3.2**) reveals virtually no change in hybrid thermal stabilities upon going from a stretched to a looping linker conformation (**Figure 3.8**, panel **D**), in marked contrast to the situation that occurs with exclusively *antisense*

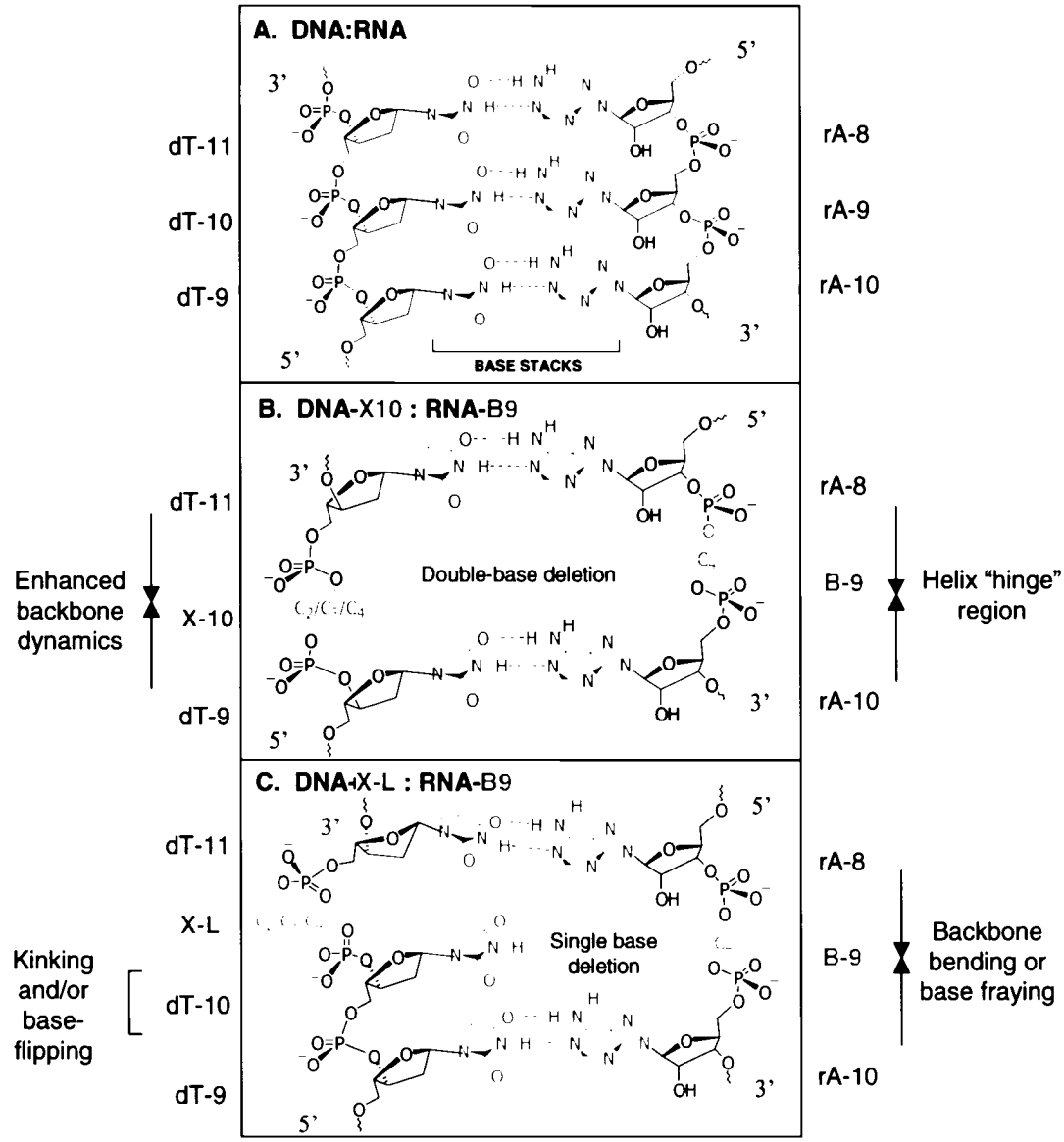

Figure 3.9: Native (**A**) and bistrand-modified hybrids (**B** & **C**), showing the central 3 base stacks unique to each duplex along with associated interresidue numbering; X denotes C2 (ethyl), C3 (propyl), or C4 (butyl) interphosphate linkages. Possible structural consequences common to all linker-modified duplexes are shown alongside the deformable helix sites and discussed in the text.

modified constructs (**Table 3.2** & **Figure 3.8**, panel **C**). In fact, this is quite expected, given the consequent inability of any one of the bistrand-modified hybrids to retain base pairing at the linker junction (**Figure 3.9**). Furthermore, given the large degree of backbone internal mobility at the acyclic junctions, it is possible that both types of symmetrically-modified duplexes also experience some breathing or 'fraying' of adjacent

base pairs, perhaps dictated by the size of the resulting hydrophobic cavity created by the double-linker insertions.

In bistrand-modified hybrids of the X-L series, other structural departures from normal helical stereoregularity are further possible in addition to the above: (i) the unpaired base might maintain the internal hydrophobic stack, but would be accompanied by a 'kinking' or bending of the duplex at the linker hinge to accommodate the extra steric bulk; (ii) extrahelical rotation or flipping of the orphaned base away from the internal cavity could conceivably occur, perhaps accompanied by a localized compression of the phosphate backbone which would thereby favour stacking of the adjoining helical halves, in a manner similar to that which might occur in the less sterically demanding situation encountered in the X10 series of symmetrically-modified hybrids (**Figure 3.9**, panels **B** & **C**). In fact, interdomain stacking seems most probable for E10 and E-L AONs (**3.3** & **3.4**) when paired with RNA-B9 **3.5**, whose thermal stabilities are equal in magnitude and significantly greater than similar hybrids in which a propyl unit replaces the ethyl spacer ($\Delta\Delta T_M$ = + 3-4°C *vs.* **3.1** & **3.2** bound to **3.5**; **Table 3.2**). External displacement of helical lesions is not an uncommon phenomenon and has frequently been observed for abasic and mismatched sites as well.[274,276-279]

Obviously, such a dynamic picture of intrinsic helical plasticity cannot be dissected from this work alone, and thus necessitates further examination through the implementation of refined methods (*e.g.* NMR and X-ray crystallographic analyses) to probe the individual conformational properties unique to each duplex type.

3.5. Hyperchromic^{280} and First Derivative Analysis of Helix Interdomain Cooperativity

One structural feature that we were capable of probing however, was the ability of each of the anucleosidic hybrids to undergo *cooperative* transitions upon heat denaturation and dissociation of the respective complexes into single strands. This characteristic is derived upon examination of hyperchromic changes in UV absorption profiles that accompany the melting of a duplex when monitored at a single wavelength (*i.e.* λ_{max} *ca.* 260 nm).

Such associated spectral changes by which the denaturation process is measured thus constitute an optical phenomenon that reflects a diminished capacity of the chromophoric

nucleobases within the duplex to absorb UV light relative to their absorbances in the single stranded (disordered) state. At low temperatures, there is a relative decrease in absorption intensity (*i.e.* a 'hypochromic' effect) that is predominantly manifest from the ordered array of transition dipole moments originating from the neighbouring nucleobase chromophores residing uniformly within the intertwined helix, which themselves possess optical densities that are consequently lower than the sum of their constituent unpaired mononucleotides.[281-283] As the duplex is denatured, this ordered stacking of adjacent nucleobases is sharply disrupted with a concomitant increase (*i.e.* hyperchromism) in the absorption profile. Upon further heating of the nucleic acid solution, the monitored absorbance displays a plateau effect, in which the absorption intensity exhibits only negligible increases with increasing temperature. Hence, spectral differences that accompany the heating of a nucleic acid complex are highly indicative of the helix-random coil equilibria and the order-disorder state of the intertwined strands.[257]

Indeed, the concept of hyperchromism is based on well-established theoretical and experimental foundations that thereby provide a solid basis for understanding the cooperative nature by which two complementary single strands exhibit association/dissociation behaviour. Accordingly, a cooperative melting process is one that is characterized by a sharp increase in absorption over a narrow temperature range, and is represented by a single sigmoidal curve with inflection point centered on the temperature at which half the duplex population has dissociated to the single strands; it is also indicative of abrupt destacking and unzipping of the duplex. Hyperchromism and cooperativity are therefore interdependent properties that are proportional to the number of nucleotide units involved in neighbouring interactions (*i.e.* polynucleotide chain length) and can thus serve as useful probes of the 'randomness' of nucleic acid secondary structure.[280,283,284]

We applied these principles to discern the qualitative influence of the aliphatic spacers on the integrity of duplex formation, in particular to determine whether the inclusion of an anucleosidic site within the duplex would affect its overall ability to associate with the intended RNA target as a single unit. For comparative purposes, we also synthesized a set of short AONs designed to mimic the pairing interactions common to each of the linker-containing hybrids (**Figure 3.10**). These derivatives were specifically constructed

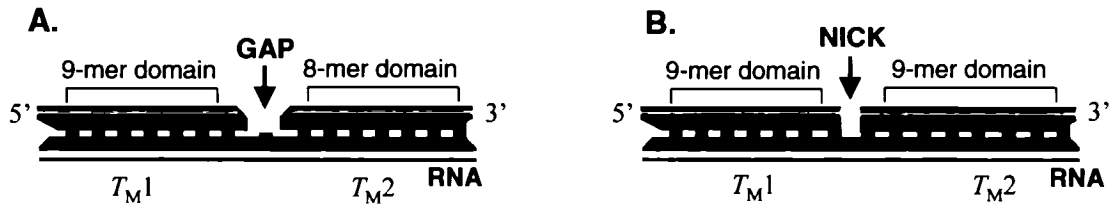

Figure 3.10: Structural representation of 2'F-ANA 'gapped' (**A**) and 'nicked' (**B**) duplexes with RNA (**2.24**), constructed to mimic 'stretched' or 'looped' DNA designs, respectively. These sequences were designed to show that in the absence of an internal tether on the AON domains, the two helical units no longer support interdomain communication. 2'F-ANA sequences (5'→3') are: TTA TAT TTT (nonamer 5'-unit; **3.6**), TC TTT CCC (octamer 3'-unit; **3.7**), and TTC TTT CCC (nonamer 3'-unit; **3.8**).

using 2'-fluoroarabinonucleotide units, which have been shown to mimic the conformational properties of the native deoxynucleotides at both the monomer and oligomer levels, yet exhibit substantial increases in thermal stability when directed toward RNA complements (ΔT_M = + 1 – 2°C/nt modification), likely as a result of the enhanced preorganization of the relatively rigid fluoroarabinose sugar framework over its deoxyribose-based counterparts.

As such, we surmised this modification to be beneficial for retaining tight RNA pairing affinity, despite the complete disconnection of a fragment of the phosphodiester backbone, which ultimately divides the resultant AON/RNA duplex into two defined 'subhelical' segments. Such tandemly arranged segments could therefore provide insight on the extent to which the melting cooperativity might be disrupted in the DNA-based anucleosidic AONs.

3.5.1. Melting Cooperativity of Asymmetric and Bistrand-Modified Duplexes

It is apparent from the data presented in **Figure 3.9** that all anucleosidic duplexes – whether singly- or doubly-modified – undergo relatively monophasic transitions with increasing temperature as demonstrated by a lack of pronounced deviations in melting cooperativity relative to the fully matched hybrids. This is further evident upon inspection of normalized plots illustrating the temperature-dependent changes in hyperchromicity (**Figure 3.11**, inset), which itself is proportional to the fraction of each helical domain melting as an isolated unit.[285]

A. 'Stretched' Duplexes (X-10 Series)

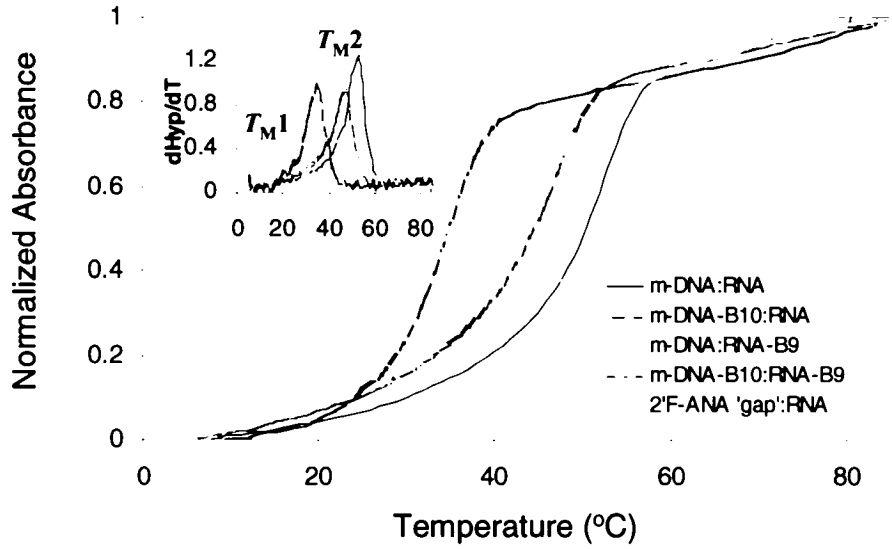

B. 'Looped' Duplexes (X-L Series)

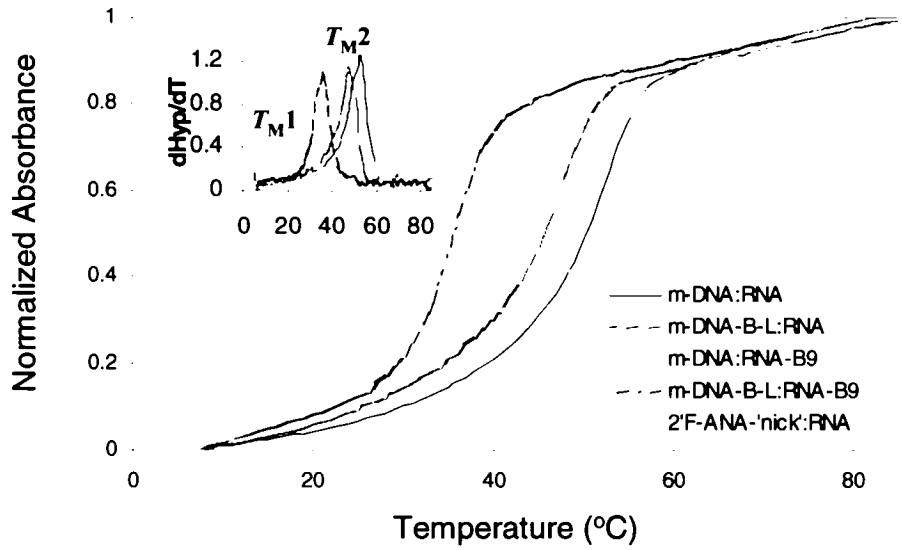

Figure 3.11: Temperature-dependent UV absorption profiles of single- and double-modified 'flexible' AON:RNA hybrids at 260 nm; data for propyl and ethyl-containing AONs were analogous to the above and have thus been omitted for clarity. The 'gapped' and 'nicked' sequences were derived from 2'F-ANA AONs, which bind more stably than DNA to the target and were thus designed to illustrate two independent melting transitions in the absence of cooperativity transfer from one helical unit/domain to the other. Normalized melting profiles were obtained by equating the fractional absorbance change using the formula $A_{norm} = (A_T - A_o)/(A_F - A_o)$, to facilitate comparative visualization of the component behaviour.[286] Inset: First derivative hyperchromic curves illustrating single- *vs.* double transitions of duplex domains in linker-modified *vs.* 'gapped' or 'nicked' duplexes respectively. Peak maxima correspond to the T_M of each transition, and are respectively denoted as T_M1 and T_M2.

Consequently, in the complete absence of a linker in the pairing strands, melting of one of the octameric or nonameric hybrid domains is completely decoupled from the second, even for a thermally more stable duplex such as that obtained upon annealing a 2'F-ANA-derived AON to the corresponding segment along the RNA complement. The melting curves for these analogues are clearly biphasic, indicating that at least 2 steps could be reliably detected in the melting process. As such, melting of 'nicked' or 'gapped' hybrid duplexes (**Figure 3.10**) is accompanied by an additional transition not observed in the melting of any of the anucleosidic hybrid duplexes (**Figure 3.11**), thereby demonstrating the domains to be paired in these latter cases, rather than exhibit decoupled melting as in the former. Indeed, such an occurrence of 2 well-defined melting transitions is strongly indicative of regions exhibiting noncooperativity, associated with the removal of the intervening tether and substantial loss of nearest-neighbour nucleobase interactions at this junction.

Interestingly, bistranded linker insertions do not exhibit further alterations in melting cooperativity relative to single strand (*i.e.* asymmetric) modifications, again suggesting that the presence or type of helical imperfection in both of the annealing strands does not divide the overall duplex into isolated halves of differing thermal stabilities. In light of this consideration, and the fact that virtually no thermal stability is lost upon stretching or looping the linkers in the AON (**Table 3.2**; AONs bound to RNA-B9 **3.5**), it is conceivable that the flexible bistranded 'joints' connecting the 2 helical halves of these doubly-modified duplexes simply allow the nucleotide pairs flanking the linkers to maintain the stacking interaction in a manner which is not possible in discontinuous or 'nicked' duplexes by virtue of the relatively larger degree of unrestricted internal motion in the latter. That cooperativity effects between two divided segments may be communicated through rearrangement of the phosphate backbone, is in full agreement with studies by Becaud and coworkers,[285] who inserted single or multiple propyl units either asymmetrically or symmetrically (*i.e.* bistrand defects) and found duplex melting to become gradually decoupled only upon contiguous incorporation of more than two units. In conclusion, all anucleosidic duplexes exhibit only mild reductions in hyperchromicity relative to the full Watson-Crick based paired duplexes. In addition, there appears to be extensive interdomain communication within each of the linker-modified constructs,

suggesting that any associated compromises in duplexation affinity are not a consequence of impaired cooperativity, and that the linkers impart only localized structural defects to the integrity of the corresponding hybrids by achieving a position within the duplex that is compatible with full target binding of the anchoring deoxynucleotide tracts (see also **section 3.6.**).

3.6. Effect of Linker Length, Composition and Flexibility on RNase H-Mediated Sense Strand Hydrolysis

We next attempted to define the contributions of each nucleic acid structural imperfection in terms of its potential biological relevance as an antisense therapeutic, by examining the relative abilities of both asymmetric (monostrand) and symmetric (bistrand) linker-containing duplexes to undergo processing by human RNase H1. Not only was this work encouraged by our previous observations on the superior abilities of butyl-modified antisense to induce rapid RNase H-mediated sense strand hydrolysis (see chapter **2**), we also speculated that the inherent flexibility and associated composition of each anucleosidic site might impart different degrees of curvature, or bending, within the hybrid substrate, allowing for preferential contact with and cleavage by RNase H.

3.6.1. Linker Placement in the Antisense Strand (Single-Strand Defects)

To evaluate the influence of antisense strand promoted-effects on the ensuing enzymatic activity, each of the AON-modified hybrids was bound to an all-RNA complement (**2.24**) and incubated with human RNase H1 over varying time intervals. The temperature at which these assays were conducted (*i.e.* 22°C) was chosen on the basis of the melting temperature of the weakest hybrids of the series, in order to ensure full duplexation and equivalent availability of each substrate for the enzyme under the experimental conditions. Aliquots of each solution were removed over the course of the incubation, and enzyme activity was abruptly quenched, followed by electrophoretic separation of the 5'-labeled RNA digestion products to evaluate the precise position and extent of cuts generated along the labile RNA component.

General inspection of the resolved cleavage fragments arising via RNase H-mediated hydrolysis reveals that the linker-modified AONs support efficient enzyme recruitment in

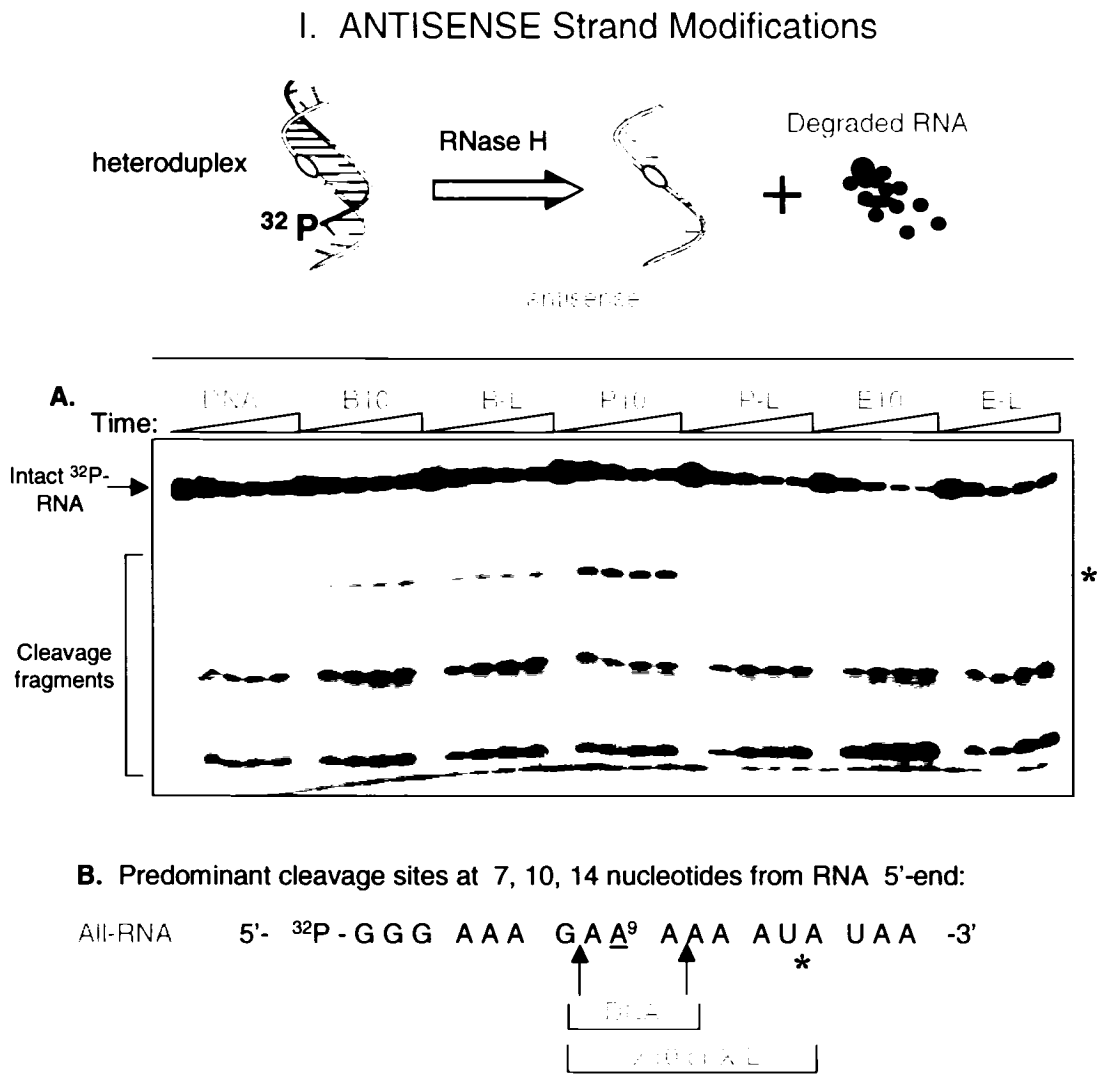

Figure 3.12: Human RNase H1 assays on linker-modified AON hybrids with all-RNA. **A.** PAGE results showing RNA cleavage products generated from full length 5'-^{32}P-labeled-RNA (**2.24**, 1 pmol) incubated with 10 pmol of each AON. Complementary strands were mixed in buffer (60 µL final volume) containing 60 mM Tris-HCl (pH 7.8), 60 mM KCl, 2.5 mM $MgCl_2$, and 2 mM DTT, then heated at 90°C for 5 minutes and slowly cooled. Reactions were initiated by the addition of purified human RNase H1 (0.4 ng) and the substrate solutions were further incubated for 5, 10, 20 and 30 min at 22°C. After the alloted incubation time, samples were quenched by the addition of an equal volume of denaturing loading buffer (98% deionized formamide, 10 mM EDTA, 1mg/mL BPB and 1 mg/mL XC). Reaction products were denatured by heating at 100°C for 5 min, followed by electrophoretic resolution on 16% polyacrylamide sequencing gels containing 7M urea. **B.** Position of primary cleavage sites generated in the RNA target. $\underline{A}^9$ denotes the identity and position of the ribonucleotide opposite the linker insertion site in the AON. The asterisk denotes the position of the 14 nt RNA fragment arising exclusively in the digestion profiles of linker-containing substrates.

a manner that only loosely depends on the composition of the linker insert. A most prominent feature of the degradation reaction is an intriguing ability of stretched (X10) and looped (X-L) hydrocarbon linkers residing in the antisense strand to promote an additional site-specific cut within the target RNA species when in the presence of the enzyme, as indicated by the appearance of a single intense band of low electrophoretic mobility, consistent with the migration of a 14 nt RNA fragment (**Figure 3.12**). Accordingly, under conditions favouring partial hydrolysis of duplexed substrates, we observed a consistent shift in the pattern of cleavage for each of the linker modified hybrids, indicating a broader degree of tolerance by RNase H to act upon multiple locations in the 'test' substrates. The extra cleavage site is surprisingly absent in the fully matched parent hybrids (*i.e.* DNA **2.3** bound to RNA **2.24**) in which the predominant scissile locations are always found to occur 7 and 10 nucleotides away from the 5'-end of the RNA within this sequence context. In the latter case, this 'normal' cleavage pattern is consistent with the proposed biological role of human RNase H1 in nuclear[236,287] and mitochondrial DNA replication[239,288] in which the enzyme is implicated to remove Okazaki primer fragments during discontinuous or 'lagging' strand DNA synthesis.[229,289,290] This occurs by the introduction of strongly site-specific cuts in the RNA strand of the primer-template complex near the RNA-DNA junction of the replicating strand that spans a window of 7 – 12 nucleotides from the 5'-terminus of the initiator RNA segment.[242,291] Also consistent with this biological mode of action is the ability of the enzyme to discriminate the precise antiparallel arrangement of duplexed strands, preferentially exerting its effects upon the 5'-RNA/3'-DNA part of the hybrid in an endonucleolytic manner with little evidence of subsequent exonucleolytic processivity.[288,292]

As such, not only is the apparent stringency in site selection by RNase H alleviated by the presence of a hydrocarbon linker in the AON, accumulation of the 14 nt RNA fragment seems to exhibit some dependence on linker composition, with a gradual reduction in the abundance of this band observed upon interchanging a longer member of the acyclic series for a shorter analogue.

Clearly, both a flexible helical junction and/or gap size somehow affect the scanning mechanism by which RNase H selects a particular position for cleavage. That the

induced cuts always occur at a specific distance upstream of the flexible region in the AON (*ca.* 4-5 nts) strongly suggests that the linkers steer the enzyme-hybrid interaction in an *exclusively* directional manner, perhaps through facilitated binding at the linker site which – when coupled with the ensuing downstream RNA cleavage event – would account for the observed product distribution. In fact, the 3'-shift in the digestion profiles along the complementary RNA strands correlates well with the spatial separation between a general nucleic acid binding region at the N-terminus of the human enzyme and the nearby catalytic center, which are estimated to span little more than a half turn of the duplex (*ca.* 5-7 nts).[293]

It is noteworthy that the *overall* extent to which sense strand hydrolysis occurs is uniformly enhanced by the linker-modified AONs, irrespective of likely differences in

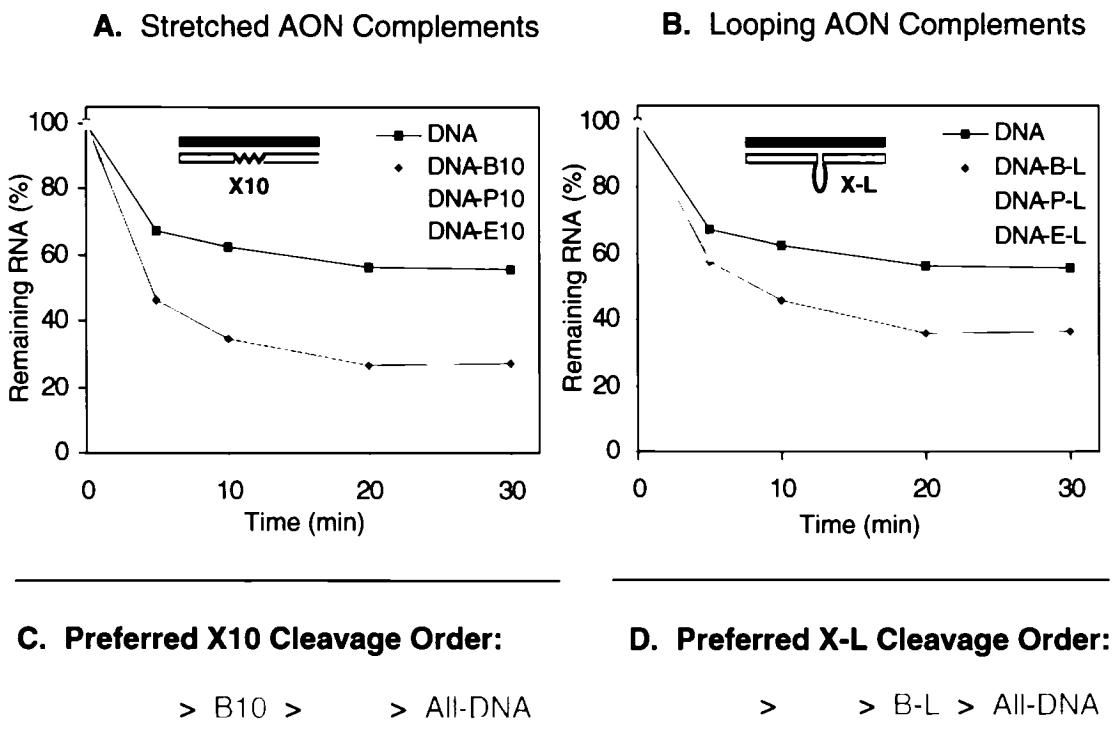

Figure 3.13: Levels of target RNA cleavage in antisense-modified DNA:RNA heteroduplexes, as determined in the presence of human RNase H1 (0.4 ng). Although all modified constructs elevate the extent of target scission that occurs over the native hybrids, complements with a stretched linker (**A**) tend to work as well as, or better than, their looped counterparts (**B**). The observed order of enzyme-mediated RNA degradation noted within each series of hybrids (panels **C** & **D**) conforms to the following overall preference of the enzyme to act upon the RNA partner of a given AON-modified substrate as follows: E10 >> B10 ~ P-L > E-L > P10 ~ B-L > all-DNA.

local structure and interresidue motility surrounding the modification junction. Accordingly, *all* anucleosidic AON hybrids with RNA are more proficient at activating the enzyme as compared to the native heteroduplex, with moderate differences in scissile susceptibility reflected by the type of linker comprising the central site and its assumed spatial disposition at the helix periphery, whether forced to lie parallel to the duplex axis or extrahelically projected (*i.e.* X10 *vs.* X-L; **Figure 3.13**, panels **A** & **B**). Stretched DNA-X10 complements, in particular, generally tend to accelerate target strand scission by RNase H as well as, or somewhat better than their 'looping' counterparts, with the interresidue X10 hydrocarbon length and local architecture further highlighting the fickle nature of substrate recognition and enzyme processing. This trend is largely reflected by a comparatively variable spread in the overall amounts of RNA cleaved within this series as compared to the X-L constructs, the latter showing only a modest degree of dependence on the identity of the linker at the insertion site (**Figure 3.13**).

In summary, these results collectively demonstrate that productive interactions between the enzyme and a respective linker-modified heteroduplex substrate can evidently be promoted in a somewhat general manner that is primarily influenced by local helical flexibility, with only a secondary influence on activity arising from the nature of the residue constituting the flexible helical junction. This is a striking observation in view of the stringent requirement for structural preservation at the atomic level of other nucleic acid recognition elements as previously established by us and other groups (*i.e.* global helix morphology as dictated by local sugar conformation).[48,111-113,115] It is appealing to envision that consequent RNase H recognition of 'defective' duplexes is associated with an adaptive binding mechanism that is somehow made more favourable in the presence of increased backbone plasticity or the strategic placement of 'holes' within target substrates. Indeed, structural reorganization of the substrate by the enzyme is likely a process that must occur for effective catalysis, and also implicated to account for the observed enhancements in this work.

3.6.2. Sense (RNA) Strand Placement & Effects of Anucleosidic Sites on RNase H Action

In a logical progression of the above principles, our next goal involved an attempt to scrutinize the nature of the underlying molecular mechanisms giving rise to the observed enhancements by examining possible influences on the binding *vs.* catalytic activities accompanying overall enzymatic function. To address this question, we designed hybrids comprising a singly-modified *RNA* strand, in an effort to determine the extent to which enzyme recruitment and subsequent target destruction might further depend on the origin of the strand hosting the flexible modification. Heteroduplexes of this type were quite simply derived by an *interstrand* inversion in the helical placement of the linker, such that the internal flexible gap region in the resultant heteroduplexes would now ultimately reside within the RNA rather than the DNA component, while still retaining the same *intrastrand* distance from terminal base pairs at the duplex poles. As such, hybrid substrates containing the 'inverted' anucleosidic site were assembled by annealing the respective butyl-modified ssRNA (RNA-B9; **3.5**) with a contiguous oligodeoxynucleotide complement (all-DNA; **2.1**) to construct the inverse gap region. The corresponding degradation profile of this derivative was contrasted to that of the fully matched heteroduplex, also the poorest activator with respect to the AON-modified series of analogues (see **section 3.5.1.**).

(A) Effects on Catalysis. Autoradiographic analysis of the enzymatic digests reveals that *sense*-modified hybrids strongly suppress enzyme activity, in sharp contrast to the operative situation occurring in monostranded linker-containing AON heteroduplexes with all-RNA. Specifically, under conditions favouring complete and rapid cleavage of the fully-matched parent helices, sense-modified constructs are very poorly cleaved, indicating a pronounced inability of the enzyme to interact efficiently with the RNA linker site in a manner conducive to catalysis. Sense-modified hybrids are, in fact, profoundly resistant towards enzyme-induced degradation, requiring *ca.* a 5-fold greater concentration of enzyme in order to attain roughly the same level of activity as that which occurs with either unmodified or antisense-modified derivatives. A second surprising occurrence in the digestion mixtures of these substrates is the apparent absence of a

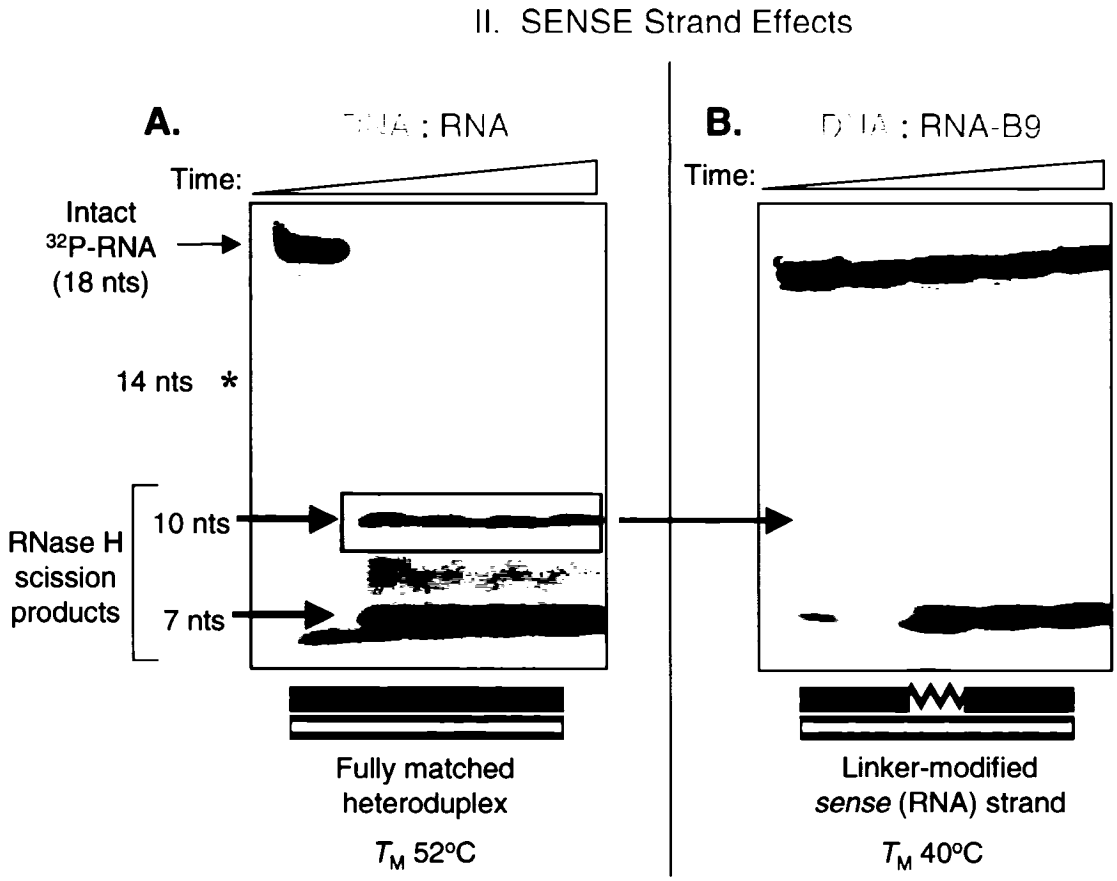

Figure 3.14: A linker-modified RNA target impedes RNase H action. Incorporation of a linker into the sense strand is detrimental to activity in all tested substrates, as demonstrated by the pronounced decrease in abundance of full-length RNA-B9 (**3.5**; panel **B**) *vs.* the native all-RNA mixed sequence target (**2.24**; panel **A**) over time. Lanes (left to right) correspond to 0, 5, 10, 20 and 30 min enzyme incubations in the presence of human RNase H1 (2.0 ng, 22°C), in buffer consisting of 60 mM Tris-HCl (pH 7.8), 60 mM KCl, 2.5 mM $MgCl_2$, and 2 mM DTT. The asterisk denotes the expected migration of the 14 nt RNA scission product, which is only observed in linker-modified AON hybrids with RNA (see **Figure 3.12**).

primary cut at the 10^{th} ribonucleotide in the target (**Figure 3.14**), again strongly contrasting with the observed degradation profiles of all analogous hybrids thus far examined. As this region in particular should exactly coincide with the precise positioning of the catalytic subunit of the enzyme upon binding, it is entirely conceivable that the ablated activity owes to severely adverse effects on the catalytic rather than the binding event, arising from an inhibitory influence of the linker at the adjacent upstream (*i.e.* 9^{th}) position in the RNA strand. This proposal is consistent with the established role

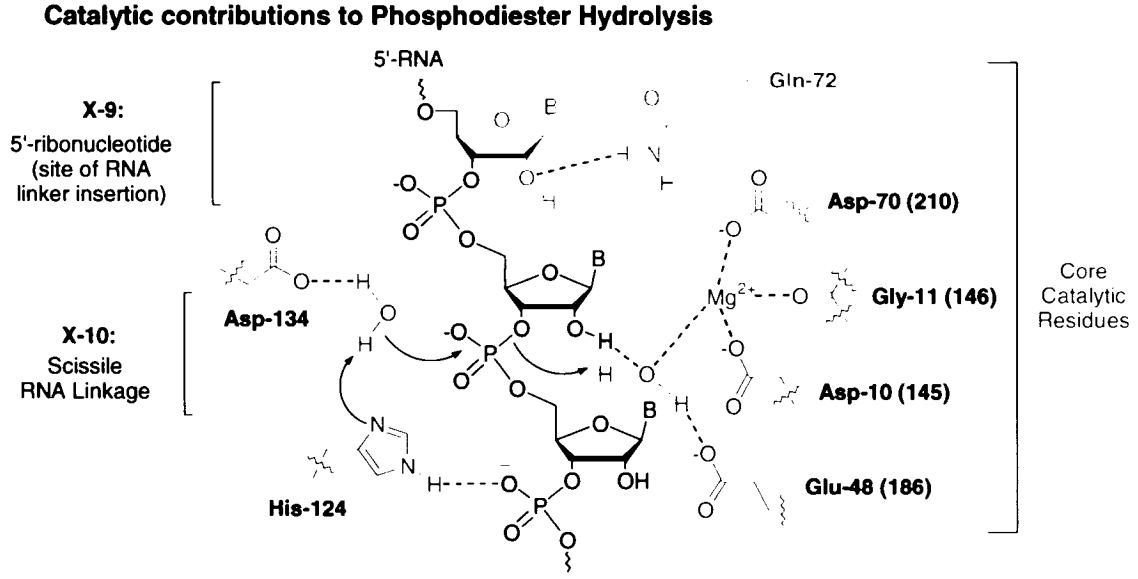

Figure 3.15: Proposed general acid-base catalytic mechanism of *E. coli* RNase H1. Metal-dependent catalysis proceeds via coordination of an outer-sphere water molecule with Mg^{2+}, itself anchored by multivalent contacts to the enzyme active site (implicated residues are shown alongside with human RNase H1 numbering in parentheses). In-line cleavage of the scissile phosphodiester bond is mediated by a second water molecule that supplies the nucleophilic hydroxyl ion, with a histidine residue acting as a proton sink. A conserved Gln residue (Gln-72) stabilizes the bound complex through hydrogen bond formation with the 2'-hydroxyl group of the ribonucleotide 5' to the scissile site[40,294,295] (gray shaded residue); linker insertion at this site likely disrupts this contact and abolishes scission at the adjacent position. Based on a similar model discussed by Haruki *et al.*[100] and reported by others.[247,296]

of the 2nd ribonucleotide 5' to the scissile phosphodiester linkage, in which the 2'-hydroxyl of this residue favourably contributes to the structural integrity of the nucleoprotein complex with *E. coli* RNase H1 by maintaining hydrogen-bonded contacts with a conserved glutamine (Gln) residue at the active site surface of the enzyme[101,295-297] (**Figure 3.15**). Inferences from site-directed mutagenesis of critical residues and molecular modeling of the human core catalytic domain have further extended this obligatory role for a similar Gln residue in substrate recognition by the human homologue.[298] Accordingly, the observed drop in activity accompanying replacement of the ribonucleotide upstream of the cleavage site with an aliphatic linker supports previous observations, and further implicates a similar functional dependence of the enzyme for

the 5'-ribonucleotide unit in organizing the formation of the enzyme-substrate complex directly at the active site for the ensuing hydrolytic event.

(B) Effects on Binding – Cleavage Site Specificity. While the disappearance of the canonical 10 nt RNA scission product is consistent with an obstruction in catalysis of RNA-B9 substrates, absence of the 14 nt cleavage band normally accompanying linker-induced site-specific cleavage in AON-modified derivatives (see **Figures 3.12 & 3.14**) implies suboptimal enzyme binding at the new RNA-B9 junction, despite the associated flexibility imparted to the hybrid structure by the butyl insert. That the thermal stability of this sequence is equal in magnitude to that of the most potent AON-modified analogue (DNA-E10, **3.3**), further suggests exquisite differences in enzyme recruitment, rather than suboptimal duplexation. Indeed, such a rationale presupposes a biased mode of strand selection by RNase H during binding at specific helix loci, in which the enzyme preferentially locates the antisense strand at the linker junction (**Figure 3.8 C**) and uses it as a landmark for subsequent positioning along the heteroduplex. The induced flexure in RNA-modified hybrids may alternatively distort the trajectory of the duplex unfavourably upon interacting with the RNase H binding domain, such that the downstream duplex segment no longer interacts efficiently with the distal catalytic site. Evidently as in unmodified hybrids, enzyme recognition of, and downstream cleavage from the RNA-linker site is lost. As such, the accompanying elevations in the activation potency and broader site tolerance of 'flexible' duplexes appears to be exclusively strand-specific within this particular base sequence and/or locus, with beneficial effects observed only upon localizing the linker to the AON – rather than the RNA – component of the nucleic acid pairing partners.

3.6.3. Antisense + Sense Strand Effects: Restoration of Enzyme Activity via Bistranded Linker Modifications

In agreement with the preceding hypotheses, such a trend reversal in hybrid discriminatory activities by RNase H stops short at *dual* modification of both sense and antisense strands in the respective substrates. In this case, a sizeable improvement in enzyme-mediated target degradation is realized upon examining the rates of RNA

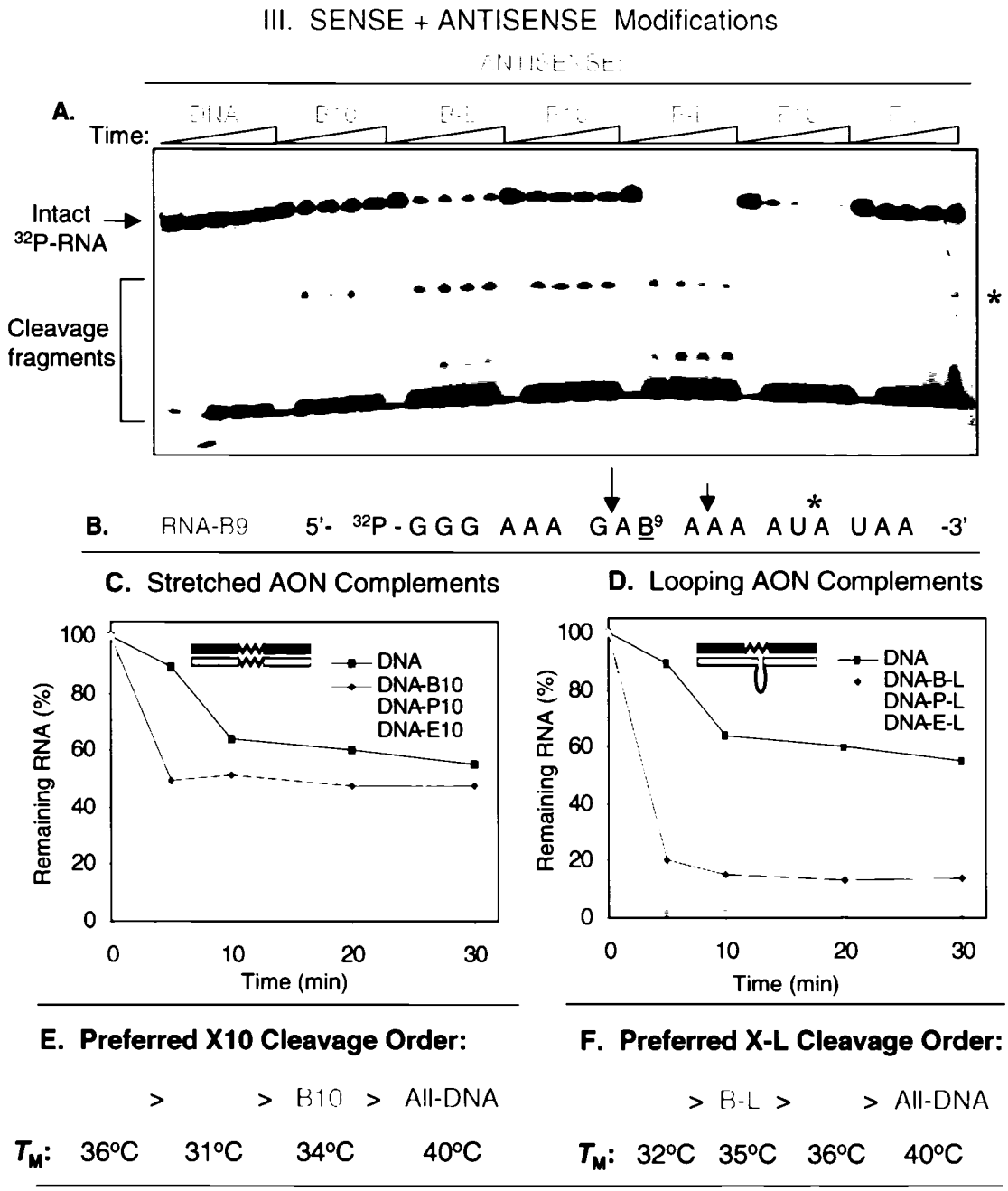

Figure 3.16: Bistrand-modified duplexes support variable levels of target strand cleavage. **A.** PAGE results showing RNA cleavage products generated from full length 5'-^{32}P-labeled-RNA-B9 (**3.5**, 1 pmol) incubated with 10 pmol of each AON. Lanes (left to right) correspond to 0, 5, 10, 20 and 30 min enzyme incubations in the presence of human RNase H1 (2.0 ng, 22°C). **B.** Position of primary cleavage sites generated in the RNA target; $\underline{B}^9$ indicates the modification site in the duplexed species. The asterisk denotes the position of the 14 nt RNA fragment arising exclusively in the digestion profiles of substrates with a linker-modified AON component. Panels **C** – **F** illustrate the observed preference of enzyme-mediated target hydrolysis for a given AON modification, and roughly noted as: P-L > E10 > B-L >> P10 > B10 ~ E-L > all-DNA.

scission in substrates containing double aliphatic substitutions for the central base pair in the helix, in contrast to the single-RNA strand modified 'control' duplexes. This is exemplified in **Figure 3.16**, where not only does the extent of target cleavage always exceed that attainable in RNA-B9 control hybrids with all-DNA, but bistrand flexible duplexes also proficiently restore cleavage lability at the cryptic downstream (*i.e.* 14^{th}) position in the RNA target. Furthermore, the propensity with which each of the modified hybrids activates RNase H in this case is rather variable (see **Figure 3.16**, panels **C** & **D**) and demonstrates little, if any, reliance on the intrinsic pairing stability of the two strands constituting the recognizant substrate. This is strongly evident upon comparing the activation potencies of each of the hybrids with their respective duplexation strengths. For example, all DNA complements with a linker in the stretched or looped conformation, when bound to butyl-modified ssRNA-B9 (**3.5**), are equally thermostable for a given linker composition (**Table 3.2** and **Figure 3.16**, panels **E** & **F**), yet show marked differences toward favouring rapid and efficient enzyme induction. This is best illustrated in DNA-E10 hybrids complexed with ssRNA-B9 (**3.5**) which serve as the most potent substrates within this series of dual modifications, yet become the weakest enzyme activators when the ethyl spacer is extruded away from the helical core (*i.e.* DNA-E-L) despite strong similarities in pairing affinities to the RNA component (see **Table 3.2**). Accordingly, the competency of a given antisense composition is seemingly dictated by the relative ease with which the enzyme can bind to and manipulate a given substrate, rather than on differences arising from hybrid dissociation-reassociation events succeeding enzyme action (*i.e.* higher turnover).

While extraordinary advantages on enzyme recognition and subsequent RNA hydrolytic susceptibility seem to generally be derived exclusively upon antisense-strand placement of a central aliphatic unit, it should be emphasized that none of the dually-modified duplexes could support target scission nearly as efficiently as that of the fully matched DNA:RNA cognates. This partial compensatory nature of a flexible antisense component on enzymatic recognition of dual interstrand structural deformities is illustrated in the following trend, which summarizes the overall preference for a given class of hybrids to support RNase H action: AON-linker:RNA (flexible antisense) > AON:RNA (fully

matched, unmodified duplex) > bistrand-modified AON:RNA > sense (RNA)-modified heteroduplexes with all-DNA ('inverted' flexible region).

Clearly, sense strand derivatization is highly inhibitory to enzyme induction in all contexts examined thus far, the effects of which are only partially counteracted by the accelerating potential associated with antisense-localized flexible regions. Although a precise molecular picture currently remains undefined, the apparent contradictory behaviour between the two pairing components might perhaps arise from anisotropic (*i.e.* directional) axial flexure[255] which could conceivably aid in orienting the substrate at the active site surface of the enzyme. Such an event may be favoured by antisense-modified analogues in particular, presumably by establishing local interactions with key amino acids specifically within the vicinity of the flexible AON region. As noted previously (*vide supra*), this proposal would further imply an asymmetric mode of contact by the enzyme across the minor groove of the substrate, in which sense strand deformability would contribute minimally, if at all, to eventual catalysis.

3.7. Structural Implications of Hybrid Helicity Derived from Circular Dichroism (CD) Studies[299]

We lastly examined the circular dichroic (CD) profiles of each class of modified hybrid in an effort to determine whether a flexible junction within the heteroduplex could impart a detectable curvature in the overall conformation that might ultimately aid in nucleic acid/protein complex formation. In this respect, CD spectroscopy, when applied to structural studies of nucleic acids, can provide powerful comparative information on the chiroptical properties intrinsic to oligonucleotides in the duplexed state. The induced circular dichroism (*i.e.* differential absorption of left- and right-circularly polarized light) of such irradiated molecules subsequently enables the qualitative assignment of overall hybrid conformation to be made and classed into one of the various families of nucleic acid polymorphs. Assignments are typically made upon reference to a duplex of known conformation in order to elucidate the overall binding mode of the macromolecular complex in question. CD signatures of dsRNA duplexes, for example, reveal adoption of the canonical A-form, whereas dsDNA duplexes typically assume a pure B-form helical arrangement as dictated by the molecular stereochemistry of the entwined strands and

intrahelical orientation of the chromophoric bases. Notable differences in the appearance of these spectra are strictly enforced by nucleobase sequence and interactions, which in turn are exquisitely sensitive to various geometric parameters including rise per base pair, base inclination or tilt relative to the helical axis and number of base pairs per turn. However, obtaining detailed structural information regarding the preferred disposition of individual nucleotides constituting the biomolecular framework is certainly a more challenging venue, and represents a primary shortcoming of this technique, yet adequate structural insight may still conveniently be derived without the need to resort to more refined methods (*e.g.* X-ray, NMR).[300] Consequently, our examination of duplex secondary structure by CD was further prompted by its intrinsically nondestructive nature, combined with its requirement for relatively small amounts of material, and applicability to a wide range of samples, including those difficult to obtain by crystallization.

Visual inspection of the CD spectral signatures of each of the anucleosidic duplexes in **Figure 3.17** confirms that inclusion of a deformable site at the central helical position does not alter the overall global morphology of these derivatives to any appreciable degree *vs.* the native heteroduplex. This is clearly evident by the strongly superimposable nature of each signature to that of the fully matched DNA:RNA pair, which itself assumes a profile intermediate in shape to that of the pure A- and B-form dsRNA and dsDNA helicities, respectively (**Figure 3.17**, panel **A**). As such, the atypical hybrid morphology is characterized by the presence of a positive CD band centered at *ca.* 270 nm, with a crossover occurring just below 255 nm and a low intensity negative band in the high wavelength region of the spectrum, all features which further corroborate the intermediacy of these hybrids to those of pure A- or B-form global geometries. Bistrand modified duplexes in particular show slight variations in amplitude intensity of the long and short wavelength bands, but as these peaks have been assigned to transitions associated with base stacking and sugar-phosphate backbone conformation, the differences are likely to be more artifactual rather than real and associated with the absence of the extra base-pairing partners at the central duplex region.

Indeed, the presence and close mimicry of the intermediate A-like conformation adopted by fully matched DNA:RNA heteroduplexes and likewise maintained in each of their

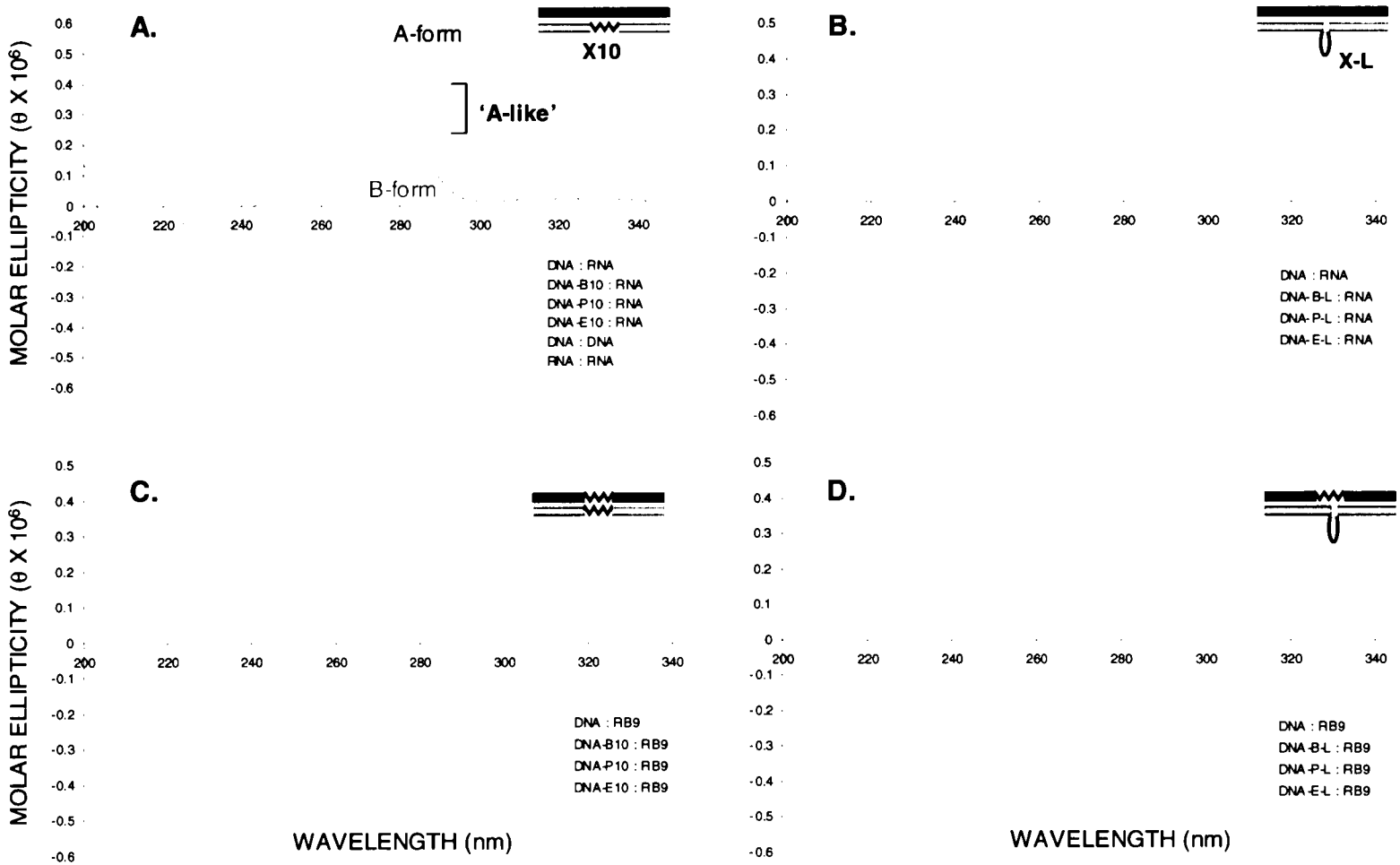

Figure 3.17: A - D. CD spectra of unmodified, mono- and bistrand-modified anucleosidic DNA:RNA duplexes. Scans represent 5 independent runs recorded at 5°C in buffer consisting of 140 mM KCl, 1 mM $MgCl_2$, 5 mM Na_2HPO_4 at pH 7.2 (2.5 μM duplex concentration). Pure A- and B-form reference spectra of analogous dsRNA and dsDNA duplexes given in panel **A** are those reported by Wasner *et al.*, 1998.[301]

anucleosidic derivatives is well known to be a critical factor in the consequent ability of the hybrids to invoke productive enzyme recognition.[42,48,101] Importantly, the absence of strong departures in structure from the unmodified duplex negates the likelihood of any observable static axial bending – as possibly facilitated in linker-modified surrogates – that thereby implies an active rather than passive role for these molecules in an RNase H mechanism of activation, perhaps involving adaptive binding to the enzyme surface prior to target hydrolysis.

3.8. CONCLUSIONS

The rather controversial issue of nucleic acid structural preorganization has, in fact, adopted mainstream attention as a means of improving many desirable therapeutic properties in promising antisense candidates. This has typically been accomplished by rigidifying the structure of the AON to maximize tight binding with its intended RNA counterpart (see **section 3.2.** & chapter **2**). However, such an approach usually serves only to sequester the targeted species from further cellular activity for example, and owes to a general inability of the respective heteroduplexes to invoke subsequent RNase H-mediated RNA destruction.

Our unconventional shift in emphasis to more flexible chimeric alternatives was initially prompted upon recognizing this class of compounds to elicit unprecedented levels of RNase H activity, usually far surpassing their native surrogates in this regard - such elevations have never been observed using 'stiff' AON counterparts. These observations have collectively validated our further exploration of flexibly-designed duplexes as efficient activators of an RNase H pathway for controlling aberrant gene suppression, which itself has proven to be a highly elusive yet vitally important contributor to the antisense approach.

We have systematically examined the concept of interspersed substrate flexibility to assess the impact of different flexible elements within potential substrates. Importantly, RNase H recognition of these derivatives is generally associated with beneficial effects only when the flexible region is centrally incorporated into the antisense strand of enzyme-competent substrates (*i.e.* A-like geometries), while detrimental effects on activity accompany the placement of the flexible units within the opposing site of the

intended target RNA counterpart. The interresidue chain length of the flexible junction exerts only a secondary effect on cleavage site selection and avidity by the enzyme, as all AON-modified analogues comparably elevate target strand hydrolysis and support broader site tolerance by the enzyme. Indeed, the contrasting properties of sense- and antisense-modified DNA:RNA heteroduplexes support a proposed model (**Figure 3.18**) in

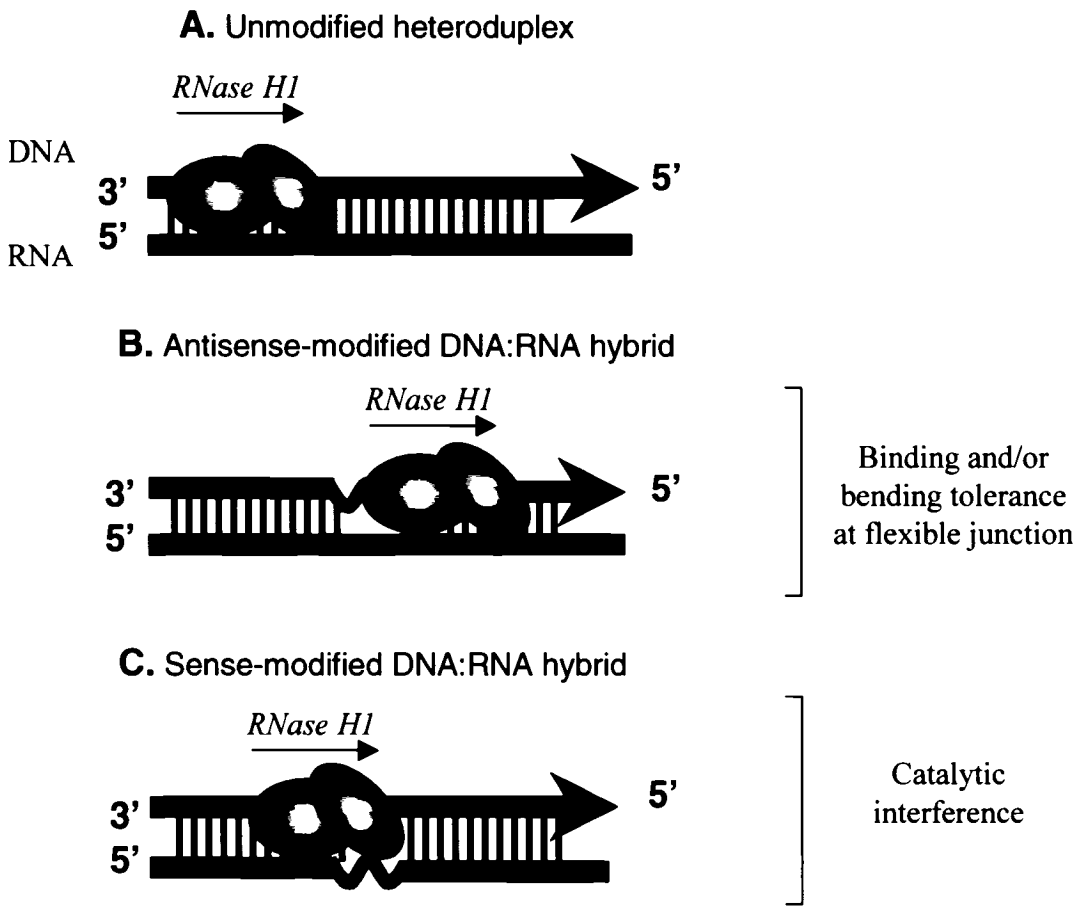

Figure 3.18: Possible modes of hybrid interaction with RNase H as suggested by the results presented herein. **A.** RNase H binds in the minor groove near the 3'-end with respect to the DNA strand of the hybrid and induces 2 simultaneous cuts[288] in the duplexed RNA species before dissociating (not drawn to scale). **B.** A local site of flexibility may provide facilitated interaction with the enzyme and block premature dissociation from the substrate to enable nucleolytic cleavage at downstream sites. Alternatively, the linker might enable the duplex to kink upon enzyme interaction and bring the distant downstream elements in close proximity to the catalytic center. **C.** Sense-modified hybrids do not support a second enzyme cut, likely due to disrupted active site contacts (see **Figure 3.15** for details). Absence of the 3rd downstream cleavage position further implies lack of an effective binding interaction with the RNA strand at the linker location. B = binding region; C = catalytic subunit.

which RNase H seemingly contacts its substrate in an asymmetric fashion, whereby binding at the flexible site in the antisense partner of the substrate somehow ameliorates enzyme processivity, while catalysis is obliterated upon sense strand modification. Accordingly, our studies suggest a vastly different functional role for the antisense *vs.* the sense strand members at this particular junction.

Furthermore, aliphatic linker containing duplexes, despite expected reductions in thermal stability, are capable of maintaining fully cooperative macromolecular units when bound to an RNA complement. Importantly, the recognizant heteroduplexes are only characterized by localized structural imperfections, such that the overall helical character of the substrate maintains the requisite A-like conformation known to invoke the enzyme. These studies clearly indicate and corroborate other findings[255] in that a picture of protein-nucleic acid interactions based only on static structures does not adequately describe the dynamic nature of molecular events that must occur for efficient hydrolysis to be realized. The dynamic aspect of enzyme binding and ensuing catalysis would likely be affected by conformational deformations of both the protein and substrate in which each partner seeks regions of the other that maximize the initial interaction. Optimal formation of the nucleic acid – protein complex would then entail some level of structural distortion in one or both partners as well to improve direct recognition. Such a phenomenon would well be supported in flexibly-designed duplexes which presumably possess both the plasticity and conformation required to optimally induce RNase H action. As these duplexes are likely characterized by unusually low energy barriers to structural dislocations or kinks in the hybrid helical axis, any abrupt or discontinuous change in the direction of the helical axis may be brought about by enzyme interaction to provide an improved fit rather than observable characteristics associated with static bending.

Nevertheless, in addition to providing evidence that general flexibility near the site of RNase H cleavage is essential for activity, these observations have direct implication for the design of novel and more potent AON drugs in future therapeutic pursuits. They also provide insight into the dynamic role of duplex structure on ensuing recognition events.

CHAPTER 4. STRUCTURAL AND MECHANISTIC INSIGHTS ON RNASE H CLEAVAGE OF POOR, NON-CLEAVABLE AND OTHER FLEXIBLY-MODIFIED NUCLEIC ACID HYBRIDS

4.1. INTRODUCTION – AN ELEGANT ENZYME-SUBSTRATE BINDING INTERACTION

In addition to a highly conserved core catalytic triad of amino acids, the RNase H tertiary structure consists of one or more nearby clusters of basic and polar amino acids primed to participate in general nucleic acid binding and orientation.[40,218,302] The initial formation of the nucleic acid:protein complex occurs rather nonspecifically through electrostatic contacts made between the negatively charged phosphodiester backbone of the nucleic acid and a precise arrangement of enzyme cationic residues in the substrate binding domain, termed a 'phosphate ruler'. These residues collectively orchestrate the discriminate recognition and cleavage of A-like hybrid substrates, with proper binding at multiple sites hypothesized to dictate the location and extent of scission generated along the RNA backbone. However, the way in which duplex characteristics are scrutinized, allowing for selective cleavage of A-like hybrids remains unclear.

Interestingly, several RNases H also require the presence of at least one aromatic amino acid residue in order to optimally position the substrate for ensuing enzymatic events. An excellent example is that of HIV-1 RT RNase H, which accomplishes this using a highly conserved, solvent-exposed tyrosine residue located adjacent to the RNase H domain, within the so-called 'primer grip' or connection subdomain.[294,303-305] Mutation of this amino acid (*i.e.* Y501) to Phe, Trp or Arg – all residues capable of undergoing stacking interactions with the nucleotide heterocycles – can fully restore the retroviral RNase H activity towards known DNA/RNA hybrid substrates to levels comparable with the wild type enzyme. In contrast, mutants harboring any of the other amino acids at this position are rendered deficient for RNase H-mediated cleavage events, suggesting an important role for Tyr-501 in the binding process.[306] The reverse transcriptase-associated RNase H domain of the *S. cerevisiae* Ty3 retrotransposon group likewise steers DNA:RNA intermediates for specific cleavage events using a Tyr residue (Y459) located near the catalytic site, despite a relatively distant evolutionary relationship from the retroviral counterpart.[307] Consistent with this role, site-directed mutagenesis of the aromatic

residue arrests enzyme site selective hydrolysis of bound hybrid substrates with an ultimate loss of transposition activity, further suggesting functional conservation of this residue in substrate discrimination.

Combined kinetic and mutational analyses of an archaeal RNase H isolated from the *Archaeoglobus fulgidus* family of thermophiles have recently validated a mode of substrate binding in which a structurally implicated tyrosine residue appears to form localized contacts with substrate nucleic acids through hydrophobic base stacking with the nucleotide heterocycles[308] (**Figure 4.1**). Together with basic and polar residues lining the substrate binding cleft (*i.e.* Arg-Lys-Arg 'ruler'), the architectural arrangement of the enzyme is one in which *general* A-form duplex binding through hydrogen bonding with the phosphodiester backbone is apparently coupled to substrate-specific (A-like) hydrolysis, likely mediated by an intercalative orienting mechanism.

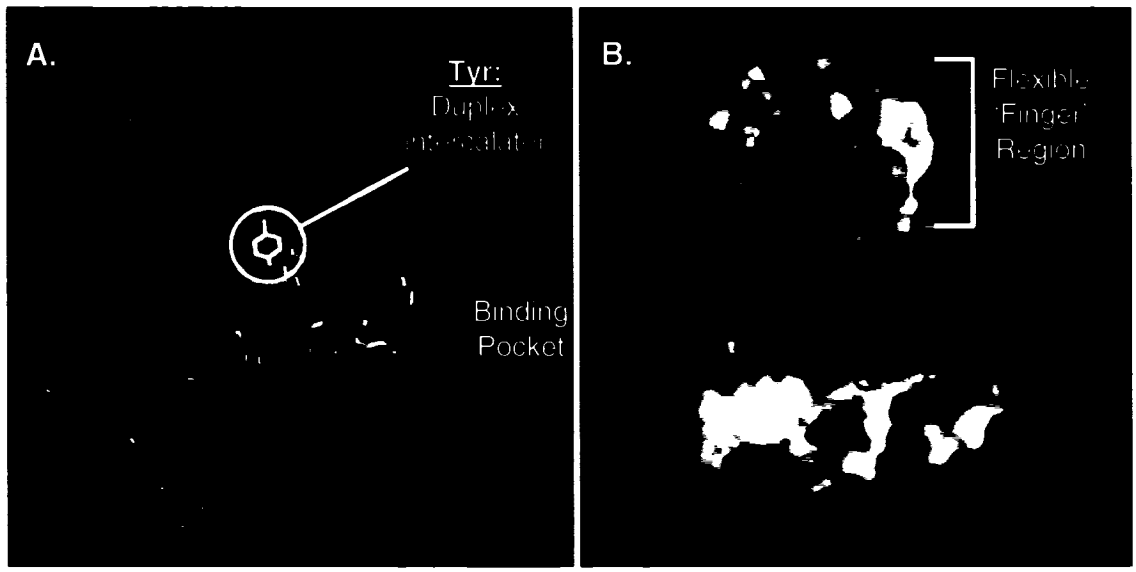

Figure 4.1: A. Binding and active site features of an archaeal RNase HII. Location of the tyrosine residue, along with proximal basic/polar amino acids housed in the substrate binding cleft and implicated in general nucleic acid hydrogen bonding (*i.e.* Arg-Lys-Arg phosphate ruler) are shown. **B.** Space-filling model of the enzyme showing the proposed substrate binding mode of an A-like substrate, generated by manually docking the nucleic acid onto the enzyme electrostatic surface. The active site groove surface forms a claw-like shape through which the substrate passes, oriented by the phosphate ruler motif and intercalating tyrosine side chain. Adapted from Chapados *et al.*, 2001.[308]

The coordinated action of these residues places the bound substrate directly within the adjacent active site situated at the floor of an open, claw-like groove on the enzyme surface, that thereby promotes subsequent hydrolysis. The key tyrosine residue allowing for such selective discrimination of A-like substrates is located in a flexible loop region of the enzyme residing *ca.* 7 Å above the general substrate binding domain and as such, is precisely poised to interact with incoming nucleic acid substrates via intercalation, with kinking or 'flexing' of the duplex probably occurring upon binding to position the scissile linkage within the active site. Indeed, a large body of evidence, including that from CD and NMR analyses of bound enzyme-substrate complexes, supports a model in which the duplex conformation is kinked upon enzyme binding, with altered base stacking observed in the hybrid that may corroborate an intercalative mode of substrate recognition and manipulation.[42,101,250,251,302,309,310] As the induced flexure is likely to occur more readily in a flexible substrate, this may further explain why DNA:RNA heteroduplexes having 3'-ssRNA extensions for example, still serve as efficient substrates for *E. coli* RNase H1, with cleavage directed as far as 4 ribonucleotides into the single stranded overhang region.[311]

Only recently have some of the above principles loosely been speculated to operate in the human RNase H mechanism of action. As with virtually all other eukaryotic RNases H1,[241,312-314] the human isotype possesses a strongly conserved tryptophan residue (*i.e.* W43) in the N-terminal domain of the protein, with the principal binding site formed by a nearby cluster of lysine residues that interact with the phosphates of the substrates.[293] Two of these, K58 and K59, confer general binding to both dsRNA and DNA:RNA hybrids,[240,313] while proper substrate alignment of the latter heteroduplex type for subsequent hydrolysis appears to be achieved by the aromatic partner of the three, possibly via intercalation.[293]

Together with our findings,[147,249,315] these studies suggest that an altered trajectory of the duplex substrate as promoted by an intercalating amino acid on the enzyme surface, may be a necessary feature of enzyme-inducing hybrid substrates.[250,251] Accordingly, productive enzyme scission might depend on the correct placement of flexible regions within the heteroduplex, themselves acting to serve as local recognition signals for such

an event, with consequent substrate reorientation. The notion that RNase H may also assume a role in DNA repair[230,231] makes this hypothesis even more attractive, in view of the fact that many repair enzymes (*e.g.* DNA photolyase,[316] uracil glycosylase,[317] endonuclease IV[318]) operate by intercalating within the lesion to mend the damaged site.

4.2. Project Objective: RNase H Cleavage in Poor or Non-Cleavable Nucleic Acid Duplexes

Inspired by these general observations and their potential relevance to the accelerating potential of linker-modified AON:RNA heteroduplexes (either DNA or 2'F-ANA as antisense), we investigated the likelihood that poorly cleaved or non-cleavable substrates might also become endowed with beneficial RNase H activating ability upon transformation to their flexible (*i.e.* linker-modified) duplex surrogates.

In accord with this rationale, we first examined the biophysical and enzymological properties of certain heteroduplexes with a strictly biased sequence composition (*i.e.* dPu:rPy hybrids). These complexes in particular, occupy a conformational class that differs considerably from that derived upon exchanging the sugars of the 2 strands (*i.e.* dPy:rPu) or evaluating mixed sequence DNA:RNA heteroduplexes,[319-321] and as such are notoriously poor activators of RNase H function.[55,322,323] Similarly, double stranded RNA (dsRNA) has never been identified as a substrate for pro- or eukaryotic RNases H, despite its ability to strongly bind to the enzymes. The reasons for this have been ascribed to a suboptimal minor groove width, either too narrow or too wide respectively, to properly align with the enzyme surface. However, enhancing flexibility in the double stranded structure through the introduction of an acyclic tether has not been explored in these or other currently inactive duplex classes. As this design should effectively introduce localized regions within the duplexes that might be accessible to intercalation with backbone plasticity also conceivably enhanced, any kinking of the substrate by enzyme for ensuing hydrolysis would likely be facilitated as well.

4.2.1. Sequence Design

Representative homopolymeric duplexes of these structurally inactive substrate classes were first investigated, specifically comprising 18 nucleotides in length but with chosen

alterations in one of the 2 pairing components to reflect a more diverse range of global nucleic acid conformations. This was accomplished by exchanging the anchoring carbohydrate in the polymer strand with one of three sugar appendages, that varied only by the chemical constituent at the 2'-position (**Figure 4.2**). The strands when complexed would thus form homopurine (Pu) – homopyrimidine (Py) hybrids spanning a broader area of the B → A conformational spectrum than those structures investigated in previous chapters. We hoped that the placement of an aliphatic connection unit within the noncompetent backbone would ideally transform these molecules to accept enzyme access, thereby gaining entry to a much broader assortment of possible substrates. Prior to discerning effects on enzyme activity however, the biophysical characteristics of each duplex were first investigated by a combination of thermal and circular dichroic analyses in order to evaluate the influence of the structural defect on duplex stability and structure.

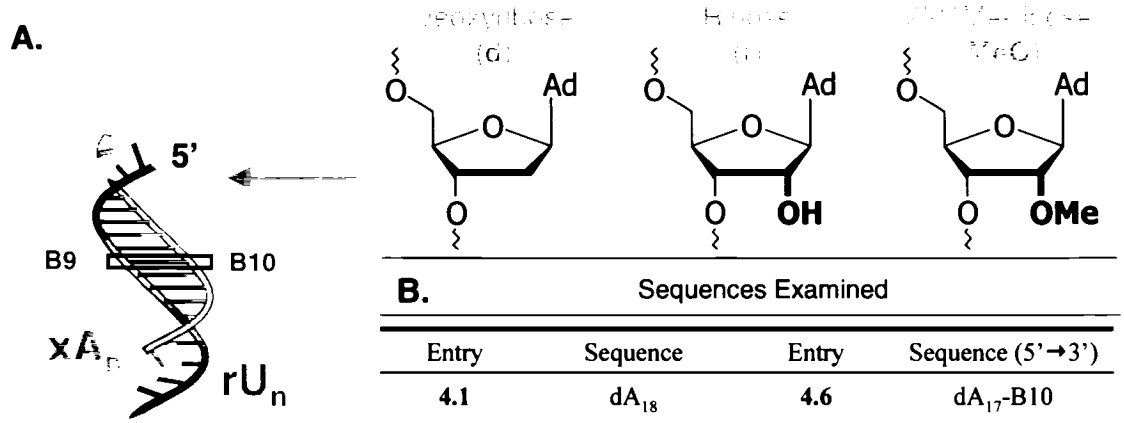

B. Sequences Examined

Entry	Sequence	Entry	Sequence (5'→3')
4.1	dA_{18}	**4.6**	dA_{17}-B10
4.2	rA_{18}	**4.7**	rA_{17}-B10
4.3	MeO-A_{18}	**4.8**	MeO-A_{17}-B10
4.4	rU_{18}	**4.9**	rU_{17}-B9
4.5	MeO-U_{18}[a]	**4.10**	MeO-U_{17}-B9[a]

Figure 4.2: **A.** Design, sequence and sugar composition of homopolymeric A:U duplexes incorporating interresidue butyl connections. Sugar anatomies of constituent nucleotides in the AON (top) are designated as d, r, or MeO in the corresponding sequence. Sequence descriptions are given in (**B**), in which the associated numbering of the butyl linker (B9, B10) indicates its position in the strand relative to the 18mer 5'-oligonucleotide terminus, designated as position 1. [a]These AONs were used in the construction of 'reverse complementary' hybrids, *i.e.* those having a purine-rich RNA target strand. See text for further details.

4.3. Thermal Stability of Homopolymeric Nucleic Acid Complexes with Central Single or Double Butyl Inserts

To assess the thermal effect of single- or double-strand linker modifications in duplexes hosting contiguous deoxyribose (d), ribose (r) or 2'O-methylribose (MeO) sugar units in one of the 2 annealing strands, hybrids were first assembled by mixing an equimolar ratio of strands to ultimately generate 16 distinct heteroduplexes that differed either by sugar composition and/or central butyl modification. All sequences were assembled by standard phosphoramidite chemistry, with the exception of the methylated strands which were purchased from UCDNA Services (Calgary, AB). All oligonucleotides were characterized by gel electrophoresis, HPLC and MALDI analysis (see chapter **6**) prior to conducting biophysical measurements and enzymatic assays.

4.3.1. Duplexes with a Pyrimidine Rich RNA Component

The relative ability of each heteroduplex to form a stable double stranded structure is illustrated in **Table 4.1**. Indeed, the tabulated data (panel **A**) indicates exceptional destabilization for unmodified deoxy-A_{18} sequences when paired with rU_{18} (*i.e.* dA_{18}:rU_{18}), consistent with the available literature on these and similar dPu:rPy complexes.[109,323,324] While it is not surprising that the deoxyribofuranose moiety in the AON is intrinsically the weakest pairing partner of the 3 sugar types in this class, rA_{18} and MeO-A_{18} hybrids with rU_{18} display similar stabilities upon duplexation. The higher T_Ms for these latter 2 classes corroborate previous claims demonstrating these sugars to adopt a preferred C3'-*endo* conformation upon RNA binding, thereby elevating duplex stability relative to a deoxyribofuranose counterpart, which itself has been shown to prefer a C2'-*endo* pucker and heteronomous structure in the duplex[319] (*i.e.* the 2 strands of the heteroduplex maintain different conformations).

Interestingly, the 2'-methylated strands appear to offer practically no advantages in thermal stabilities over the native ribosylated oligoadenylates (ΔT_M = +0.05°C / MeO modification *vs.* ribose), a property not usually the case when evaluating mixed sequences, in which the 2'-OMe moiety generally confers increases of *ca.* 1°C per MeO residue.[77,82,325] The origins for these enhancements normally owe primarily to two components: (i) a 'conformational effect', which shifts the sugar moiety to the N-type

Duplex Stability (T_M °C):	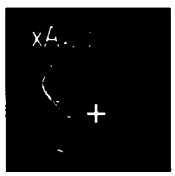	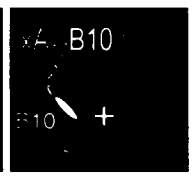	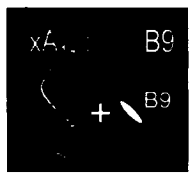	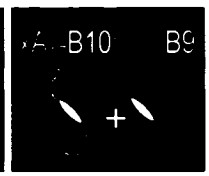
x = Purine sugar	*Group 1*	*Group 2*	*Group 3*	*Group 4*
A. Purine Rich Antisense	Polypyrimidine targets			
	4.4		**4.9**	
dA	28.2	28.0	14.3	14.2
rA	34.9	32.6	22.0	20.8
MeO-A	35.8	33.6	23.7	17.1
B. Reverse Complementary Duplex	**4.5**		**4.10**	
rA : MeO-U	46.6	35.2	34.9	27.1

Table 4.1: Melting temperatures of heteroduplexes depends on the sugar unit. Measurements were determined using an equimolar ratio of single strands (2.5 μM duplex concentration) in buffer consisting of 140 mM KCl, 1 mM $MgCl_2$, and 5 mM Na_2HPO_4 (adjusted to pH 7.2). All transitions displayed sharp, two-state melting behaviour, indicative of formation of a single cooperative complex. The T_M data were derived by computing the maxima of the first derivative curves obtained from the A_{260} *vs.* T profiles; reported values are those from independent measurements conducted in triplicate, with an estimated uncertainty of ± 0.5°C.

(C3'-*endo*) pucker, and (ii) a 'hydrophobic effect', arising from favourable interactions of the 2'-methoxy groups lining the hybrid minor groove surface (see chapter **1**). However, studies on 2'-O-methyl ApA dimers in aqueous media have noted neither an increase in nucleobase stacking nor an enhanced stabilization of the N sugar conformation.[326-328] Moreover, Lesnik and Freier have observed the magnitude of the hydrophobic effect to decrease linearly with increasing 2'-methoxy adenylate content in the AON component of AON:RNA heteroduplexes.[80] Sequences comprising short tracts of homopurine:homopyrimidine pairs in particular have further demonstrated that no added stabilization occurs for 2'-OMe-A residues relative to their ribose surrogates upon binding to an RNA complement.[80] These findings collectively support our observations on the unusually similar thermal stabilities of rA:rU and MeO-A:rU systems (see also **section 4.4.**).

Perhaps the most unusual finding centers upon the fact that target tenacity *does not decrease* upon single interchange of a purine nucleotide with a hydrocarbon linker in the A:U system. This is typified among 'Group 2' hybrids (xPu_{17}-B10 sequences **4.6** – **4.8** with rU_{18}; **Figure 4.2** & **Table 4.1**), which have an unexpected propensity to retain the characteristics of full target pairing despite the inclusion of a butyl linker within the oligoadenylate strand. This property occurs irrespective of flanking sugar composition, such that deoxy-, ribo- and 2'-methoxy sugar surrogates all display roughly no declines in binding affinities to a common ribouridylate target. On the other hand, substitution of an internal uridine nucleotide in the oligopyrimidylate partner (*i.e.* rU_{18}) with the acyclic spacer (Groups 3 and 4; **Table 4.1**, sequences bound to rU_{17}-B9 **4.9**), produces a substantial effect on the magnitude of the resulting heteroduplex T_M. Accordingly, each of these respective duplexes – regardless of oligoadenylate sugar or associated linker anatomies – now become severely compromised in their abilities to bind stably to the modified target ($\Delta T_M \sim -13^{\circ}C$ *vs.* rU_{18} as complement). These results are collectively summarized in **Tables 4.2** and **4.3** below.

Table 4.2: Thermal comparisons of unmodified and linker-modified AON complements with a common ribopyrimidylate target[a]

AON Complement	rU_{18} Target ΔT_M (°C)	rU_{17}-B9 Target ΔT_M (°C)
dA_{18} *vs.* dA_{17}-B10	0.2	0.1
rA_{18} *vs.* rA_{17}-B10	1.3	1.2
MeO-A_{18} *vs.* MeO-A_{17}-B10	2.2	6.6

[a]Listed values represent the reduction in binding affinity associated with linker incorporation within the oligoadenylate system.

Table 4.3: Thermal depressions induced by linker-modified oligoribouridylates when bound to a common oligoadenylate complement[a]

AON Complement	rU_{18} *vs.* rU_{17}-B9 ΔT_M (°C)	AON Complement	rU_{18} *vs.* rU_{17}-B9 ΔT_M (°C)
dA_{18}	13.9	dA_{17}-B10	13.8
rA_{18}	12.9	rA_{17}-B10	11.8
MeO-A_{18}	12.1	MeO-A_{17}-B10	16.5

[a]Listed values represent the reduction in binding affinity associated with linker incorporation into the oligouridylate sequence relative to its contiguous parent.

Table 4.2 illustrates a consistent ability for B10 oligoadenylates to maintain comparably strong heteroduplexation affinities relative to unmodified polyA tracts, whereas disruption of the contiguous polyU segment in the RNA complement strongly depresses the T_M, and consequently the overall complexation strength (**Table 4.3**).

The conflicting duplexation behaviours of butyl-modified oligouridylates and similarly modified oligoadenylates may partly be rationalized in terms of the contributions made by the two types of nucleobases toward organizing the secondary structure of the single stranded species. Stacking propensity in single stranded RNA follows the order G > A > C > U, with uracil stacking significantly less than the other bases.[329-331] Accordingly, in single strands formed by 2 contiguous nucleotide tracts tethered by a flexible unit, aromatic π-π stacking among adjacent bicyclic adenine bases should preferentially drive the formation of an ordered helical structure that preserves intrastrand stacking of the bases,[332] even those surrounding the linker junction. Conversely, polyU segments joined by an intervening linker are significantly more disordered in the single stranded state, by virtue of the poorer stacking proficiency of the uracil heterocycles.[333,334] Upon duplexation, our results suggest these properties to be manifest in the ensuing structural integrity of the formed complexes (**Tables 4.2 & 4.3**). Evidently, in the purine rich strands, the adenine heterocycles strongly influence the pairing orientation around the linker insertion site likely by forcing the linker to loop out upon complex formation with an unmodified RNA complement. This would be accompanied by collapse of the adjacent coaxial stacks to form a single, continuously base-paired structure with the linker projected away from the helix. Such a situation is quite possible given the pairing degeneracy of the 2 homopolymeric partners, which would accommodate misaligning or 'slipping' of the structure equally well. Butyl-modified poly-rU strands meanwhile, appear to adopt a stretched orientation of the linker upon binding to an unmodified target, which produces an internally unpaired base in the opposing strand, and is manifest as a sharp reduction in hybridization avidity (**Table 4.3**). Certainly many pairing modes other than those discussed here are possible and a heterogenous population of hybrids is also likely to exist perhaps with one conformational state preferred over another. However, as both linker configurations *(i.e.* stretched or looped) are indeed acceleratory with respect to

RNase H activity, we did not attempt to define the precise conformational properties of these two systems to any greater level of detail.

4.3.2. Duplexes with a Purine Rich RNA Component ('Reverse' Complements)

In contrast to the above, heteroduplexes designed with a purine- rather than pyrimidine-rich RNA strand (*i.e.* MeO-U sequences bound to rA complements, **Table 4.1,** panel **B**) exhibit similar reductions in binding affinity when *either* the purine *or* pyrimidine component is modified with a butyl linker. The associated decreases for either duplex carrying a single butyl modification (ΔT_M *ca.* –11°C *vs.* MeO-U_{18}:rA_{18}) seem to be independent of sequence composition, suggesting that the nature of binding is also affected by the structures and conformational variabilities of the two complements as they

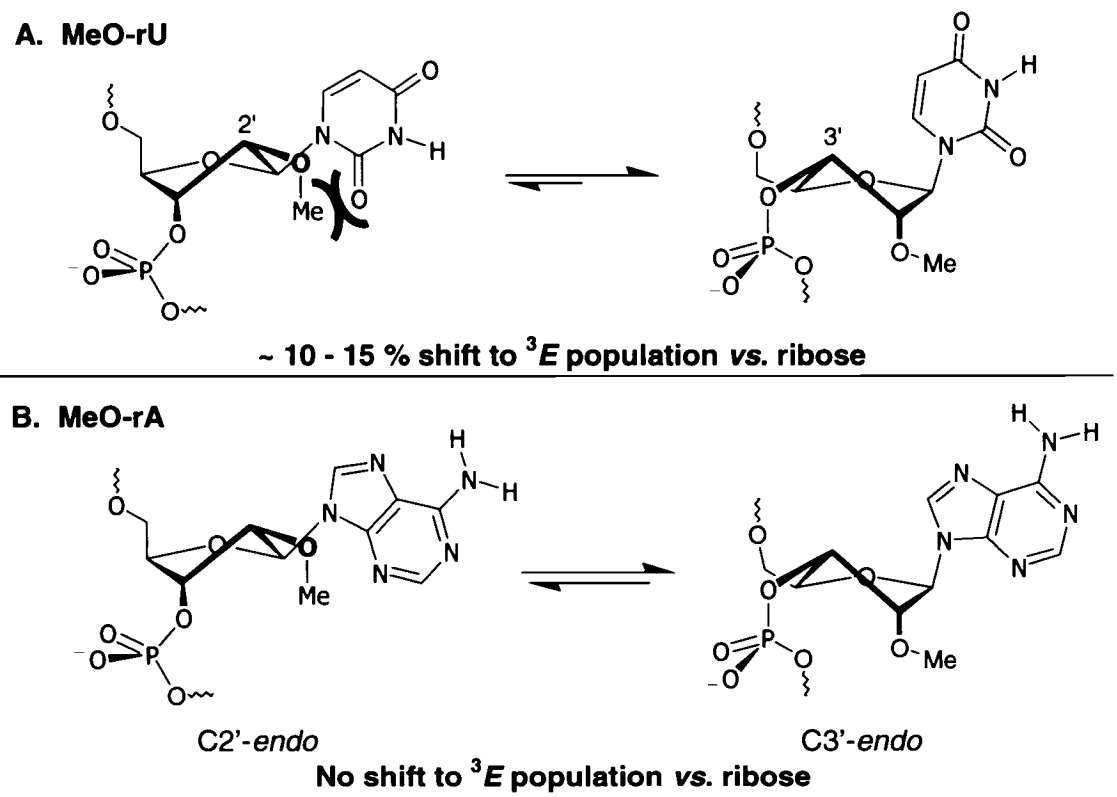

Figure 4.3: **A.** Steric clashes between the 3'-phosphate and 2'-O-methyl substituents orients the latter toward the uracil base. The consequent steric repulsion between the 2-carbonyl and the 2'-OMe group drives the pyrimidyl sugar to the North (C3'-*endo*) antipode and preorganizes the structure relative to ribose counterparts.[335] **B.** Purine nucleotides can stably accommodate both sugar conformations and thus show no relative preference for the C3'-*endo* conformation.[328,335,336]

associate and ultimately intertwine. In accord with this reasoning, it is important to note that 2'-O-methylation of rU stretches has been shown to significantly alter the topology of the resulting polymer,[335] while methylation of rA tracts has very little effect.[80,336] Consequently, while the MeO-A:rU system only confers T_M increases of 0.05°C per 2'-OMe modification relative to the rA:rU system, the reverse complements (*i.e.* MeO-U:rA) are significantly more stabilizing (ΔT_M = 0.65°C per modification; **Table 4.1**). These differences have been ascribed to the presence of an intraresidue steric repulsion occurring specifically between the pyrimidine 2-carbonyl group and the 2'-methoxy substituent when in the C2'-*endo* form, which thereby leads to a stabilization of the C3'-*endo* isomer (**Figure 4.3**). The resulting equilibrium shift from the S → N sugar antipode alleviates the added steric strain, placing the pyrimidine bases in a pseudoaxial position, which in turn enhances the base stacking and structural rigidity of the oligouridylate strand.[335] As this effect is absent in methylated strands with an appended purine base, this may explain why MeO-U:rA and not MeO-A:rU systems are overall more stable than rA:rU derivatives.

4.4. Heteroduplex Polymorphism in A:U Hybrids: Evidence for Different Structural Classes

Without question, the sugar scaffold and chemistry largely controls the gross secondary structural characteristics of the associating biomolecules, and butyl modification does not measurably alter this global property (**Figure 4.4,** panels **A-D**). All heteroduplexes exhibit distinct CD profiles indicating a pronounced transformation of the helix shape from an intermediate A/B helicity (dA:rU) to the classical A-form (MeO-U:rA), as monitored by changes in both the amplitude and position of the CD bands for a given structural type.

The dA:rU system, for example, assumes a rather peculiar double-stranded conformation under the conditions of our experiments, namely those representative of the intracellular cationic environment.[114] This is exemplified by the appearance of: (a) a broad positive peak of relatively moderate intensity at *ca.* 255-290 nm (270 nm), (b) a weak negative band with minimum centered at *ca.* 247 nm, and (c) strong positive (218 nm) and negative (205 nm) maxima at the low wavelength region of the spectrum (**Figure 4.4**,

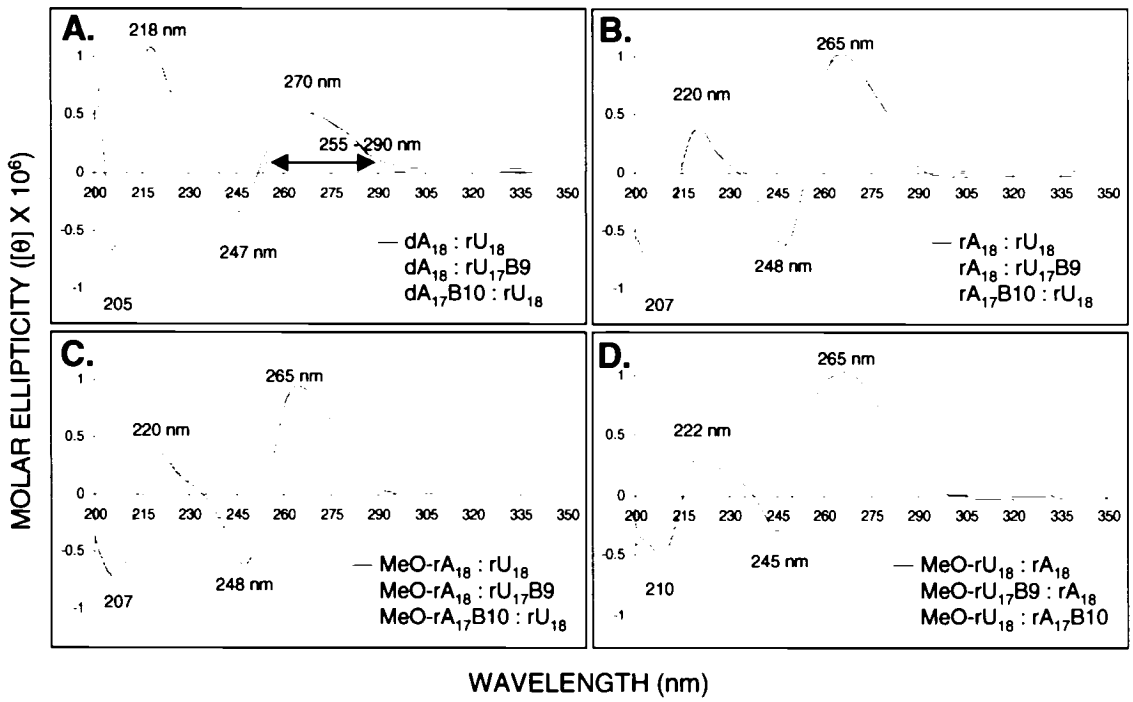

Figure 4.4: A – D. Circular dichroism spectra of duplexes at 5°C, illustrating lack of structural perturbation following butyl modification. All spectra are the cumulative average of 3 scans, obtained in buffer consisting of 140 mM KCl, 1 mM $MgCl_2$, and 5 mM Na_2HPO_4 (adjusted to pH 7.2).

panel **A**). The shape of this curve is, in fact, consistent with the formation of a double-helical complex.[321] A further comparison to published spectra of the dA:dT system,[323,337] which belongs to the B'-conformational family,[9] shows some retention of these spectral properties, specifically: (a) the presence of shallow positive bands above 255 nm, and (b) peak maxima centered at 247 nm and 217 nm, with the latter dominating the spectrum in terms of amplitude intensity, much like that seen in the signature for dA:rU hybrids. However, dA:rU hybrids do not adopt the B-form, but can more precisely be regarded as a unique conformational blend of the B-form typified by the dA:dT system and the A-like helicity adopted by their chemically homologous counterparts, the dT:rA hybrid class (data not shown). Thus, while dA:rU and dT:rA hybrids in particular differ primarily by a simple strand exchange of the sugars (*i.e.* dPu → dPy and rPy → rPu), the latter resemble the secondary structure of the A-family more closely.[338,339] Studies supporting this interpretation have further indicated the cavity of the major groove in dPu:rPy hybrids to be wider, and that of the minor groove smaller, than otherwise

expected for a typical A-like DNA:RNA heteroduplex, thereby justifying the assignment of the former in a structurally distinct conformational class.[319,320,340] These observations may also explain why hybrids generally having purine-rich DNA and pyrimidine-rich RNA strands (*e.g.* dA_{18}:rU_{18}) are exceptionally poor substrates for RNase H whereas dT_{18}:rA_{18} serves as one of the most potent activators (*vide infra*).[55,322]

The spectral properties of the rA:rU series, meanwhile, are entirely reminiscent of the preferential adoption of pure A-form helicity by this system,[9] again with no global structural disturbances imparted to the helices upon butyl incorporation within either of the two pairing strands (panel **B**). Relative to the dA:rU system however, a sizeable increase in the magnitude of the positive peak at the near-UV end of the spectral region (*i.e.* 260 nm – 290 nm) can be seen, along with a slight blue-shift of the corresponding wavelength maximum. Both of these characteristics are indicative of the increased stacking in the rA versus dA component of these hybrids and further reconciles the notion that heteroduplexes of the former tend to form tighter structures than those of the latter (see **section 4.3.1.**). On the other hand, rA:rU and MeO-A:rU hybrids exhibit nearly identical CD spectra (**Figure 4.4,** panels **B** & **C**), again indicating that 2'-O-methylation of the anchoring ribose sugars in the homoadenine strand does not appreciably affect the intraresidue dynamics or the resulting helix morphology.[336] In fact, larger spectral differences only become evident upon going from the MeO-A:rU → MeO-U:rA systems (panel **D**), despite identical chemical constitutions between these two classes in particular. Moreover, these discrepancies appear to justify the heterocycle-specific influence/role of the 2'-OMe groups in orienting the adjoining pyrimidine bases pseudoaxially, leading to improved intrahelical stacking as well as to minor structural perturbations of the sugar-phosphate backbone, the latter being manifest in the CD spectrum through a depression in peak amplitude at the far-UV spectral region (*ca.* 210 nm). Accordingly, while the signature is one of classical A-form global helicity, the observed spectral variations may further be rationalized in terms of the enhanced preorganization (*i.e.* greater rigidity) inherent to the 2'-O-methylated homouridine strands,[341] which would presumably lead to less conformational averaging in the spectrum as well.

4.5. Impact of Global Helix Twist *vs.* Local Geometry on RNase H Discrimination

As noted in the preceding sections, the single unifying feature of each of the homopolymeric heteroduplexes centers on their relatively high resilience to RNase H action, likely because the minor groove dimensions for each fall outside the optimum window size deemed necessary to trigger productive cutting by the enzyme. As butyl modification does not alter the helix twist at the global level, we hypothesized that its presence might locally aid the enzyme in gripping and manipulating the substrate with the concomitant execution of cuts in the labile RNA strand. Such an event would clearly emphasize for the first time, the importance of the local microenvironment in sensitizing these noncompetent duplexes toward possible improvements in enzyme processing, with little to no reliance on duplex minor groove width size.

Substrate specificity was assessed following the introduction of a ^{32}P tag at the 5'-terminus of the RNA component of each test substrate in a phosphoryl transfer reaction from γ-^{32}P-ATP, as catalyzed by T4 polynucleotide kinase (see **section 6.6.1.**). The purified, radiolabeled single strands were subsequently purified and annealed with a respective AON complement (d, r or MeO sugar backbones), and allowed to equilibrate overnight prior to initiating the assays.

Special consideration was given to the choice of optimal incubation temperature, *i.e.* one that could sustain adequate RNase H activity without compromising the integrity of the preformed substrates. As such, the maximum permissive temperature at which all of these assays could accurately be conducted was defined as 4°C, and was chosen upon inspection of the two-state melting behaviour of the weakest test species (*e.g.* dA_{17}-B10:rU_{17}-B9; $T_M \approx 14$°C), such that complete duplexation could be realized (data not shown). Enzyme assays were performed using either human RNase H1 or *E. coli* RNase HI, both of which were cloned, purified, and kindly provided by Dr. Kyung-Lyum Min of the Damha research group (see **section 6.6.2.**). The enzyme concentration was accordingly adjusted in a round of preliminary optimization experiments to compensate for the sluggish activity at the reduced temperature, and viability was routinely checked using dT_{18}:rA_{18} and its centrally-modified counterpart (dT_{17}-B10:rA_{18}) as positive controls.

4.5.1. dA:rU Hybrids and Enzyme Action – A/B-Like Helix Twist

Neither bacterial nor human or bovine (mammalian) sources of RNase H can effectively digest substrates when the antisense partner is composed of an oligodeoxyadenylate strand.[102,322,342] This is also true of sugar-modified oligoadenylates with a normally enzyme competent backbone (*e.g.* PS-dA_{18}, ara-A_{18}, and araF-A_{18}),[323] demonstrating that even certain DNA:RNA hybrids and their enzyme-active mimics, when designed to bind with a U-rich RNA target sequence, likely possess unusual polymorphism[338] which in turn diminishes the ability of the enzyme to recognize and cleave these duplex substrates.

Consistent with these claims, we have likewise observed dA_{18}:rU_{18} substrates to display an unusual resistance towards enzyme-mediated cleavage, specifically under conditions that favour rapid and complete digestion of dT_{18}:rA_{18} heteroduplexes (**Figure 4.5,** panels **A** & **B;** lanes 2-4). Indeed, both human and *E. coli* RNases H are unable to efficiently act upon the former substrate class, further highlighting the high degree of functional conservation shared by these two homologues. As the particular structure of dA:rU hybrids is therefore not very relevant for antisense work, many have instead preferred to pursue the development of modified AONs initially modeled in base sequence after the prototypical dT_{18}:rA_{18} system as a basis for which to establish enzyme competency in new AON candidates.[228]

4.5.1.1. Sense (rU) Strand Modification

While dA_{18}:rU_{18} can largely be regarded as a noncompetent substrate for RNase H, certain flexibly-designed dA:rU duplexes (*i.e.* those containing the central anucleosidic region in the uridylate strand) strikingly reverse this tendency and restore considerable enzyme competency to the targeted duplex, regardless of the source of enzyme used to execute target degradation (**Figure 4.5**; compare lanes 4 & 5). For dA_{18}:rU_{17}-B9 substrates in particular, butyl incorporation strongly sensitizes the corresponding derivatives to RNase H activity, which now triggers multiple strand breaks along the duplexed RNA complement. The human enzyme accomplishes this task with remarkable efficiency, as evidenced by a conspicuous absence of intact RNA following digestion of dA_{18}:rU_{17}-B9 hybrids (panel **B**, lane 4). In general however, the overall preference of the

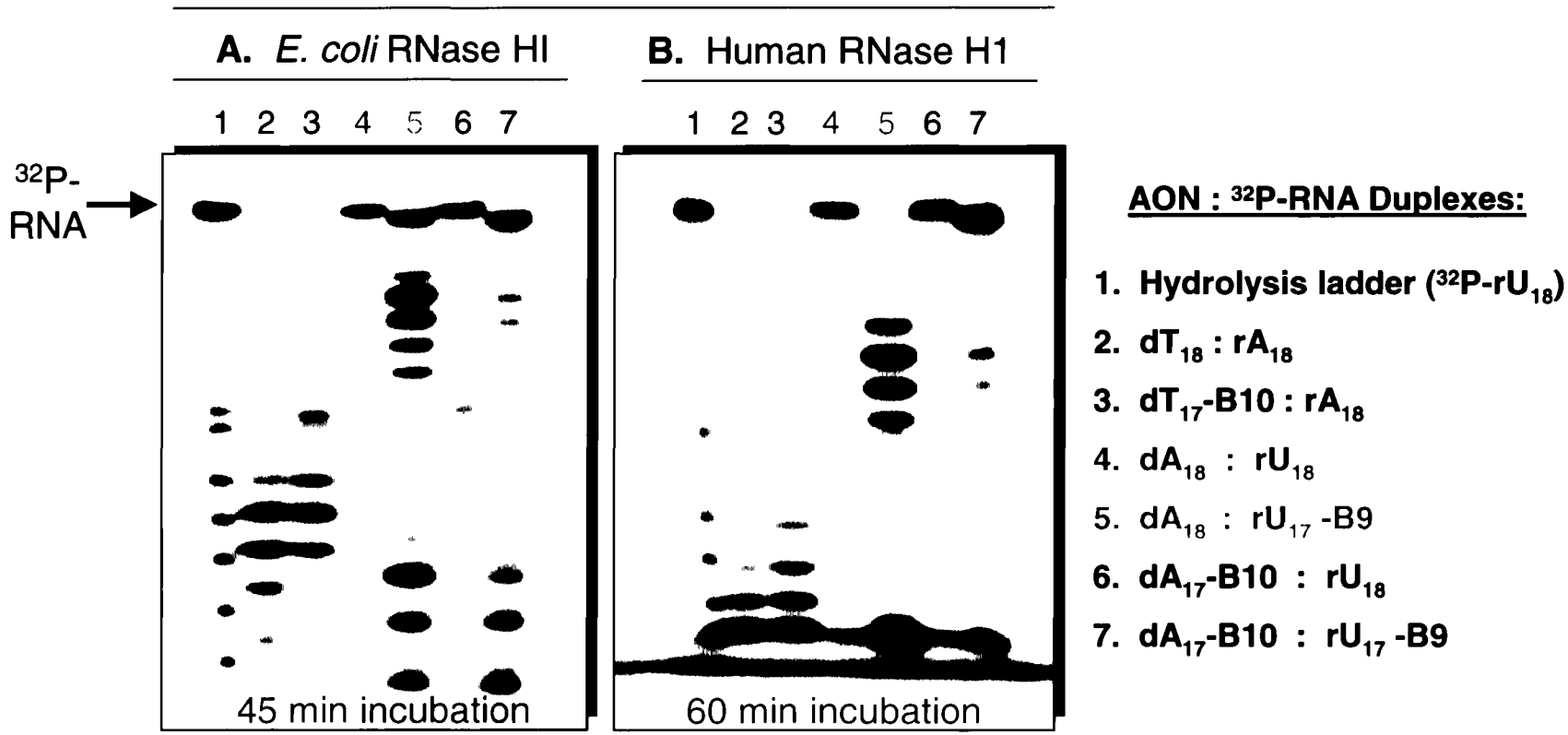

Figure 4.5: 16 % PAGE of 5'-^{32}P-RNA species showing the pattern of cuts generated after treatment with (**A**) *E. coli* RNase HI or (**B**) human RNase H1. Test reactions comprised 1 pmol of 5'-^{32}P-RNA with 3 pmol of test AON in buffer consisting of 60 mM Tris-HCl, 60 mM KCl, 2.5 mM $MgCl_2$ and 2 mM DTT. Reactions were initiated by the addition of enzyme and conducted at 4°C for the times specified. Reaction products were visualized by autoradiography (Kodak X-OMAT).

bacterial and mammalian enzymes for a given substrate is clearly quite similar, and both enzymes produce a similar distribution of fragmentation products over the specified incubation period. As noted throughout this work, the hydrolytic profiles are entirely consistent with the idea that enzyme-mediated strand scission occurs predominantly in a site-specific and unidirectional fashion upon the helix presumably by establishing local interactions at the linker insertion site. Interestingly, linker-promoted cleavage of the duplexed homopolymers is certainly less well-defined than that of hybrids containing other sequence compositions (*e.g.* mixed substrates, see chapter **3**). This is shown by the accumulation of numerous hydrolysis bands within rU_{17}-B9 targets, each being of variable intensity and progressively shorter than the other by a single nucleotide (lanes 5 & 7). The wider dispersion of cuts can be traced to lie roughly within a 4 nt segment of duplex and probably does not reflect any real sliding of the enzyme along the substrate, but – given the degenerate nature of the pairing strands – might intuitively suggest the occurrence of species with duplexed strands slightly misaligned prior to enzyme hydrolysis. As such, the location of cuts in the target may alternately indicate a strong participation of the anucleosidic region in orienting the heteroduplex at this junction for subsequent hydrolysis of the upstream duplexed RNA region, which may perhaps be facilitated through an intercalative positioning mechanism intrinsic to the enzyme (discussed in **sections 4.1. & 4.7.**).

4.5.1.2. Antisense (dA) Strand Modification

Further demonstrating the exquisite specificity of the enzyme-substrate interaction is the finding that duplexes hosting the non-nucleotidic linker in the antisense strand *do not* induce any discernible enhancements on the level of enzyme-mediated degradation relative to the all-RNA target (lanes 4 *vs.* 6). For substrates containing linkers in both strands, an effect intermediate to that of sense- or antisense-modified constructs is observed (compare lanes 4 & 5 *vs.* 7 for both enzymes), thereby providing the first indication that derivatizing the *antisense* component might in fact be somewhat inhibitory to conducive enzyme catalysis within this sequence context. Thus in a twisted turn of events, dA:rU hybrids apparently favour flexibility only in the *sense* and not in the *antisense* strand when the duplex is modified at the central helical residue. By contrast, it

is the antisense-modified variants of the dT_{18}:rA_{18} system (*i.e.* dT_{17}-B10:rA_{18}) to which considerable advantages are imparted in terms of substrate susceptibility towards enzyme action (**Figure 4.5**; see also chapter **2**).

To confirm the existence of such seemingly irregular trends, each dA:rU duplex substrate was re-evaluated for enzyme activation specifically following incubation with human RNase H, in order to establish a time-dependent profile of the degradation reactions. The time span within which these particular assays were conducted (30 min total) necessitated as a consequence the use of a slightly higher enzyme concentration, amounting to a 2-fold increase as compared to previous experiments. This single adjustment was key to ensuring adequate induction of enzyme activity within the shorter time period, so that a

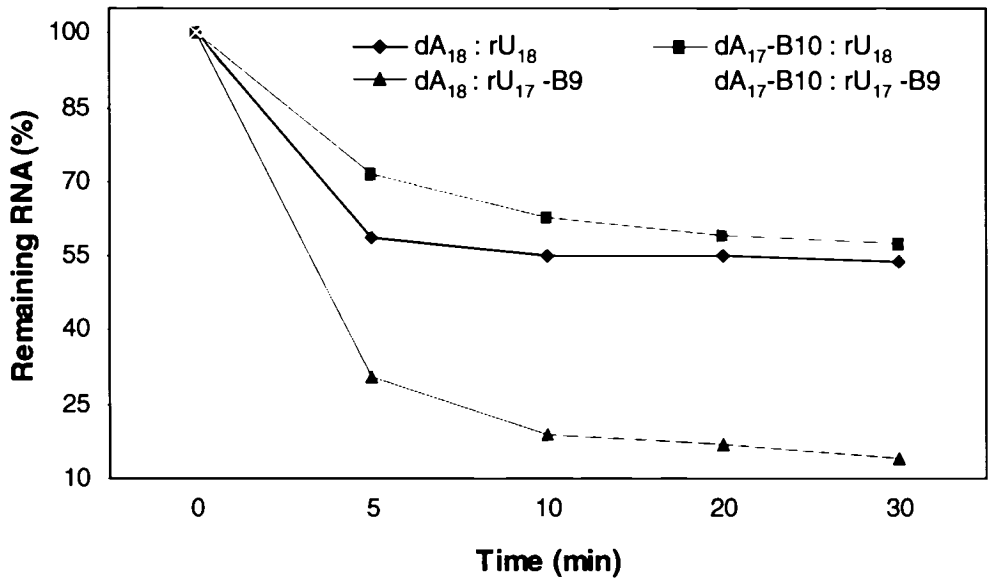

Figure 4.6: Relative levels of human RNase H1-mediated scission in linker modified dA:rU heteroduplexes. Assays were conducted at 4°C, using 0.9 pmol duplex concentration for 30 min, with timed aliquots removed at 5, 10, 20 and 30 min, quenched with loading buffer and heated prior to sample electrophoresis. Bands were quantified using UN-Scan-It digitizing software (Silk Scientific Inc., Orem, UT).

representative picture of partial digestion encompassing all tested substrates could ultimately be extracted from the data. The results are summarized in **Figure 4.6**, which illustrates the extent of RNase H-mediated hydrolysis for dA_{18}:rU_{18} and related derivatives at multiple time points, following electrophoretic resolution and densitometric

quantification of bands in the corresponding autoradiograms (not shown).

As expected, each of these test substrates could support some level of RNase H induction, although to a substantially lesser degree than that of the reverse complements (dT_{18}:rA_{18} and dT_{17}-B10:rA_{18} controls), which were fully cleaved by the enzyme at the earliest time point of this experiment (5 min). As a consequence, adequate comparisons could not be drawn between these two series without adjusting the enzyme concentration for the latter to slow the initial cleavage rate, again underscoring the importance of overall helical geometry in determining preferential substrate selection by RNase H.

We were however, able to define the relative propensity of enzyme-mediated cleavage within the dA:rU system more precisely. Interestingly, the unmodified heteroduplex can be cleaved albeit with moderate efficiency under these conditions, while a milder decline in target RNA levels occurs upon butyl introduction exclusively into the AON component of the cognate substrates (dA_{17}-B10:rU_{18}; **Figure 4.6**). Accordingly, linker incorporation within the antisense retards hydrolysis of the respective heteroduplex independently of the target RNA strand composition, which itself becomes acceleratory when modified, as reflected in the degradation profiles above and noted as follows:

dPu : rPy Hybrids

dA_{18} : rU_{17} -B9 (SENSE) **>>** **dA_{17}-B10 : rU_{17} -B9** (SENSE + ANTISENSE) **>** **dA_{18} : rU_{18}** (UNMODIFIED) **≥** **dA_{17}-B10 : rU_{18}** (ANTISENSE)

For comparison, the noted order of enzyme susceptibility exhibited by mixed sequence hybrids upon linker modification (discussed in chapter **3**) is as follows:

Mixed Hybrids (A-Like)

AON : RNA -B9 (SENSE) **<** **AON-B10 : RNA-B9** (SENSE + ANTISENSE) **<<** **AON : RNA** (UNMODIFIED) **<** **AON-B10 : RNA** (ANTISENSE)

Collectively, these observations may justify the likelihood that substrate recognition by RNase H proceeds by asymmetric docking and selection of one of the two strands at a given site within the heteroduplex. This is demonstrated by the fact that butyl inclusion

exerts contradictory effects on enzyme activity depending on: (1) its *inter*strand replacement of either one of a given helical base pair, and (2) the overall geometric disposition of the parent duplex. The latter consideration is particularly relevant for dPu:rPy hybrids, which exhibit a complete and dramatic reversal of trends relative to those of mixed sequences when analogously modified (*vide supra*). This surprisingly disparate behaviour may further reconcile evidence showing $dA_n:rU_n$ homopolymeric substrates to reside in a conformational class that is sufficiently distinct[319,320,340] from the requisite A-like geometries possessed by mixed sequence or $dT_{18}:rA_{18}$ hybrids that normally render these latter species much more amenable than the former towards productive enzyme hydrolysis.

For human RNase H in particular, earlier evidence also suggests that the scissile event might be preceded by the ease with which the docked enzyme can insert an aromatic side chain within the helix to reorient the trajectory of the bound complex within the distal catalytic region (see **section 4.1.**). The following 4 observations thus far strengthen this hypothesis: (1) As amino acid intercalation would presumably constitute a very defined interaction at a given helix locus, it might partly explain why duplexes hosting a linker at the same position but in alternate strands are never equally proficient at inducing the enzyme; (2) duplexes with a stretched *vs.* a looped linker are hydrolyzed somewhat more efficiently (chapters **2** & **3**) perhaps because the former can better accommodate the presumed intercalation; (3) the appearance of new cuts in linker-modified *vs.* unmodified substrates roughly coincides with the spatial placement of binding and catalytic domains on the enzyme, as well as with a putative tryptophan residue located within the former which itself has been shown to be necessary for strong site-specific downstream RNA cleavage;[293] and (4) heteroduplexes with global geometries that are slightly suboptimal from the A-like twist – while normally being very poor activators of function[55,322,323] (*e.g.* dA:rU) – are transformed to potent substrates upon butyl insertion and yield a distribution of fragmented products consistent with facilitated binding; they nonetheless seem to interact with the enzyme at initially different helix loci than otherwise expected for an A-like substrate.

4.5.2. A-form Heteroduplexes and RNase H Activation (rA:rU, MeO-rA:rU and MeO-rU:rA Systems)

To expand upon these observations and deduce the relative importance of the helix minor groove at the same time, other linker-modified heteroduplexes with identical base composition to that of the dA:rU series were likewise fashioned, yet now designed to comprise a completely enzyme-inactive backbone (*i.e.* dsRNA or MeO-RNA:RNA). The salient features of these hybrids, as compared to dA_{18}:rU_{18} (A/B-form) or dT_{18}:rA_{18} (A-like) hybrids, include an expanded minor groove, and the consequential adoption of pure A-form helical geometries, characterized by an overall 'compressed' twist of the double-stranded structure. As discussed in **section 4.3**, duplexes of this type also form relatively more stable pairing partners than those of the dA:rU system, and although not cleaved, can tightly bind to RNase H.[46] The anucleosidic derivatives of these duplexes (**Table 4.1**; Groups 2-4) should therefore serve as satisfactory candidates for which to assess any change in substrate recognition properties, as these would solely be brought about by linker incorporation rather than a predetermined minor groove size.

4.5.2.1. Experimental Considerations: Analysis of Cleavage Profiles

All test substrates were initially evaluated against human and *E. coli* RNases H using conditions identical to those supporting strong cleavage of 'flexible' dA:rU hybrids. In cases where either one of the two complexing strands could potentially serve as the labile RNA 'target' during the degradation reaction (*i.e.* rA_{18}:rU_{18} and butyl-modified variants; **Table 4.1**), both of the cognate single strands were individually radiolabeled with the phosphorus probe, then hybridized with an unlabeled complement and sequentially tested for enzyme competency. Accordingly, each duplex of the four variants in the rA:rU series ultimately comprised two separate test reactions, with the substrates themselves differing only in the strand location of the probe, as for example ^{32}P-rA_{18}:rU_{18} and its counterpart rA_{18}:^{32}P-rU_{18}. Following the hydrolysis reaction in this manner would thereby enable us to isolate and separately account for the fate of each strand.

From the cleavage data depicted for MeO-RNA:RNA duplexes in **Figure 4.7**, it is evident that no single linker modification is capable of eliciting a response by RNase H when placed in an established noncompetent backbone, regardless of whether the target RNA

strand is engineered to comprise a homoadenine (comparable to dT_{18}:rA_{18} substrates; panel **A**) or homouridine base sequence (dA_{18}:rU_{18} sequence analogues; panel **B**). The inability of either enzyme to cleave these substrates is further exemplified by the relative ease with which the dT_{18}:rA_{18} duplex (positive control) is hydrolyzed, with complete degradation occurring in under 5 minutes. By contrast, all heteroduplexes consisting of 2'-O-methylated AONs remain uncleaved, despite the use of prolonged incubation times (12 h) and high concentrations of enzyme in the reaction mixtures.

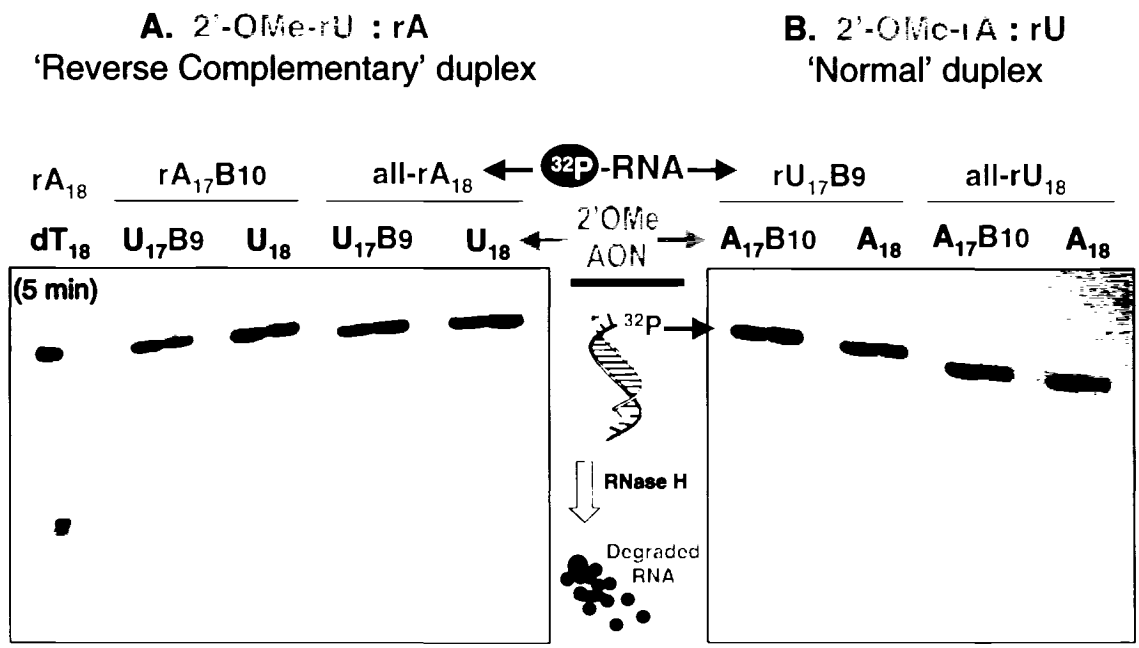

Figure 4.7: 16% denaturing PAGE analysis of duplexes treated with human RNase H1. Assays comprised *ca.* 1 pmol of test duplex incubated with enzyme at 4°C (0, 12 h) with the exception of dT_{18}:rA_{18} (left panel) which was only incubated with the enzyme for 5 min to ensure viability. Reactions were quenched by the addition of loading buffer and heat denatured (5 min, 70°C) prior to electrophoretic analysis.

A possible reason for the observed inactivity of the enzyme could arise from the combined effects of an unfavourably low assay temperature and an expectedly high substrate tolerance to cleavage. Our subsequent attempts to induce target recognition by RNase H thus involved a mild elevation of the incubation temperature (from 4 to 10°C), particularly since these duplexes could tolerate the increase somewhat better than those of dA:rU compositions without appreciably dissociating (T_M of weakest test substrate in this series *ca.* 17°C; **Table 4.1**). The combined results for bacterial- or human-mediated

RNase H induction towards each of the linker-modified homopolymeric duplexes and their unmodified parents are presented in **Table 4.4**. Although still far below the reported temperature optima for the enzymes (*i.e.* 37°C), these experiments confirm the relatively intractable nature of the A-form hybrid anatomy in constituting a cleavable substrate. Accordingly, in no case does linker inclusion at the central nucleotide pair of a respective helix render any of the targets with the ability to recruit either of the enzyme homologues.

Table 4.4: Attempts at cleaving linker-modified RNA:RNA or MeO-RNA:RNA duplexes with bacterial and human RNases H

Non-cleavable backbone type[a] tested:	Human[b]	*E. coli*[b]	Assay Conditions[c]
^{32}P-rA : rU	-	-	10°C, 24 h
^{32}P-rU : rA	-	-	10°C, 24 h
^{32}P-rA : MeO-rU	-	-	10°C, 24 h
^{32}P-rU : MeO-rA	-	-	10°C, 24 h

[a]Each entry represents unmodified, sense-, antisense- and bistrand-modified butyl containing duplexes; see **Figure 4.1** and **Table 4.1** for a complete description of sequences and hybrid design. [b]Enzyme concentrations used were *ca.* 10-fold greater than those employed for the dA:rU system; minus sign indicates no change in substrate recognition. [c]Assay temperature was defined as the maximum upper limit for which full duplexation of each test species could be achieved.

Consequently, the size of the duplex minor groove is certainly important for establishing multiple enzyme contacts and exclusively governs the feasibility of target strand hydrolysis in this context, irrespective of linker incorporation within the flanking ribose or 2'-methoxyribose sugar frameworks. However, this work does not decisively negate a presumed role for an enzyme-mediated intercalative mode of substrate recognition. The reasons for this are clarified upon consideration of the following: (1) Normal dsRNA and MeO-RNA:RNA duplexes, in addition to possessing a disproportionately sized minor groove cavity, might further block the impending catalytic event simply by projecting their respective 2'-substituents toward this face of the duplex (see chapter **1**). Such steric obstructions in productive hydrolysis alone would not necessarily disqualify a preferential association of the enzyme binding surface at the linker region, but rather might render remote internucleotide linkages along the helix impervious to scission by the distal catalytic domain (*i.e.* densely packed minor groove). (2) Alternatively, the linker may

reside at a position on the helix that does not coincide with the preferred locus of enzyme action and/or intercalation. This possibility might be relevant given that the sequence design and chemical site of linker modification, while chosen to be similar to that of our previously identified most potent substrates (A/B geometries; **section 4.5.1.**), were nonetheless arbitrarily defined in the structural context of pure A-form helicity. Stated another way, the ultimate spatial location of the linker, being governed not only by sequence but also by overall duplex morphology, might inadequately be positioned to interact with the enzyme when the helical twist of the hosting biomolecule is varied.

4.6. ATTEMPTS AT CLEAVING MIXED SEQUENCE RNA:RNA DUPLEXES

To assess the probability that an alternate region on the A-form duplex might trigger a cleavage event when modified, we next constructed duplexes in which the linker was shifted *ca.* one-quarter turn away from the helix center. The target sequence for these studies (herein referred to as U5-RNA) was designed to correspond to a 24-nt segment within the U5 region of the HIV-1 viral genome, instead of the prototypical homopolymeric systems that had previously been evaluated. Notwithstanding its potential biomedical significance, we anticipated this system to offer a number of technical advantages over the latter. Most obvious of these concerns the inherent inability of contiguous A:U base pairs to contribute to a stable duplex form, such that the greater the A:U content, the weaker the hybrid.[339] Consequently, any therapeutic utility conferred to such sequences upon linker modification is probably not practical for use in an *in vivo* setting, where the duplex must be preformed at physiological temperature prior to RNase H recognition and cleavage. Sequences of mixed nucleobase composition on the other hand, are not only more representative of the genetic diversity typified within the intracellular situation, but also generally ensure much tighter target hybridization under physiological cationic conditions. This is exemplified in the thermal behaviours of parent and derivatized dsRNA duplexes, constructed by annealing fully matched or butyl-modified RNA AONs with the complementary U5-RNA sense sequence (oligoribonucleotides bound to **4.14**; **Table 4.5**). Evidently, all duplexes form exceptionally stable structures that display sharp, monophasic melting transitions at temperatures sufficiently above physiological, in buffer approximating the intracellular

Table 4.5: Sequence design and stabilities of U5-RNA duplexes with RNA AONs

Entry	Duplex Code	5' → 3' AON Complement[a]	Buffer A[b]	Buffer B[c]
4.11	dsRNA	GUU ACC AGA CUG ACA CAA CAG ACG	82.3	83.2
4.12	dsRNA-2B_S	GUU ACC A**B**A GUC ACA **B**AA CAG ACG	59.3	60.1
4.13	dsRNA-2B_L	GUU ACC AG**B**A CUG ACA C**B**AA CAG ACG	70.0	71.0

[a]All AONs comprise a ribose backbone; the 'antisense' designation used here denotes complementarity to the viral target RNA sense strand (**4.14**), with sequence: 5'-CGU CUG UUG UGU GAC UCU GGU AAC-3'. B = butyl linker. [b]Phosphate buffer: 140 mM KCl, 1 mM $MgCl_2$, and 5 mM Na_2HPO_4 (pH 7.2); [c]RNase H assay buffer: 60 mM Tris-HCl (pH 7.8), 60 mM KCl, 2.5 mM $MgCl_2$, and 2 mM DTT.

cationic environment. Also notable is the extent to which the double-stranded form is destabilized by butyl replacement at *multiple sites* within one strand of the helix (entries **4.12** & **4.13**), the magnitudes of which roughly corroborate the expected internal (stretched) *vs.* extrahelical (looped) orientation of the linker at the respective insertion sites (**Figure 4.8**). Indeed, both of these types of structural defects support amplified enzymatic activity in native DNA or 2'F-ANA heteroduplexes with RNA,[147] and were therefore equally desirable for evaluation in this system. Furthermore, as all duplexes are nonetheless sufficiently stable over a relatively large range of temperature as conferred by paired ribonucleotide flanks, the need to restrict the enzyme assay

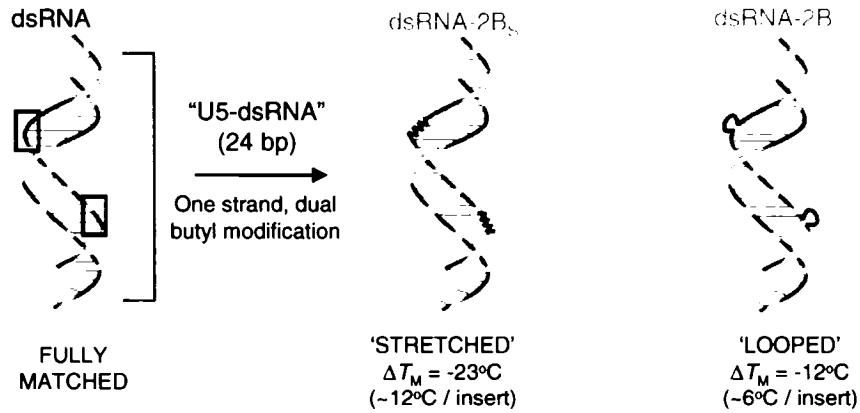

Figure 4.8: Anatomies of mixed sequence duplexes derived upon double-linker modification within one of the pairing strands. Disruption of G:C base pairs at either hydrocarbon site significantly reduces the T_M relative to the fully matched hybrid, although some stability can be recovered by forcing the linker to extrude away from the core of the biomolecule (dsRNA-2B_L). Importantly, both configurations accelerate RNase H-mediated target RNA hydrolysis in competent substrates.[147,249]

temperature to a suboptimal upper boundary (*i.e.* less than 37°C) is significantly relaxed, which essentially allows for the use of more aggressive conditions favouring maximal enzyme induction during the incubation reaction.

The single-most important aspect particularly unique to the dsRNA system pertains to the facility with which dual, remotely spaced flexible regions in the duplex may simultaneously be probed for possible enzyme action. This consideration is mostly one of synthetic convenience, and relates to the fact that both strands could potentially serve as the primary scissile locations for RNase H. A concomitant loss in binding directionality may also be envisioned, such that either duplex pole may now adequately promote the initial enzyme binding interaction (**Figure 4.9**). Accordingly, 'sense' (U5-RNA) and

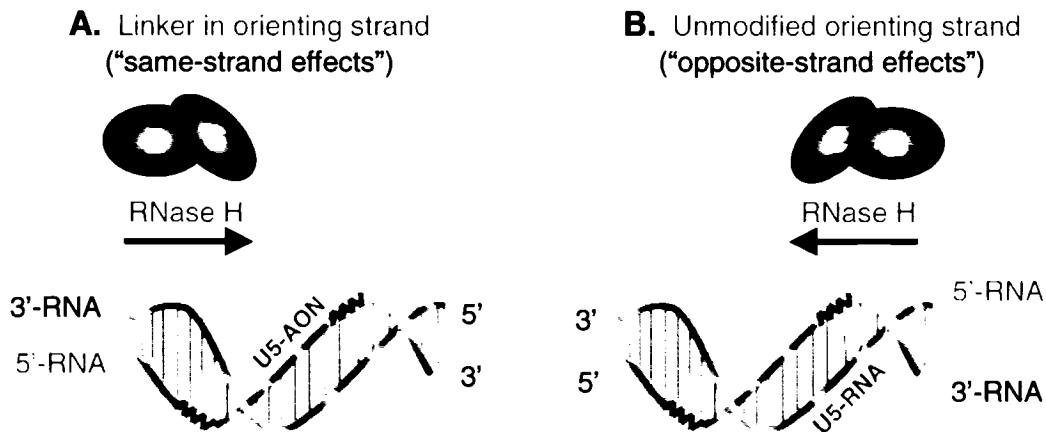

Figure 4.9: RNase H binds to native heteroduplexes by orienting with the sense strand (5'-RNA) pole of the 3'-DNA/5'-RNA hybrid. In dsRNA, however, either end of the duplex could theoretically serve equally well as recognition sites for binding, thereby allowing evaluation of intra- (**A**) and inter-strand (**B**) linker modifications within a single sequence design in a manner akin to 'sense' and 'antisense' derivatization of DNA:RNA substrates. As such, multiple targets to scrutinize each type of interaction need not be synthesized separately. B = RNase H binding domain; C = catalytic subunit.

'antisense' (U5-AON) strands should presumably be recognized by the enzyme in a nondiscriminate fashion; hence, the need to design and test linker-containing analogues of each pairing strand individually (*e.g.* **section 4.2.**) can be circumvented by integrating the double linker design within a single sequence, which thereby reduces the number of test substrates to be synthesized and ultimately analyzed.

Degradation reactions were monitored as before in the presence of *E. coli* or human RNase H type 1 enzymes, yet neither homologue was able to initiate any detectable cuts

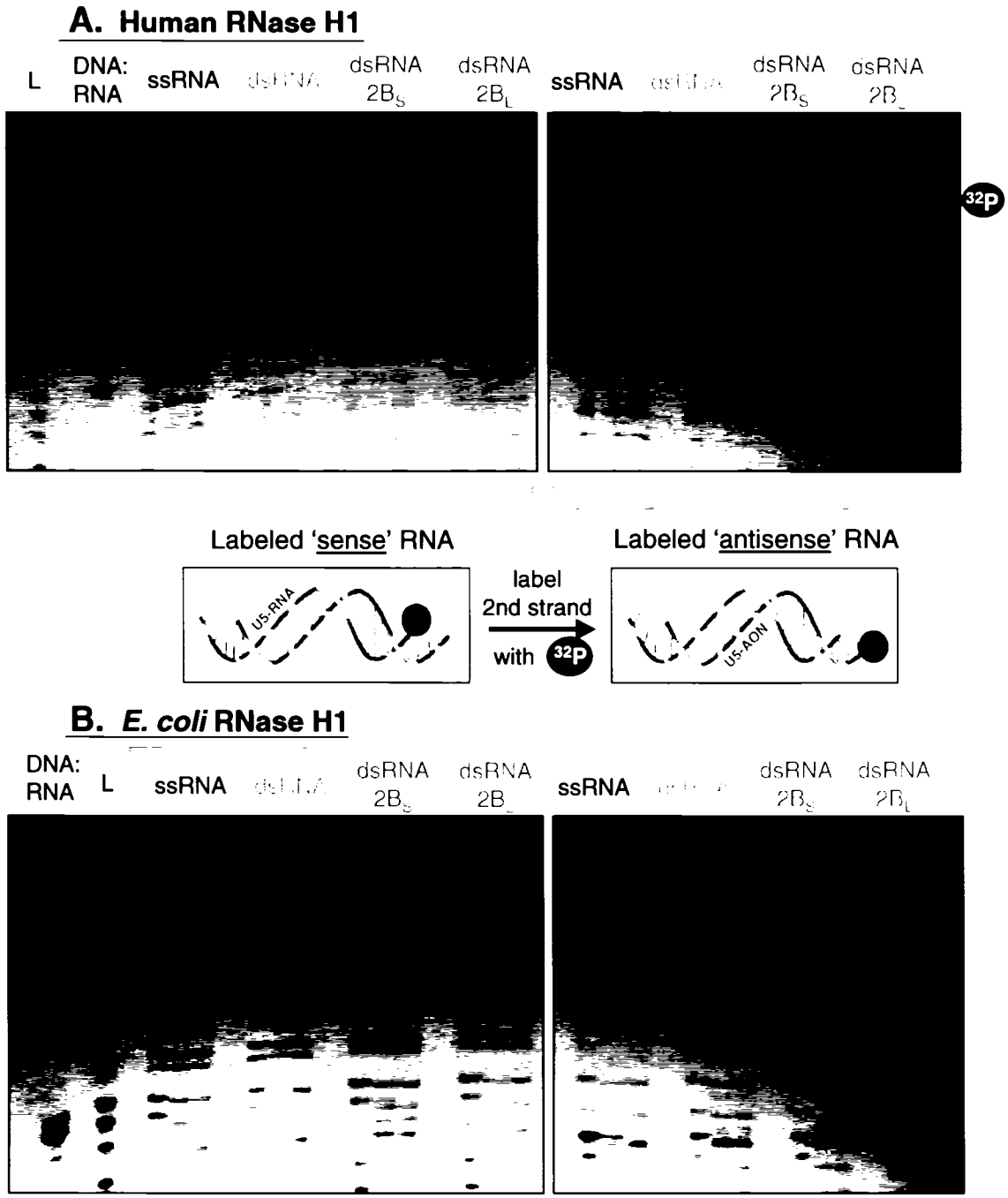

Figure 4.10: Attempts at cleaving butyl-modified U5-dsRNA derivatives. Preformed duplexes (1 pmol) were incubated at 37°C for 0, 12 and 24 h with human (**A**) or bacterial enzymes (**B**), with both pairing strands sequentially labeled and separately assayed for activity. Sequence descriptions are given in **Table 4.1**. L – Base ladder; ssRNA – ^{32}P-labeled single strand (negative control); DNA:RNA – mixed sequence 18 bp heteroduplex (positive control), degraded upon a 5 min treatment with either enzyme. The slowly migrating bands in the dsRNA lanes correspond to the unmodified duplexes, which withstand denaturation upon heating (5 min, 100 °C) and subsequent electrophoresis.

along the duplexes within the specified incubation time (24 h at 37°C; **Figure 4.10**), despite our best efforts to refine the A-form duplex structure to one of acceptable enzyme competency. These findings are thus consistent with the generally noncompliant anatomy of the dsRNA duplex to support enzyme scission, but do not rule out the possibility that one or more linker regions might serve to ameliorate enzyme binding and manipulation of the substrate perhaps through intercalation, rather than actual catalysis (discussed in **section 4.7.**). In support of this notion, duplexes of identical base composition have previously been shown to interact and competitively inhibit RNase H-mediated degradation of native substrates,[301] indicating that the intractability of the dsRNA backbone is probably not due to any real loss of enzyme-substrate contacts but rather to an inability of the substrate to associate with key regions on the protein, despite the presence of local deformable sites in the former. As such, the molecular mechanisms by which general A-form duplex binding could conceivably be coupled to the exquisite catalytic specificity of the enzyme may eventually be delineated as crystal structure data of the bound complexes becomes available.

4.7. Mechanistic Studies on RNase H: Mimicking Core Nucleoprotein Interactions by Oligopeptide Intercalation

To further acquire mechanistic insights into the role of intercalation in enzyme activity, we next conducted competition experiments involving linker-containing AON/RNA enzyme-active hybrids in the presence of RNase H, using as inhibitor a unique tripeptide designed to intercalate within the hole created by the linker site along the hybrid.[343,344] Our choice of nucleic acid substrates to perform these studies was based on those possessing the requisite A-like duplex morphology, and prompted by the capacity of stretched or looped linker orientations to amplify RNase H-assisted target degradation upon central helical insertion within the antisense member of the duplex (*i.e.* DNA sequences **2.3**, **2.4** and **2.6** bound to all-RNA target **2.24**; see chapter **2**).

The competitor tripeptide consisted of an internal aromatic amino acid side chain, flanked by 2 lysine termini (*i.e.* Lys-Trp-Lys), spanning an area of 3 – 4 nucleotides on the helix once bound.[345] Indeed, pioneering studies conducted in the laboratory of Dr. Claude Hélène first demonstrated this design in particular to elegantly mimic core interactions

that frequently occur in nature by certain repair enzymes (*e.g.* AP endonucleases[318]) which are implicated to act locally at UV-damaged or apurinic DNA duplex sites by positioning the protein for nucleotide excision via specific intercalation at the site of the lesion (*i.e.* "cut-and-patch" reaction).[343,346-348] Interestingly, oligopeptides of the general structure Lys-X-Lys (where X is an aromatic residue,[349] either Phe, Trp, or Tyr) could simulate this activity rather remarkably, both with respect to binding specificity at the vicinity of the damaged region and catalytic activity at the adjoining phosphate linkage.[344,348,350-352]

The exquisite site specificity by which oligopeptides of this specific amino acid composition form precise contacts with abasic duplexes in particular occurs via sequential formation of: (i) nonspecific electrostatic attractions between positively charged terminal lysine α- and ε-amino groups along the phosphodiester backbone to form an 'outside complex'[349] **(Figure 4.11**, panel **A)**; and (ii) specific intercalation within the helix cavity at the minor groove,[353] as conferred by the aromatic component of the tripeptide to form the 'inside complex', characterized by a complete quenching of the tryptophyl fluorescence[345,354] **(Figure 4.11**, panel **B)**. The overall interaction is obviously much stronger when an abasic region is present along the native duplex, simply because this facilitates the precise ordering of the second component of the complex, namely the insertion of the aromatic residue between adjacent base pairs.[351,352]

The mode of binding exhibited by these small molecules is in fact conceptually similar to that proposed in the human RNase H mechanism – itself hypothesized to play a role in repair – whereby the duplex is triangulated along the enzyme for site-specific catalysis by the concerted binding of 2 downstream Lys side chains in conjunction with a Trp residue near the N-terminus of the protein[293] (*i.e.* 'KKW' motif; see **section 4.1.**). Accordingly, we speculated that the precision by which the catalytic function of RNase H might be blocked by specifically disrupting these associations would help to clarify whether the enhanced cleavage activity observed among linker-containing duplexes is indeed promoted by an intercalating aromatic amino acid residue intrinsic to the enzyme that participates in reorienting the substrate for ensuing catalysis. This possibility is discussed

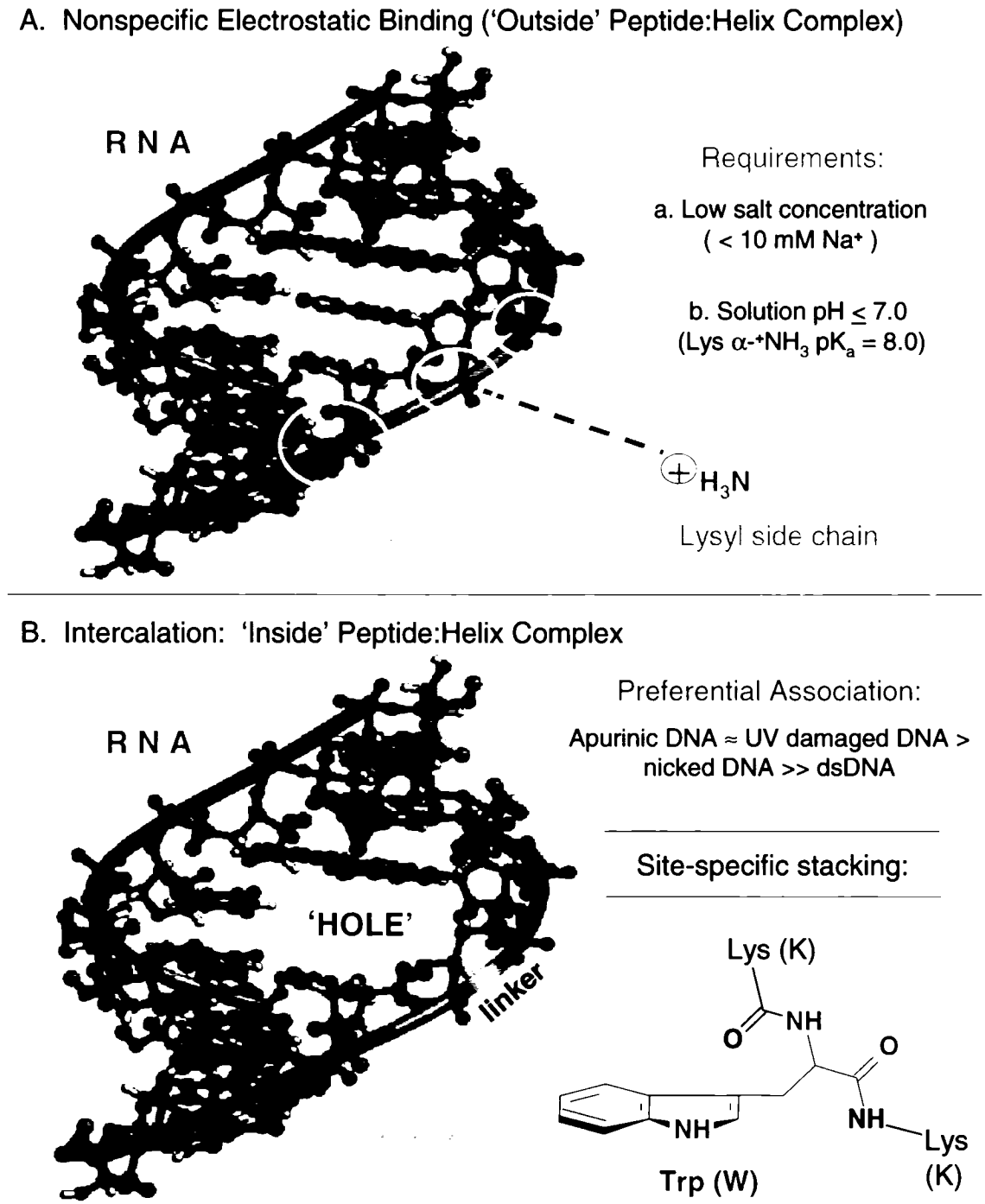

Figure 4.11: Probing amino acid side chain interactions with nucleic acids. **A.** Nonspecific electrostatic attractions between the negatively charged phosphate oxygens and the basic lysyl side chain do not markedly differ among the various duplexes, and depend only on the solution ionic strength and pH. **B.** Removal of an internal heterocycle introduces strong binding sites for the tripeptide through efficient stacking of the tryptophyl residue with adjacent nucleic acid bases, allowing for discriminant recognition of abasic over native duplexes; see text for details. K = Lys; W = Trp.

with respect to the role that stacking interactions could play in the specificity of recognition of duplex alterations by RNase H.

4.7.1. Maximizing Peptide:Helix Complex Association

Because a number of factors can influence the integrity of peptide:helix complexation, these must be taken into consideration in the initial experimental design and implemented prior to evaluating the extent by which RNase H hybrid cleavage levels might be affected by the presence of competing tripeptide. For instance, lysine binding across the duplex backbone to form the 'outside' complex occurs under rather stringent solution conditions, with adequate complex formation only observed in media of extremely low ionic strength (*e.g.* 1 – 10 mM Na^+), usually much lower than those in which oligonucleotide hybridization and melting are monitored (100 mM – 1 M Na^+).[355-357] CD, proton NMR and fluorescence studies have further revealed a pH dependence of binding, in which the association is strongly decreased in moderately alkaline conditions (pH $\geq$ 8.0).[345,358] Indeed, both of these environmental variables exclusively perturb the electrostatic component of the peptide:duplex interaction either by shielding the phosphate oxygens along the helix backbone or by neutralizing positive charges on lysyl amine groups via deprotonation.

In accord with this rationale, our initial attempts to block RNase H activity on linker-modified heteroduplexes by tripeptide:nucleic acid associations using standard solution conditions known to support high enzyme activity were unsuccessful, likely due to the unfavourable combination of high solution ionic strength (60 mM K^+) and pH (7.8) in the assay medium. As such, buffers were chosen that were capable of supporting complexation of the peptides with duplex while still sustaining appreciable enzyme activity. Test buffers were designed to consist of 2.5 mM $MgCl_2$ and 2 mM dithiothreitol (DTT) in solutions of 1 – 50 mM sodium cacodylate (adjusted to pH 7.0).

Inclusion of both DTT, a protective reducing reagent that inhibits disulfide cross-linking and RNase H inactivation,[359,360] and Mg^{2+} to stimulate phosphodiester bond hydrolysis, is critical for ensuring viability of the metalloprotein which itself executes target RNA cleavage most efficiently in neutral to slightly basic media (pH 7 – 8).[292] Hence, these variables were incorporated into the reaction buffer to maximize RNase H compatibility

during subsequent incubation reactions, and were not further adjusted. Only the sodium salt content was varied, primarily in an attempt to minimize the destabilizing effect of weak ionic conditions on duplex stability without rendering the phosphodiester charges completely inaccessible to the tripeptide (*vide supra*). However, at Na^+ concentrations of 1 – 5 mM, the extent of duplexed oligonucleotide species in solution was imperfect, as deduced from the broad nature of hyperchromic thermal transitions indicating a loss in duplex cooperativity (data not shown). Increasing the sodium content slightly ($Na^+ \geq 10$ mM) could restore adequate hybridization, whereas at higher ionic conditions (50 mM Na^+), we did not expect the association with tripeptide to be maintained.[356] Based on the hybridization data, we thus surmised the intermediate ionic concentration (10 mM) to acceptably fulfill a maximal balance of nucleic acid duplexation and charge interaction with the peptide. Notably, this concentration exactly coincides with the reported upper

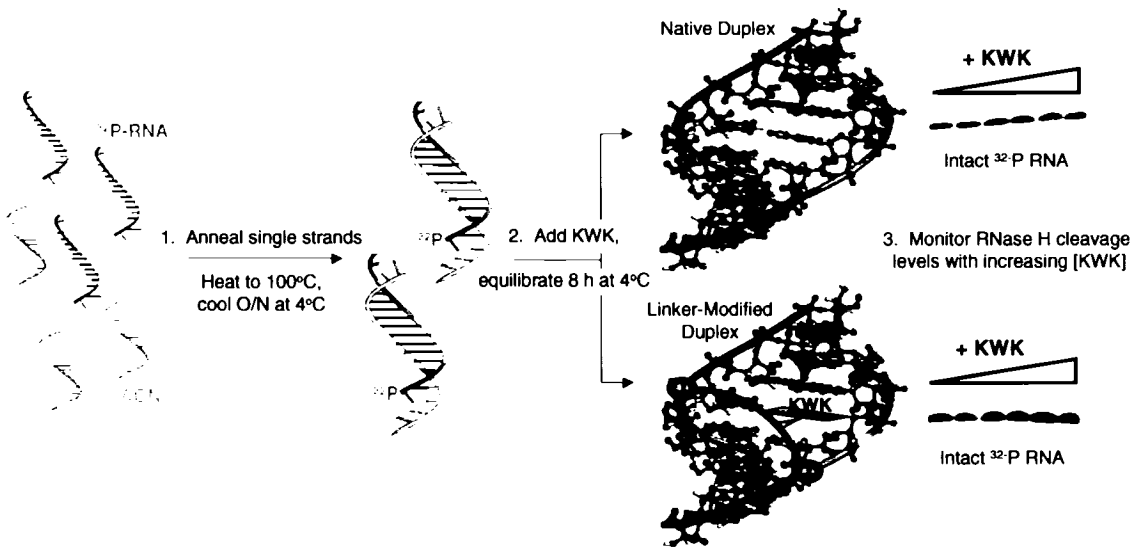

Figure 4.12: Steps required for successfully inducing inhibition of RNase H hybrid cleavage by aromatic tripeptides. Complementary single strands (1:2 RNA:AON) were preannealed in assay buffer (2.5 mM $MgCl_2$, 2 mM DTT and 10 mM sodium cacodylate; pH 7.0) prior to adding the Lys-Trp-Lys oligopeptides (Bachem Bioscience Inc., PA) to prevent premature association with and sequestration of single stranded species.[345] Upon further equilibration of heteroduplexes with increasing levels of KWK, the contents were incubated with human RNase H1 for a specified period of time, after which the reactions were quenched by the addition of denaturing buffer. The reaction products were heated (100°C, 5 min), resolved by gel electrophoresis (16%, 7 M urea) and the ^{32}P-labeled fragments were visualized by autoradiography.

limit for effective electrostatic attraction and also falls within the optimum range required to invoke RNase H activity (*i.e.* 10 – 50 mM Na^+).[292] Following buffer optimization, the tripartite complexes were sequentially prepared in an ordered series of reactions that were anticipated to maximize the abundance of active peptide:heteroduplex population prior to initiating enzyme assays. As outlined in **Figure 4.12**, all heteroduplexes were preformed prior to adding the tripeptides, primarily since the oligopeptide is known to discriminate between single- and double-stranded native structures through stacking interactions favoured with the former (*i.e.* unpaired oligonucleotides in 'relaxed' or random coil conformations).[345,355] The ratio of annealing strands employed during the hybridization reactions was also kept low, again to minimize the occurrence of preferential peptide associations with excess single strands in solution, which might otherwise reduce the effective concentration of inhibiting KWK peptide by precluding its ability to associate with duplex. Hybrids incubated with KGK (Lys-Gly-Lys; Bachem Bioscience Inc., PA) as control peptide were prepared in a similar fashion and comparatively assayed with the enzyme to discern the specific origin of inhibition and role of intercalation in the RNase H mechanism.

4.7.2. Tripeptide-Mediated Competitive Inhibition of Human RNase H1 Activity

The ability of RNase H to cleave native and anucleosidic duplexes in the presence of tripeptide inhibitor is shown in **Figure 4.13**. Of importance to the current analysis is the fact that incubation of substrates and enzyme at the new media conditions does not alter the characteristic pattern of hybrid site selection by the enzyme, with native duplexes stimulating two strong cuts in the duplexed RNA strand while linker-modified hybrids support a third cut 4 nts upstream of the butyl insert as well (*e.g.* compare to **Figure 3.12**, chapter **3**). Thus, apart from a mild reduction in the overall efficiency of RNase H-induced cleavage that thereby necessitates the use of a higher enzyme concentration, the enzyme evidently interacts with each type of duplex analogously in this environment, illustrating that the intrinsic features of linker site discrimination do not become compromised upon adjusting the solution to accommodate the tripeptide association. There is however, a striking relationship between the ability of the oligopeptides to associate with the linker-modified duplexes and concomitant reductions in levels of target

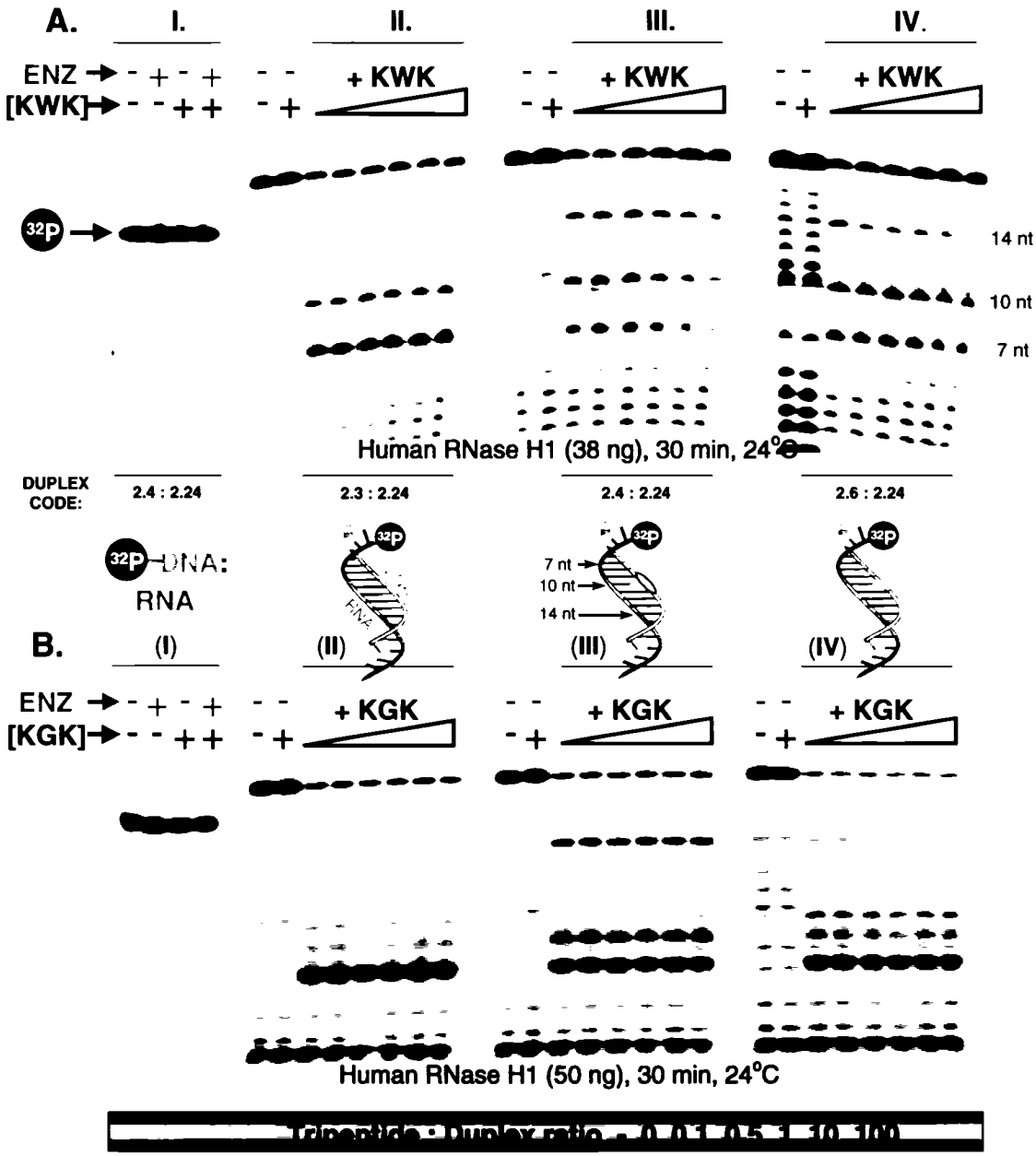

Figure 4.13: RNase H-mediated degradation of native (**II**) and butyl-modified mixed sequence heteroduplexes (**III** & **IV**) in the presence of Lys-Trp-Lys (KWK; panel **A**) or Lys-Gly-Lys (KGK; panel **B**), as inhibiting tripeptide. Preformed complexes were incubated with enzyme (30 min, 24°C) and the levels of inhibition monitored in buffer consisting of 10 mM sodium cacodylate, 2.5 mM $MgCl_2$, and 2 mM DTT, adjusted to pH 7.0. Lanes labeled with a (–) or (+) sign indicate negative and positive controls respectively, to provide confirmation that the RNA phosphodiester backbone remains intact in the absence of enzyme or presence of tripeptide (added in 100-fold excess over duplex). Duplexes **I** and **III** are identical in composition but differ in the strand location of the phosphorus probe [^{32}P-DNA (**I**) *vs.* ^{32}P-RNA (**III**); sequences **2.4** bound to **2.24**] and serve to verify that DNA strand cleavage does not occur.

RNA scission by RNase H. Indeed, aromatic peptides (KWK; panel **A**) exclusively block RNase H cleavage of anucleosidic duplexes, while no inhibition is observed in the unmodified hybrid surrogates (duplexes **III** & **IV** *vs.* **II**). This is manifest as a uniform increase in the levels of intact RNA upon elevating the peptide concentration only for duplexes carrying the deformable site, with a specific effect first apparent at a 1:1 ratio of KWK:duplex (panel **A**, *e.g.* duplex **III**). The accumulation of intact RNA roughly coincides with a gradual disappearance of fragmented products, most notably those corresponding to scission at the 10^{th} and 14^{th} nt positions in the 18mer RNA target. While some inhibition at the 10 nt scissile site is to be expected as this exactly coincides with the site of tripeptide binding, the decreased abundance of the 14 nt product (*e.g.* panel **A**, duplex **IV**) strongly suggests that the tripeptide association inhibits this upstream cleavage event site-specifically by 'plugging' the remote helix hole at the linker locus and thereby creating a local obstruction for RNase H binding. Not only would such a phenomenon be expected to decouple ensuing catalysis at the upstream position, it also agrees well with the binding and catalytic directionality of the enzyme.

Conversely, the fact that no inhibition occurs when the aromatic tripeptide presumably associates with the backbone in a nonspecific fashion (duplex **II**) as suggested by other studies,[344,357] indicates that this mode of helix binding alone does not interfere with the RNase H mechanism of action. Thus, the inhibitory effect appears to arise only when the indole ring of the tryptophan residue is allowed to insert within the helix, especially in light of the notion that the electrostatic component of the oligopeptide interaction should otherwise be similar among the three types of hybrids. The results might alternatively imply the presence of only weak charge associations between tripeptide and native duplexes altogether, especially as the strength of this 'outside' component is known to drop exponentially at solution ionic conditions exceeding a 10 mM cation concentration,[345,357,361] as used in these experiments.

Accordingly, analogous experiments with Lys-Gly-Lys reveal a failure by this species to arrest scission by the enzyme at any concentration, irrespective of the presence of heteroduplex defects (KGK; **Figure 4.13**, panel **B**). This clearly suggests intercalation to be the predominant mode by which peptide binding interferes with RNase H cleavage of anucleosidic duplexes, particularly since substitution of the tryptophyl side chain with a

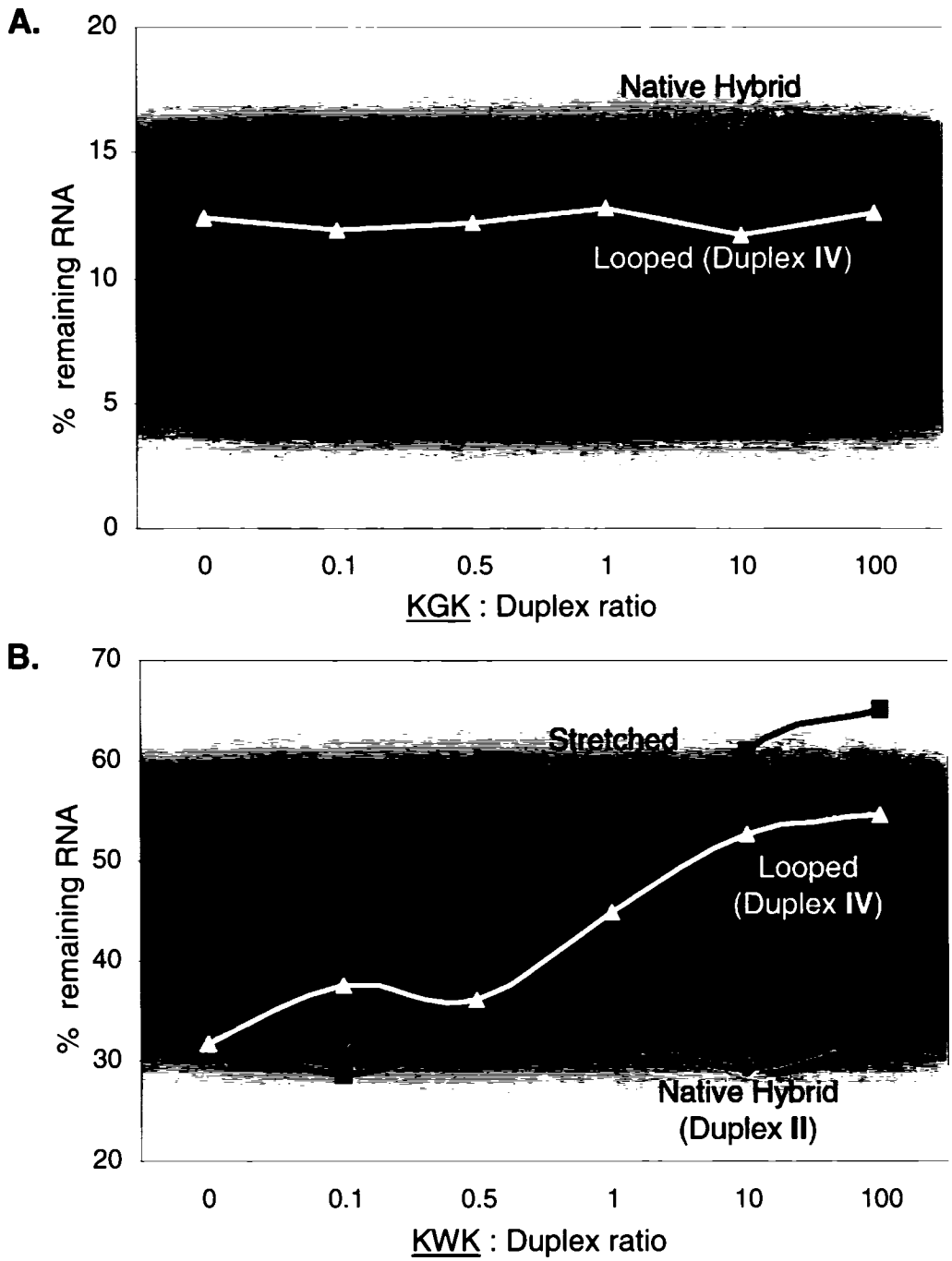

Figure 4.14: KGK tripeptides do not induce RNase H-mediated inhibition of native or anucleosidic duplexes (**A**), while aromatic tripeptides markedly affect enzyme activity (**B**) in a manner that depends on the local accessibility of the internal helix cavity. Oligopeptides were added to preannealed duplexes and reactions initiated with human RNase H1 (50 ng or 38 ng) for 30 min at 24°C in buffer consisting of 10 mM sodium cacodylate, 2.5 mM $MgCl_2$, and 2 mM DTT (pH 7.0). Reaction products were electrophoresed (16% denaturing PAGE) and RNA levels quantified by densitometry using UN-Scan-It software (Silk Scientific Inc., Orem, UT).

hydrogen atom (*i.e.* Trp → Gly) removes only this element of the peptide:duplex interaction.

These results are collectively summarized in **Figure 4.14**, which illustrates the extent of inhibition attainable for each of the duplex variants in the presence of KWK or KGK duplex decoys, determined upon quantification of the intact RNA signal as a function of the total radioactivity present after each degradation reaction. The trends highlight a remarkable correlation between the relative ability of each heteroduplex to elicit enzyme activity and subsequent peptide-mediated resistance to enzyme action. Indeed, linker-containing hybrids normally capable of supporting the highest levels of cleavage (anucleosidic duplexes with a 'stretched' butyl linker, panel **A**; see also chapter **2**) are likewise the most susceptible to inhibition via tryptophyl ring stacking at the vacant helix position (panel **B**), with an intermediate effect evident in hybrids where the linker is forced to reside extrahelically ('looped' duplexes). Thus, the degree to which target RNA hydrolysis by RNase H occurs is apparently related to the accessibility of anucleosidic sites in the duplexes, and the specificity conferred by stacking interactions between aromatic amino acid residues and adjacent nucleic acid bases. The notion that only aromatic tripeptides interact and do so with variable efficiency to stretched and looped linker-modified hybrids, indirectly suggests that these holes can also form strong binding pockets for RNase H, and that this local structure markedly affects cleavage activity.

It is, however, necessary to appreciate that the natural enzyme-substrate interaction probably involves additional binding components unique within the protein microenvironment beyond those exploited in this work, if intercalation is a general mechanism by which native duplexes are likewise cleaved. Although tripeptides do not associate with these duplexes, adaptive binding or bending, for example, of such substrates by the enzyme (see **section 4.1.**) may precede and therefore facilitate the presumed intercalation, a feat that is likely to be impossible with fully matched hybrids when using tripeptides to preform a 'protected' tripartite complex. Conversely, the pre-existing cavity within flexible anucleosidic duplexes (*e.g.* duplexes **III** & **IV**, **Figure 4.13**) would not only be expected to better accommodate a tripeptide-mediated intercalation, but in its absence might also conceivably accelerate the hydrolysis event through reduced energetics associated with enzyme-induced manipulations.

4.8. CONCLUSIONS

This chapter has examined the molecular factors by which anucleosidic duplexes elicit superior RNase H activity over their native counterparts, and the structural requirements for this task. The emerging picture from this work illustrates several important points. First, duplexes with compressed minor grooves (*i.e.* hybrids with intermediate A/B geometries), while inefficiently recognized by both bacterial and human RNases H, become strongly susceptible towards enzyme-mediated degradation upon central insertion of an aliphatic linker within the heteroduplex. Enzyme activation within this context strikingly depends on the exact helical placement of the anucleosidic region, with different functional consequences owing to which strand of the complexed nucleic acid pair houses the local deformation. Along these lines, our evidence suggests that the helical twist of the linker-hosting biomolecule markedly affects subsequent enzymatic recognition of the anucleosidic site, with dPu:rPy biased sequences (*i.e.* dA:rU systems) exhibiting enhancements only upon central linker modification in the RNA target strand, whereas canonical substrates with a slightly wider minor groove (A-like geometries) strongly activate the enzyme upon antisense strand modification.

However, neither MeO-RNA:RNA nor dsRNA homopolymeric derivatives with single or dual linker modifications at the analogous duplex regions were able to stimulate RNase H cleavage. As these hybrids were generally shown to invoke adoption of pure A-form helicity with no global perturbances of the helix structure upon linker insertion, the associated biological consequences of a relatively expanded minor groove thus appear to invariably preclude enzyme-assisted RNA hydrolysis. Our attempts to optimize the structure to one of acceptable competency (*i.e.* terminal *vs.* central linker incorporation) in mixed sequence duplexes capable of tolerating higher incubation temperatures during the enzyme assay were likewise incapable of rousing productive hydrolysis. While these observations do emphasize the established importance of the minor groove width for maintaining other critical enzyme interactions, we do not entirely dismiss the possibility that derivatization of alternate helical regions and/or multiple 'gap' modifications might still impart considerable enzyme competency to these systems.

Of clear relevance to the above premise is the likelihood with which the linker-modified double-stranded structure may conceivably be recognized by a precise positioning

mechanism used by the enzyme to steer bound substrates into a catalytically active conformation. Accordingly, our preliminary attempts to rationalize the exquisite site selectivity of human RNase H1 towards competent (*i.e.* A-like) substrates in the presence of competing tripeptides fashioned to associate with and discriminately block the vacant helix position from enzyme access, support pre-existing evidence[293,306,308] illustrating the probable importance of an intercalating amino acid residue on the enzyme binding surface that participates in manipulating the substrate for catalysis.

Although all previous studies point to a putative role for a tryptophan residue at the N-terminal region of the human enzyme, it remains unclear at this time whether this and/or other aromatic side chain(s) participate in the recognition process, especially in view of the fact that similar residues with as yet unassigned functions residing adjacent to the catalytic site have also shown high sequence conservation. Consistent with this view, most RNases H for which sequence data is available have an aromatic residue at virtually

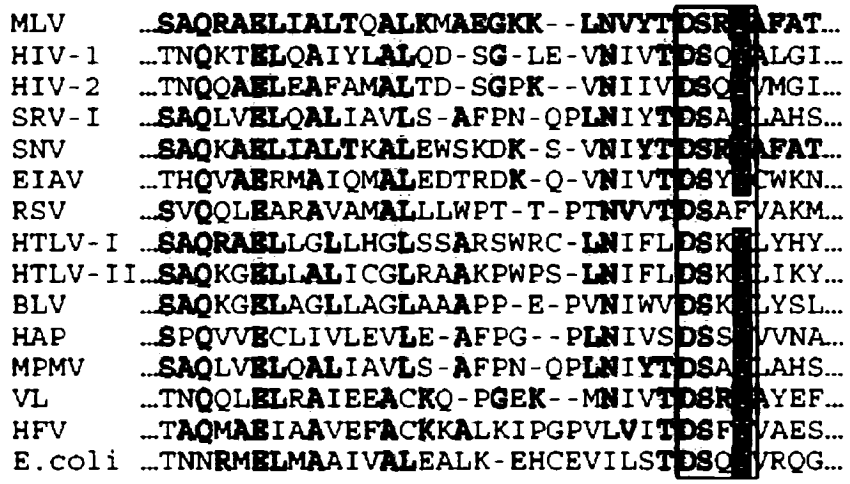

Figure 4.15: Amino acid sequence alignment of a portion of the reverse transcriptase (RT) and *E. coli* RNase H1 domains showing the highly conserved DSXY motif (boxed residues). The analogous region in the type 1 human enzyme corresponds to DSMF (residues 210 – 213) where F = phenylalanine, as found within the RSV RNase H sequence; see **Appendix A** for the full primary sequence of the type 1 human homologue. Note also that the aspartic (D) residue of this motif has been shown to be necessary for RNase H catalytic activity.[40,362] MLV = murine leukemia virus; SRV-I = simian retrovirus type I; SNV = spleen necrosis virus; EIAV = equine infectious anemia virus; RSV = Rous sarcoma virus; HTLV-I and HTLV-II = human T cell leukemia virus types I and II; BLV = bovine leukemia virus; HAP = hamster A particle; MPMV = Mason–Pfizermonkey virus; VL = visna lentivirus; HFV = human foamy virus. Adapted from Zhang *et al.*, 2002.[363]

identical positions in the primary structure.[364] We specifically note that one of these residues in the human isotype (Phe-213) aligns suspiciously well to that of Y501 in the HIV-1 RT RNase H domain (see **section 4.1.**), falling within a highly conserved region of the protein structure termed a 'DSXY' motif,[101,362,363] where X is any amino acid (**Figure 4.15;** see also **Appendix A**). This sequence motif may well comprise the functionally active intercalating amino acid side chain, and in this sense would well mimic the function and properties of the analogous tyrosine residue in the retroviral RNase H.[306]

Along with this intriguing evidence, our results collectively suggest that an acyclic linker within the duplex structure ameliorates enzyme-substrate binding presumably by promoting a specific intercalated complex with a Trp, or quite possibly, a Phe side chain housed within a critical binding region on the human enzyme. The flexibility of the duplex backbone at the linker insertion site may further aid duplex 'kinking' and reorientation as necessary for ultimate enzyme hydrolysis. Such a hypothesized interaction may also explain why the activity of linker-modified hybrid substrates varies as the linker is moved along the helix backbone,[147] or shifted to the opposing strand of the nucleic acid pair. Further studies should therefore aim to clarify the identity and role of the participating amino acid(s) in this process, while also reconciling the relatively broad substrate binding affinities of this family of enzymes with their exquisite catalytic specificities.

CHAPTER 5. CONTRIBUTIONS TO KNOWLEDGE

5.1. CONCLUSIONS AND FUTURE WORK

SYNTHESIS OF SECONUCLEOTIDES AND THEIR INCORPORATION INTO 2'F-ANA

Acyclonucleotides based on uridine and lacking the characteristic connectivity of 2'- and 3'-sugar carbons were successfully synthesized and characterized by a combination of 1- and 2D-NMR and FAB-mass spectral techniques. The acyclic synthons (*i.e.* seconucleoside 2'-phosphoramidites) were entirely amenable to solid phase synthesis, and were conveniently incorporated within 2'F-ANA oligonucleotides without the need to adjust the standard coupling times to accommodate the reactivities of these relatively unhindered molecules. Each of the newly synthesized oligonucleotides was characterized by HPLC and/or gel electrophoresis as well as MALDI-TOF mass spectrometry to confirm the success of solid-phase chain assembly and the purity of the isolated oligonucleotides.

THERMAL & ENZYMATIC STUDIES OF 'FLEXIBLE' DNA & 2'F-ANA/RNA HYBRIDS

Hybridization studies assessing the affinities of the modified AONs toward complementary RNA revealed an interesting finding, namely that the contribution to duplexation affinity as afforded by the secouridine modification was no greater than otherwise observed for homopolymeric 2'F-ANA strands when modified with a simple butyl insert (*i.e.* an anucleosidic site lacking an appended heterocycle) at the same position within the duplex. Such similarities in hybridization behaviours between the two types of acyclic residues were ultimately ascribed to a loss of normal Watson-Crick base pairing arising from the conformationally flexible butanediol moiety or the pseudosugar anchoring the uridine base. However, the associated drop in overall thermal stability of these duplexes with RNA as compared to strands lacking either of the acyclic insertions was more than compensated for by the high affinities of surrounding deoxy- or 2'F-ANA residues in the hosting antisense oligonucleotide.

Both of the localized structural modifications ultimately proved to vastly accelerate the degradative potential of 2'F-ANA heteroduplexes with RNA by both human and bacterial RNases H, far superseding the rate of target RNA hydrolysis attainable with the all 2'F-

ANA or DNA strands. Enzyme activity was also exquisitely sensitive to the site of AON linker-modification, with constructs housing a centrally placed linker affording the greatest amount of target strand hydrolysis after brief incubations. Differences between 5'- *vs.* 3'-end insertion were also apparent, with a greater amount of enzyme processing occurring when the linker was placed near the 3'-end of the AON. Interestingly, seconucleotide derivatization of the AON strand was second in rate only to those modified counterparts containing the butyl interresidue connection at the analogous helical position. Selection of the most potent AON members of this series of modifications was therefore based upon the superior RNase H activation ability of butyl over secouridine inserts, coupled with its commercial accessibility and consequent ease of oligonucleotide synthesis and applications.

Linker-modified DNA AON heteroduplexes, like 2'F-ANA derivatives, demonstrated strong elevations in enzyme recruitment and activation, with cleavage specifically directed at sites within the target sequence appearing exclusively downstream of the inserted acyclic residues. High activity could likewise be achieved upon looping the flexible linker extrahelically as opposed to stretching it along the hybrid axis, thereby providing the first indication that these helical structural defects could invoke a *general* acceleratory response from the enzyme, in contrast to its usually high structural stringency and selection of candidates possessing O4'-*endo* geometries in the AON strand (A-like heteroduplexes). Our evidence suggests these phenomena to be attributed to the flaccid character of the flexible inserts and the improved responsiveness of the duplex backbone to ensuing conformational changes brought about by the enzyme interaction.

RNase H Destruction of a Folded RNA Target Species

Given the remarkable potencies observed with both 'flexible' DNA and 2'F-ANA butyl-containing AONs, butyl-containing DNA and 2'F-ANA constructs were designed to invade and induce RNase H mediated degradation of a biologically relevant RNA target species using as model system a portion of the human *HRAS* oncogene, to determine whether the linker-induced enhancements could be reproduced in a target containing regions of significant secondary structure. The susceptibility of the *RAS* target to ensuing enzyme hydrolysis was most markedly affected following hybridization with linker-

modified 2'F-ANA AONs, indicating that the high structural preorganization of flanking residues, when coupled with a local region of helical flexibility, could offer the greatest advantages toward accelerating enzyme scission.

Optimization of the Anucleosidic Structure and Length

Subsequent efforts to introduce linkers of different intraresidue lengths further revealed that extending or compressing the AON helix backbone at the insertion site induced rather variable effects on heteroduplexation strength. However, any enhanced backbone dynamics associated with the linker region were unobservable at the global scale as deduced by circular dichroism, thereby confirming the discrete nature of the various structural defects on the overall A-like duplex morphology, and further implying an active/adaptive role for these molecules in an RNase H mechanism of activation. Interestingly, the identity of the flexible linker produced only a secondary influence on activity, with the primary influence predominantly arising from its general presence within the helix. However, ensuing acceleratory effects on enzyme activity proved to dramatically depend upon the *inter*strand location of the flexible linker in addition to its intrastrand placement, as substrates containing the modification in the RNA component of the duplexed pair were only poorly processed by the enzyme.

Poorly Cleaved & Non-Cleavable Linker-Modified Substrates

Conversely, heteroduplexes possessing relatively narrow minor groove widths (*e.g.* dPu:rPy substrates with A/B intermediate helicities), while normally serving as very poor activators of RNase H function, were cleaved more efficiently upon inclusion of the anucleosidic site exclusively within the sense (RNA) – and not the antisense – strand of the hybrids. Our evidence for this unusual and dramatic reversal of strand preference strongly suggests an asymmetric or 'biased' mode of contact by the enzyme across the minor groove of the substrate, likely arising from subtle differences in the overall intrinsic twist of the helical biomolecule. A-form surrogate hybrids with analogous modifications were, however, unable to invoke *E. coli* or human RNase H1-mediated cleavage, despite further refinements of the duplex structure by strategic displacement of the flexible region to alternate sites along the hybrid. Further work in this area should therefore attempt to

clarify whether the general resistance of the A-form duplex anatomy to RNase H hydrolysis can indeed be reversed upon introducing similar and/or multiple isolated flexible modifications at sites in the helix other than those examined herein.

Mechanistic Basis for RNase H Substrate Selection & Cleavage

Work aimed at unravelling some of the discriminatory properties by which RNase H selects and cleaves a particular hybrid substrate strongly suggests that the linkers likely exert their effects primarily through enhanced binding rather than catalysis. The precise helical placement of the linker is also crucial for ameliorating this component of the recognition process. To further scrutinize a hypothetical intercalative orienting mechanism intrinsic to the enzyme, competition experiments involving hybrids in the presence of human RNase H1 were conducted using as inhibitor a tripeptide designed to intercalate within the 'hole' of the linker-containing AON/RNA hybrid. From these preliminary studies emerged a relationship between the ability of the aromatic tripeptides to associate with the linker-modified duplexes and accompanying reductions in target RNA scission by RNase H. For example, hybrids with a stretched intrahelical linker showed the highest levels of inhibition at increasing concentrations of tripeptide, whereas unmodified duplexes exhibited no response. In fact, linker-containing hybrids normally capable of supporting the greatest levels of RNase H cleavage were also most susceptible to inhibition via tripeptide associations. Analogous experiments with Lys-Gly-Lys (KGK) as inhibiting tripeptide failed to show any response, demonstrating the possible significance of intercalation as a specific mode of interaction in these duplexes and highlighting its potential role in the mechanism of action of RNase H.

In conclusion, the studies described in this thesis highlight important structural differences that give rise to proficient enzymatic activity and further delineate the role of substrate conformation on the discriminatory properties of RNase H. The high enzyme activities observed with this class of antisense candidates imply that a strong biological effect may ultimately be achieved even in the presence of very low concentrations of antisense molecule. Our results should therefore stimulate renewed interest in acyclic compounds as integral structural components for triggering enzyme activity within other

AON classes as well. Furthermore, an extension of this work to current non-cleavable substrates with stiff backbones, yet otherwise possessing requisite A-like helix geometries (*e.g.* α-L-LNA/RNA or bc-ANA/RNA heteroduplexes) should surely prove to be one of many exciting and imminent future possibilities to explore.

5.2. CONTRIBUTIONS TO KNOWLEDGE

As a direct result of the studies described herein, the following publications have recently emerged, or are currently in preparation for submission in the near future:

(1) Maria M. Mangos and Masad J. Damha. "Accelerated Cleavage of Anucleosidic Hybrids Provides Evidence for Substrate Intercalation by Human RNase H1," manuscript in preparation.

(2) Maria M. Mangos and Masad J. Damha. "Thermal, Structural and Molecular Effects of Linker Anatomy and Location in RNase H – Competent Heteroduplexes," manuscript in preparation.

(3) Annie Galarneau, Kyung-Lyum Min, Maria M. Mangos and Masad J. Damha. "Assay for Evaluating Ribonuclease H – Mediated Degradation of RNA/Antisense Oligonucleotide Duplexes." In *Methods in Molecular Biology: Oligonucleotide Synthesis*; Herdewijn, P., Ed.; The Humana Press Inc.: Totowa NJ, vol. 288, **2005**, pp. 65 – 80.

(4) Maria M. Mangos, Kyung-Lyum Min, Ekaterina Viazovkina, Annie Galarneau, Mohamed Elzagheid, Michael A. Parniak and Masad J. Damha. "Efficient RNase H-Directed Cleavage of RNA Promoted by Antisense DNA or 2'F-ANA Constructs Containing Acyclic Nucleotide Inserts," *Journal of the American Chemical Society*, **2003**, *125*, 654 – 661.

(5) Ekaterina Viazovkina, Maria M. Mangos, Mohamed I. Elzagheid, and Masad J. Damha. "Solid-Phase Synthesis of 2'-Deoxy-2'-Fluoro-β-D-Oligoarabinonucleotides (2'F-ANA) and Their Phosphorothioate Derivatives." In *Current Protocols in Nucleic Acid Chemistry*; Beaucage, S.L., Glick, G.D., Bergstrom, D.E., Jones, R.A., Eds.; John Wiley & Sons: New York, Unit 4.15 **2002**, pp. 1 – 22.

(6) Maria M. Mangos and Masad J. Damha. "Flexible and Frozen Sugar-Modified Nucleic Acids - Modulation of Biological Activity through Furanose Ring Dynamics in the Antisense Strand," *Current Topics in Medicinal Chemistry*, **2002**, *2*, 1145 – 1169.

On account of some of the results disclosed in this thesis, the following provisional patent has been compiled:

Masad J. Damha, Maria M. Mangos, Kyung-Lyum Min, Ekaterina Viazovkina, and Michael A. Parniak. "Acyclic Linker-Containing Oligonucleotides and Uses Thereof." Int. PCT Appl. # WO03037909, 104 pp. Publication date: May 8, **2003**.

Publications resulting from studies not reported in this thesis:

(1) Jonathan K. Watts, Maria M. Mangos, B. Mario Pinto and Masad J. Damha. "Conformational Influences on 2'F-ANA Nucleosides and Nucleotides," manuscript in preparation.

(2) Sandra Carriero, Maria M. Mangos, Kazim A. Agha, Anne M. Noronha and Masad J. Damha. "Branchpoint Sugar Stereochemistry Determines the Hydrolytic Susceptibility of Branched RNA Fragments by yDBR," *Nucleosides, Nucleotides & Nucleic Acids*, **2003**, *22*, 1599 – 1602.

(3) Ekaterina Viazovkina, Maria M. Mangos and Masad J. Damha. "Synthesis and Physicochemical Properties of 2'-Deoxy-2',2"-Difluoro-β-D-Ribofuranosyl and 2'-Deoxy-2',2"-Difluoro-α-D-Ribofuranosyl Oligonucleotides," *Nucleosides, Nucleotides & Nucleic Acids*, **2003**, *22*, 1251 – 1254.

Conference Presentations and Invited Lectures:

Oral Presentations (underlined name represents presenting author):

(1) M.M. Mangos and M.J. Damha. *Substrate Specificity of Ribonuclease H: Impact of Backbone Flexibility on the Cleavage of DNA-RNA & Antisense Oligonucleotide – RNA Hybrids.* **16th International Conference on Phosphorus Chemistry**, Birmingham, UK, July 2004.

(2) M.M. Mangos, B. Patureau, R.H.E. Hudson and M.J. Damha. *Modulating RNase H Sensitivity of DNA/RNA and RNA/RNA Duplex Substrates using "Flexible" and "Frozen" Oligonucleotides.* **87th Annual CSC Conference and Exhibition**, London, ON, June 2004.

(3) M.M. Mangos and M.J. Damha. *Making Sense Out of Antisense Drugs – Synthesis and Properties of Arabinonucleic Acids.* Invited speaker, **Topics in Drug Design and Development**, jointly coordinated by the Departments of Chemistry and Pharmacology, McGill University, Montreal, QC, Nov. 2003.

(4) M.M. Mangos and M.J. Damha. Sh*aping RNase H Sensitivity of Duplex Substrates Using Flexible and Frozen Sugar Modified Antisense Nucleic Acids.* **McGill University Organic Seminar Series**, Montreal, QC, January 2003.

(5) M.M. Mangos and M.J. Damha. *RNase H: Probing Mechanism of Action through the use of Arabinonucleic Acid Analogues.* **INSERM: International Symposium on Nucleic Acids**, Paris, France, February 2003.

(6) M.M. Mangos, K.-L. Min, E. Viazovkina, M. Elzagheid, A. Galarneau and M.J. Damha. *New Antidotes in Antisense: RNase H and the Balance of Oligonucleotide Flexibility and Rigidity.* **XV International Roundtable: Nucleosides, Nucleotides and Their Biological Applications**, Leuven, Belgium, September 2002.

(7) M.M. Mangos, S. Carriero, K. Agha, A. Noronha and M.J. Damha. *Substrate Specificity of the Yeast Lariat Debranching Enzyme.* **85th Annual CSC Conference and Exhibition**, Vancouver, BC, June 2002.

(8) M.M. Mangos and M.J. Damha. *New Antidotes in Antisense: RNase H and the Balance of Oligonucleotide Flexibility and Rigidity.* **85th Annual CSC Conference and Exhibition**, Vancouver, BC, June 2002.

(9) M.M. Mangos and M.J. Damha. *Flexibility in Oligonucleotides? Anticipating New Antisense Antidotes with Ribonuclease H.* **Eastern Ribo-Club Meeting**, University of Sherbrooke, Sherbrooke, QC, February 2002.

Poster Presentations (underlined name represents presenting author):

(1) M.M. Mangos and M.J. Damha. *Shaping RNase H Sensitivity of Duplex Substrates using Flexible and Frozen Oligonucleotides.* **5th Cambridge Symposium in Nucleic Acids Chemistry & Biology**, Cambridge, UK, September 2003.

(2) M.M. Mangos, S. Carriero, K. Agha and M.J. Damha. *Synthesis of 'Y' RNA Fragments Containing Altered Sugar Residues at the Branchpoint: Substrate Recognition and Hydrolysis by the Lariat Debranching Enzyme.* **Eastern Ribo-Club Conference**, Mont-Orford, QC, September 2002.

(3) M.M. Mangos, S. Carriero, K. Agha, A. Noronha, and M.J. Damha. *Substrate Specificity of the Yeast Lariat Debranching Enzyme.* **XV International Round Table: Nucleosides, Nucleotides and Their Biological Applications**, Leuven, Belgium, September 2002.

(4) E. Viazovkina, M.M. Mangos and M.J. Damha. *Synthesis and Properties of Oligonucleotides Comprised of 2',2"-Difluoro-β-Ribofuranosyl & 2',2"-Difluoro-α-D-Nucleoside Units.* **XV International Round Table: Nucleosides, Nucleotides and Their Biological Applications**, Leuven, Belgium, Sept. 2002.

(5) M.M. Mangos and M.J. Damha, M.J. *Design of Novel Nucleic Acids Bearing Flexible "Seco"-Nucleotidyl Inserts.* **Eastern Ribo-Club Conference**, Mont-Orford, QC, September 2001.

(6) M.M. Mangos and M.J. Damha. *Synthesis and Properties of Oligonucleotides With Acyclic Nucleoside Inserts.* **4th Annual Chemistry & Biochemistry Graduate Research Conference**, Concordia University, Montreal, QC, September 2001.

(7) M.M. Mangos and M.J. Damha. *Synthesis of Oligonucleotides Containing Acyclic Nucleotide Units.* **84th Annual CSC Conference and Exhibition**, Montreal, QC, May 2001.

CHAPTER 6. EXPERIMENTAL MATERIALS AND METHODS

6.1. GENERAL METHODS

6.1.1. General Reagents

All solvents were generally dried and fractionally distilled under reduced pressure in an inert atmosphere (*i.e.* Nitrogen gas). Dichloromethane was distilled from calcium hydride (BDH Ltd., Toronto, ON) and refluxed prior to use. Pyridine, collidine (2,4,6-trimethylpyridine) and N,N-dimethylformamide (DMF) were obtained from Caledon Laboratories Inc. (Georgetown, ON) and dried by refluxing over calcium oxide, barium oxide (Fischer Scientific, Toronto, ON) or calcium hydride and also used fresh. HPLC grade ethyl acetate was shaken with a 5% aqueous solution of sodium bicarbonate and dried over anhydrous sodium sulfate (BDH). N,N-diisopropylethylamine (Aldrich Chemical Company, Milwaukee, WI) was stirred over sodium hydroxide pellets (BDH) and distilled before use. Solutions of 1 M tetra-*n*-butylammonium fluoride (TBAF) in THF or triethylamino trihydrogen fluoride (TREAT-HF) were obtained from Aldrich and used as received. Chloroform was purchased from BDH and hydrochloric acid from Caledon Laboratories Inc.

Analytical reagent grade acetic acid, aqueous ammonia, ethyl acetate, anhydrous sodium sulfate, magnesium chloride, sodium dihydrogen phosphate, disodium hydrogen phosphate (Fisher Scientific, NJ), sodium chloride, diethyl ether, *n*-butanol, anhydrous and 95% ethanol, acetone and triethylamine (BDH) were used as received. The following reagents were purchased from the Aldrich Chemical Company and also used as received: sodium periodate, sodium borohydride, sodium cacodylate, 4-dimethylaminopyridine and lithium perchlorate.

6.1.2. Chromatography

Thin-layer chromatography (TLC) was performed on Merck Kieselgel 60 F_{254} silica gel-coated aluminum sheets (EM Science, Gibbstown, NJ) with fluorescent indicator (0.2 mm x 20 cm x 20 cm). Coupounds were visualized on TLC plates by illumination with a UV light source (Mineralite, emission wavelength *ca.* 254 nm), or for trityl-containing

compounds, by brief immersion in a solution of cysteine stain followed by oven-drying. The cysteine stain is used to differentiate sugar, base and trityl groups, and consists of cysteine (0.5 g), concentrated sulfuric acid (16 mL) and water (100 mL). Consequently, both UV and non-UV active compounds could easily be detected using these methods.

Gravity and flash column chromatography were performed using silica gel (40-63 micron particle size, F60) as obtained from Silicycle Inc., QC. In the latter of the 2 methods, compounds were eluted under a constant stream of air or nitrogen where specified, using a flow rate of 1-2 mL/min.[365]

6.1.3. Instruments

UV-Vis Spectra. UV and visible absorption spectra/measurements, including those for thermal denaturation profiles of oligonucleotides, as monitored at 260 nm, were recorded with a Varian Cary I or Cary 300 spectrophotometer (Varian: Mulgrave, Victoria, Australia) equipped with a thermostatted cell holder. All data were collected using the manufacturer's supplied software (Cary Win UV, versions 1.3e or 2.00). All readouts were acquired on a personal computer (see **section 6.5.1.** for details).

NMR Spectra. Routine nuclear magnetic resonance (NMR) spectra were acquired at ambient temperature using Varian XL-200, 300 or 400 MHz spectrophotometers. In addition to ^{1}H-NMR and ^{31}P-NMR, new compounds were further characterized using 2D-NMR. Assignments were deduced primarily from homonuclear correlated spectra (^{1}H-^{1}H COSY), and all chemical shifts were reported as ppm downfield from tetramethylsilane (TMS) as internal reference. Deuterated solvents (*e.g.* $CDCl_3$, acetone-d_6, and dimethylsulfoxide-d_6) for recording spectra were obtained from Cambridge Isotope Laboratories, Andover, MA.

FAB-Mass Spectrometry. Fast atom bombardment (FAB) mass spectra were collected by the McGill University Analytical Services using a Kratos MS25RFA high resolution mass spectrometer. In all cases, the compounds were analyzed exclusively using nitrobenzyl alcohol (NBA) as matrix.

MALDI-TOF Mass Spectrometry. Matrix-assisted laser desorption/ionization time-of-flight mass spectra (MALDI-TOF) were recorded on a Kratos Kompact-III TOF instrument with a minimum laser output of 6 mW at a wavelength of 337 nm, 3 ns pulse width, and 100 mm diameter spot. The MALDI instrument was operated in the negative mode.

Circular Dichroism Measurements. Circular dichroic spectra (CD) were collected on a JASCO J-710 or J-810 spectropolarimeter fitted with a thermoelectrically controlled external constant temperature NESLAB RTE-111 circulating waterbath (JASCO, Inc.). The data were processed using Windows based software as supplied by the manufacturer.

All spectra were recorded between 200 – 350 nm. The scan speed was 50 nm/min, sampling wavelength was 0.2 nm, with 3 – 5 repetitive scans that were summed and cumulative. All CD spectra were recorded from oligonucleotides at total single strand concentrations of *ca.* 5 μM in aqueous buffered solutions unless noted otherwise (see **section 6.5.2.** for details).

6.2. Automated Solid-Phase Oligonucleotide Synthesis: Protocols & Reagents

6.2.1. Reagents for Nucleoside Monomer Phosphoramidite Functionalization

The reactions described in this section are highly sensitive to trace amounts of moisure, and as such necessitate the use of oven-dried glassware and anhydrous reagents during handling. All reagents used toward phosphoramidite preparation were obtained from the highest quality synthesis grade materials. Appropriate diluents/solvents (*e.g.* acetonitrile, THF, DIPEA) were refluxed under inert atmosphere and collected via oven-dried syringe from a septum-sealed glass bulb immediately preceding use. All phosphoramidites, including the phosphitylating reagent used for derivatization [β-cyanoethyl-(N,N-diisopropylamino) phosphochloridite; ChemGenes Corp.] were stored in brown glass vials fitted with rubber septa under an inert atmosphere at –20°C and desiccated under vacuum over P_2O_5 for at least 2 h prior to use.

DNA and RNA Phosphoramidites. Deoxy- and ribonucleoside 3'-phosphoramidites were generally purchased from ChemGenes Corp. (Ashland, MA) or otherwise synthesized via established protocols.[206,209,366,367] The former consist of a 5'-O-dimethoxytrityl-2'-deoxy – (N – protected ribonucleoside) – 3' – O – (β – cyanoethyl) N,N – diisopropyl phosphoramidite building block, whereas the latter comprise an additional 2'-OH function masked by silyl protection to give the corresponding 5'-O-dimethoxytrityl-2'-O-*tert* – butylsilyl – 2' – deoxy – (N – protected ribonucleoside) – 3' – O – (β – cyanoethyl) N,N-diisopropyl phosphoramidites. The exocyclic N^6- and N^4-amines of respective adenine (Ade) and cytosine (Cyt) heterocycles were conveniently masked in the form of benzoyl (Bz) amides, whereas the N^2-amine of quanine (Gua) was protected with an isobutyryl (*i*-Bu) group; the thymine heterocycle required no protection.

2'F-ANA Monomers. Suitably protected 2'-deoxy-2'-fluoro-β-D-arabinonucleosides employed in the solid phase synthesis of 2'F-ANA oligonucleotides were kindly provided by Drs. Katya Viazovkina and Mohamed Elzagheid and consisted of: N^6-Benzoyl-9-[2-deoxy-2-fluoro-5-*O*-(4-methoxytrityl)-β-D-arabinofuranosyl] adenine, N^2-Isobutyryl-9-[2-deoxy-2-fluoro-5-*O*-(4-methoxytrityl)-β-D-arabinofuranosyl] guanine, N^4-Benzoyl-1-[2-deoxy-2-fluoro-5-*O*-(4-methoxytrityl)-β-D-arabinofuranosyl] cytosine, and 1-[2-deoxy-2-fluoro-5-*O*-(4-methoxytrityl)-β-D-arabinofuranosyl]thymine.[212,368]
Derivatization of these nucleosides to their corresponding phosphoramidites was carried out by appending a β-cyanoethyl-*N,N*-diisopropylaminophosphinyl group to the free 3'-hydroxyl position on the 2-fluoro-arabinose sugar. To simplify purification, the reactions were completed using a minimal amount of phosphitylation reagent.

Acyclic Linker Phosphoramidites. With the exception of the secouridine 2'-phosphoramidite synthon which was synthesized in house (see **section 6.7.1.**), the 4-(4,4'-dimethoxytrityloxy)butyl-1-O-[(2-cyanoethyl)-(N,N-diisopropyl)]-phosphoramidite and similarly protected appropriate 3-(4,4'-dimethoxytrityloxy)propyl-1-O-[(2-cyanoethyl)-(N,N-diisopropyl)]-phosphoramidites, and 1-dimethoxytrityl-3-levulinyl glycerol-2-phosphoramidites (used to provide the respective butyl, propyl and ethyl interresidue

hydrocarbon spacers; see chapter **3**) were purchased from ChemGenes Corp. (Ashland, MA) and used as received.

6.2.2. Derivatization of Solid Support[369]

Long chain alkylamine controlled-pore glass (LCAA-CPG, 4 g, 500 Å pore diameter) was obtained from Dalton Chemical Laboraties (Toronto, ON) and acid activated by treatment with a 3% w/v solution of TCA in dichloroethane (DCE) for 4 h at room temperature to liberate a maximal number of amino sites on the support. The activated support was filtered on a fritted glass funnel and sequentially washed with triethylamine:DIPEA (9:1, 50 mL), dichloromethane and diethyl ether. The washed CPG was then dried *in vacuo* over $CaCl_2$ for 12 – 24 h.

Succinylation of exposed amino termini on solid support proceeded using an anhydrous mixture of acid-activated LCAA-CPG (1 g), succinic anhydride (0.20 g, 2 mmol) and 4-DMAP (0.33 mmol, 40 mg) in dry pyridine (6 mL). The contents were combined in an oven-dried hypovial purged with N_2 and gently shaken on a Mistral Multi-Mixer® (Lab-Line Instruments, Inc.; Melrose Park, ILL) at room temperature for 24 h. After this time, they were filtered and successively washed with pyridine, dichloromethane and diethyl ether, then dried overnight under vacuum.

The 5'-tritylated, base-protected nucleosides were then directly coupled through their free 3'- or 2'-OH termini to the polymer support. Condensation of the nucleoside (0.1 mmol) to succinylated LCAA-CPG (0.5 g) proceeded at room temperature over 16 h in a mixture of 4-DMAP (6 mg, 0.05 mmol) and 1-(3-dimethylaminopropyl)-3-ethylcarbodiimide (192 mg, 1.0 mmol) in a shaken solution of TEA (40 μL) and anhydrous pyridine (6 mL). Following nucleoside derivatization of the support, any residual carboxyl groups were converted to amides by stepwise addition of pentachlorophenol (65 mg, 0.24 mmol) pre-dissolved in pyridine (100 μL) for 16 h and final treatment with piperidine (2 mL) for 5 min.[369] The derivatized CPG was filtered, and washed sequentially with DCM and diethyl ether before drying under reduced pressure. The extent of nucleoside coupling to the support was calculated from the measured absorbance of released trityl ions after subjecting an accurately weighed amount of CPG to mild acid treatment (3% TCA in

DCE). By this method, nucleoside loadings were generally calculated to fall between 30 –50 μmol/g of CPG.

An alternate derivatization procedure relying on uronium-mediated nucleoside coupling was also employed to reduce the coupling time and increase the loading volume.[370] This was accomplished using *O* – (7 – azabenzotriazol – 1 – yl) – 1,1,3,3 – tetramethyluronium hexafluorophosphate (HATU; 38 mg, 0.1 mmol), 4-DMAP (12 mg, 0.1 mmol), succinyl-CPG (250 mg), and appropriately protected nucleoside (0.1 mmol) in acetonitrile (1 mL). The contents were combined and shaken at room temperature for 2 – 4 h. After successive washing with DCM, MeOH, and DCM once more, the filtered support was dried and nucleoside loading quantified by trityl analysis. Average coupling yields were calculated to lie between 50 – 75 μmol/g.

6.2.3. Automated Solid-Phase Oligonucleotide Synthesis on Solid Support

6.2.3.1. General Reagents

As phosphoramidite oligonucleotide chemistry is extremely water-sensitive, all solvents were distilled just before use to ensure they were of utmost purity while further lacking any traces of water. Fresh reagents were also routinely prepared prior to commencing a synthesis, as these were critical for eventual success. Accordingly, all materials used toward oligonucleotide assembly were of the highest quality grade (see **section 6.2.1.**). The acetylation or 'capping' of any unreacted hydroxyl groups on solid support prior to oligonucleotide extension was performed either manually or by using a dedicated synthesis cycle on the gene machine. The capping reagents ('Cap A' and 'Cap B') were prepared as follows: Cap A – 10% (v/v) acetic anhydride and 10% (v/v) dry 2,4,6-collidine in anhydrous THF; Cap B – 16% (v/v) dry N-methylimidazole (NMI) in anhydrous THF. Deblocking of trityl-masked terminal nucleoside hydroxyl groups was performed in a solution of 3% (w/v) trichloroacetic acid (TCA) in 1,2-dichloroethane (DCE). Internucleotide bond formation between free incoming nucleoside phosphoramidites and terminal support-bound hydroxyl groups was catalyzed using either 0.5 M tetrazole or 0.5 M 4,5-dicyanoimidazole in anhydrous acetonitrile as phosphoramidite activation reagent. Newly formed trivalent phosphite triester linkages

were oxidized to the more stable pentavalent phosphotriesters in a solution of 0.1 M iodine (Aldrich) in THF/pyridine/water (25:20:2, v/v/v).

6.2.3.2. Chain Assembly of DNA and RNA Oligonucleotides

Automated syntheses of oligonucleotides consisting of ribose or 2'-deoxyribose sugars were conducted almost exclusively on an Applied Biosystems (ABI) 381A synthesizer using standard β-cyanoethyl chemistry and 1 μmol synthesis scales as specified in the manufacturer's protocol.

Prior to oligonucleotide assembly, the nucleoside-derivatized glass beads, consisting of 1 μmol total nucleoside loading, were packed into an ABI-compatible synthesizer column, installed on the instrument and pretreated with a mixture of Cap A and B reagents using a dedicated capping cycle programmed into the machine. Acetylation, or capping, prevents undesirable side reactions from occurring during chain assembly by masking any potentially reactive hydroxyl or amino sites on the support surface,[371] and also ensures the removal of trace amounts of moisture prior to initiating the synthesis.[213,369]

Assembly of the oligonucleotides was generally carried out by the stepwise addition of phosphoramidite building blocks to nucleoside or nucleotide hydroxyl termini preimmobilized on solid support until the desired sequence was obtained. The individual monomers were dissolved in freshly distilled acetonitrile to give final concentrations of 0.1 M in the case of 2'-deoxyribonucleoside phosphoramidites, or 0.15 M for ribonucleoside phosphoramidites. The diluted solutions were kept under an inert atmosphere in septum-fitted brown glass vials and quickly transferred to the respective port on the instrument immediately preceding oligonucleotide synthesis.

Each addition of new building block required four steps: detritylation, coupling, capping, and oxidation. Adjustments to the standard protocols were made primarily to compensate for reduced reactivities of certain phosphoramidites and/or protecting groups and included the following protocol modifications: *(i) Detritylation* – a solution of 3% TCA in DCE was continuously delivered to the column for 120 seconds to quantitatively remove DMT-groups; for the less labile MMT-protected nucleosides, the delivery time was extended to 200 seconds. *(ii) Nucleoside coupling* – the coupling time or 'wait' step for incoming 2'-deoxynucleoside phosphoramidites (dA, dC, dT) was set to 120 seconds, whereas dG

phosphoramidites were delivered over 240 seconds; ribonucleoside phosphoramidites (rA, rC, rU) typically required 450 seconds for efficient coupling and 600 seconds for rG. Specialized monomers (*i.e.* 2'-methoxyribonucleotides, seconucleoside phosphoramidites) and acyclic linkers are discussed in their respective sections (*vide infra*). *(iii) Capping* – unreacted 5'-hydroxyl groups were acetylated by continuous delivery of a mixture of Cap A and Cap B reagents over 17 seconds, followed by a 45 second 'wait' step. *(iv) Oxidation* – internucleotide phosphite triester linkages were oxidized by treatment with an aqueous iodine solution which was delivered to the column for 20 seconds followed by a 20 second 'wait' step.

All oligonucleotides were synthesized in the 'trityl-off' mode to facilitate subsequent purification by either preparative PAGE (**section 6.4.2.**) or anion exchange HPLC (**section 6.4.3.**). At completion of the synthesis, exposed 5'-hydroxyl termini were capped with acetic anhydride on the instrument, the column contents thoroughly washed with acetonitrile, then dried by flushing under a constant stream of argon for 15 minutes.

The coupling efficiencies for successive cycles were determined spectrophotometrically by quantitation of released MMT^+ or DMT^+ cations (ε_{MMT} = 56000 L mol^{-1} cm^{-1}, λ_{max} 478 nm; ε_{DMT} = 76000 L mol^{-1} cm^{-1}, λ_{max} 504 nm). The range of coupling efficiencies as monitored by this assay were generally found to fall between 98 – 99%.

6.2.3.3. Chain Assembly of 2'F-ANA Phosphodiester Oligonucleotides

The chemical synthesis of 2'-deoxy-2'-fluoro-β-D-oligoarabinonucleotides (2'F-ANA) containing phosphodiester linkages was accomplished with the assistance of Dr. Katya Viazovkina.

Briefly, the assembly of 2'F-ANA sequences was conducted under similar conditions as those employed in the construction of DNA sequences, but longer coupling times for 2'-fluoroarabinose phosphoramidite monomers were required.[212] The 2'F-ANA oligonucleotides were exclusively synthesized on an Expedite 8909 DNA synthesizer equipped with a workstation (PerSeptive Biosystems) and online trityl monitor system. All syntheses were performed on 1 μmol scales, using typical amidite concentrations of 50 mg/mL in anhydrous acetonitrile, which was introduced by syringe through the septum of the appropriate amidite vial prior to its attachment on the instrument port. The

reagents were blanketed under a steady stream of argon gas to protect them from humidity during the synthesis. The volume of amidite solution delivered to the column during each coupling step was *ca.* 240 μL. The coupling time for successive extension of the support-bound oligonucleotide chain with 2'-fluoroarabinonucleoside phosphoramidites required a 15-min wait step, as compared to 1.5 min for 2'-deoxynucleosides on the Expedite instrument. Likewise, the detritylation time was extended from 120 to 150 seconds to allow for effective removal of the monomethoxytrityl (MMT) protection as opposed to the more labile dimethoxytrityl (DMT) groups that are commonly used with the standard DNA monomers. Upon obtaining the full length 2'F-ANA oligomer, complete deprotection, analysis and purification proceeded in a manner identical to that of the oligodeoxynucleotides.

6.3. Complete Deprotection of Synthetic Oligonucleotides

6.3.1. General Reagents

Nuclease and microbial contaminants from double distilled, deionized water (Millipore; Billerica, MA) were removed by treatment with 0.1% (v/v) diethyl pyrocarbonate (DEPC; Aldrich). The contents were stirred for at least one hour prior to autoclaving to ensure general RNase inactivation and decontamination via active site acylation and permanent blocking of necessary catalytic residues.[372] Residual DEPC was eliminated after autoclaving at *ca.* 121°C in an electric steam sterilizer. Plasticware, glassware and pipet tips were similarly decontaminated, while solutions of thermolabile materials (*e.g.* DTT, manganese salts) used in the analysis of oligonucleotides were prepared by dissolving the solids in DEPC-treated water and passing the solution through a 0.2 μm filter to sterilize.[373,374] Similarly, compounds with amine groups (*e.g.* Tris buffers) were prepared by dissolving the base in DEPC-treated and autoclaved water. All sterilized materials were subsequently handled while wearing gloves to minimize contamination and degradation of oligonucleotides from nucleases present on the skin. Double-distilled, deionized water for HPLC analyses of crude and purified oligonucleotides was pre-filtered through a 0.45 μm nylon membrane (Millipore) to remove any residual particulates and contaminants.

6.3.2. Cleavage from CPG and Removal of Phosphate, Base and Hydroxyl Protecting Groups

Fully protected oligonucleotides, attached to the solid support in the synthesis column, were transferred to a microtube, and cleaved from the CPG using a mild alkaline solution of aqueous ammonia (29%) and absolute ethanol (3:1, 1 mL). This treatment ensured complete cleavage of the succinate tether from the oligonucleotide 3'-terminus while concurrently affording removal of phosphate-protecting cyanoethyl moieties and exocyclic amino protecting groups. Deprotection times generally required 24 h at room temperature with constant shaking of the contents using a hand shaker; for those sequences containing the less labile N^2-isobutyryl protected guanine heterocycles, extended times (*ca.* 48 h) were required.

Upon complete deprotection, the CPG was separated by centrifugation, and the supernatant collected and transferred to a sterile microtube. The residual material was washed with ethanol (3 x 1 mL) to maximize oligonucleotide recovery, and the recovered fractions were dried under low vacuum for 1-2 h or left to stand at room temperature for 1 day to remove all traces of ammonia, in order to prevent subsequent bumping of the liquid and loss of the sample during lyophilization. The ammonia-free fractions were then lyophilized to dryness in a Speed-vac® concentrator.

Additional silyl protection of ribose-containing oligonucleotides necessitated the use of one extra step following alkaline treatment, namely the removal of the 2'-O-*tert*-butyldimethylsilyl (TBDMS) group. This was accomplished by treating the crude pellet with 100-200 μL of neat triethylamine trihydrofluoride [$Et_3N(HF)_3$; Aldrich] for 48 h at r.t.[216,375] At the end of this time, the reaction was quenched with sterile water (500 μL) and lyophilized to dryness. Alternatively, the crude oligoribonucleotides could be directly precipitated by adding 25 μL of sodium acetate (3 M, pH 5.5) and 1 mL of chilled *n*-butanol and placing the contents on dry ice (–78°C) for 1 h or at –20°C overnight.[376] The pellet was then recovered following centrifugation (10 min, 18000 rpm), washing with 70% ethanol (2 x 500 μL) and lyophilization under high vacuum. Crude oligonucleotides obtained in this way were then purified by anion-exchange high-performance liquid chromatography or denaturing polyacrylamide gel electrophoresis (PAGE; **section 6.4.**). All oligonucleotides were quantitated prior to separation by PAGE

or HPLC by UV absorbance (A_{260}) so as not to under- or overload the matrix. The yield of recovered oligonucleotide was thus measured by diluting the lyophilized pellet in 1 mL of deionized water, followed by removal of a 10 μL aliquot and its further dilution with 1 mL of dd water in a UV cell. Upon measuring the sample absorption at 260 nm, the amount of crude oligonucleotide (in A_{260} units) could subsequently be calculated.

6.4. Analysis and Purification of Synthetic Oligonucleotides

6.4.1. General Reagents

All aqueous solutions were made with double distilled, deionized water (Millipore). High quality molecular biology grade acrylamide, *N,N'*-methylene-bisacrylamide (BIS), ammonium persulfate (APS), *N,N,N',N'*-tetramethylethylenediamine (TEMED) and urea used for electrophoresis were purchased from Amersham Biosciences. Bromophenol blue (BPB), xylene cyanol FF (XC), 2-amino-2-(hydroxymethyl)-1,3-propanediol (Tris), boric acid, and disodium ethylenediaminetetraacetate dihydrate (EDTA) were purchased from Bio-Rad Laboratories (Mississauga, ON) and used as received.

Denaturing polyacrylamide gel solutions were generally prepared by mixing the appropriate amount of a 50% aqueous acrylamide stock solution (w/v), consisting of 19:1 acrylamide:BIS, with 10 x TBE buffer (0.89 M Tris, 0.89 M boric acid, 25 mM EDTA; pH 8.3). Whenever possible, commercially prepared solutions of polyacrylamide (Laboratoire Mat Inc., QC) were used to avoid direct handling of the neurotoxic acrylamide powder. Ultrapure urea (7 M) was added to the mixture to ensure disruption of all secondary structure and thereby simplify resolution of the full length oligomer species from contaminating failure sequences. A final dilution with sterile double distilled, deionized water was necessary to obtain typical working concentrations of 14 – 24% acrylamide for oligonucleotide separations.

Formamide was obtained from Sigma and deionized before use by stirring over a mixed bed ion-exchange resin (Bio-Rad AG 501-X8) for 30 min. After filtering, it was then used to prepare the loading buffer (denaturing) which consisted of 9:1 (v/v) formamide : 10 x TBE buffer. Running dye markers were prepared in exactly the same manner as the loading buffer, but also incorporated 2% (w/v) of both XC and BPB tracking dyes. The running buffer used for filling the upper and lower chamber reservoirs was 1 x TBE.

Aqueous solutions of lithium perchlorate (Aldrich) for anion-exchange HPLC analysis and purification were filtered through a 0.45 μm pore nylon membrane filter and degassed under vacuum before use.

6.4.2. Polyacrylamide Gel Electrophoretic (PAGE) Resolution and Purification of Oligonucleotides

The overall success of a synthesis was primarily evaluated by monitoring the migratory behaviour of fully deprotected oligonucleotides under denaturing PAGE conditions. Samples were typically run using a dual cooled vertical slab electrophoresis unit (Hoefer Scientific SE600, Fisher Scientific) powered by a variable adjust DC voltage supply unit (Model 2000/200, BioRad Labs, Inc).

Both analytical and preparative gel solutions (30 – 50 mL) were generally sonicated for 20 min to degas the solution prior to casting the gel. Polymerization was then induced by adding a free radical initiator, consisting of freshly prepared 10% (w/v) ammonium persulfate (APS; 200 μL) and TEMED (20 μL) as catalyst. The gel porosity was controlled by adjusting the percentage of acrylamide; typically 24% (w/v) solutions were used for analytical runs while preparative gels consisted of 16 – 20% acrylamide to facilitate isolation. Gels were cast in 18 cm x 16 cm silanized glass plates either as 0.75 or 1.5 mm thick, the latter to accommodate larger sample loadings for preparative scales. Polymerization was usually complete at 0.5 – 1.5 h, at which time the wells were gently aspirated with 1 x TBE running buffer to remove any settled debris and urea in the wells immediately preceding sample application. The amount of material to be resolved was quantitated by UV absorbance such that final loadings corresponded to 0.5 A_{260} units of crude sample (analytical PAGE) or 30 – 40 A_{260} units for preparative PAGE. The lyophilized samples were dissolved in 10 μL or 50 – 100 μL of loading buffer depending on the type of application, and heated at 90°C for 10 mins prior to sample loading. For RNA species, desalting prior to PAGE purification was sometimes required to prevent band distortion and maximize resolution, either by precipitating the sample (*vide supra*) or by size exclusion chromatography (**section 6.4.4.**). Electrophoresis was generally started immediately after sample loading to prevent band broadening by diffusion, and the

gels were run at 500 – 800 V until the faster moving BPB dye had migrated *ca.* two-thirds down the length of the gel surface (*ca.* 2 – 4 h).

6.4.2.1. Post-Electrophoresis Treatment

Once the current was stopped, the glass plates were carefully dismantled to expose the gels, which were removed from the plates and covered in Saran Wrap®. The wrapped gels were photographed over a fluorescent plate while illuminated by a handheld UV lamp (*e.g.* Mineralight, model UVG-54). Photographs were normally taken in the dark using a Polaroid PolaPan® camera (f 4.5 aperture setting, 16 sec exposure time) with instant film (Polaroid #52, ISO 400/21°C, 4" x 5") through a Kodak Wratten gelatin filter (#58 green). Gel images were also conveniently captured using a Canon PowerShot A70 3.2 MP digital camera.

In some instances, band migration on analytical gels was better visualized after soaking the gel in a solution of Stains-All[377] (Sigma) for 20 – 60 min according to the manufacturer's specifications. All stained bands appeared purple when placed over a white background, and were photographed without UV shadowing, with the camera filter removed and the aperture set at f 11 with a 30 sec exposure time.

Oligonucleotide isolation from preparative resolutions then proceeded by excising the desired band from the gel with a sterile scalpel. The gel slice was transferred to a sterile Falcon™ conical centrifuge tube (15 mL capacity; BD Biosciences), finely crushed with a spatula, and the oligonucleotide was extracted into *ca.* 5 mL of autoclaved water by shaking the contents for 24 h at room temperature. The slurry was centrifuged (2 min, 18000 rpm) to separate the insoluble gel matter, the supernatant was collected and the residue was washed with water (3 x 2 mL). The supernatant and washings were ultimately combined in a 15 mL conical tube and lyophilized to dryness *in vacuo*. Recovered yields of purified oligonucleotides were generally greater than 80%, but were isolated with generous amounts of low molecular impurities such as salts and urea, and so underwent a further purification or 'desalting' by size exclusion chromatography (**section 6.4.4.**) prior to subsequent biophysical characterizations.

6.4.3. Anion-Exchange HPLC Resolution and Purification of Synthetic Oligonucleotides

Oligonucleotides were also conveniently analyzed and purified by anion-exchange HPLC using a Waters 1525 HPLC instrument (Milford, MA) equipped with 2 solvent delivery pumps, a dual wavelength absorbance detector (Waters Model 2487), in-line degasser and internal column heater driven by Windows-based (*i.e.* Breeze® v. 3.20) software. The crude samples were resolved on a Protein Pak™ DEAE-5PW anion exchanger column, consisting of DEAE-bonded, hydrophilic, porous (1000 Å pore size) polymer particles 10 μm in size and with overall column dimensions of 75 mm x 7.5 mm (internal diameter). Samples for analytical injections were prepared by dissolving 0.5 – 1 ODU of oligonucleotide in 10 – 20 μL of starting buffer (*i.e.* dd H_2O) and sonicating for 10 minutes to ensure the complete dissolution of lyophilized sample. The samples were then heated to 60°C for 5 mins to denature any bound regions and centrifuged before injection to settle any insoluble material that might otherwise clog the injection port. Preparative analyses were prepared in a manner entirely analogous to the above, but typically involved much larger sample loadings, *ca.* 30 – 50 ODU of crude material dissolved in 300 – 500 μL of starting buffer. All separations were conducted using a linear gradient of 0 – 20% $LiClO_4$ or $NaClO_4$ and flow rate of 1 mL/min, with the ionic strength of the mobile phase gradually adjusted by varying the ratio of the starting buffer, or 'Buffer A' (dd H_2O) to Buffer B (1 M $LiClO_4$ or $NaClO_4$) over the course of the run (60 min). This gradient system enabled selective desorption of the purified full-length oligonucleotide as the last eluting component of the crude mixture within a reasonable period of time. In addition to equilibrating the column with starting buffer for 20 min between successive analyses, blanks were periodically run to ensure no cross contamination or 'carry-over' between runs, particularly after preparative injections. The column was maintained at a constant temperature of 55°C throughout each run, to denature all intra- or intermolecular associations between complementary regions on the oligonucleotides. The detector was tuned to monitor the absorbance at 260 nm for analytical scales, whereas preparative separations were simultaneously monitored at dual wavelengths (*i.e.* 260 and 290 nm) in order to avoid saturating the detector. In this case, detection at the latter wavelength had the advantage of enabling more accurate control over sample collection, thereby

maximizing recovered yield and minimizing any potential peak overlap with n-1 failure sequences eluting just before the peak of interest. The retention time of the desired peak was estimated from the corresponding analytical-scale chromatogram, and was collected as a series of 1 mL fractions in sterile microtubes. The fractions containing the desired oligonucleotide were then pooled and concentrated *in vacuo* to a total volume of 1 mL, and subsequently desalted using one of the methods described in **section 6.4.4**. A typical chromatographic profile of an 18 nt 2'F-ANA oligonucleotide before and after HPLC purification is shown in **Figure 6.1**. Isolation of the full length oligonucleotide is achieved upon collection of the last eluting peak of the series, with those fractions corresponding to n-1 failure sequences eluting at earlier times during the run.

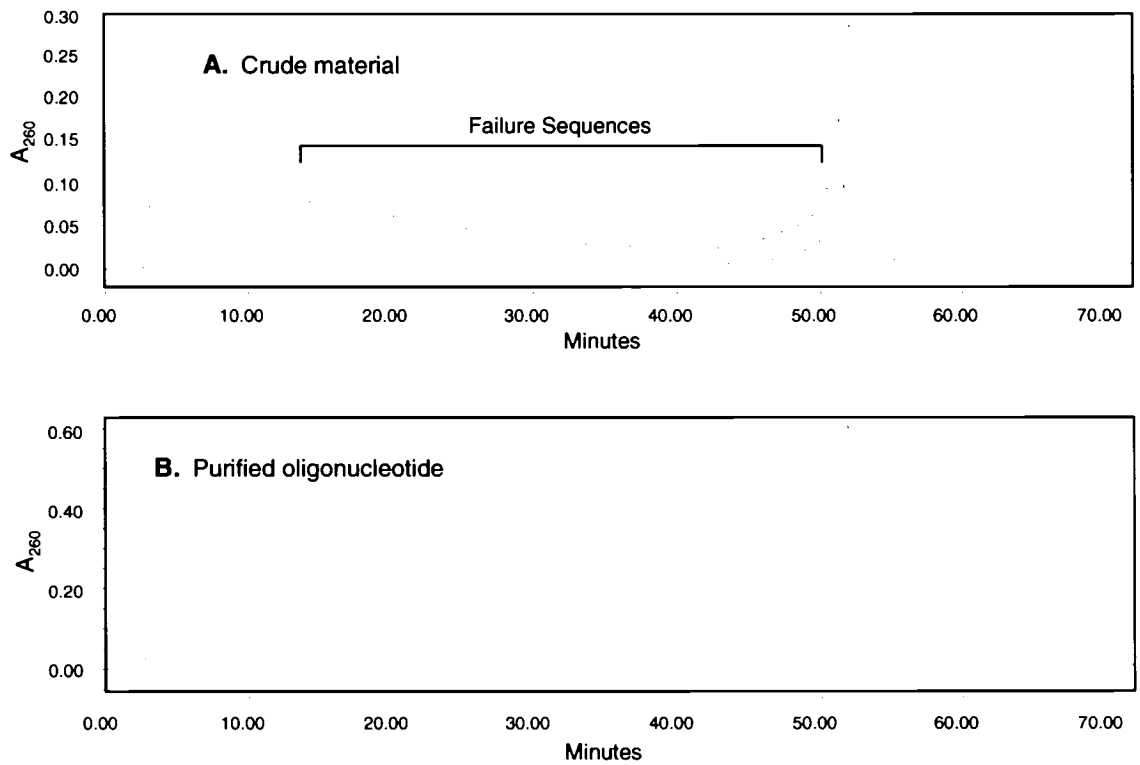

Figure 6.1: Representative anion exchange HPLC chromatogram of a fully deprotected 2'F-ANA butyl-containing oligonucleotide (sequence **2.8**) before (**A**) and after (**B**) purification of the crude sample. HPLC conditions: Protein Pak-DEAE-5PW (75 x 7.5 mm i.d.) column pre-equilibrated at 55°C; Buffer A: ddH_2O; Buffer B: 1 M $LiClO_4$ run at a 0 – 20 % gradient of Buffer B over 60 min.

6.4.4. Sample Desalting

In order to be useful for subsequent characterizations, the oligonucleotides must be isolated in the free form of the acid, thereby necessitating the removal of contaminating counterions. As such, they were purified from these and other low molecular weight impurities (*e.g.* urea) and water-soluble salts by size exclusion chromatography (SEC) on a gel filtration matrix. Effective desalting was achieved using Sephadex® G-25 Superfine medium (Amersham), prepared by cross-linking dextran with epichlorohydrin.[378,379] This size-exclusion matrix allows small impurities with nominal masses < 5000 Da, to travel a longer mean flow path and to elute later than the relatively large full-length nucleic acid species (*ca.* ≥ 5000 Da), which elutes first in the void volume by exclusion from the internal pores of the media.

The gel matrix, supplied in its dry form (20-50 μm size), was first mixed with an equal volume of dd H_2O for at least 1 h to hydrate and swell the beads (52 μm average size) prior to sterilization. The hydrated gel was then placed in an All American 25X Electric Sterilizer (Wisconsin Aluminum Foundry Co. Inc; Manitowoc, WI) and autoclaved (121°C, 15 psi, 1.5 h) in the presence of 0.1% DEPC. After cooling, the slurry was loaded into a sterile 10 mL disposable syringe barrel (8.5 cm x 1.5 cm i.d.) plugged with silanized glass wool, and packed to a volume of *ca.* 8 – 10 mL by flushing the column with DEPC-treated dd H_2O (20 – 25 mL). Once the contents had settled and the matrix was adequately washed, the 'contaminated' oligonucleotide was carefully applied to the column, with care taken to avoid disturbing the gel surface. Generally, samples were dissolved in 1 mL of dd water and allowed to fully enter the gel bed before subsequent additions of eluent. A total of 10 x 1 mL fractions were collected in sterile tubes, with each fraction individually assayed by UV absorbance (λ = 260 nm) to determine which tubes contained the pure, desalted oligonucleotide. Positive fractions containing the oligomer were typically concentrated within the second to fifth tubes. Accordingly, these were pooled and evaporated to dryness under reduced pressure, then redissolved in 1 mL of sterile H_2O for subsequent UV quantitation.

Hydrated SEC matrices of the above dimensions could rapidly effect efficient separation of up to 100 ODU of salted oligonucleotide with recovered yields generally ranging between 80 – 95% of purified material. The aqueous solutions of salt-free

oligonucleotide were stored at –20°C and thawed immediately preceding further analyses (**section 6.5.**).

6.4.5. Characterization of Oligonucleotides by MALDI-TOF Mass Spectrometry

The purity of desalted oligonucleotide samples was primarily assessed using matrix assisted laser desorption / ionization time-of-flight mass spectrometry (MALDI-TOF MS). This soft ionization method minimizes extensive fragmentation of gas phase ions, enabling accurate molecular weight determination of the intact ionized species with high signal intensities. All spectra were acquired on a Kratos Kompact-III instrument operated in the negative ion linear or reflectron mode.

Sample preparation for mass spectral analysis was done as follows: 1 μL of an aqueous solution of oligonucleotide (100 – 200 pmol) was mixed with 2 μL of a matrix consisting of 1 μL saturated 6-aza-2-thiothymine/spermine (80 mg/mL ATT dissolved in 1:1 dd H_2O/CH_3CN containing 25 mM spermine) and 1 μL of a freshly prepared 50 mM aqueous fucose solution. This matrix/co-matrix combination was especially useful for limiting adduct formation between the negative nucleic acid phosphodiester backbone and bound cations by proton exchange supplied from the spermine additive. As such, it was the matrix of choice for attaining high resolution mass spectra while increasing the abundance of the molecular ion by allowing more efficient desorption-ionization of polyionic analytes.[380,381]

A 1 μL aliquot of the matrix-analyte mixture was applied in duplicate to a stainless steel sample plate, and allowed to air dry for a minimum of 30 min to evaporate the solvent and crystallize the sample. Typically, 20-70 laser shots were fired for each spectrum, which were averaged and processed using software supplied by Kratos. Generally, the molecular ion peak also corresponded to the base peak of the spectrum and afforded correct molecular weight determinations (*m/z* values) for each sample, with excellent signal-to-noise ratios. The calculated and observed masses for each of the synthesized oligonucleotides discussed in this work are presented in their respective sections (*vide infra*).

6.5. BIOPHYSICAL CHARACTERIZATION OF OLIGONUCLEOTIDES

6.5.1. Hybrid Stability Studies: UV Thermal Denaturation Profiles

Oligonucleotide hybridizations were investigated by monitoring the hyperchromic change in UV absorbance at 260 nm with increasing temperature, thereby generating thermal denaturation profiles, or 'melting curves' over a broad temperature range, typically 5 – 90°C unless otherwise noted. These studies were conducted using a Varian Cary I or Varian Cary 300 UV-visible multiple cell spectrophotometer equipped with a Peltier temperature controller interfaced to a PC running Windows based software (Win 3.1 or Win 2000 Professional).

Molar extinction coefficients (ε_{260}) of single strands were calculated based on those of mono- and dinucleotides using the nearest-neighbour approximation method of Puglisi and Tinoco.[257] Single strand extinction coefficients for 2'F-ANA, a DNA mimic, and 2'F-ANA seconucleotide-containing chimeras were assumed to be the same as those of normal DNA strands, and were estimated from an internet-based biopolymer calculator (see **sections 6.7. – 6.9.** for reported values).

In general, samples were prepared by lyophilizing an equimolar mixture of complementary strands to dryness and then redissolving in 0.5 – 1 mL of the appropriate buffer for a total strand concentration of *ca.* 5 μM (*i.e.* 2.5 μM duplex concentration). Hybridization buffers typically consisted of one or more of the following: (a) 140 mM KCl, 5 mM Na_2HPO_4, 1 mM $MgCl_2$ (pH 7.2); (b) 60 mM Tris-HCl, 60 mM KCl, 2.5 mM $MgCl_2$, 2 mM DTT (pH 7.8); (c) 1 mM sodium cacodylate, 2.5 mM $MgCl_2$, 2 mM DTT (pH 7.0); (d) 5 mM sodium cacodylate, 2.5 mM $MgCl_2$, 2 mM DTT (pH 7.0); (e) 10 mM sodium cacodylate, 2.5 mM $MgCl_2$, 2 mM DTT (pH 7.0); or (f) 50 mM sodium cacodylate, 2.5 mM $MgCl_2$, 2 mM DTT (pH 7.0). All solutions were prepared with double-distilled DEPC-treated autoclaved water.

Each solution was rapidly heated to 90°C for 10 – 15 min to dissociate any non-specifically bound regions, and slowly cooled to room temperature for 0.5 – 4 h, after which time they were placed at 4°C for at least 12 – 24 h prior to spectral acquisition. The annealed samples were quickly transferred to pre-chilled Hellma QS-1.000 quartz cells (Cat # 114) and sealed with a Teflon-wrapped stopper to prevent solvent evaporation

during the thermal analysis. The solutions were degassed by sonication for 15-20 sec and further equilibrated to 5°C for 5 min in the cell chamber of the spectrophotometer immediately preceding the start of the acquisition. The absorbance at 260 nm was recorded at 0.5°C intervals as the temperature was ramped at increments of 0.5 °C/min. Nitrogen was continuously flushed through the sample compartment to prevent condensation at low temperature (5 – 25°C). Calculations of the thermal melting temperature were extracted using Cary WIN UV software (version 2.00) as supplied by the manufacturer. Plotting the first derivative of the resulting curve yields a maximum value, the thermal melting temperature (T_M), which corresponds to the inflection point of the transition from duplexed to single-stranded species and represents the temperature at which 50 % of the duplex population has dissociated. Spectra were typically acquired in triplicate and the calculated values were consistently reproducible with an average deviation usually less than ± 0.5°C.

The absorbance *vs.* temperature data were converted to ASCII binary format and imported into spreadsheet software (Microsoft Excel™ 2000) for subsequent manipulation and presentation.

Relative changes in absorbance (*i.e.* hyperchromicity) were compared using the formula: $\%H = [(A_T - A_o)/A_f] \times 100$ where H is the hyperchromicity, A_T is the absorbance at a given temperature (T), A_o is the initial absorbance at the low temperature (*i.e.* 5°C), and A_f is the absorbance at the highest temperature. Alternatively, plots of nonequivalent absorbance, such as those of internal non-complementary regions (*e.g.* 'nicked' or 'gapped' tandem 2'F-ANA duplexes; see chapter **3**) were normalized according to the method of Kibler-Herzog *et al.*[286] which derives the fraction absorbance change on a scale of 0 – 1 using the formula $A_{norm} = (A_T-A_o)/(A_f-A_o)$, to facilitate comparative visualization of the component behaviour.

6.5.2. Conformational Assignment by Circular Dichroism Spectroscopy (CD)

Samples were prepared for CD spectral analysis in a manner entirely analogous to those used in the UV melting experiments. Briefly, equimolar mixtures of single strands were annealed by preheating the solution and cooling to r.t. as for T_M analysis, and left at 4°C at least 12 – 24 h to equilibrate prior to spectral sampling. The samples were transferred

to Hellma QS-1.000 (Cat # 114) fused quartz cells and maintained at 5°C for at least 15 min preceding the start of the acquisition. Spectral scans were acquired on a JASCO Model J-710 or J-810 spectropolarimeter where a constant temperature of 5°C was maintained by an external circulating waterbath (VWR Scientific). All acquired spectra represented the average of 3 – 5 independent scans, and were typically recorded at wavelengths ranging from 200 – 350 nm in buffer consisting of 140 mM KCl, 5 mM Na_2HPO_4, 1 mM $MgCl_2$ (pH 7.2), unless noted otherwise. Individual scans were recorded at a rate of 50 nm/min using a sampling wavelength of 0.2 nm and a bandwidth of 1 nm. The raw data was processed using the J-700 Windows software (version 1.00) as supplied by the manufacturer, and were corrected for background effects including buffer subtraction, noise reduction (*i.e.* line smoothing), and normalized concentration, such that the molar ellipticity could be determined. The molar ellipticity, $[\theta]$, was calculated using the equation $[\theta] = \theta/Cl$, where θ is the relative ellipticity (mdeg), C is the oligonucleotide concentration (mol/L) and l is the path length of the cell (cm). All corrected data were imported to Microsoft Excel™ 2000 speadsheet software for further analysis and presentation.

6.6. General Molecular Biology Techniques: Oligonucleotide Labeling and Characterization

6.6.1. 5'-End [^{32}P]-Labeling of Synthetic Oligonucleotides

Linear oligonucleotide molecules were radioactively labeled at the 5'-hydroxyl terminus with a radioactive phosphorus probe and the enzyme T4 polynucleotide kinase (T4 PNK) according to the manufacturer's specifications (MBI Fermentas Life Sciences, Burlington, ON).

Incorporation of the ^{32}P label was accomplished in reaction mixtures consisting of: DNA or RNA oligonucleotide substrate (100 – 1000 pmol), 3.5 μL 10 x reaction buffer (consisting of 500 mM Tris-HCl, pH 7.6; 100 mM $MgCl_2$; 50 mM DTT; 1 mM spermidine; and 1 mM EDTA), 20 U of T4 PNK enzyme (diluted to 10 U/μL in a solution of 20 mM Tris-HCl, pH 7.5; 25 mM KCl, 0.1 mM EDTA, 2 mM DTT and 50% glycerol), 40 pmol of [γ-^{32}P]-ATP (6000 Ci/mmol, 10 mCi/mL; Amersham Biosciences, Inc.) and DEPC-treated sterile water to a final volume of 35 μL.

The reaction mixture was incubated for *ca.* 45 – 60 min at 37°C, followed by a second incubation for 20 min at 75°C to heat denature and deactivate the kinase enzyme. The solution was lyophilized under reduced pressure using a SpeedVac® concentrator, and redissolved in 6 μL each of sterile water and gel loading dye (98 % v/v deionized formamide in 10 x TBE, 1 mg/mL XC, 1 mg/mL BPB and 10 mM EDTA). This mixture was applied across 2 – 3 lanes of a 40-well vertical slab denaturing polyacrylamide sequencing gel (16%, 7 M urea, 0.4 mm thickness) to prevent sample overloading and subsequent smearing of bands during the electrophoresis. Full-length oligonucleotides were purified from residual degradation products and remaining ADP on a T-Rex Aluminum Backed Sequencer System, Model S3S (Owl Separation Systems Inc., Portsmouth, NH). The gel was run at 2000 V for 1.5 h, at which time the pre-silanized glass plates were disassembled and a previously used autoradiogram film was placed over the entire gel surface to create a tight seal between the gel and the film. The 'hot' gel was peeled off the glass plate and covered with Saran Wrap®, placed in a Kodak X-Omatic® cassette and the labeled oligonucleotides were visualized with an intensifying screen on X-OMAT-AR film (Kodak). Autoradiographic detection of the ^{32}P-labeled species

typically required a 5 – 30 sec exposure to the film and in most cases coincided with the most intense band, also the slowest moving on the gel. This band was circled with a permanent marker, excised, and placed in an Eppendorf® tube where it was crushed and extracted into 1.0 mL of sterile water at 37°C for 8 – 12 h. The purified oligonucleotides were desalted by elution with sterile water on a pre-packed NAP-10™ size exclusion column containing Sephadex® G-25 medium (Amersham Biosciences, Inc.) and stored at –20°C. The full-length ^{32}P-5'-RNA was subsequently quantitated for radioactive content using a Bioscan Quick-Count QC-2000 high energy benchtop beta-counter (Bioscan Inc., Washington, DC) to determine the percent of recovered material. Incorporation of the label was usually greater than 90%, with isolated yields of ^{32}P-5'-RNA following gel extraction averaging 50%.

6.6.2. Preparation of cloned RNases H

The purification and isolation of cloned *E. coli* RNase HI and human RNase H1 homologues was conducted and graciously provided by Dr. Kyung-Lyum Min under the supervision of Dr. Michael Parniak at the Lady Davis Institute, Jewish General Hospital (Montreal, QC).

Molecular biological reagents were generally purchased from MBI Fermentas Inc. (Hanover, MD) and were used as recommended by the manufacturers. Heparin-Sepharose and [γ-^{32}P]ATP were obtained from Amersham Pharmacia Biotech (Piscataway, NJ). Protein concentrations were determined by either the calculated OD_{280} value or by the Bio-Rad protein assay kit (Bio-Rad, CA). *Pfu* DNA polymerase, derived from the hyperthermophilic archaebacterium *Pyrococcus furiosus*, was obtained from Stratagene (La Jolla, CA).

6.6.2.1. Expression and purification of human RNase H1

An *hrnh* cDNA gene fragment from the pcDNA/GS/*hrnh* plasmid vector (Invitrogen, Carlsbad, CA) was obtained by polymerase chain reaction (PCR) using the following primers: AGC TAT CTC GAG ATG AGC TGG CTT CTG TTC CTG GCC and GGC CGC AAG CTT TCA GTC TTC CGA TTG TTT AGC TCC (underlined regions denote

the respective *Xho*I and *Hin*dIII palindromic recognition sequences). PCR was performed in 22 amplification cycles with *Pfu* polymerase, after which the correct sequence of the amplified cDNA product was confirmed by DNA sequencing. The amplified gene was then cloned into a pBAD/His prokaryotic expression vector (Invitrogen; Carlsbad, CA) between the *Xho*I and *Hin*dIII restriction endonuclease cleavage sites.

Recombinant human RNase H1 from the pBAD/His/*hrnh* expression plasmid was purified as follows. To overcome codon bias in *E. coli*, the expression vector was transformed into an *E. coli* BL21 codonplus host strain (Stratagene; La Jolla, CA). This strain contains a ColE1-compatible plasmid encoding extra copies of rarely used *E. coli* tRNA genes (*e.g. argU*, *proL*), and so is able to rescue the expression of heterologous mRNA whose translation might otherwise be slowed or prematurely aborted by a limited availability of the corresponding rare endogenous tRNA.[382,383] The cells were cultured in LB broth containing 100 μg/mL ampicillin and 32 μg/mL chloramphenicol at 37°C until the medium reached a density of 0.5 – 0.6 (mid-log phase) as measured spectrophotometrically by the OD_{600}. In addition to chloramphenicol resistance, transformed *E. coli* cells contain an intact *amp*^{r} gene and as such are viable in the presence of the antibiotic, allowing for their selective enrichment in this medium. Expression of the recombinant fusion protein was then induced over a 4 h period by adding 0.002 % L-arabinose to the medium.

After induction, *E. coli* cells were harvested by centrifugation (1500 x g, 15 min), and the cell paste was washed in chilled wash buffer (100 mM phosphate, pH 8.0, 300 mM NaCl), resuspended in chilled lysis buffer (100 mM phosphate, pH 8.0, 10 Units/mL DNase, 2 mM phenylmethylsulfonyl fluoride, 300 mM NaCl, 200 μg/mL lysozyme), and lysed by 0.5 % NP-40.

After centrifuging the contents, the supernatant was applied to a Ni^{2+}-nitrilotriacetate-agarose column, and the recombinant polyhistidine-tagged protein was purified in denatured form on the metal-chelating resin according to the manufacturer's directions (Qiagen). The eluate was treated with 2 mM EDTA to chelate any residual Ni^{2+} ions, dialyzed against 10 mM Tris-HCl (pH 8.0) and concentrated by ultrafiltration.

The recovered protein was treated with enterokinase (1 unit/20 μg of protein) in 50 mM Tris (pH 8.0) 1 mM $CaCl_2$, and 0.1% Tween-20 overnight at 37°C to remove the 6 x His

tag by specific cleavage at an adjacent Asp_4-Lys pentapeptide stretch,[384,385] located at the N-terminus of the fusion protein. Following proteolytic removal of the affinity peptide tag, the digested sample was loaded onto a Heparin-Sepharose column pre-equilibrated with a 20 mM aqueous solution of phosphate buffer (pH 8.0) and eluted with a gradient of 0.1 – 0.5 M NaCl, after which the desired peak was pooled, dialyzed, and concentrated.

The purified protein was refolded by dialysis against a solution of 50 mM Tris-HCl (pH 7.8), 10 mM sodium sulfate, 0.2 mM phenylmethylsulfonyl fluoride, 2 mM dithiothreitol and 8 M urea. At the last step of refolding, EDTA was added to a final concentration of 5 mM. The refolded protein was then further dialyzed against 20 mM Tris buffer (pH 7.8) to eliminate residual EDTA and sodium sulfate and then concentrated with an Amicon Centricon® centrifugal filter device (Millipore, Billerica, MA). A 20% solution of glycerol was added to the concentrated protein, and the purified enzyme was stored indefinitely as a stock solution of 2.0 μg/μL of human RNase H1 at –20°C.

6.6.2.2. Purification of *E. coli* RNase HI

E. coli BL21 (DE3) pLysS cells transformed with plasmid pET-21c/*rnhA*, which contains the RNase H gene (*rnhA*) of *E. coli*, were induced to overproduce bacterial RNase HI with 1 mM isopropyl-β-thiogalactopyranoside (IPTG). The cell pellets were suspended in 50 mM Tris buffer (pH 7.9), 0.2 KCl, 5 mM $MgCl_2$, 0.1 mM EDTA, 1 mM 2-mercaptoethanol, and lysed by the addition of NP-40. The RNase H in the soluble fraction was purified as described above (**section 6.6.2.1.**), and the purified enzyme was stored indefinitely as a stock solution of 1.2 μg/μL in 20% glycerol storage buffer.

6.6.3. RNase H Induction Assays

6.6.3.1. General Considerations

RNase H degradation assays were generally carried out to monitor the relative efficiencies of each of the modified duplexes to support activity under a given set of experimental conditions. The temperature at which the assays were run was usually chosen to correspond to a value at least 10 degrees lower than the determined thermal melting temperature of the least stable hybrid in the series. This value was empirically

chosen by inspection of thermal melting curves of each of the duplexes, which suggested full duplexation at this temperature (see **section 6.5.1.**). Whenever possible, assays were also performed at 37°C to simulate intracellular conditions.

6.6.3.2. Preparation of Duplex Substrates

Nucleic acid duplex substrates for enzyme assays were generally prepared by mixing 150 pmol of antisense oligonucleotide with 50 pmol of 5'-^{32}P-labeled RNA (**section 6.6.1.**) in buffer consisting of 60 mM Tris-HCl (pH 7.8), 60 mM KCl, 2.5 mM $MgCl_2$, and 2 mM dithiothreitol (500 µL final volume). Samples were heated at 90°C for 10 minutes and slowly cooled to room temperature to allow duplex formation. They were then placed in a beta-blocking plexiglass sample holder and left to hybridize overnight at –20°C. Stock duplex solutions could then directly be used for analysis by aliquoting 9 µL of the thawed solutions to sterile microtube vials, followed by incubation at the assay temperature for at least 1 h prior to initiating enzymatic cleavage reactions.

6.6.3.3. Preliminary Optimizations: Enzyme Dilution Assays

Because the specific activities of *E. coli* and human RNase H enzymes were not known, the choice of an optimal working enzyme concentration was evaluated from a series of preliminary RNase H dilution assays, which were prepared as follows. A 1 µL aliquot of purified stock enzyme solution was transferred to a microtube and diluted with varying amounts of sterile dd H_2O to obtain final enzyme concentrations generally ranging from a 10- to 5000-fold dilution of stock enzyme. Chosen dilutions were generally considered on the basis of the assay temperature, with lower dilutions necessary at suboptimal temperatures (*i.e.* $T < 37°C$). The enzyme was handled over ice to avoid any loss of activity, and reactions were initiated in parallel at the specified temperature by the addition of purified human or *E. coli* RNases H (1 µL) in sterile dd H_2O. The resulting mixtures (10 µL final volume) were vortexed briefly and centrifuged to ensure reaction homogeneity and consistency between vials. Trial runs were typically performed on single or multiple representative test substrates of a given series using 1 or 2 time points, usually the first and/or last points of the experiment (*e.g.* 5 min, 1 h) in the presence of 3 – 5 different enzyme dilutions. At the end of the incubation time, samples were quenched

with an equal volume of denaturing loading buffer (98% deionized formamide, 10 mM EDTA, 1mg/mL BPB and 1 mg/mL XC) and vortexed to mix the contents. The reaction products were then heated at 90°C for 5 min to denature the strands, which were ultimately resolved on 16% polyacrylamide sequencing gels containing 7 M ultrapure urea (see **section 6.6.1.**). Cleavage patterns were analyzed by autoradiography following exposure to X-ray film, which typically required a few hours to a few days depending on the level of radionuclide incorporation. Visual inspection of the resulting images enabled selection of the optimal working enzyme concentration at which only partial cleavage of the duplexed RNA component was likely to occur under the given conditions.

6.6.3.4. Determination of Relative Enzyme Acceleration Profiles

These assays evaluated the enzyme-induced degradation rates of all test substrates in a given series, using a single optimized enzyme concentration as determined above. Duplex substrate solutions generally consisted of a 3-fold excess of antisense oligonucleotide relative to the target RNA strand unless otherwise specified. Assays for a given series were conducted in parallel, and initiated by the addition of 6 μL of freshly prepared human RNase H1 or *E. coli* RNase HI in sterile water (diluted as described in the preceding section) to each test substrate (60 μL final volume). Relative levels of target RNA hydrolysis were monitored throughout the incubation by removing aliquots (10 μL) of the reaction mixtures at defined times and quenching these with an equal volume of loading buffer, followed by heating at 90°C for 5 min. Data were customarily collected over 4 or 5 time points to characterize cleavage trends and quantify overall changes in levels of enzyme-mediated RNA scission. At the completion of the experiment, the samples were heat denatured and rapidly cooled on ice prior to electrophoresis, which was normally performed by 16% denaturing PAGE (1.5 h, 2000 V). It was necessary however, that the gels be pre-run for 30 – 60 min at 1500 V before loading the samples, particularly to minimize 'frowning' effects and prevent band distortion otherwise caused by non-homogenous gel surface temperatures.

Base ladders, generated by alkaline hydrolysis of the ssRNA target, were prepared by heating the RNA (90°C; 10 μL reaction volume) in a 1.0 M solution of $NaHCO_3$ for 4, 6 or 10 min, in order to select the ladder giving the best distribution of nucleic acid

fragments for precise identification of cut sites in the enzyme-treated samples. Importantly, this mode of internucleotide cleavage forms a mixture of 2'/3'-monophosphate and 5'-hydroxyl products[386] as opposed to enzymatically hydrolyzed 5'-^{32}P-labeled fragments originating from RNase H digestion of strands,[245,246] and as such, there exists a slight shift in electrophoretic mobility between the two types of hydrolysis products. However, ensuing differences in the migratory behaviour of alkaline *vs.* enzymatically digested RNA fragments are rather small and thus do not complicate subsequent analyses of cleavage locations the latter.

Degradation profiles of the various substrates were visualized and further quantified from the resulting autoradiograms by densitometric analysis of the band intensities within each lane. This data was extracted using UN-Scan-It digitizing software (Silk Scientific Inc., Orem, UT) to process the scanned images. The resulting data was imported to Microsoft Excel™ spreadsheet software for further manipulation and presentation. Alternatively, relative rates of degradation (k_{rel}) were calculated from the pseudo-first order reactions wherever possible, using either SigmaPlot 9.0 (Systat Software, Inc., Point Richmond, CA) or Prism® 4.0 (GraphPad Software, Inc., San Diego, CA) statistical software. Rates were then normalized according to those of the parent (uniformly modified or unmodified) heteroduplexes within a given series as specified.

6.7. CHAPTER 2: SYNTHESIS AND EVALUATION OF FLEXIBLE ANTISENSE 2'F-ANA AND DNA WITH ACYCLIC / ALIPHATIC LINKERS

These experiments evaluated the effect of an aliphatic or acyclic linker within an antisense DNA or 2'F-ANA backbone against a variety of targets, including a biologically relevant folded RNA species (**section 6.7.3.**). The synthesized antisense oligomers containing the acyclic moieties were prepared as described previously,[54,110] and were characterized by analytical PAGE, anion exchange HPLC and MALDI-TOF mass spectrometry. Sequences of the oligonucleotides and complementary targets along with mass spectral characterization data are provided in **Table 6.1**. Aliphatic linkers for AON incorporation included the 4-(4,4'-dimethoxytrityloxy)butyl-1-O-[(2-cyanoethyl)-(N,N-diisopropyl)]-phosphoramidite precursor **IV**, which was purchased from ChemGenes Corp. (Ashland, MA) and was used as received. Secouridine

Table 6.1: MALDI-TOF Spectral Analysis and Calculated Extinction Coefficients of Oligonucleotides Evaluated in Chapter **2**.

Entry	Sequence (5'→3')[a,b]	ε x 10^4 ($L \cdot mol^{-1} \cdot cm^{-1}$)	Calc. Mass (g/mol)	Observed Mass (g/mol)	Observed Molecular Ion
2.1	ttt ttt ttt ttt ttt ttt	14.640	5413.6	5413.7	$(M-H)^-$
2.2	ttt ttt ttt Btt ttt ttt	13.890	5260.5	5259.2	$(M-2H+Na)^-$
2.3	tta tat ttt ttc ttt ccc	15.490	5371.6	5372.1	$(M-H)^-$
2.4	tta tat ttt Btc ttt ccc	14.740	5218.5	5219.1	$(M-2H+Na)^-$
2.5	tta tat ttt ctc ttt ccc	15.400	5339.6	5339.8	$(M-H)^-$
2.6	tta tat ttt B ttc ttt ccc	15.550	5522.7	5522.4	$(M-H)^-$
2.7	TTT TTT TTT TTT TTT TTT	14.640	5737.4	5739.1	$(M-H)^-$
2.8	TTT TBT TTT TTT TTT TTT	13.890	5566.3	5568.1	$(M-2H+Li)^-$
2.9	TTT TTT TTT BTT TTT TTT	13.890	5566.3	5567.1	$(M-2H+Na)^-$
2.10	TTT TTT TTT TTT BTT TTT	13.389	5566.3	5567.2	$(M-H)^-$
2.11	TTT TTT TTT STT TTT TTT	14.640	5722.4	5720.7	$(M-2H+Na)^-$
2.12	TTT TTT TTS STT TTT TTT	14.640	5707.4	5707.0	$(M-3H+2Li)^-$
2.13	TTA TAT TTT TTC TTT CCC	15.490	5695.4	5694.5	$(M-3H+2Li)^-$
2.14	TTA TAT TTT BTC TTT CCC	14.740	5524.3	5525.9	$(M-H)^-$
2.15	TTA TAT TTT CTC TTT CCC	15.400	5663.4	5665.2	$(M-2H+Li)^-$
2.16	TTA TAT TTT tTC TTT CCC	15.490	5677.4	5677.1	$(M-H)^-$
2.17	TTA TAT TTT B TTC TTT CCC	15.550	5828.5	5828.0	$(M-2H+Li)^-$
2.18	ATT CCG TCA TCG CTC CTC	15.540	5685.2	5684.3	$(M-H)^-$
2.19	ATT CCG TCA BCG CTC CTC	14.790	5514.2	5514.2	$(M-H)^-$
2.20	att ccg tca tcg ctc ctc	15.540	5361.5	5361.3	$(M-H)^-$
2.21	att ccg tca Bcg ctc ctc	14.790	5190.4	5190.9	$(M-H)^-$
2.22	att ccg tca ccg ctc ctc	15.350	5346.5	5346.3	$(M-4H+3Li)^-$
	Target RNA Sequences[c]				
2.23	*AAA AAA AAA AAA AAA AAA*	21.940	5863.8	5864.1	$(M-H)^-$
2.24	*GGG AAA GAA AAA AUA UAA*	21.130	5881.7	5882.4	$(M-2H+Li)^-$
2.25	*GAGGAGCGAUGACGGAAU*	19.140	5897.7	5898.5	$(M-2H+Na)^-$
2.26	*CGCAGGCCCCUGAGGAGCGAUGACG-GAAUAUAAGCUGGUG*	39.760	12991.9	12992.4	$(M-H)^-$
2.27	*CGGGCCGCAGGCCCCUGAGGAGCGA-UGACGGAAUAUAAGCUGGUGGUGGU*	49.100	16285.9	16285.9	$(M-H)^-$

[a]Oligonucleotides were synthesized on a 1 μmol scale; see **Table 3.1** for crude and isolated yields of representative sequences. Upper case letters, 2'F-ANA nucleotides; lower case letters, deoxynucleotides; C, arabinofluoro- or c, deoxycytidine mismatch residue; B, butanediol linker; S, 2'-secouridine insert. [b]2'F-ANA and seconucleotide-containing chimeras were assumed to have the same molar extinction coefficient as DNA and were calculated using the nearest-neighbour approximation method.[257] [c]RNA residues are italicized; underlined regions within the 18, 40, and 50mer *RAS* RNA sequences (entries **2.25** – **2.27**) denote the AON complementary binding site.

2'-phosphoramidites of the secouridine diol precursor **2.3** were prepared by variations of published protocols.[203] Briefly, the acyclic or 'seco'-nucleoside residues consist of a 1-[1,5-dihydroxy-4(*S*)-hydroxymethyl-3-oxapent-2(*R*)-yl]-uracil unit which has been appropriately protected and functionalized for oligonucleotide incorporation as described below.

6.7.1. Solution Syntheses of Acyclic 'Seco'-Nucleoside Monomers

(A) 5'-O-MMT-β-D-uridine (**2.2**). Uridine ribonucleosides were protected according to the method of Wu *et al.*[387] For these reactions, the less chemically labile monomethoxytrityl group was used as opposed to hydroxyl protection with DMT, in order to prevent premature detritylation during subsequent manipulations (*vide infra*). Accordingly, uridine (**2.1**; 6.11 g, 25 mmol) was dried by coevaporation with anhydrous pyridine (3 x 30 mL) and resuspended in 180 mL (7.2 mL/mmol nucleoside) of dry pyridine. The mixture was cooled to 0°C prior to the addition of MMT-Cl (9.26 g, 30 mmol, 1.2 eq), which was added in 4 equal portions over a 3 h period. After the last addition, the reaction was gradually warmed to ambient temperature and allowed to stir overnight under an inert atmosphere. Reaction progression was monitored by TLC, which enabled rapid visual assessment of the extent of conversion to monotritylated product. Upon substantial conversion to product, methanol (10 mL) was added to the mixture to quench any remaining reactants and stirring was continued for an additional 20 min period at r.t. The solution was concentrated to a gum, redissolved in CH_2Cl_2 (*ca.* 300 mL), and washed with an aqueous solution of 5% $NaHCO_3$ (3 x 100 mL). The aqueous layer was back-extracted (2 x 100 mL CH_2Cl_2), and the combined organic layers were dried (anhydrous Na_2SO_4), filtered and evaporated *in vacuo* to a crude brown oil. The desired product was purified using flash column chromatography in a gradient of 0 – 5% MeOH in DCM and flow rate of *ca.* 2.0 cm/min (column dimensions 15 cm x 40 mm i.d.). Generally, the desired product eluted at 2 – 3 % of the gradient and was collected in 4 – 5 fractions. The fractions were pooled, and the solvent evaporated under reduced pressure to yield the product as a pure white foam in 80% isolated yield (10.33 g; 20 mmol). R_f (CH_2Cl_2:MeOH, 9:1) 0.55; FAB-MS (nitrobenzyl alcohol matrix): 517.3; Calc: 516.55.

*(B) 5'-O-MMT-2',3'-*seco*-uridine* (**2.3**). To a 0.1 M solution of 5'-monomethoxytrityluridine (**2.2**; 5'-MMT-Ur, 5.16 g, 10 mmol) in dioxane was added a saturated solution of $NaIO_4$ in H_2O (2.26 g, 10.6 mmol, 1.06 eq) and the reaction allowed to proceed at r.t. for 2 – 3 h until complete conversion to the dialdehyde was observed by TLC visualization (R_f 0.57 in CH_2Cl_2:MeOH, 9:1). The reaction was diluted with dioxane (100 mL), filtered to remove $NaIO_3$ salts and followed by *in situ* reduction of the dialdehyde via treatment with $NaBH_4$ (0.378 g, 10 mmol, 1.0 eq) for 10-20 min. at r.t. The reaction mixture was quenched with acetone, neutralized with 20% acetic acid and concentrated to an oil under reduced pressure. The residue was then diluted with CH_2Cl_2 (200 mL) and washed with H_2O. The aqueous layer was back-extracted and the combined organic layers were dried using anhydrous Na_2SO_4, filtered and evaporated to give the product as a pure white foam in 98% isolated yield (5.08 g; 9.8 mmol). R_f (CH_2Cl_2:MeOH, 9:1) 0.52; (CH_2Cl_2:Acetone, 3:1) 0.13; FAB-MS (NBA): 519.0; Calc: 518.57.

(C) 5'-O-MMT-2'-O-t-butyldimethylsilyl-2',3'-secouridine (**2.4**) *and 5'-O-MMT-3'-O-t-butyldimethylsilyl-2',3'-secouridine* (**2.5**). Monoprotection of either of the free hydroxyl functions of **2.3** was achieved nonselectively by adding *t*-butyldimethylsilyl chloride (0.81 g, 5.4 mmol, 1.1 eq) to a stirred 0.1 M solution of **2.3** (2.55 g, 4.9 mmol) in dry THF at 0°C containing a suspension of $AgNO_3$ (0.92 g, 5.39 mmol, 1.1 eq). The reaction temperature was returned to r.t. after 20 min and maintained as such for 24 h. The workup was initiated by filtering the mixture directly into an aqueous solution of 5% $NaHCO_3$ (50 mL), followed by extraction of the aqueous layer twice with CH_2Cl_2. The combined organic layers were dried (anhydrous Na_2SO_4), filtered and evaporated under reduced pressure to give the crude product as a yellow oil. The residue was purified by flash silica gel column chromatography using a gradient of 0-25% acetone in CH_2Cl_2 to recover both monosilyl isomers as pure white foams. Isolated yields for **2.4** and **2.5** were 22% and 14%, respectively. R_f (CH_2Cl_2:Et_2O, 3:1) **2.4**, 0.18; **2.5**, 0.05. FAB-MS (NBA): 633.4; Calc: 632.83.

(D) 5' – O – MMT – 3' – O – t – butyldimethylsilyl – 2', 3' – secouridine – 2' – O – [N,N-diisopropylamino-(2-cyanoethyl)]phosphoramidite (**2.6**). To a nitrogen-purged solution of 4-dimethylaminopyridine (DMAP; 12 mg, 0.10 mmol, 0.1 eq), N,N-diisopropylethylamine (DIPEA; 0.68 mL, 3.9 mmol, 4 eq) and **3c** (620 mg, 0.98 mmol) in THF (0.2 M) at 0°C was added N,N-diisopropylamino-β-cyanoethylphosphonamidic chloride (0.24 mL, 1.1 mmol, 1.1 eq) dropwise over 5 min. The immediate appearance of a white precipitate due to the rapid formation of diisopropylethylammonium hydrochloride signified sufficiently anhydrous conditions, and the reaction was allowed to warm to r.t., whereupon it was stirred for 2.5 h prior to the reaction workup. Briefly, the reaction mixture was diluted with EtOAc (50 mL, prewashed with 5% $NaHCO_3$) and washed with saturated brine (2 × 20 mL). The recovered organic layer was dried (anhydrous Na_2SO_4), filtered and the solvent removed via reduced pressure, yielding a crude yellow oil. Coevaporation of the crude product with Et_2O afforded a pale yellow foam. Purification of the product by flash silica gel column chromatography using a CH_2Cl_2:Hexanes:TEA gradient system (25:74:1 adjusted to 50:49:1) afforded a white foam in 99% isolated yield. R_f (EtOAc:Tol, 4:1) 0.77, 0.65. FAB-MS (NBA): 833.3; Calc: 833.05.

6.7.2. Relative Turnover of DNA, 2'F-ANA and 2'F-ANA-B10 AONs

These assays were conducted to evaluate the influence, if any, of duplex thermal stability on rates of cleavage by human RNase H1. Turnover experiments were performed at room temperature over a 15 to 30 min time interval using different concentrations (1 – 16 pmol) of nonlabeled rA_{18}, 0.05 pmol of 5'-^{32}P labeled rA_{18}, and 1 pmol of dT_{18}, 2'F-ANA or 2'F-ANA-B10 oligothymidylates as antisense oligonucleotide, respectively, in buffer consisting of 50 mM Tris-HCl, pH 7.9, 60 mM KCl, and 10 mM $MgCl_2$. After the addition of human RNase H1, samples were incubated for the specified time period followed by quenching of the reaction contents with an equal volume of gel loading dye (9:1 (v/v) formamide : 10 x TBE buffer with 2% (w/v) of both XC and BPB tracking dyes). RNase H-generated degradation products were resolved by electrophoresis using 14% acrylamide sequencing gels containing 7 M urea as denaturant, visualized by autoradiography, and quantified by densitometry using Un-Scan-It software.

6.7.3. Synthesis and Structural Modeling of *HRAS* RNA Secondary Structure

The *HRAS* RNA target sequence investigated in these studies spans a region in the full length mRNA transcript that encompasses the translation initiation site of human *RAS* and corresponds to residues –19 to +21 within this gene (with +1 denoting the position of the first nucleotide in the AUG codon triplet with respect to the 5'-terminus of the mRNA). A Basic Local Alignment (BLASTn) search of this sequence identified its location within a coding region of exon 1 of *c-Harvey ras* mRNA (+1054 to +1075; accession no. M15077), and corresponding to an endogenous gene of many species. With this information in hand, both 40 and 50 nt *RAS* target mimics of the full length transcript (**2.26** & **2.27**) were obtained from a commercial source (UCDNA Services, Calgary, AB) and desalted on arrival, while the synthesis and purification of the shorter 18 nt target species (**2.25**) was performed in house.

Prediction of likely *HRAS* RNA secondary structures of these three targets was generated using the mfold computer-based algorithm (version 3.1.2) running under a Unix environment. The software estimates ΔG°_{37} values for self-complementary duplex formation using nearest neighbour thermodynamic rules,[224] and incorporates many adjustable parameters to improve the predictions, which were set as follows. The entire sequence was set to be folded at a simulated temperature of 37°C with the P value, or percent suboptimality, set to 5 or 25 in order to search for all structures within 5 or 25% of the computed overall minimum folding free energy. The concentration of Na^{+} and Mg^{2+} counterions were set to 145 mM and 1 mM, respectively, to mimic the experimental solution ionic conditions. All other input parameters were default values as generated by the program and based on nucleotide length of the input sequence.

RNA 5'-^{32}P-end labeling by T4 PNK for subsequent analysis of RNase H degradation profiles in the presence of complementary AON was performed as described (**section 6.6.1.**). Assays were ultimately conducted in the presence of a general nuclease inhibitor (RNaseIn®; Promega, WI) to protect the targets from possible contaminating nucleases.

6.8. CHAPTER 3: LINKER ANATOMY AND HELIX LOCATION IN RNASE H–COMPETENT DUPLEXES

In order to assess the structure- and strand-specific role of the aliphatic linker on enzyme competency, this chapter examined the effect of oligodeoxy- and ribonucleotide complements comprising centrally placed linkers in one or both of the pairing strands. The sequences of some of these oligonucleotides and their complementary RNA targets, along with mass spectral characterization data are provided in **Table 6.2**.

Table 6.2: MALDI-TOF Spectral Analysis and Calculated Extinction Coefficients of Representative Oligonucleotides Evaluated in Chapter **3**.

Entry	Sequence (5'→3')[a,b]	ε x 10^4 ($L \cdot mol^{-1} \cdot cm^{-1}$)	Calc. Mass (g/mol)	Observed Mass (g/mol)	Observed Molecular Ion
3.1	tta tat ttt Ptc ttt ccc	14.740	5203.4	5200.1	$(M-H)^-$
3.2	tta tat ttt P ttc ttt ccc	15.550	5507.6	5507.0	$(M-H)^-$
3.3	tta tat ttt Etc ttt ccc	14.740	5219.4	5218.9	$(M-H)^-$
3.4	tta tat ttt E ttc ttt ccc	15.550	5523.6	5522.1	$(M-2H+Na)^-$
3.6	TTA TAT TTT	8.530	2855.7	2854.5	$(M-2H+Na)^-$
3.7	TC TTT CCC	6.210	2455.5	2454.9	$(M-2H+Li)^-$
3.8	TTC TTT CCC	7.020	2777.7	2777.6	$(M-H)^-$
	Target RNA Sequence[c]				
3.5	*GGG AAA GAB AAA AUA UAA*	20.270	5703.6	5703.3	$(M-2H+Na)^-$

[a]Oligonucleotides were synthesized on a 1 μmol scale; crude and isolated yields of representative sequences are reported in **Table 3.1**. Upper case letters, 2'F-ANA nucleotides; lower case letters, deoxynucleotides; P, propyl linker; E, ethyl backbone linker. [b]2'F-ANA oligonucleotides were assumed to have the same molar extinction coefficient as DNA and were calculated using the nearest-neighbour approximation method.[257] [c]RNA residues are italicized; B, butyl interresidue linker.

All oligonucleotides were synthesized on an ABI 381A DNA synthesizer (Applied Biosystems Inc.; Foster City, CA), with the exception of 2'F-ANA oligonucleotides (**3.6 – 3.8**) which were separately synthesized on an Expedite 8909 DNA synthesizer by Dr. Katya Viazovkina and supplied in crude, protected form for subsequent deprotection and purifications. The acyclic phosphoramidite synthons (*i.e.* used for the construction of

respective ethyl, propyl or butyl internucleotide units) were successfully incorporated into the synthesis cycle using standard oligodeoxyribonucleotide coupling times (120 sec). All sequences were deprotected under standard conditions with no additional steps required for levulinyl removal from the protected glycerol unit (*i.e.* used to provide an ethyl interresidue spacer). Conversely, removal of the sugar 2'-O-*t*-BDMS protection on butyl-modified oligoribonucleotides was effected by a final treatment with TREAT-HF (150 μL) at room temperature for 48 h, followed by quenching with water and drying under vacuum. These sequences were desalted prior to preparative PAGE purification.

6.8.1. Human RNase H1 Incubation Assays

All enzyme assays were conducted in parallel, using identical conditions in order to obtain comparative information on the behaviour of the various linker-modified AON hybrids with that of their fully matched heteroduplex counterparts. Hybrid duplexes were generally prepared by mixing complementary strands (1:10 of 5'-^{32}P-labeled-RNA to AON) in RNase H assay buffer [60 μL final volume, containing 60 mM Tris-HCl (pH 7.8), 60 mM KCl, 2.5 mM $MgCl_2$, and 2 mM DTT], followed by heating of the samples at 90°C for 5 minutes and slow cooling overnight (4 or –20°C in a plexi-glass beta block). Choice of the enzyme assay temperature (22°C) was made on the basis of hybrid duplex stabilities and substrate solutions were allowed to equilibrate for 1 h at this temperature prior to initiating the degradation reaction. Reactions were started by the addition of purified human RNase H1 with general incubation times spanning 5, 10, 20 and 30 min at 22°C. After the alloted incubation times, samples (10 μL) were aliquoted out of each reaction mixture, and quenched upon mixing with an equal volume of denaturing loading buffer (98% deionized formamide, 10 mM EDTA, 1mg/mL BPB and 1 mg/mL XC). Reaction products were denatured by heating at 100°C for 5 min, followed by electrophoretic resolution on 16% polyacrylamide sequencing gels containing 7 M urea.

6.9. CHAPTER 4: STRUCTURAL AND MECHANISTIC STUDIES ON RNASE H CLEAVAGE OF POOR AND NON-CLEAVABLE NUCLEIC ACID HYBRIDS

Oligonucleotides used in the ensuing studies were synthesized on an ABI 381A DNA synthesizer using standard coupling times and phosphoramidite chemistry, with the

exception of 2'-OMe RNA homopolymeric and U5 RNA mixed sequences which were custom synthesized by UCDNA Services (Calgary, AB). Commercially obtained oligonucleotides were desalted by size-exclusion chromatography prior to subsequent biophysical measurements and enzymatic assays. The sequence compositions of all oligonucleotides and complementary RNA targets are provided along with mass spectral characterization data in **Table 6.3**.

Table 6.3: MALDI-TOF Spectral Analysis of Oligonucleotides and Calculated Extinction Coefficients for Sequences Evaluated in Chapter **4**.

Entry	Sequence (5'→3')[a,b]	ε x 10^4 ($L \cdot mol^{-1} \cdot cm^{-1}$)	Calc. Mass (g/mol)	Observed Mass (g/mol)	Observed Molecular Ion
4.1	aaa aaa aaa aaa aaa aaa	21.940	5575.8	5576.1	$(M-2H+Li)^-$
4.3	m-AAA AAA AAA AAA AAA AAA	21.940	6115.8	6115.4	$(M-H)^-$
4.4	*UUU UUU UUU UUU UUU UUU*	17.480	5449.1	5447.1	$(M-4H+3Li)^-$
4.5	m-UUU UUU UUU UUU UUU UUU	17.480	5701.1	5700.8	$(M-H)^-$
4.6	aaa aaa aaa Baa aaa aaa	21.080	5413.7	5413.7	$(M-2H+Li)^-$
4.7	AAA AAA AAA BAA AAA AAA	21.080	5685.7	5685.1	$(M-H)^-$
4.8	m-AAA AAA AAA BAA AAA AAA	21.080	5923.7	5923.8	$(M-H)^-$
4.9	*UUU UUU UUB UUU UUU UUU*	16.530	5294.0	5292.9	$(M-2H+Li)^-$
4.10	m-UUU UUU UUB UUU UUU UUU	16.530	5532.0	5531.5	$(M-H)^-$
	U5-RNA Sequences				
4.11	*GUU ACC AGA CUG ACA CAA CAG ACG*	24.540	7681.8	n.d.[c]	n.a.[d]
4.12	*GUU ACC ABA GUC ACA BAA CAG ACG*	23.350	7333.5	n.d.	n.a.
4.13	*GUU ACC AGBA CUG ACA CBAA CAG ACG*	24.870	7984.0	n.d.	n.a.
4.14	*CGU CUG UUG UGU GAC UCU GGU AAC*	22.980	7623.6	n.d.	n.a.

[a]Oligonucleotides were synthesized on a 1 μmol scale. Upper case letters, 2'-OMe ribonucleotides (also designated by the prefix m-); lower case letters, deoxynucleotides; italicized upper case letters, ribonucleotides; B, butyl linker. [b]Molar extinction coefficients of 2'-OMe RNA sequences were calculated using the nearest-neighbour approximation method[257] while assuming similar values as for native oligoribonucleotides. [c]n.d. – not determined; [d]n.a. – not applicable.

6.9.1. RNase H Cleavage of U5-dsRNA Mixed Sequence Duplexes

These assays examined the possibility of achieving RNase H-mediated RNA strand hydrolysis within a therapeutically relevant dsRNA duplex upon its modification with dual aliphatic linkers. The U5-RNA target sequence for these studies was initially located by a nucleotide-nucleotide alignment (BLASTn) search[388] of sequence data in the GenBank database (publicly available from the National Center for Biotechnology Information, NIH; Bethesda, MA) and corresponds to a contiguous stretch of 24 nucleotides located at the 5'-UTR of the *ca.* 10 kB human immunodeficiency virus type 1 genome [linear ss + (plus) strand]. Duplex substrates were prepared for subsequent RNase H incubation reactions by 5'-end ^{32}P-labeling of either one of the two pairing strands of the duplex in order to assay both members for enzymatic susceptibility. Respective end-labeled and nonlabeled RNA complements were mixed in a 1:3 ratio in RNase H assay buffer [60 μL final volume of 60 mM Tris-HCl (pH 7.8), 60 mM KCl, 2.5 mM $MgCl_2$, and 2 mM DTT; 100 nM total duplex concentration]. The samples were heated (100°C, 10 min) and slowly cooled to r.t. (4 h), then allowed to equilibrate overnight (–20°C) in a beta block plexi-glass holder. The preformed duplexes were slowly warmed to 37°C and maintained as such for 1 h prior to initiating the degradation reactions. Subsequent enzyme assays were evaluated in the presence of high concentrations of purified human or *E. coli* RNases H1 (**section 6.6.2.**) for 0, 12 and 24 h. Following the alloted incubation times, aliquots of each test substrate (10 μL) were removed and quenched by mixing with an equal volume of gel loading buffer, followed by sample heating (100°C, 15 min) prior to electrophoresis. Respective hydrolysis profiles were analyzed on 16% denaturing polyacrylamide sequencing gels.

6.9.2. Tripeptide-Induced Inhibition of Human RNase H1-Mediated Cleavage in Linker-Modified Hybrids

These experiments were conducted to determine whether an inhibitory effect on RNase H activity upon linker-modified DNA:RNA heteroduplexes could be realized in the presence of increasing amounts of tripeptide inhibitor. Upon 5'-end ^{32}P-labeling and purification of RNA targets, complementary single strands (1:2 RNA:AON) were preannealed in various assay buffers (2.5 mM $MgCl_2$, 2 mM DTT and 1 – 50 mM sodium

cacodylate; pH 7.0) for 12 – 16 h at 4°C prior to adding KWK or KGK oligopeptides (Bachem Bioscience Inc., PA) to the reaction mixture. Heteroduplexes comprising a 5'-radiolabeled DNA strand were prepared in a similar fashion as those with the label on the RNA counterpart. Enzyme assays were ultimately conducted using either RNase H activity buffer [60 mM Tris-HCl (pH 7.8), 60 mM KCl, 2.5 mM $MgCl_2$, and 2 mM DTT; 100 nM total duplex concentration] or atypical solution conditions that consisted of 2.5 mM $MgCl_2$, 2 mM DTT and 10 mM sodium cacodylate, adjusted to pH 7.0.

Following further equilibration of the preformed nucleic acid substrates with increasing levels of oligopeptide (*i.e.* 0.01 – 10 μM of KWK or KGK tripeptide mixed with 0.1 μM of each test duplex for 8 h at 4°C), the contents were incubated with human RNase H1 for a single 30 min time interval. At the end of the incubation period, the degradation reactions were quenched by the addition of denaturing buffer, followed by heating of the products to 100°C for 5 min. Cleavage fragments were electrophoretically resolved (16% sequencing PAGE with 7 M urea) and the ^{32}P-labeled fragments were visualized by autoradiography. Scanned images of the autoradiograms were quantified by densitometry and the resulting data was imported into Microsoft Excel™ 2000 for further processing and presentation.

APPENDIX A

HUMAN RIBONUCLEASE H1 PRIMARY STRUCTURE

Human Ribonuclease H1 – 286 amino acids

```
  1 - ATGAGCTGGCTTCTGTTCCTGGCCCACAGAGTCGCCTTGGCCGCCTTGCCCTGCCGCCGC - 60
  1 - M  S  W  L  L  F  L  A  H  R  V  A  L  A  A  L  P  C  R  R

 61 - GGCTCTCGCGGGTTCGGGATGTTCTATGCCGTGAGGAGGGGCCGCAAGACCGGGGTCTTT - 120
 21 - G  S  R  G  F  G  M  F  Y  A  V  R  R  G  R  K  T  G  V  F

121 - CTGACCTGGAATGAGTGCAGAGCACAGGTGGACCGGTTTCCTGCTGCCAGATTTAAGAAG - 180
 41 - L  T  W[43] N  E  C  R  A  Q  V  D  R  F  P  A  A  R  F  K[59] K[60]

181 - TTTGCCACAGAGGATGAGGCCTGGGCCTTTGTCAGGAAATCTGCAAGCCCGGAAGTTTCA - 240
 61 - F  A  T  E  D  E  A  W  A  F  V  R  K  S  A  S  P  E  V  S

241 - GAAGGGCATGAAAATCAACATGGACAAGAATCGGAGGCGAAAGCCAGCAAGCGACTCCGT - 300
 81 - E  G  H  E  N  Q  H  G  Q  E  S  E  A  K  A  S  K  R  L  R

301 - GAGCCACTGGATGGAGATGGACATGAAAGCGCAGAGCCGTATGCAAAGCACATGAAGCCG - 360
101 - E  P  L  D  G  D  G  H  E  S  A  E  P  Y  A  K  H  M  K  P

361 - AGCGTGGAGCCGGCGCCTCCAGTTAGCAGAGACACGTTTTCCTACATGGGAGACTTCGTC - 420
121 - S  V  E  P  A  P  P  V  S  R  D  T  F  S  Y  M  G  D  F  V

421 - GTCGTCTACACTGATGGCTGCTGCTCCAGTAATGGGCGTAGAAGGCCGCGAGCAGGAATC - 480
141 - V  V  Y  T  D[145] G  C  C  S  S  N  G  R  R  R  P  R  A  G  I
                *
481 - GGCGTTTACTGGGGGCCAGGCCATCCTTTAAATGTAGGCATTAGACTTCCTGGGCGGCAG - 540
161 - G  V  Y  W  G  P  G  H  P  L  N  V  G  I  R  L  P  G  R  Q

541 - ACAAACCAAAGAGCGGAAATTCATGCAGCCTGCAAAGCCATTGAACAAGCAAAGACTCAA - 600
181 - T  N  Q  R  A  E[186] I  H  A  A  C  K  A  I  E  Q  A  K  T  Q
                   *
601 - AACATCAATAAACTGGTTCTGTATACAGACAGTATGTTTACGATAAATGGTATAACTAAC - 660
201 - N  I  N  K  L  V  L  Y  T  D[210] S  M  F  T  I  N  G  I  T  N
                            *
661 - TGGGTTCAAGGTTGGAAGAAAAATGGGTGGAAGACAAGTGCAGGGAAAGAGGTGATCAAC - 720
221 - W  V  Q  G  W  K  K  N  G  W  K  T  S  A  G  K  E  V  I  N

721 - AAAGAGGACTTTGTGGCACTGGAGAGGCTTACCCAGGGGATGGACATTCAGTGGATGCAT - 780
241 - K  E  D  F  V  A  L  E  R  L  T  Q  G  M  D  I  Q  W  M  H

781 - GTTCCTGGTCATTCGGGATTTATAGGCAATGAAGAAGCTGACAGATTAGCCAGAGAAGGA - 840
261 - V  P  G  H  S  G  F  I  G  N  E  E  A  D  R  L  A  R  E  G

841 - GCTAAACAATCGGAAGACTGA - 861
281 - A  K  Q  S  E  D  *  - 286
```

Supplementary Material A: Amino acid sequence of human RNase H1, shown underneath the corresponding cDNA sequence for the cloned protein. Residues 1 – 27 comprise a mitochondrial localization signal; 28 – 73, a general nucleic acid binding region (dsRBD-like domain); 74 – 135, spacer region; 136 - 286, core RNase H domain. KKW residues (boldface) implicated in nucleic acid binding, along with position from the N-terminus are noted; critical catalytic residues (bold, underlined) are indicated by an asterisk and amino acids corresponding to the highly conserved 'DSXY' motif are boxed. Residues Y and T immediately upstream of this region (bold) are less strictly conserved.

REFERENCES

1) Watson, J. D.; Crick, F. H. C. *Nature* **1953**, *171*, 737-738.

2) Watson, J. D.; Crick, F. H. C. *Nature* **1953**, *171*, 964-967.

3) Chargaff, E. *Experientia* **1950**, *6*, 201-209.

4) Klug, A. *Nature* **1968**, *219*, 808-10, 843-844.

5) Klug, A. *Nature* **1974**, *248*, 787-788.

6) Maddox, B. *Rosalind Franklin: The Dark Lady of DNA*; HarperCollins Publishers Inc.: New York, NY **2002**.

7) Henry, C. M. *Chemical & Engineering News* **2003**, *81*, 49-60.

8) Pennisi, E. *Science* **2003**, *300*, 282-285.

9) Saenger, W. *Principles of Nucleic Acid Structure*; Springer-Verlag: New York, NY **1984**.

10) Blackburn, G. M.; Gait, M. J.; *Nucleic Acids in Chemistry and Biology, Second Edition*; Oxford University Press: New York, NY **1996**.

11) Myers, K. J.; Dean, N. M. *Trends Pharm. Sci.* **2000**, *21*, 19-23.

12) Crooke, S. T. *Biochim. Biophys. Acta* **1999**, *1489*, 31-44.

13) Uhlmann, E.; Peyman, A. *Chem. Rev.* **1990**, *90*, 543-584.

14) Nirenberg, M. W.; Matthaei, J. H.; Jones, O. W.; Martin, R. G.; Barondes, S. H. *Fed. Proc. Symp.* **1963**, *22*, 55-61.

15) Belikova, A. M.; Zarytova, V. F.; Grineva, N. I. *Tetrahedron Lett.* **1967**, *37*, 3557-3562.

16) Zamecnik, P. C.; Stephenson, M. L. *Proc. Natl. Acad. Sci. U.S.A.* **1978**, *75*, 280-284.

17) Winkler, K. E. *Nat. Rev. Drug Discov.* **2004**, *3*, 823-824.

18) Agrawal, S.; Zhao, Q. *Curr. Opin. Chem. Biol.* **1998**, *2*, 519-528.

19) Eckstein, F. *Antisense Nucleic Acid Drug Dev.* **2000**, *10*, 117-121.

20) Henry, S. P.; Monteith, D.; Levin, A. A. *Anti-Cancer Drug Des.* **1997**, *12*, 395-408.

21) Weidner, D. A.; Valdez, B. C.; Henning, D.; Greenberg, S.; Busch, H. *FEBS Lett.* **1995**, *366*, 146-150.

22) Srinivasan, S. K.; Tewary, H. K.; Iversen, P. L. *Antisense Res. Dev.* **1995**, *5*, 131-139.

23) Akhtar, S.; Agrawal, S. *Trends Pharm. Sci.* **1997**, *18*, 12-18.

24) Kool, E. T.; Morales, J. C.; Guckian, K. M. *Angew. Chem. Int. Ed.Engl.* **2000**, *39*, 990-1009.

25) Iyer, R. P.; Roland, A.; Zhou, W.; Ghosh, K. *Curr. Opin. Mol. Ther.* **1999**, *1*, 344-358.

26) Freier, S. M.; Altmann, K.-H. *Nucleic Acids Res.* **1997**, *25*, 4429-4443.

27) De Mesmaeker, A.; Altmann, K.-H.; Waldner, A.; Wendeborn, S. *Curr. Opin. Struct. Biol.* **1995**, *5*, 343-355.

28) Uhlmann, E.; Peyman, A.; Breipohl, G.; Will, D. W. *Angew. Chem. Int. Ed. Engl.* **1998**, *37*, 2796-2823.

29) Juliano, R. L.; Alahari, S.; Yoo, H.; Kole, R.; Cho, M. *Pharm. Res.* **1999**, *16*, 494-502.

30) Walder, R. Y.; Walder, J. A. *Proc. Natl. Acad. Sci. U.S.A.* **1988**, *85*, 5011-5015.

31) Cazenave, C.; Hélène, C. In *Antisense oligonucleotides*; Mol, J. N., van der Krol, A. R., Eds.; Marcel Dekker, Inc.: New York, NY **1991**, pp. 47-93.

32) Lebedeva, I.; Stein, C. A. *Annu. Rev. Pharmacol. Toxicol.* **2001**, *41*, 403-419.

33) Itaya, M.; Kondo, K. *Nucleic Acids Res.* **1991**, *19*, 4443-4449.

34) Rumbaugh, J. A.; Murante, R. S.; Shi, S.; Bambara, R. A. *J. Biol. Chem.* **1997**, *272*, 22591-22599.

35) Peliska, J. A.; Benkovic, S. J. *Science* **1992**, *258*, 1112-1118.

36) Crouch, R. J.; Toulmé, J. J. (Eds.) *Ribonucleases H*; INSERM: Paris, **1998**.

37) Nishizaki, T.; Iwai, S.; Ohtsuka, E.; Nakamura, H. *Biochemistry* **1997**, *36*, 2577-2585.

38) Uchiyama, Y.; Miura, Y.; Inoue, H.; Ohtsuka, E.; Ueno, Y.; Ikehara, M.; Iwai, S. *J. Mol. Biol.* **1994**, *243*, 782-791.

39) Crooke, S. T.; Lemonidis, K. M.; Neilson, L.; Griffey, R.; Lesnik, E. A.; Monia, B. P. *Biochem. J.* **1995**, *312*, 599-608.

40) Katayanagi, K.; Miyagawa, M.; Matsushima, M.; Ishikawa, M.; Kanaya, S.; Ikehara, M.; Matsuzaki, T.; Morikawa, K. *Nature* **1990**, *347*, 306-309.

41) Baker, B. F.; Monia, B. P. *Biochim. Biophys. Acta* **1999**, *1489*, 3-18.

42) Oda, Y.; Iwai, S.; Ohtsuka, E.; Ishikawa, M.; Ikehara, M.; Nakamura, H. *Nucleic Acids Res.* **1993**, *21*, 4690-4695.

43) Egli, M.; Usman, N.; Zhang, S.; Rich, A. *Proc. Natl. Acad. Sci. U.S.A.* **1992**, *89*, 534-538.

44) Wahl, M. C.; Sundaralingam, M. *Curr. Opin. Struct. Biol.* **1995**, *5*, 282-295.

45) Zamaratski, E.; Pradeepkumar, P. I.; Chattopadhyaya, J. *J. Biochem. Biophys. Methods* **2001**, *48*, 189-208.

46) Lima, W. F.; Crooke, S. T. *Biochemistry* **1997**, *36*, 390-398.

47) Salazar, M.; Champoux, J. J.; Reid, B. R. *Biochemistry* **1993**, *32*, 739-744.

48) Fedoroff, O. Y.; Salazar, M.; Reid, B. R. *J. Mol. Biol.* **1993**, *233*, 509-23.

49) Cummins, L.; Graff, D.; Beaton, G.; Marshall, W. S.; Caruthers, M. H. *Biochemistry* **1996**, *35*, 8734-8741.

50) Marshall, W. S.; Caruthers, M. H. *Science* **1993**, *259*, 1564-1570.

51) Summers, J. S.; Shaw, B. R. *Curr. Med. Chem.* **2001**, *8*, 1147-1155.

52) Rait, V. K.; Shaw, B. R. *Antisense Nucleic Acid Drug Dev.* **1999**, *9*, 53-60.

53) Noronha, A. M.; Wilds, C. J.; Lok, C. N.; Viazovkina, K.; Arion, D.; Parniak, M. A.; Damha, M. J. *Biochemistry* **2000**, *39*, 7050-7062.

54) Damha, M. J.; Wilds, C. J.; Noronha, A.; Brukner, I.; Borkow, G.; Arion, D.; Parniak, M. A. *J. Am. Chem. Soc.* **1998**, *120*, 12976-12977.

55) Wang, J.; Verbeure, B.; Luyten, I.; Lescrinier, E.; Froeyen, M.; Hendrix, C.; Rosemeyer, H.; Seela, F.; Van Aerschot, A.; Herdewijn, P. *J. Am. Chem. Soc.* **2000**, *122*, 8595-8602.

56) Sørensen, M. D.; Kvaernø, L.; Bryld, T.; Håkansson, A. E.; Verbeure, B.; Gaubert, G.; Herdewijn, P.; Wengel, J. *J. Am. Chem. Soc.* **2002**, *124*, 2164-2176.

57) Zamore, P. D. *Mol. Cell* **2001**, *8*, 1158-1160.

58) Elbashir, S. M.; Lendeckel, W.; Tuschl, T. *Genes Dev.* **2001**, *15*, 188-200.

59) Zamore, P. D.; Tuschl, T.; Sharp, P. A.; Bartel, D. P. *Cell* **2000**, *101*, 25-33.

60) Parrish, S.; Fleenor, J.; Xu, S.; Mello, C.; Fire, A. *Mol. Cell* **2000**, *6*, 1077-1087.

61) Ma, M.; Benimetskaya, L.; Lebedeva, I.; Dignam, J.; Takle, G.; Stein, C. A. *Nat. Biotechnol.* **2000**, *18*, 58-61.

62) Hartmann, R. K.; Krupp, G.; Hardt, W.-D. *Biotechnol. Annu. Rev.* **1995**, *1*, 215-265.

63) Leaman, D. W.; Cramer, H. *Methods* **1999**, *18*, 252-265.

64) Adah, S. A.; Bayly, S. F.; Cramer, H.; Silverman, R. H.; Torrence, P. F. *Curr. Med. Chem.* **2001**, *8*, 1189-1212.

65) Kushner, D. M.; Paranjape, J. M.; Bandyopadhyay, B.; Cramer, H.; Leaman, D. W.; Kennedy, A. W.; Silverman, R. H.; Cowell, J. K. *Gynecol. Oncol.* **2000**, *76*, 183-192.

66) Trawick, B. N.; Daniher, A. T.; Bashkin, J. K. *Chem. Rev.* **1998**, *98*, 939-960.

67) Gee, J. E.; Robbins, I.; Van Der Laan, A. C.; Van Boom, J. H.; Colombier, C.; Leng, M.; Raible, A. M.; Nelson, J. S.; Lebleu, B. *Antisense Nucleic Acid Drug Dev.* **1998**, *8*, 103-111.

68) Bonham, M. A.; Brown, S.; Boyd, A. L.; Brown, P. H.; Bruckenstein, D. A.; Hanvey, J. C.; Thomson, S. A.; Pipe, A.; Hassman, F.; Bisi, J. E.; Froehler, B. C.; Matteucci M. D.; Wagner, R. W.; Noble, S. A.; Babiss, L. E. *Nucleic Acids Res.* **1995**, *23*, 1197-1203.

69) Schmajuk, G.; Sierakowska, H.; Kole, R. *J. Biol. Chem.* **1999**, *274*, 21783-21789.

70) Vickers, T. A.; Wyatt, J. R.; Burckin, T.; Bennett, C. F.; Freier, S. M. *Nucleic Acids Res.* **2001**, *29*, 1293-1299.

71) Shen, L. X.; Kandimalla, E. R.; Agrawal, S. *Bioorg. Med. Chem.* **1998**, *6*, 1695-1705.

72) Altona, C.; Sundaralingam, M. *J. Am. Chem. Soc.* **1972**, *94*, 8205-8212.

73) Thibaudeau, C.; Chattopadhyaya, J. *Nucleosides Nucleotides* **1997**, *16*, 523-529.

74) Thibaudeau, C.; Plavec, J.; Watanabe, K. A.; Chattopadhyaya, J. *J. Chem. Soc., Chem. Commun.* **1994**, 537-540.

75) Thibaudeau, C.; Plavec, J.; Garg, N.; Papchikhin, A.; Chattopadhyaya, J. *J. Am. Chem. Soc.* **1994**, *116*, 4038-4043.

76) Acharya, P.; Nawrot, B.; Sprinzl, M.; Thibaudeau, C.; Chattopadhyaya, J. *J. Chem. Soc. Perkin Trans. 2* **1999**, 1531-1536.

77) Cook, P. D. *Annu. Rep. Med. Chem.* **1998**, *33*, 313-325.

78) Barsky, D.; Colvin, M. E.; Zon, G.; Gryaznov, S. M. *Nucleic Acids Res.* **1997**, *25*, 830-835.

79) Monia, B. P.; Johnston, J. F.; Sasmor, H.; Cummins, L. L. *J. Biol. Chem.* **1996**, *271*, 14533-14540.

80) Lesnik, E. A.; Freier, S. M. *Biochemistry* **1998**, *37*, 6991-6997.

81) Tereshko, V.; Portmann, S.; Tay, E. C.; Martin, P.; Natt, F.; Altmann, K.-H.; Egli, M. *Biochemistry* **1998**, *37*, 10626-10634.

82) Cummins, L. L.; Owens, S. R.; Risen, L. M.; Lesnik, E. A.; Freier, S. M.; McGee, D.; Guinosso, C. J.; Cook, P. D. *Nucleic Acids Res.* **1995**, *23*, 2019-2024.

83) Kawasaki, A. M.; Casper, M. D.; Prakash, T. P.; Manalili, S.; Sasmor, H.; Manoharan, M.; Cook, P. D. *Nucleosides Nucleotides* **1999**, *18*, 1419-1420.

84) Manoharan, M.; Prakash, T. P.; Barber-Peoc'h, I.; Bhat, B.; Vasquez, G.; Ross, B. S.; Cook, P. D. *J. Org. Chem.* **1999**, *64*, 6468-6472.

85) Griffey, R. H.; Monia, B. P.; Cummins, L. L.; Freier, S.; Greig, M. J.; Guinosso, C. J.; Lesnik, E.; Manalili, S. M.; Mohan, V.; Owens S.; Ross, B. R.; Sasmor, H.; Wancewicz, E.; Weiler, K.; Wheeler, P. D.; Cook, P. D. *J. Med. Chem.* **1996**, *39*, 5100-5109.

86) Prakash, T. P.; Manoharan, M.; Fraser, A. S.; Kawasaki, A. M.; Lesnik, E. A.; Owens, S. R. *Tetrahedron Lett.* **2000**, *41*, 4855-4859.

87) Kawasaki, A. M.; Casper, M. D.; Freier, S. M.; Lesnik, E. A.; Zounes, M. C.; Cummins, L. L.; Gonzalez, C.; Cook, P. D. *J. Med. Chem.* **1993**, *36*, 831-841.

88) Prakash, T. P.; Manoharan, M.; Kawasaki, A. M.; Lesnik, E. A.; Owens, S. R.; Vasquez, G. *Org. Lett.* **2000**, *2*, 3995-3998.

89) Prakash, T. P.; Kawasaki, A. M.; Vasquez, G.; Fraser, A. S.; Casper, M. D.; Cook, P. D.; Manoharan., M. *Nucleosides Nucleotides* **1999**, *18*, 1381-1382.

90) Ozaki, H.; Sato, Y.; Azuma, S.; Sawai., H. *Nucleosides Nucleotides Nucleic Acids* **2000**, *19*, 593-601.

91) Venkateswarlu, D.; Lind, K. E.; Mohan, V.; Manoharan, M.; Ferguson, D. M. *Nucleic Acids Res.* **1999**, *27*, 2189-2195.

92) Fraser, A.; Wheeler, P.; Cook, P. D.; Sanghvi, Y. S. *J. Heterocycl. Chem.* **1993**, *30*, 1277-1287.

93) Plavec, J.; Thibaudeau, C.; Chattopadhyaya, J. *J. Am. Chem. Soc.* **1994**, *116*, 6558-6560.

94) Wolfe, S. *Acc. Chem. Res.* **1972**, *5*, 102-111.

95) Vorobjev, P. E.; Zarytova, V. F.; Bonora, G. M. *Nucleosides Nucleotides* **1999**, *18*, 2745-2750.

96) Lind, K. E.; Mohan, V.; Manoharan, M.; Ferguson, D. M. *Nucleic Acids Res.* **1998**, *26*, 3694-3699.

97) Teplova, M.; Wallace, S. T.; Tereshko, V.; Minasov, G.; Symons, A. M.; Cook, P. D.; Manoharan, M.; Egli, M. *Proc. Natl. Acad. Sci. U.S.A.* **1999**, *96*, 14240-14245.

98) Cuenoud, B.; Casset, F.; Hüsken, D.; Natt, F.; Wolf, R. M.; Altmann, K.-H.; Martin, P.; Moser, H. E. *Angew. Chem. Int. Ed. Engl.* **1998**, *37*, 1288-1291.

99) Manoharan, M. *Biochim. Biophys. Acta* **1999**, *1489*, 117-130.

100) Haruki, M.; Tsunaka, Y.; Morikawa, M.; Iwai, S.; Kanaya, S. *Biochemistry* **2000**, *39*, 13939-13944.

101) Nakamura, H.; Oda, Y.; Iwai, S.; Inoue, H.; Ohtsuka, E.; Kanaya, S.; Kimura, S.; Katsuda, C.; Katayanagi, K.; Morikawa, K. *Proc. Natl. Acad. Sci. U.S.A.* **1991**, *88*, 11535-11539.

102) Eder, P. S.; Walder, J. A. *J. Biol. Chem.* **1991**, *266*, 6472-6479.

103) Kool, E. T. *Chem. Rev.* **1997**, *97*, 1473-1487.

104) Hassan, A.; Wazeer, M. I. M.; Perzanowski, H. P.; Ali, S. A. *J. Chem. Soc. Perkin Trans. 2* **1997**, 411-418.

105) Ikeda, H.; Fernandez, R.; Wilk, A.; Barchi, J. J., Jr.; Huang, X.; Marquez, V. E. *Nucleic Acids Res.* **1998**, *26*, 2237-2244.

106) Nishizono, N.; Sumita, Y.; Ueno, Y.; Matsuda, A. *Nucleic Acids Res.* **1998**, *26*, 5067-5072.

107) Uesugi, S.; Miki, H.; Ikehara, M.; Iwahashi, H.; Kyogoku, Y. *Tetrahedron Lett.* **1979**, 4073-4076.

108) Thibaudeau, C.; Nishizono, N.; Sumita, Y.; Matsuda, A.; Chattopadhyaya, J. *Nucleosides Nucleotides* **1999**, *18*, 1035-1053.

109) Giannaris, P. A.; Damha, M. J. *Can. J. Chem.* **1994**, *72*, 909-18.

110) Wilds, C. J.; Damha, M. J. *Nucleic Acids Res.* **2000**, *28*, 3625-3635.

111) Damha, M. J.; Noronha, A. M.; Wilds, C. J.; Trempe, J. F.; Denisov, A.; Pon, R. T.; Gehring, K. *Nucleosides Nucleotides Nucleic Acids* **2001**, *20*, 429-440.

112) Venkateswarlu, D.; Ferguson, D. M. *J. Am. Chem. Soc.* **1999**, *121*, 5609-5610.

113) Denisov, A. Y.; Noronha, A. M.; Wilds, C. J.; Trempe, J.-F.; Pon, R. T.; Gehring, K.; Damha, M. J. *Nucleic Acids Res.* **2001**, *29*, 4284-4293.

114) Noronha, A. M., Ph. D. Thesis, McGill University: Montreal, **1999**, 216 pp.

115) Trempe, J.-F.; Wilds, C. J.; Denisov, A. Y.; Pon, R. T.; Damha, M. J.; Gehring, K. *J. Am. Chem. Soc.* **2001**, *123*, 4896-4903.

116) Wilds, C. J.; Damha, M. J. *Bioconjug. Chem.* **1999**, *10*, 299-305.

117) Berger, I.; Tereshko, V.; Ikeda, H.; Marquez, V. E.; Egli, M. *Nucleic Acids Res.* **1998**, *26*, 2473-2480.

118) Barbarich, T. J.; Rithner, C. D.; Miller, S. M.; Anderson, O. P.; Strauss, S. H. *J. Am. Chem. Soc.* **1999**, *121*, 4280-4281.

119) Minasov, G.; Teplova, M.; Wengel, J.; Egli, M. *Biochemistry* **2000**, *39*, 3525-3532.

120) Christensen, N. K.; Peterssen, M.; Nielsen, P.; Jacobsen, J. P.; Olsen, C. E.; Wengel, J. *J. Am. Chem. Soc.* **1998**, *120*, 5458-5463.

121) Nielsen, P.; Pfundheller, H. M.; Wengel, J. *Chem. Commun.* **1997**, 825-826.

122) Herdewijn, P. *Biochim. Biophys. Acta* **1999**, *1489*, 167-179.

123) Tommerholt, H. V.; Christensen, N. K.; Nielsen, P.; Wengel, J.; Stein, P. C.; Jacobsen, J. P.; Petersen, M. *Org. Biomol. Chem.* **2003**, *1*, 1790-1797.

124) Nielsen, P.; Petersen, M.; Jacobsen, J. P. *J. Chem. Soc. Perkin Trans. 1* **2000**, 3706-3713.

125) Altmann, K.-H.; Imwinkelried, R.; Kesselring, R.; Rihs, G. *Tetrahedron Lett.* **1994**, *35*, 7625-7628.

126) Altmann, K.-H.; Kesselring, R.; Francotte, E.; Rihs, G. *Tetrahedron Lett.* **1994**, *35*, 2331-2334.

127) Maier, M. A.; Choi, Y.; Gaus, H.; Barchi, J. J., Jr.; Marquez, V. E.; Manoharan, M. *Nucleic Acids Res.* **2004**, *32*, 3642-3650.

128) Wengel, J.; Koshkin, A.; Singh, S. K.; Nielsen, P.; Meldgaard, M.; Rajwanshi, V. K.; Kumar, R.; Skouv, J.; Nielsen, C. B.; Jacobsen, J. P.; Jacobsen, N.; Olsen, C. E. *Nucleosides Nucleotides* **1999**, *18*, 1365-1370.

129) Rajwanshi, V. K.; Håkansson, A. E.; Sørensen, M. D.; Pitsch, S.; Singh, S. K.; Kumar, R.; Nielsen, P.; Wengel, J. *Angew. Chem. Int. Ed. Engl.* **2000**, *39*, 1656-1659.

130) Rajwanshi, V. K.; Håkansson, A. E.; Dahl, B. M.; Wengel, J. *Chem. Commun.* **1999**, 1395-1396.

131) Rajwanshi, V. K.; Håkansson, A. E.; Kumar, R.; Wengel, J. *Chem. Commun.* **1999**, 2073-2074.

132) Singh, S. K.; Wengel, J. *Chem. Commun.* **1998**, 1247-1248.

133) Koshkin, A. A.; Nielsen, P.; Meldgaard, M.; Rajwanshi, V. K.; Singh, S. K.; Wengel, J. *J. Am. Chem. Soc.* **1998**, *120*, 13252-13253.

134) Bondensgaard, K.; Petersen, M.; Singh, S. K.; Rajwanshi, V. K.; Kumar, R.; Wengel, J.; Jacobsen, J. P. *Chem. Eur. J.* **2000**, *6*, 2687-2695.

135) Petersen, M.; Nielsen, C. B.; Nielsen, K. E.; Jensen, G. A.; Bondensgaard, K.; Singh, S. K.; Rajwanshi, V. K.; Koshkin, A. A.; Dahl, B. M.; Wengel, J.; Jacobsen, J. P. *J. Mol. Recognit.* **2000**, *13*, 44-53.

136) Vester, B.; Wengel, J. *Biochemistry* **2004**, *43*, 13233-13241.

137) Nielsen, K. E.; Rasmussen, J.; Kumar, R.; Wengel, J.; Jacobsen, J. P.; Petersen, M. *Bioconjug. Chem.* **2004**, *15*, 449-457.

138) Nielsen, K. E.; Singh, S. K.; Wengel, J.; Jacobsen, J. P. *Bioconjug. Chem.* **2000**, *11*, 228-238.

139) Epple, C.; Leumann, C. *Chem. Biol.* **1998**, *5*, 209-216.

140) Obika, S.; Hari, Y.; Sugimoto, T.; Sekiguchi, M.; Imanishi, T. *Tetrahedron Lett.* **2000**, *41*, 8923-8927.

141) Petersen, M.; Bondensgaard, K.; Wengel, J.; Jacobsen, J. P. *J. Am. Chem. Soc.* **2002**, *124*, 5974-5982.

142) Wahlestedt, C.; Salmi, P.; Good, L.; Kela, J.; Johnsson, T.; Hokfelt, T.; Broberger, C.; Porreca, F.; Lai, J.; Ren, K.; Ossipov, M.; Koshkin, A.; Jakobsen, N.; Skouv, J.; Oerum, H.; Jacobsen, M. H.; Wengel, J. *Proc. Natl. Acad. Sci. U.S.A.* **2000**, *97*, 5633-5638.

143) Kurreck, J.; Wyszko, E.; Gillen, C.; Erdmann, V. A. *Nucleic Acids Res.* **2002**, *30*, 1911-1918.

144) Petersen, M.; Håkansson, A. E.; Wengel, J.; Jacobsen, J. P. *J. Am. Chem. Soc.* **2001**, *123*, 7431-7432.

145) Frieden, M.; Christensen, S. M.; Mikkelsen, N. D.; Rosenbohm, C.; Thrue, C. A.; Westergaard, M.; Hansen, H. F.; Orum, H.; Koch, T. *Nucleic Acids Res.* **2003**, *31*, 6365-6372.

146) Li, J.; Wartell, R. M. *Biochemistry* **1998**, *37*, 5154-5161.

147) Mangos, M. M.; Min, K. L.; Viazovkina, E.; Galarneau, A.; Elzagheid, M. I.; Parniak, M. A.; Damha, M. J. *J. Am. Chem. Soc.* **2003**, *125*, 654-661.

148) Pradeepkumar, P. I.; Zamaratski, E.; Foldesi, A.; Chattopadhyaya, J. *Tetrahedron Lett.* **2000**, *41*, 8601-8607.

149) Peng, L.; Roth, H.-J. *Helv. Chim. Acta* **1997**, *80*, 1494-1512.

150) Nielsen, P.; Dreioe, L. H.; Wengel, J. *Bioorg. Med. Chem.* **1995**, *3*, 19-28.

151) Mikhailov, S. N.; Pfleiderer, W. *Tetrahedron Lett.* **1985**, *26*, 2059-2062.

152) Wu, T.; Froeyen, M.; Schepers, G.; Mullens, K.; Rozenski, J.; Busson, R.; Van Aerschot, A.; Herdewijn, P. *Org. Lett.* **2004**, *6*, 51-54.

153) De Clercq, E. *J. Med. Chem.* **1995**, *38*, 2491-2517.

154) Vandendriessche, F.; Augustyns, K.; Aerschot, A. V.; Busson, R.; Hoogmartens, J.; Herdewijn, P. *Tetrahedron* **1993**, *49*, 7223-7238.

155) Chu, C. K.; Cutler, S. J. *J. Heterocycl. Chem.* **1986**, *23*, 289-319.

156) Schneider, K. C.; Benner, S. A. *J. Am. Chem. Soc.* **1990**, *112*, 453-455.

157) Ogilvie, K. K.; Proba, Z. A. *Nucleosides Nucleotides* **1984**, *3*, 537-547.

158) Ogilvie, K. K.; Hamilton, R. G.; Gillen, M. F.; Radatus, B. K.; Smith, K. O.; Galloway, K. S. *Can. J. Chem.* **1984**, *62*, 16-21.

159) Ogilvie, K. K.; Nghe Nguyen, B.; Gillen, M. F.; Radatus, B. K.; Cheriyan, U. O.; Smith, K. O.; Galloway, K. S. *Can. J. Chem.* **1984**, *62*, 241-252.

160) Usman, N.; Juby, C. D.; Ogilvie, K. K. *Tetrahedron Lett.* **1988**, *29*, 4831-4834.

161) Thibon, J.; Latxague, L.; Deleris, G. *J. Org. Chem.* **1997**, *62*, 4635-4642.

162) Latxague, L.; Thibon, J.; Deleris, G. *Tetrahedron Lett.* **1998**, *39*, 4025-4028.

163) Lok, C. N.; Viazovkina, E.; Min, K. L.; Nagy, E.; Wilds, C. J.; Damha, M. J.; Parniak, M. A. *Biochemistry* **2002**, *41*, 3457-3467.

164) Min, K. L.; Viazovkina, E.; Galarneau, A.; Parniak, M. A.; Damha, M. J. *Bioorg. Med. Chem. Lett.* **2002**, *12*, 2651-2654.

165) Damha, M. J.; Parniak, M. A. Int. PCT Appl. WO 03/064441, **2003**, 63 pp.

166) Kvaernø, L.; Wengel, J. *Chem. Commun.* **2001**, 1419-1424.

167) Verbeure, B.; Lescrinier, E.; Wang, J.; Herdewijn, P. *Nucleic Acids Res.* **2001**, *29*, 4941-4947.

168) Gu, P.; Schepers, G.; Rozenski, J.; Van Aerschot, A.; Herdewijn, P. *Oligonucleotides* **2003**, *13*, 479-489.

169) Wang, J.; Verbeure, B.; Luyten, I.; Froeyen, M.; Hendrix, C.; Rosemeyer, H.; Seela, F.; Van Aerschot, A.; Herdewijn, P. *Nucleosides Nucleotides Nucleic Acids* **2001**, *20*, 785-788.

170) Thoma, C.; Hasselblatt, P.; Kock, J.; Chang, S.-F.; Hockenjos, B.; Will, H.; Hentze, M. W.; Blum, H. E.; Von Weizsacker, F.; Offensperger, W.-B. *Mol. Cell* **2001**, *8*, 865-872.

171) Steiger, M. A.; Decker, C. J. *Mol. Cell* **2001**, *8*, 732-733.

172) Wang, Z.; Kiledjian, M. *EMBO J.* **2000**, *19*, 295-305.

173) Brewer, G. *J. Biol. Chem.* **1998**, *273*, 34770-34774.

174) Ross, J.; Kobs, G. *J. Mol. Biol.* **1986**, *188*, 579-593.

175) Wang, Z.; Kiledjian, M. *Cell* **2001**, *107*, 751-762.

176) Chen, C. Y.; Gherzi, R.; Ong, S. E.; Chan, E. L.; Raijmakers, R.; Pruijn, G. J.; Stoecklin, G.; Moroni, C.; Mann, M.; Karin, M. *Cell* **2001**, *107*, 451-464.

177) Mittal, V. *Nat. Rev. Genet.* **2004**, *5*, 355.

178) Fire, A.; Xu, S.; Montgomery, M. K.; Kostas, S. A.; Driver, S. E.; Mello, C. C. *Nature* **1998**, *391*, 806-811.

179) Bosher, J. M.; Dufourcq, P.; Sookhareea, S.; Labouesse, M. *Genetics* **1999**, *153*, 1245-1256.

180) Schepers, U.; Kolter, T. *Angew. Chem. Int. Ed. Engl.* **2001**, *40*, 2437-2439.

181) McManus, M. T.; Sharp, P. A. *Nat. Rev. Genet.* **2002**, *3*, 737-747.

182) Caplen, N. J.; Parrish, S.; Imani, F.; Fire, A.; Morgan, R. A. *Proc. Natl. Acad. Sci. U.S.A.* **2001**, *98*, 9742-9747.

183) Jackson, A. L.; Bartz, S. R.; Schelter, J.; Kobayashi, S. V.; Burchard, J.; Mao, M.; Li, B.; Cavet, G.; Linsley, P. S. *Nat. Biotechnol.* **2003**, *21*, 635-637.

184) Bartel, D. P. *Cell* **2004**, *116*, 281-297.

185) Saxena, S.; Jonsson, Z. O.; Dutta, A. *J. Biol. Chem.* **2003**, *278*, 44312-44319.

186) Song, J.-J.; Smith, S. K.; Hannon, G. J.; Joshua-Tor, L. *Science* **2004**, *305*, 1434-1437.

187) Damha, M. J.; Usman, N.; Ogilvie, K. K. *Tetrahedron Lett.* **1987**, *28*, 1633-1636.

188) Damha, M. J.; Giannaris, P. A.; Marfey, P. *Biochemistry* **1994**, *33*, 7877-7885.

189) Lacombe, J.; Viazovkina, E.; Bernatchez, P. N.; Galarneau, A.; Damha, M. J.; Sirois, M. G. *Can. J. Physiol. Pharmacol.* **2002**, *80*, 951-961.

190) Crooke, S. T.; Bennett, C. F. *Annu. Rev. Pharmacol. Toxicol.* **1996**, *36*, 107-129.

191) Eckstein, F. *Annu. Rev. Biochem.* **1985**, *54*, 367-402.

192) Stein, L. D. *Nature* **2004**, *431*, 915-916, and references therein.

193) Monia, B. P.; Lesnik, E. A.; Gonzalez, C.; Lima, W. F.; McGee, D.; Guinosso, C. J.; Kawasaki, A. M.; Cook, P. D.; Freier, S. M. *J. Biol. Chem.* **1993**, *268*, 14514-14522.

194) Minshull, J.; Hunt, T. *Nucleic Acids Res.* **1986**, *14*, 6433-6451.

195) Cazenave, C.; Loreau, N.; Thuong, N. T.; Toulmé, J. J.; Hélène, C. *Nucleic Acids Res.* **1987**, *15*, 4717-36.

196) Baker, B. F.; Lot, S. S.; Condon, T. P.; Cheng-Flournoy, S.; Lesnik, E. A.; Sasmor, H. M.; Bennett, C. F. *J. Biol. Chem.* **1997**, *272*, 11994-12000.

197) Khym, J. X.; Cohn, W. E. *J. Am. Chem. Soc.* **1960**, *82*, 6380-6386.

198) Davoll, J.; Lythgoe, B.; Todd, A. R. *J. Chem. Soc.* **1946**, 833-838.

199) Brown, D. M.; Lythgoe, B. *J. Chem. Soc.* **1950**, 1990-1991.

200) Bessodes, M.; Antonakis, K. *Tetrahedron Lett.* **1985**, *26*, 1305-1306.

201) Maggio, A. F.; Boyer, V.; Aubertin, A. M.; Obert, G.; Kirn, A.; Imbach, J. L. *Nucleosides Nucleotides* **1991**, *10*, 1431-1449.

202) Pizarro, J. M.; Pizarro, J. L.; Fernandez, J.; Sandino, A. M.; Spencer, E. *Virology* **1991**, *184*, 768-772.

203) Mikhailov, S. N.; Florentiev, V. L.; Pfleiderer, W. *Synthesis* **1985**, 399-400.

204) Ogilvie, K. K.; Beaucage, S. L.; Schifman, A. L.; Theriault, N. Y.; Sadana, K. L. *Can. J. Chem.* **1978**, *56*, 2768-2780.

205) Ogilvie, K. K.; Hakimelahi, G. H. *Carbohydrate Res.* **1983**, *115*, 234-239.

206) Damha, M. J.; Ogilvie, K. K. *Methods Mol. Biol.* **1993**, *20*, 81-114.

207) Yu, C.; Liu, B.; Hu, L. *Tetrahedron Lett.* **2000**, *41*, 4281-4285.

208) Bouzide, A.; Sauve, G. *Tetrahedron Lett.* **1997**, *38*, 5945-5948.

209) Hakimelahi, G. H.; Proba, Z. A.; Ogilvie, K. K. *Can. J. Chem.* **1982**, *60*, 1106-1113.

210) Ogilvie, K. K.; Sadana, K. L.; Thompson, E. A.; Quilliam, M. A.; Westmore, J. B. *Tetrahedron Lett.* **1974**, 2861-2863.

211) Beaucage, S. L.; Caruthers, M. H. *Tetrahedron Lett.* **1981**, *22*, 1859-1862.

212) Viazovkina, E.; Mangos, M. M.; Elzagheid, M. I.; Damha, M. J. In *Current Protocols in Nucleic Acid Chemistry*; Beaucage, S. L., Bergstrom, D. E., Glick, G. D. and Jones, R. A., Eds.; John Wiley & Sons, Inc.: New York, NY, **2002**; Vol. 4.15, 22 pp.

213) Temsamani, J.; Kubert, M.; Agrawal, S. *Nucleic Acids Res.* **1995**, *23*, 1841-1844.

214) Letsinger, R. L.; Finnan, J. L.; Heavner, G. A.; Lunsford, W. B. *J. Am. Chem. Soc.* **1975**, *97*, 3278-3279.

215) Letsinger, R. L.; Lunsford, W. B. *J. Am. Chem. Soc.* **1976**, *98*, 3655-3661.

216) Gasparutto, D.; Livache, T.; Bazin, H.; Duplaa, A. M.; Guy, A.; Khorlin, A.; Molko, D.; Roget, A.; Teoule, R. *Nucleic Acids Res.* **1992**, *20*, 5159-5166.

217) Jarvinen, P.; Oivanen, M.; Lonnberg, H. *J. Org. Chem.* **1991**, *56*, 5396-5401.

218) Yang, W.; Hendrickson, W. A.; Crouch, R. J.; Satow, Y. *Science* **1990**, *249*, 1398-1405.

219) Chakraborty, A. K.; Cichutek, K.; Duesberg, P. H. *Proc. Natl. Acad. Sci. U.S.A.* **1991**, *88*, 2217-2221.

220) Kiaris, H.; Spandidos, D. A. *Int. J. Oncol.* **1995**, *7*, 413-421.

221) Kiaris, H.; Spandidos, D. A. *Int. J. Oncol.* **1995**, *7*, 75-80.

222) Hua, V. Y.; Wang, W. K.; Duesberg, P. H. *Proc. Natl. Acad. Sci. U.S.A.* **1997**, *94*, 9614-9619.

223) Zuker, M.; Mathews, D. H.; Turner, D. H. In *RNA Biochemistry and Biotechnology*; Barciszewski, J. and Clarke, B. F. C., Eds.; NATO ASI Series, Kluwer Academic Publishers: Norwell MA, **1999**, pp. 11-43.

224) Mathews, D. H.; Sabina, J.; Zuker, M.; Turner, D. H. *J. Mol. Biol.* **1999**, *288*, 911-940.

225) Vorobjev, P. E.; Pyshnaia, I. A.; Pyshnyi, D. V.; Repkova, M. N.; Venmiaminov, A. G.; Zenkova, M. A.; Ivanova, E. M.; Scalfi-Happ, C.; Seliger, H.; Bonora, G.; Zarytova, V. F. *Russ. J. Bioorg. Chem.* **2000**, *26*, 844-851.

226) Vorobjev, P. E.; Pyshnaya, I. A.; Pyshnyi, D. V.; Repkova, M. N.; Venyaminova, A. G.; Zenkova, M. A.; Ivanova, E. M.; Scalfi-Happ, C.; Seliger, H.; Bonora, G. M.; Zarytova, V. F. *Russ. J. Bioorg. Chem.* **2000**, *26*, 758-764.

227) Vorobjev, P. E.; Pyshnaya, I. A.; Pyshnyi, D. V.; Venyaminova, A. G.; Ivanova, E. M.; Zarytova, V. F.; Bonora, G. M.; Scalfi-Happ, C.; Seliger, H. *Antisense Nucleic Acid Drug Dev.* **2001**, *11*, 77-85.

228) Toulmé, J. J.; Frank, P.; Crouch, R. J. In *Human Ribonucleases H*; Crouch, R. J. and Toulmé, J. J., Eds.; INSERM: Paris, **1998**, pp 147-162.

229) Turchi, J. J.; Huang, L.; Murante, R. S.; Kim, Y.; Bambara, R. A. *Proc. Natl. Acad. Sci. U.S.A.* **1994**, *91*, 9803-9807.

230) Arudchandran, A.; Cerritelli, S. M.; Narimatsu, S. K.; Itaya, M.; Shin, D.-Y.; Shimada, Y.; Crouch, R. J. *Genes Cells* **2000**, *5*, 789-802.

231) Rydberg, B.; Game, J. *Proc. Natl. Acad. Sci. U.S.A.* **2002**, *99*, 16654-16659.

232) Moelling, K.; Bolognesi, D. P.; Bauer, H.; Buesen, W.; Plassmann, H. W.; Hausen, P. *Nat. New Biol.* **1971**, *234*, 240-243.

233) Stein, H.; Hausen, P. *Science* **1969**, *166*, 393-395.

234) Frank, P.; Albert, S.; Cazenave, C.; Toulmé, J.-J. *Nucleic Acids Res.* **1994**, *22*, 5247-5254.

235) Frank, P.; Braunshofer-Reiter, C.; Wintersberger, U.; Grimm, R.; Busen, W. *Proc. Natl. Acad. Sci. U.S.A.* **1998**, *95*, 12872-12877.

236) Frank, P.; Braunshofer-Reiter, C.; Poeltl, A.; Holzmann, K. *Biol. Chem.* **1998**, *379*, 1407-1412.

237) Crouch, R. J.; Arudchandran, A.; Cerritelli, S. M. *Methods Enzymol.* **2001**, *341*, 395-413.

238) Johnson, M. S.; McClure, M. A.; Feng, D. F.; Gray, J.; Doolittle, R. F. *Proc. Natl. Acad. Sci. U.S.A.* **1986**, *83*, 7648-7652.

239) Cerritelli, S. M.; Frolova, E. G.; Feng, C.; Grinberg, A.; Love, P. E.; Crouch, R. J. *Mol. Cell* **2003**, *11*, 807-815.

240) Cerritelli, S. M.; Crouch, R. J. *RNA* **1995**, *1*, 246-259.

241) Evans, S. P.; Bycroft, M. *J. Mol. Biol.* **1999**, *291*, 661-669.

242) Wu, H.; Lima, W. F.; Crooke, S. T. *J. Biol. Chem.* **2001**, *276*, 23547-23553.

243) Ohtani, N.; Haruki, M.; Morikawa, M.; Kanaya, S. *J. Biosci. Bioeng.* **1999**, *88*, 12-19.

244) Frank, P.; Braunshofer-Reiter, C.; Wintersberger, U. *FEBS Lett.* **1998**, *421*, 23-26.

245) Berkower, I.; Leis, J.; Hurwitz, J. *J. Biol. Chem.* **1973**, *248*, 5914-5921.

246) Crouch, R. J.; Dirksen, M. L. In *Ribonucleases H*; Linn, S. M. and Roberts, R. J., Eds.; Cold Spring Harbor Laboratory Press: Cold Spring Harbor, NY **1982**; Vol. 14, pp. 211-254.

247) Krakowiak, A.; Owczarek, A.; Koziolkiewicz, M.; Stec, W. J. *ChemBioChem* **2002**, *3*, 1242-1250.

248) Lai, L.; Yokota, H.; Hung, L.-W.; Kim, R.; Kim, S.-H. *Structure* **2000**, *8*, 897-904.

249) Mangos, M. M.; Damha, M. J. *Curr. Topics Med. Chem.* **2002**, *2*, 1147-1171.

250) Nielsen, J. T.; Stein, P. C.; Petersen, M. *Nucleic Acids Res.* **2003**, *31*, 5858-5867.

251) Premraj, B. J.; Raja, S.; Yathindra, N. *Biophys. Chem.* **2002**, *95*, 253-272.

252) Barsky, D.; Foloppe, N.; Ahmadia, S.; Wilson, D. M., III; MacKerell, A. D., Jr. *Nucleic Acids Res.* **2000**, *28*, 2613-2626.

253) Gelfand, C. A.; Plum, G. E.; Grollman, A. P.; Johnson, F.; Breslauer, K. J. *Biochemistry* **1998**, *37*, 12507-12512.

254) Kung, H. C.; Bolton, P. H. *J. Biol. Chem.* **1997**, *272*, 9227-9236.

255) Harrington, R. E.; Winicov, I. *Prog Nucleic Acid Res. Mol. Biol.* **1994**, *47*, 195-270.

256) Wu, H.; Lima, W. F.; Zhang, H.; Fan, A.; Sun, H.; Crooke, S. T. *J. Biol. Chem.* **2004**, *279*, 17181-17189.

257) Puglisi, J. D.; Tinoco, I., Jr. *Methods Enzymol.* **1989**, *180*, 304-325.

258) Dahl, B. H.; Nielsen, J.; Dahl, O. *Nucleic Acids Res.* **1987**, *15*, 1729-1743.

259) Beaucage, S. L.; Iyer, R. P. *Tetrahedron* **1992**, *48*, 2223-2311.

260) Xin, Z.; Just, G. *Tetrahedron Lett.* **1996**, *37*, 969-972.

261) Vargeese, C.; Carter, J.; Yegge, J.; Krivjansky, S.; Settle, A.; Kropp, E.; Peterson, K.; Pieken, W. *Nucleic Acids Res.* **1998**, *26*, 1046-1050.

262) Welz, R.; Muller, S. *Tetrahedron Lett.* **2002**, *43*, 795-797.

263) Berner, S.; Muhlegger, K.; Seliger, H. *Nucleic Acids Res.* **1989**, *17*, 853-864.

264) Krotz, A. H.; Klopchin, P. G.; Walker, K. L.; Srivatsa, G. S.; Cole, D. L.; Ravikumar, V. T. *Tetrahedron Lett.* **1997**, *38*, 3875-3878.

265) Iwai, S.; Ohtsuka, E. *Tetrahedron Lett.* **1988**, *29*, 5383-5386.

266) Iwai, S.; Ohtsuka, E. *Nucleic Acids Res.* **1988**, *16*, 9443-9456.

267) Muller, E.; Gasparutto, D.; Lebrun, C.; Cadet, J. *Eur. J. Org. Chem.* **2001**, 2091-2099.

268) Van Boom, J. H.; Burgers, P. M. J. *Tetrahedron Lett.* **1976**, 4875-4878.

269) Meldgaard, M.; Nielsen, N. K.; Bremner, M.; Pedersen, O. S.; Olsen, C. E.; Wengel, J. *J. Chem. Soc. Perkin Trans. 1* **1997**, 1951-1955.

270) Sorensen, M. D.; Meldgaard, M.; Rajwanshi, V. K.; Wengel, J. *Bioorg. Med. Chem. Lett.* **2000**, *10*, 1853-1856.

271) Shida, T.; Arakawa, M.; Sekiguchi, J. *Nucleosides Nucleotides* **1994**, *13*, 1319-1326.

272) Vesnaver, G.; Chang, C. N.; Eisenberg, M.; Grollman, A. P.; Breslauer, K. J. *Proc. Natl. Acad. Sci. U.S.A.* **1989**, *86*, 3614-3618.

273) Gelfand, C. A.; Plum, G. E.; Grollman, A. P.; Johnson, F.; Breslauer, K. J. *Biochemistry* **1998**, *37*, 7321-7327.

274) Gelfand, C. A.; Plum, G. E.; Grollman, A. P.; Johnson, F.; Breslauer, K. J. *Biopolymers* **1996**, *38*, 439-445.

275) Beger, R. D.; Bolton, P. H. *J. Biol. Chem.* **1998**, *273*, 15565-15573.

276) Thomas, D. C.; Kunkel, T. A.; Casna, N. J.; Ford, J. P.; Sancar, A. *J. Biol. Chem.* **1986**, *261*, 14496-14505.

277) Guest, C. R.; Hochstrasser, R. A.; Sowers, L. C.; Millar, D. P. *Biochemistry* **1991**, *30*, 3271-3279.

278) Cuniasse, P.; Fazakerley, G. V.; Guschlbauer, W.; Kaplan, B. E.; Sowers, L. C. *J. Mol. Biol.* **1990**, *213*, 303-314.

279) Coppel, Y.; Berthet, N.; Coulombeau, C.; Coulombeau, C.; Garcia, J.; Lhomme, J. *Biochemistry* **1997**, *36*, 4817-4830.

280) Tinoco, I. *J. Am. Chem. Soc.* **1960**, *82*, 4785-4790.

281) Rhodes, W. *J. Am. Chem. Soc.* **1961**, *83*, 3609-3617.

282) Rich, A. *J. Am. Chem. Soc.* **1960**, *82*, 6409-6411.

283) Applequist, J.; Damle, V. *J. Am. Chem. Soc.* **1965**, *87*, 1450-1458.

284) Felsenfeld, G.; Rich, A. *Biochim. Biophys. Acta* **1957**, *26*, 457-468.

285) Becaud, J.; Pompizi, I.; Leumann, C. J. *J. Am. Chem. Soc.* **2003**, *125*, 15338-15342.

286) Kibler-Herzog, L.; Zon, G.; Whittier, G.; Mizan, S.; Wilson, W. D. *Anti-Cancer Drug Des.* **1993**, *8*, 65-79.

287) Cazenave, C.; Frank, P.; Toulmé, J.-J.; Busen, W. *J. Biol. Chem.* **1994**, *269*, 25185-25192.

288) Pileur, F.; Toulmé, J.-J.; Cazenave, C. *Nucleic Acids Res.* **2000**, *28*, 3674-3683.

289) Busen, W.; Peters, J. H.; Hausen, P.; Crystalla, G. *Eur. J. Biochem.* **1977**, *74*, 203-208.

290) Turchi, J. J.; Bambara, R. A. *J. Biol. Chem.* **1993**, *268*, 15136-15141.

291) Bambara, R. A.; Murante, R. S.; Henricksen, L. A. *J. Biol. Chem.* **1997**, *272*, 4647-4650.

292) Wu, H.; Lima, W. F.; Crooke, S. T. *J. Biol. Chem.* **1999**, *274*, 28270-28278.

293) Lima, W. F.; Wu, H.; Nichols, J. G.; Prakash, T. P.; Ravikumar, V.; Crooke, S. T. *J. Biol. Chem.* **2003**, *278*, 49860-49867.

294) Sarafianos, S. G.; Das, K.; Tantillo, C.; Clark, A. D., Jr.; Ding, J.; Whitcomb, J. M.; Boyer, P. L.; Hughes, S. H.; Arnold, E. *EMBO J.* **2001**, *20*, 1449-1461.

295) Iwai, S.; Kataoka, S.; Wakasa, M.; Ohtsuka, E.; Nakamura, H. *FEBS Lett.* **1995**, *368*, 315-320.

296) Yazbeck, D. R.; Min, K.-L.; Damha, M. J. *Nucleic Acids Res.* **2002**, *30*, 3015-3025.

297) Davies, J. F., II; Hostomska, Z.; Hostomsky, Z.; Jordan, S. R.; Matthews, D. A. *Science* **1991**, *252*, 88-95.

298) Lima, W. F.; Nichols, J. G.; Wu, H.; Prakash, T. P.; Migawa, M. T.; Wyrzykiewicz, T. K.; Bhat, B.; Crooke, S. T. *J. Biol. Chem.* **2004**, *279*, 36317-36326.

299) Rodger, A.; Norden, B. *Circular Dichroism and Linear Dichroism*; Oxford University Press: New York, NY **1997**.

300) Gray, D. M.; Ratliff, R. L.; Vaughan, M. R. *Methods Enzymol.* **1992**, *211*, 389-406.

301) Wasner, M.; Arion, D.; Borkow, G.; Noronha, A.; Uddin, A. H.; Parniak, M. A.; Damha, M. J. *Biochemistry* **1998**, *37*, 7478-7486.

302) Iwai, S.; Wakasa, M.; Ohtsuka, E.; Kanaya, S.; Kidera, A.; Nakamura, H. *J. Mol. Biol.* **1996**, *263*, 699-706.

303) Ding, J.; Das, K.; Hsiou, Y.; Sarafianos, S. G.; Clark, A. D., Jr.; Jacobo-Molina, A.; Tantillo, C.; Hughes, S. H.; Arnold, E. *J. Mol. Biol.* **1998**, *284*, 1095-1111.

304) Huang, H.; Chopra, R.; Verdine, G. L.; Harrison, S. C. *Science* **1998**, *282*, 1669-1675.

305) Rausch, J. W.; Lener, D.; Miller, J. T.; Julias, J. G.; Hughes, S. H.; Le Grice, S. F. J. *Biochemistry* **2002**, *41*, 4856-4865.

306) Arion, D.; Sluis-Cremer, N.; Min, K. L.; Abram, M. E.; Fletcher, R. S.; Parniak, M. A. *J. Biol. Chem.* **2002**, *277*, 1370-1374.

307) Lener, D.; Budihas, S. R.; Le Grice, S. F. J. *J. Biol. Chem.* **2002**, *277*, 26486-26495.

308) Chapados, B. R.; Chai, Q.; Hosfield, D. J.; Qiu, J.; Shen, B.; Tainer, J. A. *J. Mol. Biol.* **2001**, *307*, 541-556.

309) Metelev, V. G.; Zayakina, G. V.; Ryabushenko, I. L.; Krynetskaya, N. F.; Romanova, E. A.; Oretskaya, T. S.; Shabarova, Z. A. *FEBS Lett.* **1988**, *226*, 232-234.

310) Wyatt, J. R.; Walker, G. T. *Nucleic Acids Res.* **1989**, *17*, 7833-7842.

311) Lima, W. F.; Crooke, S. T. *J. Biol. Chem.* **1997**, *272*, 27513-27516.

312) Mushegian, A. R.; Edskes, H. K.; Koonin, E. V. *Nucleic Acids Res.* **1994**, *22*, 4163-4166.

313) Cerritelli, S. M.; Fedoroff, O. Y.; Reid, B. R.; Crouch, R. J. *Nucleic Acids Res.* **1998**, *26*, 1834-1840.

314) Arudchandran, A.; Cerritelli, S. M.; Bowen, N. J.; Chen, X.; Krause, M. W.; Crouch, R. J. *Mol. Biol. Evol.* **2002**, *19*, 1910-1919.

315) Galarneau, A.; Min, K.-L.; Mangos, M. M.; Damha, M. J. In *Methods in Molecular Biology: Oligonucleotide Synthesis*; Herdewijn, P., Ed.; The Humana Press Inc.: Totowa NJ, vol. 288, **2005**, pp. 65 – 80.

316) Komori, H.; Masui, R.; Kuramitsu, S.; Yokoyama, S.; Shibata, T.; Inoue, Y.; Miki, K. *Proc. Natl. Acad. Sci. U.S.A.* **2001**, *98*, 13560-13565.

317) Friedhoff, P.; Thomas, E.; Pingoud, A. *J. Mol. Biol.* **2003**, *325*, 285-297.

318) Hosfield, D. J.; Guan, Y.; Haas, B. J.; Cunningham, R. P.; Tainer, J. A. *Cell* **1999**, *98*, 397-408.

319) Hung, S. H.; Yu, Q.; Gray, D. M.; Ratliff, R. L. *Nucleic Acids Res.* **1994**, *22*, 4326-4334.

320) Gyi, J. I.; Conn, G. L.; Lane, A. N.; Brown, T. *Biochemistry* **1996**, *35*, 12538-12548.

321) Dubins, D. N.; Lee, A.; MacGregor, R. B., Jr.; Chalikian, T. V. *J. Am. Chem. Soc.* **2001**, *123*, 9254-9259.

322) Stavrianopoulos, J. G.; Gambino-Giuffrida, A.; Chargaff, E. *Proc. Natl. Acad. Sci. U.S.A.* **1976**, *73*, 1087-1091.

323) Wilds, C. Ph. D. Thesis, McGill University: Montreal, **1999**, 185 pp.

324) Wang, S.; Kool, E. T. *Biochemistry* **1995**, *34*, 4125-4132.

325) Lesnik, E. A.; Guinosso, C. J.; Kawasaki, A. M.; Sasmor, H.; Zounes, M.; Cummins, L. L.; Ecker, D. J.; Cook, P. D.; Freier, S. M. *Biochemistry* **1993**, *32*, 7832-7838.

326) Drake, A. F.; Mason, S. F.; Trim, A. R. *J. Mol. Biol.* **1974**, *86*, 727-739.

327) Lee, C.-H.; Ezra, F. S.; Kondo, N. S.; Sarma, R. H.; Danyluk, S. S. *Biochemistry* **1976**, *15*, 3627-3639.

328) Singh, H.; Herbut, M. H.; Ilo, R.; Lee, C.-H.; Sarma, R. H. *Biopolymers* **1976**, *15*, 2167-2184.

329) Borer, P. N.; Dengler, B.; Tinoco, I., Jr.; Uhlenbeck, O. C. *J. Mol. Biol.* **1974**, *86*, 843-853.

330) Freier, S. M.; Sugimoto, N.; Sinclair, A.; Alkema, D.; Neilson, T.; Kierzek, R.; Caruthers, M. H.; Turner, D. H. *Biochemistry* **1986**, *25*, 3214-3219.

331) Burkard, M. E.; Turner, D. H.; Tinoco, I., Jr. In *The RNA World*; Gesteland, R. F., Cech, T. R. and Atkins, J. F., Eds.; Cold Spring Harbor Laboratory Press: Plainview NY, **1999**, vol. 37, pp. 233-264.

332) Holcomb, D. N.; Tinoco, I., Jr. *Biopolymers* **1965**, *3*, 121-133.

333) Richards, E. G.; Flessel, C. P.; Fresco, J. R. *Biopolymers* **1963**, *1*, 431-446.

334) Michelson, A. M.; Monny, C. *Proc. Natl. Acad. Sci. U.S.A.* **1966**, *56*, 1528-1534.

335) Kawai, G.; Yamamoto, Y.; Kamimura, T.; Masegi, T.; Sekine, M.; Hata, T.; Iimori, T.; Watanabe, T.; Miyazawa, T.; Yokoyama, S. *Biochemistry* **1992**, *31*, 1040-1046.

336) Cheng, D. M.; Sarma, R. H. *Biopolymers* **1977**, *16*, 1687-1711.

337) Steely, H. T., Jr.; Gray, D. M.; Ratliff, R. L. *Nucleic Acids Res.* **1986**, *14*, 10071-10090.

338) Ratmeyer, L.; Vinayak, R.; Zhong, Y. Y.; Zon, G.; Wilson, W. D. *Biochemistry* **1994**, *33*, 5298-5304.

339) Lesnik, E. A.; Freier, S. M. *Biochemistry* **1995**, *34*, 10807-10815.

340) Gyi, J. I.; Lane, A. N.; Conn, G. L.; Brown, T. *Biochemistry* **1998**, *37*, 73-80.

341) Rabczenko, A.; Shugar, D. *Acta Biochim. Pol.* **1971**, *18*, 387-402.

342) Sarngadharan, M. G.; Leis, J. P.; Gallo, R. C. *J. Biol. Chem.* **1975**, *250*, 365-373.

343) Hélène, C. *Adv. Biophys.* **1985**, *20*, 177-186.

344) Behmoaras, T.; Toulmé, J. J.; Hélène, C. *Proc. Natl. Acad. Sci. U.S.A.* **1981**, *78*, 926-930.

345) Brun, F.; Toulmé, J. J.; Hélène, C. *Biochemistry* **1975**, *14*, 558-563.

346) Hélène, C. *Nature* **1971**, *234*, 120-121.

347) Héléne, C.; Toulmé, J. J.; Doan, T. L. *Nucleic Acids Res.* **1979**, *7*, 1945-1954.

348) Behmoaras, T.; Toulmé, J. J.; Hélène, C. *Nature* **1981**, *292*, 858-859.

349) Durand, M.; Maurizot, J. C.; Borazan, H. N.; Hélène, C. *Biochemistry* **1975**, *14*, 563-570.

350) Behmoaras, T.; Toulmé, J. J.; Hélène, C. *CR Seances Acad. Sci. III* **1981**, *293*, 5-8.

351) Hélène, C.; Maurizot, J. C. *CRC Crit. Rev. Biochem.* **1981**, *10*, 213-258.

352) Hélène, C.; Toulmé, J. J.; Behmoaras, T.; Cazenave, C. *Biochimie* **1982**, *64*, 697-705.

353) Behmoaras, T.; Fidy, J.; Hélène, C.; Lancelot, G.; Le Doan, T.; Mayer, R.; Montenay-Garestier, T.; Toulmé, J. J. In *Intermolecular Forces*; Pullman, B. Ed.; D. Reidel Publishing Company: Dordrecht, **1981**, vol. 14, pp. 317-330.

354) Hélène, C. In *Excited States in Organic Chemistry and Biochemistry*; Pullman, B., and Goldblum, N., Eds.; D. Reidel Publishing Company: Dordrecht, **1977**, vol. 10, pp. 65-78.

355) Toulmé, J. J.; Hélène, C. *J. Biol. Chem.* **1977**, *252*, 244-249.

356) Dimicoli, J. L.; Hélène, C. *Biochemistry* **1974**, *13*, 724-730.

357) Toulmé, J. J.; Charlier, M.; Hélène, C. *Proc. Natl. Acad. Sci. U.S.A.* **1974**, *71*, 3185-3188.

358) Dimicoli, J. L.; Hélène, C. *Biochemistry* **1974**, *13*, 714-723.

359) Cleland, W. W. *Biochemistry* **1964**, *35*, 480-482.

360) Lima, W. F.; Wu, H.; Nichols, J. G.; Manalili, S. M.; Drader, J. J.; Hofstadler, S. A.; Crooke, S. T. *J. Biol. Chem.* **2003**, *278*, 14906-14912.

361) Mayer, R.; Toulmé, F.; Montenay-Garestier, T.; Hélène, C. *J. Biol. Chem.* **1979**, *254*, 75-82.

362) Kanaya, S.; Kohara, A.; Miura, Y.; Sekiguchi, A.; Iwai, S.; Inoue, H.; Ohtsuka, E.; Ikehara, M. *J. Biol. Chem.* **1990**, *265*, 4615-4621.

363) Zhang, W.-H.; Svarovskaia, E. S.; Barr, R.; Pathak, V. K. *Proc. Natl. Acad. Sci. U.S.A.* **2002**, *99*, 10090-10095.

364) Wu, H.; Lima, W. F.; Crooke, S. T. *Antisense Nucleic Acid Drug Dev.* **1998**, *8*, 53-61.

365) Still, W. C.; Kahn, M.; Mitra, A. *J. Org. Chem.* **1978**, *43*, 2923-2925.

366) Ti, G. S.; Gaffney, B. L.; Jones, R. A. *J. Am. Chem. Soc.* **1982**, *104*, 1316-1319.

367) McLaughlin, L. W.; Piel, N.; Hellmann, T. *Synthesis* **1985**, 322-323.

368) Elzagheid, M. I.; Viazovkina, E.; Damha, M. J. In *Current Protocols in Nucleic Acid Chemistry*; Beaucage, S. L., Bergstrom, D. E., Glick, G. D. and Jones, R. A., Eds.; John Wiley & Sons, Inc.: New York, NY **2002**, Vol. 1.7, 19 pp.

369) Damha, M. J.; Giannaris, P. A.; Zabarylo, S. V. *Nucleic Acids Res.* **1990**, *18*, 3813-3821.

370) Pon, R. T.; Yu, S.; Sanghvi, Y. S. *Bioconjug. Chem.* **1999**, *10*, 1051-1057.

371) Pon, R. T.; Usman, N.; Ogilvie, K. K. *Biotechniques* **1988**, *6*, 768-770, 773-775.

372) Blackburn, P.; Moore, S. In *The Enzymes*; Boyer, P.D., Ed.; Academic Press: New York NY, **1982**, vol. 15, pp. 317-433.

373) Blumberg, D. D. *Methods Enzymol.* **1987**, *152*, 20-24.

374) Sambrook, J.; Fritsch, E. F.; Maniatis, T. *Molecular Cloning: A Laboratory Manual, 2nd Ed.*; Cold Spring Harbor Laboratory Press: Cold Spring Harbor, NY, **1989**.

375) McClinton, M. A. *Aldrichim. Acta* **1995**, *28*, 31-35.

376) Sproat, B.; Colonna, F.; Mullah, B.; Tsou, D.; Andrus, A.; Hampel, A.; Vinayak, R. *Nucleosides Nucleotides* **1995**, *14*, 255-273.

377) Dahlberg, A. E.; Dingman, C. W.; Peacock, A. C. *J. Mol. Biol.* **1969**, *41*, 139-147.

378) Porath, J.; Flodin, P. *Nature* **1959**, *183*, 1657-1659.

379) Porath, J. *Clinica Chim. Acta* **1959**, *4*, 776-778.

380) Asara, J. M.; Allison, J. *Anal. Chem.* **1999**, *71*, 2866-2870.

381) Vandell, V. E.; Limbach, P. A. *Rapid Commun. Mass Spectrom.* **1999**, *13*, 2014-2021.

382) Kane, J. F. *Curr. Opin. Biotechnol.* **1995**, *6*, 494-500.

383) Bonekamp, F.; Andersen, H. D.; Christensen, T.; Jensen, K. F. *Nucleic Acids Res.* **1985**, *13*, 4113-4123.

384) Hopp, T. P.; Prickett, K. S.; Price, V. L.; Libby, R. T.; March, C. J.; Cerretti, D. P.; Urdal, D. L.; Conlon, P. J. *Biotechnology* **1988**, *6*, 1204-1210.

385) Collins-Racie, L. A.; McColgan, J. M.; Grant, K. L.; DiBlasio-Smith, E. A.; McCoy, J. M.; LaVallie, E. R. *Biotechnology* **1995**, *13*, 982-987.

386) Roberts, G. C. K.; Dennis, E. A.; Meadows, D. H.; Cohen, J. S.; Jardetzky, O. *Proc. Natl. Acad. Sci. U.S.A.* **1969**, *62*, 1151-1158.

387) Wu, T.; Ogilvie, K. K.; Pon, R. T. *Nucleic Acids Res.* **1989**, *17*, 3501-3517.

388) Altschul, S. F.; Madden, T. L.; Schaffer, A. A.; Zhang, J.; Zhang, Z.; Miller, W.; Lipman, D. J. *Nucleic Acids Res.* **1997**, *25*, 3389-3402.